APPLYING NEXT-GENERATION CANCER GENOME SEQUENCING APPROACHES TO OVARIAN CANCER

By

Dorothy Leigh Hallberg

A dissertation submitted to Johns Hopkins University in conformity with the requirements for the degree of Doctor of Philosophy

Baltimore, Maryland

December, 2019

ABSTRACT

Ovarian cancer is the leading cause of death from gynecologic cancers. The ten year survival is less than 30% and has not improved significantly over the last 30 years. We employed next generation sequencing to address three common areas where previous studies have been lacking and insight into disease etiology would help improve survival and treatment of patients with ovarian cancer. Firstly, one of the challenges to improved diagnostic and therapeutic intervention in ovarian cancer has been a limited understanding of the natural history of the disease. It has been proposed that fallopian tube cancers may be precursors of high-grade serous ovarian carcinoma (HGSOC) but evolutionary evidence for this hypothesis has been limited. We performed whole exome sequence and copy number analyses of laser-capture microdissected fallopian tube lesions (p53 signatures, serous tubal intraepithelial carcinomas (STICs), and fallopian tube carcinomas), ovarian cancers, and metastases from nine patients. Secondly, to improve our understanding of ovarian cancer, we performed genome-wide analyses of 45 commonly used ovarian cancer cell lines. Lastly, endometrioid and mucinous ovarian cancers represent nearly a quarter of ovarian cancers and their molecular characteristics and pathologic origins are poorly understood. Whole exome sequencing analyses of HGSOC samples demonstrated that p53 signatures and STICs are precursors of ovarian carcinoma and identified a window of seven years between development of a STIC and initiation of ovarian carcinoma, with metastases following rapidly thereafter. Whole genome sequencing analyses of 45 ovarian cancer cell lines showed dose-response analyses to targeted therapies revealed unique molecular dependencies, including increased sensitivity of tumors with PIK3CA and PPP2R1A alterations to PI3K inhibitor GNE-493, MYC amplifications to PARP inhibitor BMN673, and SMAD3/4 alterations to MEK inhibitor MEK162. Finally, whole exome and genome sequencing analyses on less common ovarian cancer subtypes revealed ovarian and GI mucinous tumors were epigenetically distinct. In contrast, the number of alterations and affected genes in ovarian and uterine endometrioid cancers were not distinguishable, suggesting

that these tumors may have a similar tissue of origin. Together these analyses provide insights into the etiology of ovarian cancer, have implications for prevention, early detection and therapeutic intervention of this disease.

Thesis Advisor: Dr. Victor E. Velculescu, M.D., Ph.D.

Thesis Readers: Dr. Robert B. Scharpf, Ph.D. and Dr. Valsamo Anagnostou, M.D., Ph.D.

ACKNOWLEDGEMENTS

I would like to thank my mentor, Victor Velculescu, for his guidance and support throughout my graduate training, for his impeccable attention to detail, for always having time to discuss data, for his unwavering kindness, and for his efforts towards making the lab a warm and exciting environment. I also want to thank Robert Scharpf, Valsamo Anagnostou, and Dan Arking for their mentorship and advice as members of my thesis committee and beyond, and all the members of the Cancer Genomics Lab for their comradery. My family has also been a constant area of support, my husband, Kenny, and our three furbabies who has been with me through the highs and lows and always been a great source of encouragement and inspiration, my sisters, Charlotte and Alexis, and their whole families who have provided me many laughs and nephews to keep me sane and happy, my parents and new parents who I wouldn't be here without them, and finally my friends and labmates who have provided laughs and inspiration along the way. I greatly appreciate the contributions to research from patients with cancer as well as the support of Johns Hopkins University School of Medicine.

TABLE OF CONTENTS

Abstract		ii
Acknowledgements		iv
Table of Contents		v
List of Tables		vi
List of Figures		viii
Chapter 1:	Introduction	1
Chapter 2:	High grade serous ovarian carcinomas originate in the fallopian tube	8
Chapter 3:	Integrated genomic, epigenomic and expression analyses of ovarian cancer cell lines	113
Chapter 4:	Genomic landscapes of endometrioid and mucinous ovarian cancers	251
Chapter 5:	Discussion	289
References		298
Curriculum Vitae		306

LIST OF TABLES

Supplementary Table 2.1. Summary of Patient and Sample Characteristics 42

Supplementary Table 2.2. Summary of Next-Generation Sequencing Analyses 44

Supplementary Table 2.3. Targeted Sequencing Panel 46

Supplementary Table 2.4. Somatic Sequence Alterations 49

Supplementary Table 2.5. Somatic Sequence Alterations used for Evolutionary Cluster 99

Supplementary Table 2.6. Recurrent Somatic Sequence Alterations 105

Supplementary Table 2.7. Regions of Allelic Imbalance in CGOV62 107

Supplementary Table 2.8. Regions of Allelic Imbalance in CGOV63 109

Supplementary Table 2.9. Regions of Allelic Imbalance in CGOV280 110

Supplementary Table 2.10. Regions of Allelic Imbalance in CGOV279 111

Supplementary Table 2.11. Regions of Allelic Imbalance in CGOV278 112

Table S3.1a. Summary of ovarian cancer cell lines analyzed 146

Table S3.1c. Summary of genomic analyses 148

Table S3.1d. Summary of sequence alterations 150

Table S3.1e. Driver genes evaluated for inactivating mutations 152

Table S3.1f. Sequence alterations 160

Table S3.1h. Deletions 187

Table S3.1i. Predicted in-frame coding fusions 221

Table S3.1k. Pathway inhibitors 240

Table S3.1l. Rearrangement types identified from improperly paired reads 245

Table S3.1n. R package versions 246

Supplementary Table 4.1. Summary of Ovarian and CRC Mucinous Analyzed Through Whole-Exome and Whole-Genome Analyses Supplementary 278

Table 4.2. Summary of Next-Generation Sequencing Analyses 282

LIST OF FIGURES

Figure 2.1. Schematic of sample isolation and next-generation sequencing analyses 29

Figure 2.2. Somatic mutation and allelic imbalance profiles among different tumor lesions 30

Figure 2.3. Genome-wide allelic imbalance profile 31

Figure 2.4. Schematic of tumor evolution 32

Supplementary Figure 2.1. Loss of heterozygosity analyses for CGOV62 33

Supplementary Figure 2.2. Loss of heterozygosity analyses for CGOV63 34

Supplementary Figure 2.3. Loss of heterozygosity analyses for CGOV280 35

Supplementary Figure 2.4. Loss of heterozygosity analyses for CGOV279 36

Supplementary Figure 2.5. Loss of heterozygosity analyses for CGOV278 37

Supplementary Figure 2.6. Loss of heterozygosity analyses for CGOV65 37

Supplementary Figure 2.7. Loss of heterozygosity analyses for CGOV64 38

Supplementary Figure 2.8. Loss of heterozygosity analyses for CGOV303 38

Supplementary Figure 2.9. Loss of heterozygosity analyses for CGOV304 39

Supplementary Figure 2.10. Genome-wide copy number profile 40

Supplementary Figure 2.11. Schematic of tumor evolution using PHYLIP 41

Figure 3.1. Overview of Genomic, Epigenomic, Expression, and Therapeutic Analyses of Ovarian Cancer Cell Lines 140

Figure 3.2. Number of False-Positive Somatic Structural Variant Identifications in Lymphoblastoid Cell Lines 141

Figure 3.3. Trellis Approach for Characterization of Genomic Structural Alterations 142

Figure 3.4. Methylation of CpG Sites in Ovarian Cancers and Normal Fallopian Tissue 143

Figure 3.5. Sequence, Structural, Epigenomic, and Expression Alterations in Ovarian Cancer Cell Lines 144

Figure 3.6. Sensitivity and Resistance to Pathway Inhibitors 145

Figure 4.1. Overview of genomic analyses 265

Figure 4.2. Integrated genomic and epigenomic analyses of ovarian endometrioid and uterine endometrial cancers 272

Figure 4.3. Whole genome analyses of linked amplicons and rearrangements 273

Figure 4.4. Integrated genomic analyses of ovarian and colorectal mucinous cancers 274

Figure 4.5. Prevalence of alterations in related tumor types 275

Figure 4.6. Methylation analyses of ovarian and GI mucinous tumors 276

Supplemental Figure 4.1. Distribution number of mutations within the endometrioid samples 277

Supplemental Figure 4.2. ESR1 Y537R mutations 278

Supplemental Figure 4.3. Mutation signature analyses 279

Supplemental Figure 4.4. Circos plots of 19 ovarian endometrioid tumor samples 280

Supplemental Figure 4.5. Rearrangement analyses of ovarian endometrioid and ovarian mucinous tumors 281

Supplemental Figure 4.6. Comparison of mutation frequencies in ovarian mucinous and endometrioid tumors 282

Supplemental Figure 6.7. Proportion of methylated probes in mucinous tumor samples 283

CHAPTER 1:

INTRODUCTION

1.1 Overall introduction

Ovarian cancer is the leading cause of death from gynecologic cancers[1,2]. The ten year survival is less than 30% and has not improved significantly over the last 30 years[3]. Despite significant efforts, various screening and therapeutic strategies have generally not led to improved overall survival[4,5]. One of the major challenges to improved diagnostic and therapeutic intervention in ovarian cancer has been a limited understanding of the natural history of the disease. Ovarian carcinoma is a highly heterogeneous group of diseases including different histological subtypes with distinct clinicopathological and molecular genetic features that can be generally classified as Type I and Type II tumors[6]. Among them, high grade serous ovarian carcinoma (HGSOC, the major Type II tumor) is the most common histologic subtype of ovarian cancer, accounting for three quarters of ovarian carcinoma[7-10].

Despite significant advances in therapies for other solid tumor malignancies, the overall survival of patients with late-stage ovarian cancer has remained dismal with few new options for treatment. The standard therapy involves debulking surgery followed by chemotherapy. Part of the reason for the lack of novel therapies for ovarian cancer has been an inadequate understanding of the underlying molecular characteristics of this disease, especially in the context of cancer cell models than can facilitate the development of various cancer treatments.

Epithelial ovarian cancer comprises about 90% of all ovarian cancer malignancies and includes high grade serous, low grade serous, mucinous, endometrioid and clear cell ovarian carcinoma. High grade serous ovarian cancers (HGSOC) represent more than half of all epithelial ovarian cancers and is the most widely studied epithelial ovarian tumor, while endometrioid and mucinous account for 10% and 6%, respectively[11]. Through extensive whole genome, exome, and methylation analyses of HGSOC, a variety of genes have been identified as likely drivers in these tumors[12], and evolutionary analyses have implicated the fallopian tube as the tissue of origin of

HGSOC [13-15]. Apart from alterations in a few well known drivers including *KRAS* and *HER2* amplification in ovarian mucinous carcinomas and mutations in *ARID1A*, *PIK3CA*, and *PTEN* genes as well as MMR deficiency in ovarian endometrioid carcinomas, comparatively little is known about molecular alterations in these tumors. Comprehensive genomic analyses of these tumor subtypes could delineate additional alterations and pathways frequently altered in these cancers and shed light on their likely tissue of origin.

1.2 High grade serous ovarian carcinomas originate in the fallopian tube introduction

Genomic analyses of HGSOC have identified genetic alterations in *TP53, BRCA1, BRCA2, PTEN* and other genes although few of these discoveries have affected clinical care[16,17]. HGSOC is diagnosed at advanced stages in approximately 70% of cases, and these women have a significantly worse outcome than those with early stage disease. Until recently, the prevailing view of HGSOC was that it developed from the ovarian surface epithelium. However, early *in situ* lesions that arise from the ovarian surface epithelium and progress to invasive HGSOC have never been reproducibly identified.

Insights into the pathogenesis of HGSOC have emerged from investigating the prevalence of occult ovarian and fallopian tube carcinomas in women with germline mutations of *BRCA1/BRCA2* genes[18-22]. Potential precursor lesions of HGSOC were identified in the fimbriae of the fallopian tubes removed as part of prophylactic surgery[21]. Such lesions, including a *TP53* mutant single-cell epithelial layer (p53 signature) and serous tubal intraepithelial carcinoma (STIC)[22,23], have been identified in patients with advanced stage sporadic HGSOC of the ovary, fallopian tube and peritoneum[23]. Immunohistochemical as well as targeted sequencing analyses have shown that fallopian tube lesions harbor the same *TP53* mutation as surrounding invasive carcinomas[22-26]. These analyses suggest a clonal relationship among such tumors but given the limited number of genes analyzed do not conclusively identify the initiating lesions nor exclude the possibility of

fallopian tube metastases from primary ovarian carcinomas[26,27]. Yet additional studies have evaluated clonal intraperitoneal spread of ovarian cancer using whole genome analyses, but this effort did not analyze precursor lesions such as STICs that may give rise to this disease[28].

In this study, we use exome-wide sequence and structural analyses of multiple tumor samples from the same individual to examine the origins of HGSOC. We have previously shown that the acquisition of somatic alterations can be used as a molecular marker in the development of human cancer[29]. Here, we examine whether the compendium of somatic alterations identified in different lesions may provide insights into the evolutionary relationship between primary fallopian tube lesions, including p53 signatures and STIC lesions, ovarian carcinomas, and intraperitoneal metastases.

1.3 Integrated genomic, epigenomic and expression analyses of ovarian cancer cell lines introduction

Recent studies have highlighted the genomic complexity and heterogeneity of ovarian cancer. These have included a catalog of sequence mutations, focal changes in DNA copy number, gene expression, and methylation alterations in high grade serous ovarian cancer [16] as well as whole exome analyses of ovarian clear cell carcinoma and low grade serous carcinoma[30,31]. Genome-wide sequence analyses of high grade serous ovarian cancer identified drivers associated with primary and acquired resistance to chemotherapy[13,17]. More recently, a catalog of proteomic alterations in high grade serous TCGA samples has been integrated with structural alterations and correlated with clinical outcomes[32]. Hypothesis-generating pharmacogenomic studies involving cancer cell lines, some of which were ovarian, have revealed genetic- and expression-based alterations associated with resistance or sensitivity to a panel of drugs[33,34]. More recent cell line studies have evaluated high grade serous, clear cell and other cancers using targeted genomic and other molecular analyses[35-37]. These initial efforts were extended to demonstrate the similarity of molecular

alterations in cell lines to those in corresponding tissues, to develop approaches for incorporating multiple data types to model sensitivity, and to apply these models to larger drug panels[38]. Despite these advances, a comprehensive analysis of genome-wide structural alterations, including intra- and inter-chromosomal translocations and gene fusions, and integration of these data with whole-exome sequence, epigenetic and expression information are not available for many histological subtypes of ovarian cancer. Furthermore, the therapeutic response of these ovarian cancer subtypes to common targeted therapies is not well understood.

Here, we performed complementary molecular analyses of 45 ovarian cell lines of different histologies, including serous, clear cell, endometrioid, and mucinous cancers. As these cell lines do not have matched normal tissues, we developed novel approaches to characterize tumor-specific alterations at sequence and structural levels, and integrated these with methylation and transcript changes to identify the compendium of alterations at the gene- and pathway-levels. Using the same cell lines, we evaluated the effect of a few targeted agents of common pathways using in vitro cell survival assays. Our analyses identified novel molecular alterations in ovarian cancer, delineated genes modulated by genetic and epigenetic changes, and highlighted specific sequence, structural, and epigenetic alterations associated with sensitivity and resistance to common pathway inhibitors.

1.4 Genomic landscapes of endometrioid and mucinous ovarian cancers introduction

Accumulating evidence suggests connections between endometrioid ovarian cancers and endometrioid uterine tumors, which accounts for nearly 85% of all epithelial uterine carcinomas [39]. Synchronous endometrioid ovarian and uterine carcinomas can arise from independent primary tumors or as metastases from a single primary tumor [40,41], suggesting that these tumors may share the same cell of origin [42,43]. Women who have synchronous ovarian and uterine cancers have an improved survival as compared to those with a single cancer, in part due to early diagnosis from

the symptoms associated with uterine tumors [44]. Understanding the origin of these cancers could lead to more accurate prognoses of survival or more aggressive early intervention. While whole genome and targeted next generation sequencing analyses have been performed of ovarian endometrioid carcinomas [45,46] and whole exome studies have been performed on uterine endometroid carcinomas [47], the extent to which these cancers share similar alterations and a potentially common tissue of origin has not been systematically evaluated.

Distinguishing between primary mucinous ovarian cancer and mucinous adenocarcinoma metastases from other sites, including gastrointestinal mucinous tumors, may be challenging. Some histological features can favor primary diagnosis but there are several discordant and overlapping features that make a definitive diagnosis difficult [48]. Genomic analyses for mucinous ovarian and gastrointestinal cancers, including pancreatic, stomach and colorectal cancer, have largely been limited to targeted sequencing [49-52]. Additionally, no studies to date have compared the genomes and epigenomes of mucinous carcinomas from the ovary with those of other sites. Such analyses could establish the tissue of origin and lead to better risk stratification and treatment for patients with these cancers.

To better understand the genomic landscapes of these ovarian cancer subtypes and their histological counterparts, we performed whole exome sequencing and/or whole genome sequencing of 130 samples from 117 patients with endometrioid cancer of the ovary or uterus or mucinous cancer of the ovary or GI tissues (stomach, pancreas, or colon). Whole exome sequencing analyses identified somatic sequence mutations and structural alterations common to these cancers, including deletions, amplifications, and loss of heterozygosity. For samples with whole genome sequencing, we additionally identified novel intra- and inter-chromosomal rearrangements and in-frame fusions using our recently developed Trellis approach [53]. To further explore the differences in molecular landscapes of mucinous cancers, we compared the epigenome of 25 patients with ovarian or GI

mucinous cancer using genome-wide methylation analyses in both the cancer and adjacent normal tissues. These analyses highlight major pathways affected by genomic and epigenomics changes in these ovarian cancers, and identified a number of novel molecular alterations that may improve our understanding of their tissue of origin.

CHAPTER 2:

HIGH GRADE SEROUS OVARIAN CARCINOMAS ORIGINATE IN THE FALLOPIAN TUBE

METHODS

Specimens obtained for sequencing analysis

The study was approved by the Institutional Review Board at Brigham and Women's Hospital and the Johns Hopkins Hospital and all patients gave informed consent before inclusion. Five sequential patients with stage III sporadic HGSOC, in whom a serous tubal intraepithelial carcinoma (STIC) was identified in their fallopian tubes (FT), were included. In addition, we included isolated STICs from three patients with germline BRCA deleterious mutation alterations who underwent prophylactic bilateral salpingo-oophorectomy and as well as a fourth patient who had bilateral salpingo-oophorectomy and hysterectomy in the context of a pelvic mass. All cases underwent complete tubal examination using the SEE-FIM protocol16. Formalin-fixed paraffin embedded (FFPE) blocks were retrieved from the pathology files at Brigham and Women's Hospital and Johns Hopkins Hospital within the 3 months following surgical diagnosis and stored at 4°C to slow down nucleic acids degradation. All the cases were reviewed by a gynecologic pathologist (MH, DL, LS) that confirmed the diagnosis of STIC and /or p53 signature in the FT. Slides from each FFPE block were microdissected, including early lesions, invasive carcinomas and metastases, stained with Hematoxylin & Eosin (H&E), and using immunohistochemistry were analyzed for p53 staining. In each FT, at least one STIC and/or p53 signature was identified and microdissected separately. Importantly, STICs were not pooled together even if they were in the same section. They were considered separate STICs.

Immunohistochemistry p53 staining for and laser capture microdissection

For accurate microdissection of early lesions including STIC and p53 signature, immunohistochemistry staining of p53 was specifically adapted for Laser Capture Microdissection

(LCM) as previously described43. PEN membrane frame slides Arcturus (Life technologies, Carlsbad, CA) were used. Each slide was coated with 350 ul of undiluted poly-L-lysine 0.1% w/v (Sigma, St. Louis, MO). For drying, the slides were placed in a slide holder for 60 minutes at room temperature. Tissue sections were cut and mounted on the pretreated membrane slides. Deparaffinization was performed in fresh xylene for 5 minutes twice, followed by 100% ethanol for 2 minutes, 95% for ethanol 2 minutes and 70% ethanol for 2 minutes. Subsequently, the slides were transferred into distilled water for 5 minutes. Heat-epitope antigen retrieval (AR) was performed in Citrate Buffer (Dako, Carpinteria, CA) at low temperature (60°C) for 44 hours instead of 120°C for 10 minutes to reduce tissue and DNA damage by high temperature. Retrieval solution was pre-warmed to 60°C before usage. After incubation in the oven, the AR solution was left to cool down to room temperature and the slides were rinsed for 30 seconds in fresh 1X PBS then incubated for 40 minutes with primary antibody anti-p53 (Epitomics, Burlingame) at 1:100 in a humidifying chamber. Before adding the secondary antibody, slides were washed twice for 1 minute in fresh 1X PBS. The secondary antibody, labeled polymer-HRP anti-mouse (Dako EnVision System-HRP (DAB), Carpinteria, CA) was applied for 30 minutes. Then, slides were washed twice for 1 minute in fresh 1X PBS. Chromogenic labeling was performed with 3,3-DAB substrate buffer and DAB chromogen (Dako EnVision System-HRP (DAB), Carpinteria, CA) for 5 minutes. Slides were washed again for 30 seconds in fresh distilled water. Dehydration was performed as follows: 70% ethanol for 30 seconds, 95% ethanol for 30 seconds, 100% ethanol for 30 seconds, and xylene for 30 seconds. The stained slides were microdissected within 2 hours with the Arcturus XT LCM system (Life technologies, Carlsbad, CA).

Hematoxylin staining for laser capture microdissection

Invasive carcinomas from the ovaries, the fallopian tubes and intraperitoneal metastases or STICs from patients with negative p53 IHC staining were microdissected after Hematoxylin staining.

Briefly, deparaffinization was performed in fresh xylene for 1 minute twice followed by 100% ethanol for 1 minute, 95% for ethanol 1 minute and 70% ethanol for 1 minute. The slides were transferred into distilled water for 2 minutes before staining with Hematoxylin for 2 minutes. Subsequently, slides were rinsed in distilled water until they became clear before undergoing dehydration in 70% ethanol for 1 minute, 95% ethanol for 1 minute, 100% ethanol for 1 minute and xylene for 1 minute. The stained slides were microdissected within 2 hours.

Sample preparation and next-generation sequencing

DNA was extracted from patient whole blood using a QIAamp DNA Blood Mini QIAcube Kit (Qiagen Valencia, CA). Genomic DNA from FFPE blocks was extracted from the microdissected tissues using the QIAamp DNA FFPE Tissue kit (Qiagen, Valencia, CA). In brief, the samples were incubated in proteinase K for 16 hours before DNA extraction. The digested mixture was transferred to a microtube for DNA fragmentation using the truXTRAC™ FFPE DNA Kit with 10 min shearing time as per the manufacturer's instructions (Covaris, Woburn, MA). Following fragmentation, the sample was further digested for 24 hours followed by one hour incubation at 80ºC. DNA purification was performed using the QIAamp DNA FFPE Tissue kit following the manufacturer's instructions (Qiagen, Valencia, CA). Fragmented genomic DNA from tumor and normal samples were used for Illumina TruSeq library construction (Illumina, San Diego, CA) according to the manufacturer's instructions or as previously described44. Exonic or targeted regions were captured in solution using the Agilent SureSelect v.4 kit or a custom targeted panel according to the manufacturer's instructions (Agilent, Santa Clara, CA). Paired-end sequencing, resulting in 100 bases from each end of the fragments for exome libraries and 150 bases from each end of the fragment for targeted libraries, was performed using Illumina HiSeq 2000/2500 and Illumina MiSeq instrumentation (Illumina, San Diego, CA).

Next generation sequencing data and identification of somatic mutations

Somatic mutations were identified using VariantDx45 custom software for identifying mutations in matched tumor and normal samples. Prior to mutation calling, primary processing of sequence data for both tumor and normal samples were performed using Illumina CASAVA software (v1.8), including masking of adapter sequences. Sequence reads were aligned against the human reference genome (version hg18 or hg19) using ELAND. Candidate somatic mutations, consisting of point mutations, insertions, and deletions were then identified using VariantDx across the either the whole exome or regions of interest44. For samples analyzed using targeted sequencing, we identified candidate mutations that were altered in >10% of distinct reads. For samples analyzed using whole exome sequencing, we identified candidate mutations that were altered in >10% of distinct reads with ≥5 altered reads in at least one sample, where coverage at the altered base was at least as high as the TP53 alteration in that sample, and where the ratio of the coverage of the mutated base to the overall sequence coverage of that sample was >20%. Identified mutations were reported as present in other samples of the same patient if the mutation was present in at least 2 distinct altered reads. Mutations present in polyN tract ≥ 5 bases, or those with an average distinct coverage below 50x were removed from the analysis.

An analysis of each candidate mutated region was performed using BLAT. For each mutation, 101 bases including 50 bases 5' and 3' flanking the mutated base was used as query sequence (http://genome.ucsc.edu/cgi-bin/hgBlat). Candidate mutations were removed from further analysis, if the analyzed region resulted in >1 BLAT hits with 90% identity over 70 SCORE sequence length. All candidate alterations were examined by visual inspection, and any alteration present.

Genome-wide allelic imbalance analysis

We performed comparative analysis of loss of heterozygosity (LOH) across the tumor samples from each patient to identify copy number alterations occurring in the course of tumor evolution. Minor allele frequency (MAF) of germline heterozygous SNPs with minimum coverage of 10x in each tumor sample were segmented using circular binary segmentation algorithm (CBS)46. Genomic segments where the difference between tumor and normal MAF exceeded a threshold of 0.10 were labeled as harboring LOH. In each tumor sample, the minimum MAF across segments with minimum size of 10 Mb was calculated to provide a measure of sample purity. Each segment marked as LOH was assigned to one of the three confidence categories: (1) High confidence, segment MAF within 0.1 of the minimum sample MAF. (2) Intermediate confidence, segment MAF within 0.1 to 0.2 of the minimum sample MAF (3) Low confidence, segment MAF exceeding the minimum sample MAF by greater than 0.2.

Next, sample level segments were intersected across the entire set of samples from each patient to derive patient level segments while accounting for the possibility of variable segment break points in different samples (Supplementary Data 7-11). Patient level segments were filtered to keep those covering a minimum of 20 SNPs and with minimum length of 10 Mb. The resulting segments were further narrowed down to only include those with high confidence LOH in at least one of the samples. Genomic segments with LOH in a subset of samples can serve as informative markers to track tumor evolution similar to somatic mutations. To increase the specificity in identifying this class of genomic segments, we required a minimum distance of 0.1 between the MAF of samples with and without LOH. To minimize the possibility of over-segmentation which could result in inflated estimates of the number independent structural alterations, we evaluated patient level segments with boundaries within a 5 Mb window. In cases where the LOH calls were identical and the difference of segment minor allele frequencies were less than or equal to 0.05 in all tumor samples, the segments were merged.

For CGOV62 and CGOV63, the number of germline heterozygous SNPs meeting the coverage criteria in p53 signature samples was significantly lower than the other samples from the same patient. Thus, we modified the approach above in these two patients to enable sensitive analysis of LOH in p53 signature samples. Initially, the patient level genomic segments of interest were defined excluding p53 signature samples. Next, in each genomic segment, the minor allele of each overlapping germline SNP was determined by taking a majority vote over their minor alleles in the other samples. The coverage and minor allele read count for each SNP was derived using samtools (v0.1.19) mpileup module47. The segment minor allele frequency in p53 signature samples were calculated by dividing the sum of minor allele read counts across all SNPs by the total coverage of SNPs, circumventing the variance resulting from low coverage at individual SNPs. In each p53 signature sample, segments with MAF lower than that of the normal by at least 0.1 were marked as LOH.

Copy number analysis

The genome-wide copy number profiles were determined by analysis of the ratio of read counts in the tumor and matched normal whole exome sequenced samples. In each sample, the number of reads mapping to genomic bins located in target and off-target regions were corrected for biases arising from GC-content, repetitive sequences, and target capture process using CNVKit (v.0.7.6) [https://doi.org/10.1371/journal.pcbi.1004873]. The log ratio of the processed tumor to normal read counts provides a measure of copy number in each bin, and was segmented to yield genomic intervals at constant copy number levels. The difference in sequencing library size between the tumor and normal samples is another factor that needs to be accounted for when analyzing reads ratios in NGS-based copy number pipelines. In CNVKit, the log ratio values in each sample are adjusted by setting the median of autosomal bins to 0 in log space, assuming a median ploidy of 2

for the genome. Given the high prevalence of copy number aberrations in ovarian cancer and the high frequency of allelic imbalance in the present cohort, this assumption may not be accurate, and will manifest itself as a genome-wide bias or shift of log ratio values.

Therefore, an alternative approach for normalization of log ratio values was adopted, which takes into account the level of allelic imbalance in each genomic region. Briefly, genomic regions with the least degree of allelic imbalance were identified in each tumor sample, and used in a normalization process based on the notion that these regions can only be present in an even number of copies. The distribution of log ratio values among these regions was inspected to ensure that they belong to the same copy number level. Otherwise, a subset of regions at a common log ratio (and thus copy number) level were selected. By fixing the copy number of these segments at a specified level, one can solve for the genome-wide bias of log ratio values as follows, and thus identify the genome-wide integer copy number profile.

$$R = log_2\left(\frac{\alpha\, CN_T + (1-\alpha)CN_N}{2}\right) - \delta$$

In the equation above, R represents the observed log ratio of read counts, α is the purity of the tumor sample, CN_T and CN_N are the integer copy number of tumor and normal samples at a locus, and δ is the genome-wide bias term. Given the value of tumor purity and copy number, δ is the only unknown in the equation. To favor solutions with less complex genomes, the copy number of regions with complete allelic balance was initially set to 2. If the resulting solution was deemed implausible (e.g. by implying chromosome or chromosome arm scale homozygous deletions), the copy number of regions with complete allelic balance was assigned to 4 and an alternative solution was found (Supplementary Figure 10).

Details of the genomic segments selected to solve for the genome-wide bias term δ are as follows. In CGOV62, chromosomes 4 and 12 did not have allelic imbalance in any tumor samples. The solution assigning copy number two to these regions implied homozygous deletion of the p-arm of chrX in multiple samples; therefore, the simplest plausible solution assigned them to 4 copies. In CGOV63, chromosomes 6 and 15 did not have allelic imbalance in any of the tumor samples, and were assigned to 2 copies. No complete chromosome with absence of allelic imbalance across all tumor samples could be found in CGOV278. Therefore, four genomic regions with no allelic imbalance were selected for the normalization process above. These regions were chr8:38-69Mb, chr12:62-85Mb, chr18:7-19Mb, chr20:23-35Mb. The solution assigning these regions to 2 copies resulted in an implausible assignment of homozygous deletion to chr5:50-136Mb. Therefore, assignment of four copies to the selected regions results in the simplest solution. In CGOV279, two genomic regions were selected for the normalization procedure: chr5: 64-131Mb, chr20:17-36Mb. Evaluation of log ratio values suggested that the two regions are present at different copy levels, as evidenced by a difference of ~0.60 in the log ratio values. The region on chr5, which had the lower log ratio level, was assigned to copy number 2. In CGOV280, chr16q had no allelic imbalance in any samples excluding the left FT STIC. Examination of log ratio values of chr16q in the left FT STIC supports a copy loss in that sample. The genome-wide bias term δ was determined by assignment of 2 copies to chr16q in the four samples with no allelic imbalance, and one copy in the left FT STIC.

Subclonal hierarchy analysis

The tumor subclonality phylogenetic reconstruction algorithm SCHISM 1.0.025 was used to infer tumor subclonal hierarchies from the set of confidently called somatic mutations in each patient. Given the estimates of genome-wide copy number profile, most copy number aberrations seem to occur early in the evolution of disease and are common across the lesions analyzed from each

patient. Thus, the majority of somatic mutations can be assumed to occur following the acquisition of copy number aberrations, and can be present in cancer cells with multiplicity of one (one mutated copy per cell). Using this assumption, we can estimate mutation cellularity (or cancer cell fraction) from the observed reference and alternate read counts, and estimates of copy number, and tumor purity as follows.

$$V_{exp} = \frac{m\alpha C}{\alpha\, CN_T + (1-\alpha)CN_N}$$

In the equation above, V_expis the expected variant allele frequency of the mutation, m is the multiplicity of the mutation which is set to 1, α is the purity of the tumor sample, C is the cellularity of the mutation, and 〖CN〗_T and 〖CN〗_N are the integer copy number of tumor and normal sample at the locus of the mutation. The observed alternate read count of the mutation can be modeled as a binomial random variable drawn from a distribution with probability parameter equal to V_exp and number of trials equal to the total sequence coverage of the mutation. We calculated the likelihood for observation of the alternate read counts for cellularity values spanning the range of 0 to 1 in increments of 0.01, and derived the maximum likelihood estimate and confidence interval for the mutation cellularity.

To obtain reliable estimates of mutation cellularity, we clustered mutations by joint presence or absence across the available tumor samples. This approach makes phylogenetic reconstruction more tractable and the cellularity of the resulting clusters can be estimated with higher accuracy than that of individual mutations. For each patient, a mutation was called as present or absent in each of the available tumor samples (10 samples from CGOV62, 6 samples from CGOV63, 5 samples from CGOV280, 4 samples from CGOV279, and 3 samples from CGOV278). To call the mutation present, we used a minimum allele frequency of 2% and 2 distinct mutant reads. Mutation clustering was performed by a greedy algorithm. Tumor purity in each tumor sample was estimated

as the read count fraction of TP53 mutation in each patient. Each patient harbored a single distinct TP53 mutation that was present in all tumor samples, and we assumed the wild-type allele was lost, as supported by the ubiquitous LOH of chromosome 17. To derive a more comprehensive view of the evolution of these samples, we extended the original SCHISM framework to model acquisition of large scale somatic copy number alterations, which can be detected by analysis of allelic imbalance (including LOH). First, we extracted a set of high confidence genomic regions with ubiquitous, partially shared, or private LOH in tumor samples of each patient (Methods). These regions of LOH served as binary features that could be used for evolutionary analysis, and were clustered into LOH feature groups with identical patterns of presence or absence across samples (Figure 2). Each LOH feature group was compared to the somatic mutation clusters in each patient, with respect to its pattern of presence or absence across samples. In cases where a mutation cluster with the identical pattern could be found, the cluster and the LOH feature group were assumed to have occurred together in the course of tumor evolution. Otherwise, the LOH feature groups were modeled as distinct features, and added in post-hoc analysis by application of the lineage precedence rule from SCHISM; which requires cellularity of ancestor alterations to be greater than or equal to cellularity of descendant alterations in all tumor samples. SCHISM was run with the above inputs and default parameter settings to infer the order of somatic alterations and thus define subclonal hierarchy in each patient. SCHISM software is freely available for non-profit use at http://karchinlab.org/appSchism.

Evolutionary trees resulting from SCHISM analysis were compared with those derived by maximum parsimony phylogeny using PHYLIP (Phylip-3.695, PARS method). For CGOV280, an adjustment to the tree was applied to account for multiple subclones in Right FT STIC.

Estimating an evolutionary timeline

Following the approach of Jones et al., the observed data are the number of somatic mutations in the STIC (n_j), the number of mutations in the metastasis (n_k), and the age at which the patient was diagnosed (t_k), where somatic mutations include both sequence and structural alterations. Unknown is the birth date (t_j) of the cell that was the last common ancestor of the STIC and the metastasis. Assuming the mutation rate of somatic passenger mutations and the length of the cell cycle is constant, the number of somatic mutations in the metastasis cell that were present in the STIC follows a binomial distribution with parameters N2 and probability t_j/t_k. As t_j is unknown, we posit a conjugate beta probability distribution on the rate t_j/t_k with shape parameters a and b estimated from previous studies as described below. The posterior distribution of t_j/t_k is beta (a + n_j, b + n_k - n_j) from which 90% highest posterior density intervals can be constructed with point estimates for the birthdate reported as the posterior mean. For simplicity, we refer to the highest posterior density as a confidence interval. To construct a prior for t_j/t_k, we draw on a previous study of four colorectal cancer patients29 where a small number of additional passenger mutations were acquired by the cell that gave birth to the metastasis. On average, 95% of the mutations in the original adenocarcinoma were present in the metastases. We center the mean for the beta prior at 0.95 using shape parameters a = 34 and b = 1.6. Our prior is equivalent to one patient having 34 passenger somatic mutations in the original lesion and 1.6 additional mutations to be acquired by cells that gave birth to the metastases. For patients with three samples in a linear tree as determined by evolutionary analyses (say, samples j, k, and l where sample j is the STIC, l is the metastasis, and k is an intermediate sample), we first derived the posterior distribution for t_k comparing mutations in samples k and l. Next, we derived the posterior distribution of t_j integrating over all possible values of t_k, thereby fully incorporating the uncertainty of the intermediate timepoint in the estimate of t_j. We evaluated three additional prior models, and found that that posterior inference under these alternative models given by 90% credible intervals for t_k – t_j, results in qualitatively similar timelines among different lesions in tumor progression.

RESULTS

Overall approach

To elucidate the relationship among tumors in patients with HGSOC, we performed whole-exome sequencing of 37 samples from five patients diagnosed with sporadic HGSOC who underwent upfront debulking (Supplementary Table 2.1). This included STIC lesions, fallopian tube carcinomas, and ovarian cancers in all five patients; appendiceal, omental or rectal metastases in three of patients (CGOV62, CGOV280, CGOV278); p53 signatures in two patients (CGOV62, CGOV63); and a STIC lesion in the contralateral fallopian tube from the affected ovarian cancer (CGOV280).

In addition, we analyzed isolated STIC lesions from four patients (CGOV64, CGOV65, CGOV303 and CGOV304), three of whom had germline pathogenic *BRCA* alterations and underwent prophylactic bilateral salpingo-oophorectomy, and a fourth who had bilateral salpingo-oophorectomy and hysterectomy in the context of a pelvic mass (Supplementary Table 2.1). For all patients, laser capture microdissection was used to isolate lesions after immunohistochemistry (IHC) staining of p53 in STICs and p53 signatures if these contained a *TP53* missense mutation or after hematoxylin staining if the samples contained a *TP53* nonsense mutation (Figure 2.1). All other samples were microdissected after hematoxylin staining. Whole blood, normal ovarian stroma, normal fallopian tube stroma, or normal cervix were used as control samples.

To identify genetic alterations in the coding regions of these cancers, we used next-generation sequencing platforms to examine entire exomes in matched tumor and normal specimens of all patients (Figure 2.1). This approach allowed us to identify non-synonymous and synonymous sequence changes, including single base and small insertion or deletion mutations, as well as copy number alterations in coding genes. Given the challenges of exome-wide analyses of small tumor

samples observed in STICs and p53 signature lesions, we developed experimental and bioinformatic approaches for detection of somatic alterations from laser capture microdissected tissue. These included optimized approaches for microdissection of STICs and p53 signatures after immunohistochemical staining, improved DNA recovery from laser captured material, library construction from limited and stained tissue samples, and error correction methods in next generation sequence analyses. The analyses of p53 signatures were particularly challenging because these are extremely small lesions, representing 10-30 cells per section and less than several hundred cells total that result in minute amounts (less than a few ng) of isolated DNA. We optimized these approaches using a targeted next generation sequencing approach analyzing 120 genes in a subset of samples from patient CGOV62, and then used whole-exome analyses to evaluate coding sequence alterations in all samples (Supplementary Tables 2.2-2.4). We obtained a total of 719 Gb of sequence data, resulting in an average per-base sequence ~178-fold total coverage (~112-fold distinct coverage) for each tumor analyzed by whole-exome sequencing (Supplementary Table 2.2).

Analysis of sequence and structural changes

Whole-exome sequence analyses of the tumor samples from each patient identified somatic mutations that were present in all neoplastic samples analyzed as well as specific changes that were present in individual or subsets of tumors (Figure 2.2). As expected, we identified sequence changes in the *TP53* tumor suppressor gene, a well-known driver gene in HGSOC, in all cases. The *TP53* alterations were identical in all samples analyzed for each patient including in the p53 signatures, the STIC lesions, and other carcinomas. These data suggest that mutation of *TP53* was among the earliest initiating events for high grade serous ovarian carcinoma development as all lesions harbored this alteration.

IHC staining for p53 did not identify any nuclear positive staining of p53 on the ovarian surface epithelium in any of the cases that had *TP53* missense mutation, whereas all carcinomas, STICs, and p53 signatures in the fallopian tube were positive. Whole-exome sequence analyses of normal ovarian stroma (no p53 staining) microdissected from three patients (CGOV64, CGOV65, CGOV280) did not find any genomic abnormalities. Analysis of the resected tissues revealed that none of the nine cases had ovarian inclusion cysts. These observations suggest that there is no early lesion with *TP53* mutation in the surface epithelium or other normal regions within the ovary.

Because *TP53* mutations are expected to be clonal and were all homozygous due to loss of heterozygosity (LOH) of the remaining wild-type allele (as determined in our subsequent allelic imbalance analyses), we used the mutant allele fraction of *TP53* in each sample to estimate tumor purity. We further analyzed sequence alterations in all samples with estimated tumor purities >50%, while four samples with tumor cellularities below this threshold (omental metastasis from CGOV279 and right ovarian tumor from CGOV278), or that were miliary carcinomas (rectal and sigmoidal metastases from CGOV63) were only analyzed for structural changes.

Using a high-sensitivity mutation detection pipeline, we identified an average of 33 non-synonymous and synonymous sequence alterations per tumor sample. Candidate alterations were evaluated across samples in an individual to determine if they were present in multiple neoplastic lesions or were unique to a particular sample. To allow for the possibility that a subclone may have developed in a tumor lesion prior to becoming a dominant clone at another location, we determined if genetic alterations that were present in one tumor were also present in a low fraction of neoplastic cells of other lesions. This method required high coverage of analyzed alterations in all samples and excluded potential artifacts related to mapping, sequencing or PCR errors, allowing specific detection of alterations present in ≥1% of sequence reads (see Methods for additional information).

The composition of sequence alterations was relatively similar among the affected lesions of each patient. For example, for CGOV62, the STIC lesion, fallopian tube carcinomas, left and right ovarian cancers, and all four metastatic lesions harbored a common set of somatic mutations (Figure 2.2). In CGOV63, CGOV279 and CGOV278, while most of the sequence alterations were the same among the tumors of each patient, a subset of mutations could distinguish the STIC lesions and fallopian tube carcinomas from ovarian cancers or intraperitoneal metastases.

Given the importance of chromosomal instability in HGSOC[16], we extended our analyses to examine structural variation in the multiple tumors of each patient. We focused on regions of allelic imbalance that can result from the complete loss of an allele (LOH) or from an increase in copy number of one allele relative to the other. We divided the genome into chromosome segments and for each segment compared the minor allele (B-allele) frequency values in tumor and normal samples using the ~17,000 whole-exome germline heterozygous single nucleotide polymorphisms (SNPs) observed (Figure 2.3, Supplementary Figures 2.1-2.9 and Supplementary Tables 2.7-2.11). Overall, we observed that an average of ~26% (range 12% - 39%) of the genome had chromosomal imbalances in the samples analyzed (Figure 2.3).

Integration of sequence and structural alterations identified an average of 47 alterations per sample (range 21-74) (Figure 2.2). The combination of both types of alterations allowed robust genomic differentiation between STICs and ovarian cancers or metastatic lesions in all patients analyzed. In patient CGOV62, a loss of heterozygosity (LOH) of 9q (70.8 – 131.7 Mb) provided a clear difference between the STIC and all other carcinomas analyzed (Figures 2.2 and 2.3). Likewise, chromosomal changes in 7q were represented a distinguishing feature between the right STIC or right fallopian tube tumors and the remaining lesions (ovarian cancers, omental metastasis and left STIC) in CGOV280 (Figures 2.2 and 2.3). In patient CGOV279, multiple regions of allelic

imbalance were present in a STIC near the fallopian tube carcinoma, while these were absent in a STIC that was not adjacent to this lesion.

Evolutionary relationship of neoplastic lesions

As somatic genetic alterations can be used to recreate the evolutionary history of tumor clones, we used the somatic sequence mutations and chromosomal alterations observed in each patient to determine the history of tumor clonal evolution. We employed a subclone hierarchy inference tool called SCHISM (SubClonal Hierarchy Inference from Somatic Mutations) which enables improved phylogenetic reconstruction by incorporating estimates of the fraction of neoplastic cells in which a mutation occurs (mutation cellularity)[54]. We estimated the cellularity of each mutation by correcting the observed allele frequencies for tumor purity and copy number levels. In addition to the observed structural alterations, this approach allowed us to use 213 synonymous and nonsynonymous somatic sequence alterations to construct the phylogenetic trees illustrated in Figure 2.4 and Supplementary Table 2.5.

A SCHISM tree node represents cells harboring a unique compartment of mutations defining a subclone whereas an edge represents a set of mutations acquired by the cells in the progeny nodes that distinguish them from the cells in the parental node. By definition, for an individual cancer there could only be one parental clone, although there could be many different progeny subclones representing invasive or metastatic lesions or further evolution of the primary tumor. The optimal hierarchy among subclones is determined by examining all possible pairwise relationships between somatic alterations, and performing a heuristic search over the space of phylogenetic trees to identify the simplest model that can explain the observed alterations.

In all samples, the SCHISM analysis of sequence and structural alterations suggested that the p53 signature or STIC lesions contained the ancestral clone for the observed cancers (Figure 2.4). This

evolutionary relationship was strengthened by the observation that nearly all of the alterations within the p53 signature and STIC lesions were shared by all other lesions. For example, the ovarian tumors of all cases displayed alterations that were shared in fallopian tube lesions but also contained additional changes, suggesting that these represented daughter clones of the latter tumors (Figure 2.2). Likewise, the ovarian cancers or their immediate precursors were likely the direct parental clones for the metastases in CGOV62, CGOV278 and CGOV280 as demonstrated by the shared alterations that were not contained in earlier fallopian tube lesions. Overall, the phylogenetic model generated by these data suggests a progression from fallopian tube epithelium to p53 signatures and to STIC lesions which are then precursors of fallopian tube carcinoma, ovarian carcinoma, and metastatic lesions. In addition to the sequential accumulation of alterations in this linear evolution, we also observed branching phylogenetic trees due to continued evolution within STIC lesions as well as fallopian tube carcinomas and ovarian carcinomas (Figure 2.4). We compared evolutionary trees resulting from SCHISM analysis with those derived by maximum parsimony phylogeny using PHYLIP and the results were similar in all cases (Figure 2.4 and Supplementary Data 2.11).

Interestingly, patient CGOV280 had a right STIC, a right fallopian carcinoma, and a right ovarian cancer but also had a STIC in the left fallopian tube (Supplementary Figure 2.5). In this case the SCHISM analysis suggested that the lesion in the left fallopian tube which was pathologically determined to be a STIC actually represented a metastatic lesion of the right ovarian cancer (Figure 2.4). This lesion shared nearly all the alterations of the ovarian cancer but contained 10 single base substitutions and four additional regions of allelic imbalance on chromosomes 1, 13 and 22, and both the left STIC and right ovarian cancer had an additional region of allelic imbalance on chromosome 7 that was absent in the right STIC. These observations are consistent with the above model of STIC to ovarian cancer progression, but suggest that in advanced disease ovarian cancers

may also seed metastatic deposits throughout the peritoneum, including to the fallopian tube on the contralateral side.

Genomic alterations in isolated STICs

Neoplastic cells observed in the fallopian tubes rather than the ovaries removed from carriers of germline mutation of *BRCA1* and *BRCA2* provided the first indication of the fallopian tube as a potential cell of origin of HGSOC[20,55]. Since less than 1.25% of HGSOC are diagnosed with stage I disease[27], *BRCA* carriers provide a unique opportunity to analyze genomic alterations in isolated STICs without associated HGSOC. We examined neoplastic samples from three individuals with germline *BRCA* alterations where STIC lesions were incidentally identified after prophylactic bilateral salpingo-oophorectomy, and one patient where two STICs were identified after resection of pelvic mass (Supplementary Table 2.1). We identified *BRCA1 or BRCA2* sequence alterations or deletions in the germline of three of these patients (*BRCA1* Q1200X, *BRCA2* L2653P, and a *BRCA2* 55kb hemizygous deletion in CGOV65, CGOV64, and CGOV304, respectively), as well as somatic mutations in *TP53*, and LOH of both chromosome 13 and 17, encompassing the *BRCA1, BRCA2* and *TP53* loci in all of these cases (Supplementary Figures 2.6, 2.7, 2.8, and 2.9). Whole exome analyses showed that the STIC lesions contained a total of 91, 23, 34 and 46 non-synonymous and synonymous somatic mutations, in CGOV65, CGOV64, CGOV303, and CGOV304 respectively. Overall, these analyses revealed that STICs in isolation in patients with or without germline *BRCA* changes have a roughly similar number of sequence changes to STICs in patients with sporadic tumors. These observations provide evidence that isolated STICs may act as precursors in the same manner as those identified in patients with sporadic advanced stages HGSOC analyzed in this study.

Recurrent molecular alterations

We examined tumors from the nine patients to identify recurrent non-silent sequence or chromosomal changes. Although no genes other than *TP53* were mutated in all patients analyzed, we identified mutations in ten genes that were altered in two or more patients (Supplementary Table 2.6). These included mutations in the tumors of two patients of the *PIK3R5* gene that encodes a regulatory subunit of the PI3-kinase complex. CGOV64 also had a somatic alteration in *PTEN* that together with changes in *PIK3R5* highlight the importance of the PI3K pathway in ovarian cancer[16]. Additional genes that were observed to be altered in other ovarian cancers through other large scale sequencing efforts such as TCGA[16] are indicated in Supplementary Data 6.

In addition to recurrent sequence changes, we found alterations in regions of allelic imbalances encompassing several tumor suppressor genes involved in ovarian cancer. Remarkably, these included losses of *BRCA1, BRCA2* and *TP53* in all nine patients, and loss of *PTEN* for CGOV62, CGOV63, CGOV280 and CGOV64 (in addition to the somatic sequence alterations of these genes) (Supplementary Figures 2.1-2.9). In all cases, the LOH observed in the metastatic lesions and ovarian tumor lesions for regions encompassing these genes were already present in the fallopian tube tumor and STIC lesions. Considering the evolutionary model above, these data suggest that a combination of sequence changes in a few genes including *TP53* together with loss of the *TP53* wild-type allele as well as *BRCA1, BRCA2*, and *PTEN* may be crucial early events that are needed for the initiation of STICs[56,57].

Evolutionary timeline of ovarian cancer development

To estimate the time between the development of the earliest neoplastic clones in the fallopian tube and the development of ovarian and other metastatic lesions we used a mathematical model for comparative lesion analysis[29,58]. This model estimates the time interval between a founder cell of a tumor of interest and the ancestral precursor cell assuming that mutation rates and cell division times are constant throughout a patient's life. In the patient CGOV62, this model would suggest

~1.9 years between the development of the STIC lesion and the ovarian cancer (90% CI, 0.5 – 4.2 years). For other patients this transition appears to have been slower as the average time between STICs and ovarian cancer among all patients was 6.5 years (range 1.4 to 10.7 years). Importantly, in patients with metastatic lesions, the time between the initiation of the ovarian carcinoma and development of metastases appears to have been rapid (average 2.0 years). There were either no additional mutations in metastatic lesions (e.g. CGOV62 omental, rectal or appendiceal metastasis or CGOV280 omental metastasis) or the number of additional changes was small (e.g. three changes in CGOV278 omental metastasis), reflecting the ease with which cancer cells located on the ovaries can subsequently seed additional peritoneal sites. Although the precise timing of this progression depends on assumptions related to mutation rates, which may change during tumor progression, models employing different rates all showed longer timeline from STIC lesions to ovarian tumors followed by rapid development of metastatic lesions.

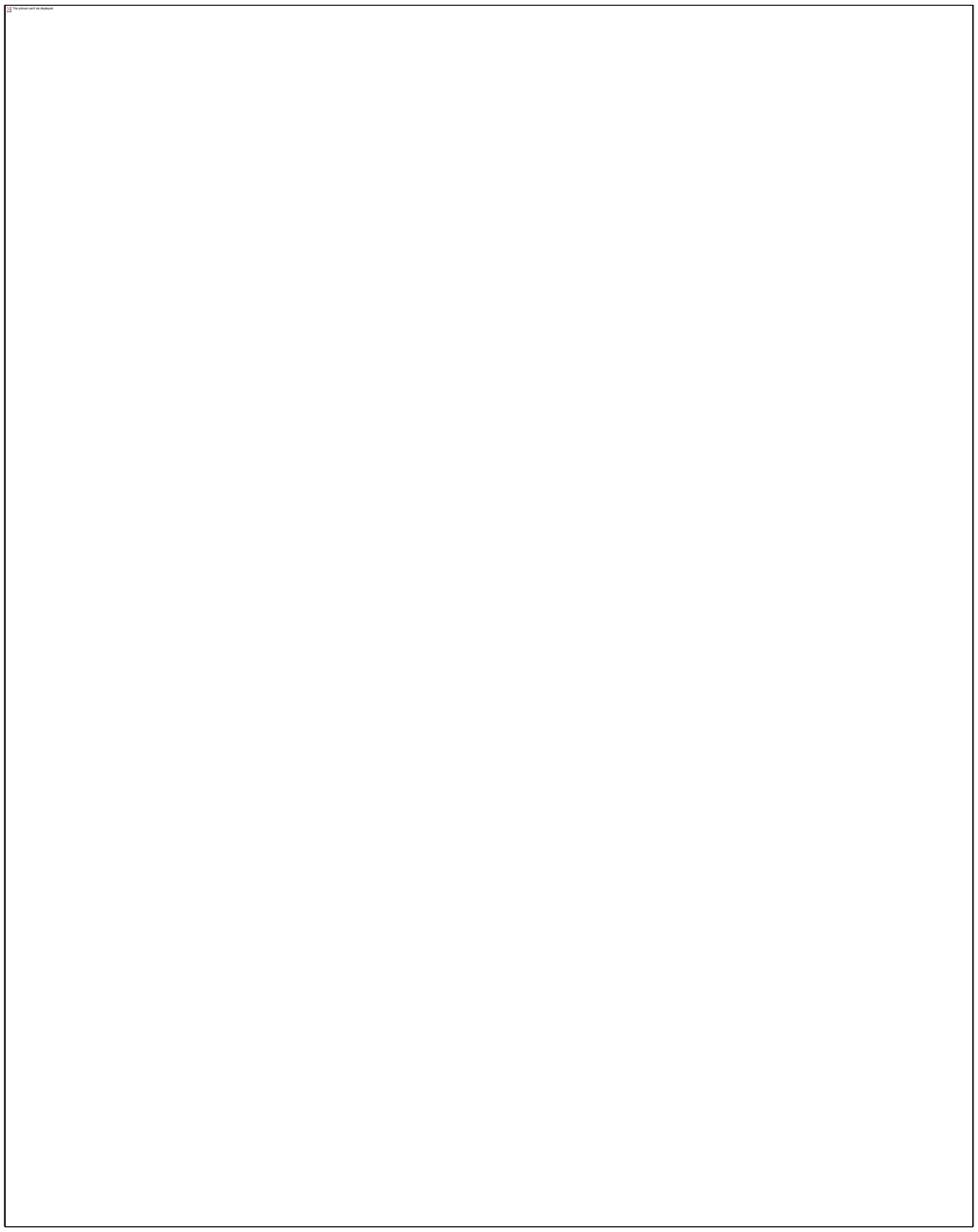

Figure 2.1. Schematic of sample isolation and next-generation sequencing analyses. (Top panel) Tumor sites analyzed from CGOV62 with stage III HGSOC. For each sample, slides were stained with hematoxylin and eosin as well as analyzed by immunohistochemical staining of p53. (Middle panel) Tumor samples were microdissected for genomic analyses. For microdissection for STIC and p53 signature lesions, tumor cells were identified using immunohistochemical staining of p53 and isolated through laser capture microdissection. (Bottom panel, left) Next-generation sequencing analyses were performed for tumor specimens using either whole-exome or targeted analyses focused on 120 genes. (Bottom panel, right) Somatic mutations and chromosomal alterations were used to evaluate tumor evolution using the tumor subclonality phylogenetic reconstruction algorithm SCHISM and to determine a timeline for tumor progression.

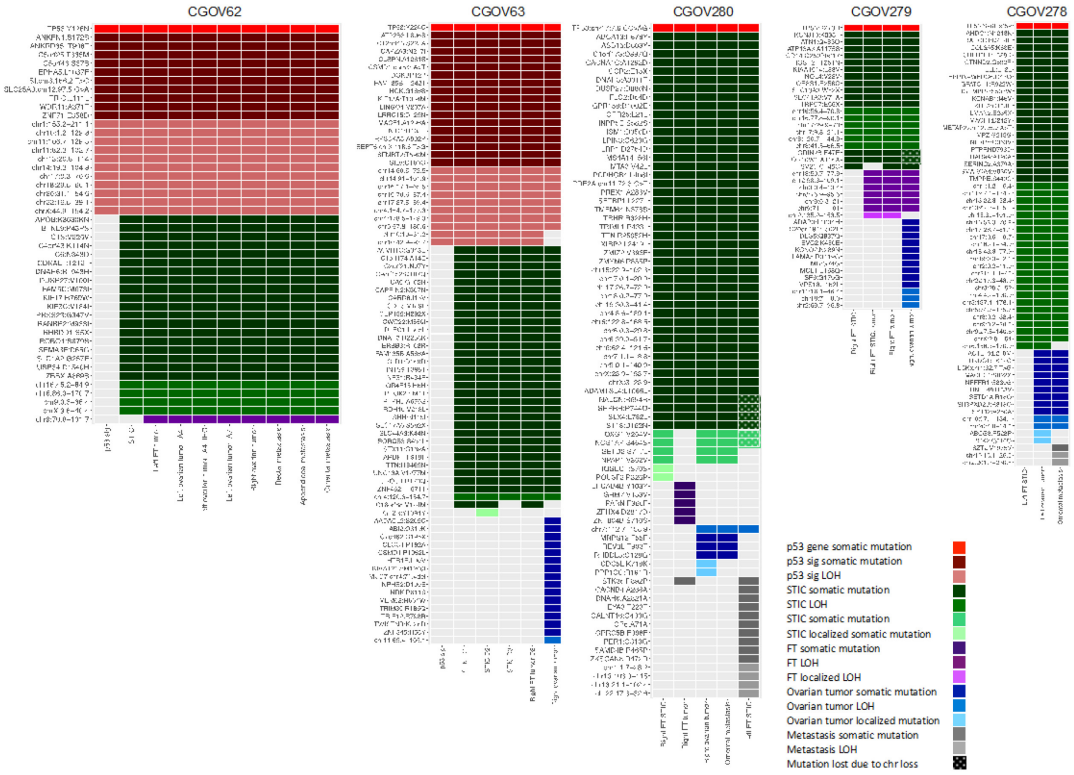

Figure 2.2. Somatic mutation and allelic imbalance profiles among different tumor lesions. Somatic mutations and segments of allelic imbalance detected by whole-exome analyses are indicated as colored cells in rows for all patients. Darker shades of each color indicate somatic mutations while lighter shades indicate allelic imbalances. The tumor samples analyzed for each patient are indicated in columns (p53 sig, p53 signature; STIC, serous tubal intraepithelial carcinoma). For ovarian tumors in CGOV62 and STIC lesions in CGOV63 multiple blocks are indicated, including one ovarian tumor where multiple sections were analyzed after hematoxylin and eosin staining or after immunohistochemistry (IHC) staining of p53. These analyses indicated that staining methods did not affect detection of somatic alterations. The color of mutations indicates the degree of relatedness among tumor samples: red, shared among all tumor samples with TP53 highlighted at the top row; green, shared among all tumor samples except p53 signature lesion; purple, shared among fallopian tube tumor and omental metastasis; blue indicates mutations that were first detected in the ovarian tumors; and gray indicates mutations that were only detected in metastatic lesions. Additional color shades or patterns indicate mutations that are localized to specific lesions or lost due to chromosome loss as shown in the legend.

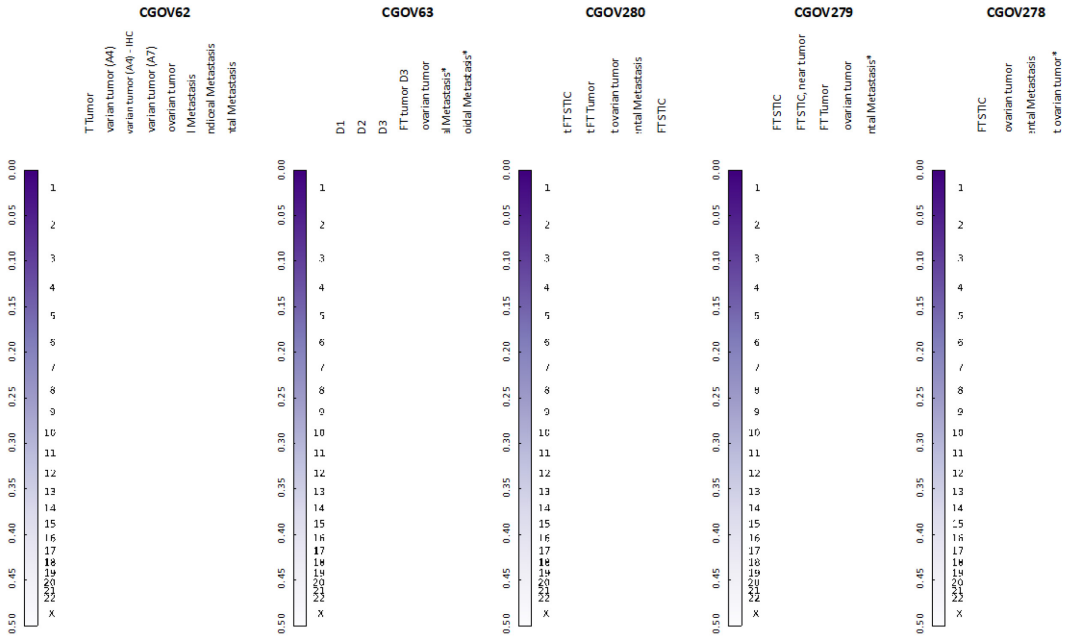

Figure 2.3. Genome-wide allelic imbalance profile. Minor allele frequency of heterozygous SNPs identified from normal tissue in each patient are derived in each tumor sample, enabling assessment of allelic imbalance in ~17,000 loci across the exome. Circular binary segmentation (CBS) is applied to minor allele frequencies of SNPs with minimum coverage of 10x in each tumor sample, and the resulting segment means are shown as a heatmap. Asterisks indicate samples where corresponding mutation analyses were not performed due to low tumor purity (omental metastasis of CGOV279, right ovarian tumor of CGOV278) or miliary pattern of tumor samples (peritoneal metastases of CGOV63). Given the relatively lower number of distinct DNA molecules available from the p53 signature samples from CGOV62 and CGOV63, these samples are subject to a more sensitive LOH analysis (Methods, Genome-wide imbalance analysis) and are not shown here.

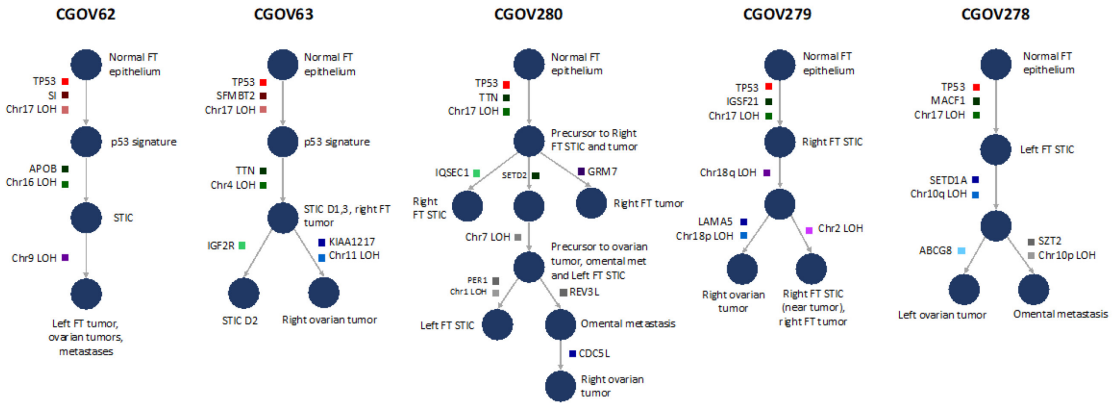

Figure 2.4. Schematic of tumor evolution. The history of tumor evolution in each patient is modeled as a subclonal hierarchy inferred from the somatic mutations and large scale genomic regions harboring loss of heterozygosity (LOH features) using the SCHISM framework, and is depicted as tree. Each tree starts from a root node corresponding the normal fallopian tube epithelium (germline). In all patients, mutations in *TP53* (red boxes) are among the earliest somatic alterations and are ubiquitously present in all tumor samples. Somatic alterations (boxes) are acquired along edges (arrows) of the tree, and example alterations are indicated in each case. Nodes of the tree represent cells whose genotype is described by the presence of somatic mutations and LOH features on the path connecting the node to the root of the tree. Each node is labeled with tumor samples harboring all upstream and lacking any downstream alterations. The trees inferred for all patients support a pattern of evolution with p53 signatures and STIC lesions as early events in tumorigenesis. Mutation clusters and LOH feature groups follow the same color code as Figure 2.

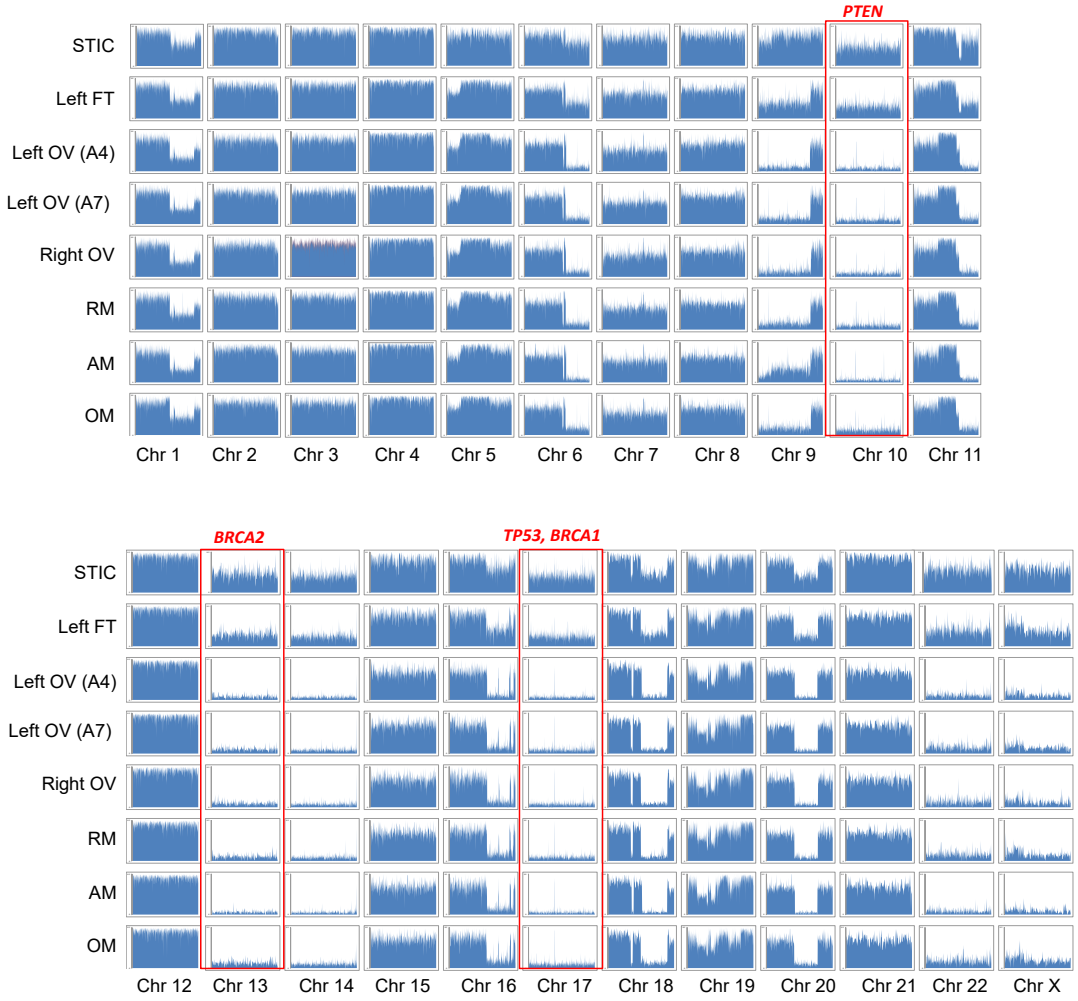

Supplementary Figure 2.1. Loss of heterozygosity analyses for CGOV62. The graphs represent B allele frequencies (BAFs) for the indicated chromosomes. A value of 0.5 indicates a heterozygous genotype (AB) whereas allelic imbalances in tumor samples are observed as a deviation from 0.5. BAF values of 0 typically indicate loss of heterozygosity, although normal contaminating tissue may limit the minimum observed value. Graphs for CGOV62 include left fallopian tube STIC, left fallopian tube tumor, left ovarian tumor block A4, left ovarian tumor block A7, right ovarian tumor, rectal metastasis, appendiceal metastasis, and omental metastasis. LOH events that contain *PTEN*, *BRCA2*, *TP53* and *BRCA1* genes are indicated by the red boxes.

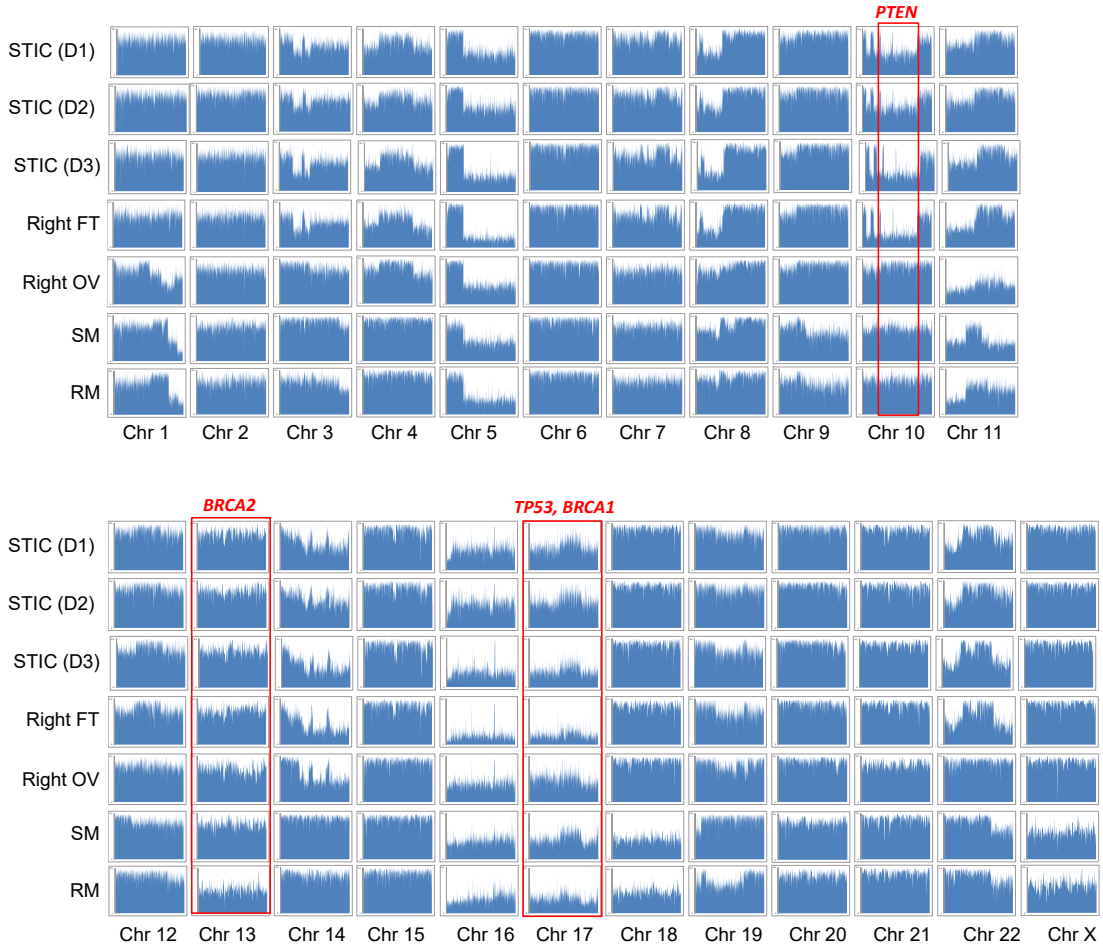

Supplementary Figure 2.2. Loss of heterozygosity analyses for CGOV63. The graphs represent B allele frequencies (BAFs) for the indicated chromosomes. A value of 0.5 indicates a heterozygous genotype (AB) whereas allelic imbalances in tumor samples are observed as a deviation from 0.5. BAF values of 0 typically indicate loss of heterozygosity, although normal contaminating tissue may limit the minimum observed value. Graphs for CGOV63 include STIC block D1, STIC block D2, STIC block D3 , right fallopian tumor, right ovarian tumor, sigmoid metastasis, rectal metastasis. LOH events that contain *PTEN*, *BRCA2*, *TP53* and *BRCA1* genes are indicated by the red boxes.

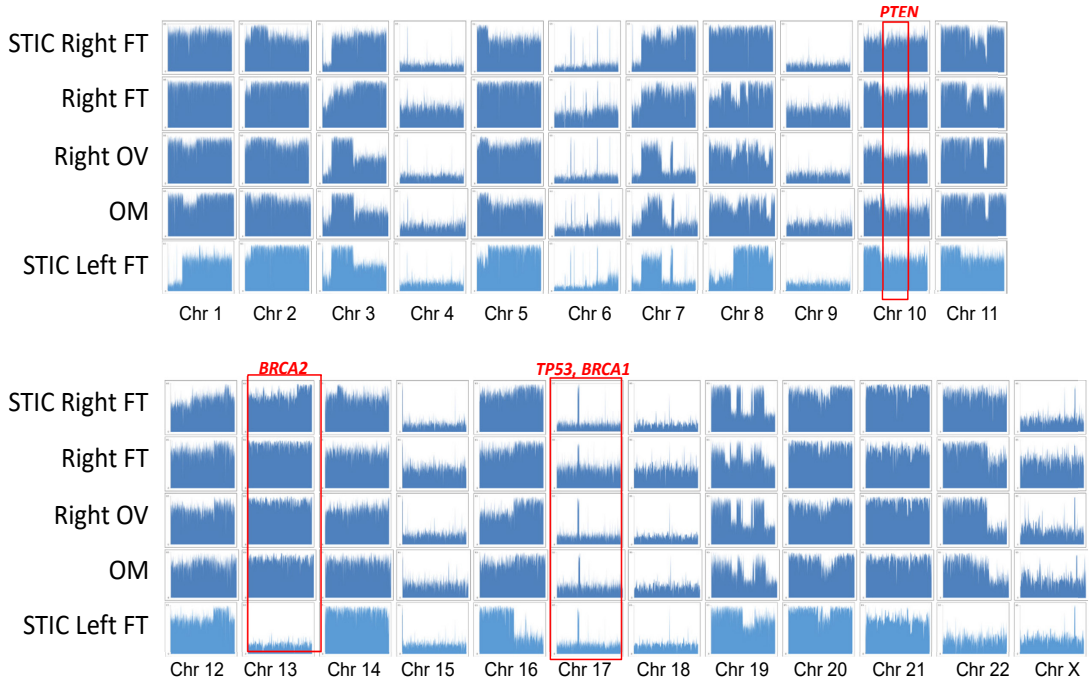

Supplementary Figure 2.3. Loss of heterozygosity analyses for CGOV280. The graphs represent B allele frequencies (BAFs) for the indicated chromosomes. A value of 0.5 indicates a heterozygous genotype (AB) whereas allelic imbalances in tumor samples are observed as a deviation from 0.5. BAF values of 0 typically indicate loss of heterozygosity, although normal contaminating tissue may limit the minimum observed value. Graphs for CGOV280 include STIC of the right fallopian tube, right fallopian tube tumor, right ovarian tumor, omental metastasis, stic of the left fallopian tube. LOH events that contain *PTEN*, BRCA2, *TP53* and *BRCA1* genes are indicated by the red boxes.

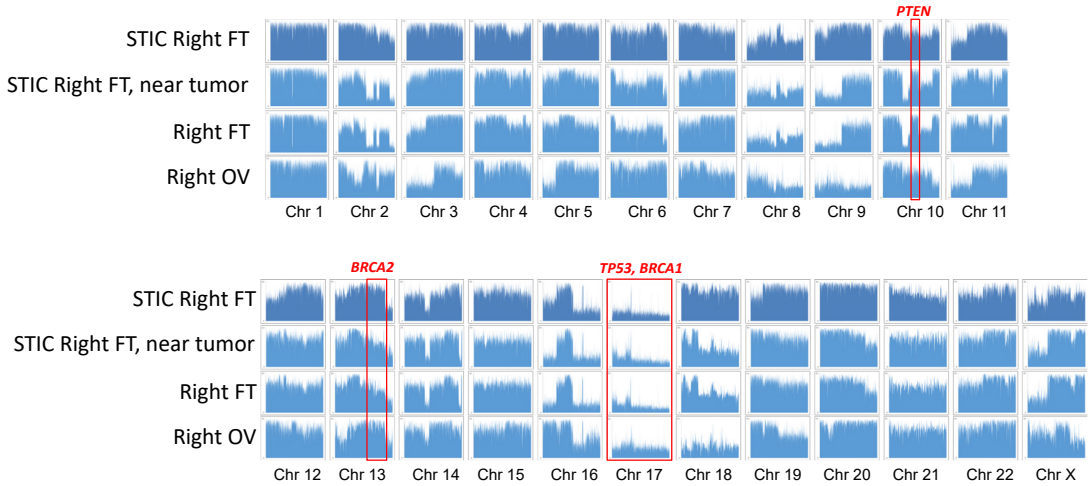

Supplementary Figure 2.4. Loss of heterozygosity analyses for CGOV279. The graphs represent B allele frequencies (BAFs) for the indicated chromosomes. A value of 0.5 indicates a heterozygous genotype (AB) whereas allelic imbalances in tumor samples are observed as a deviation from 0.5. BAF values of 0 typically indicate loss of heterozygosity, although normal contaminating tissue may limit the minimum observed value. Graphs for CGOV279 include STIC of the right fallopian tube, STIC of the right fallopian tube close to the tumor, right fallopian tube tumor, right ovarian tumor. LOH events that contain *BRCA2*, *TP53* and *BRCA1* genes are indicated by the red boxes, while the LOH region in chromosome 10 of this sample does not overlap with the *PTEN* gene.

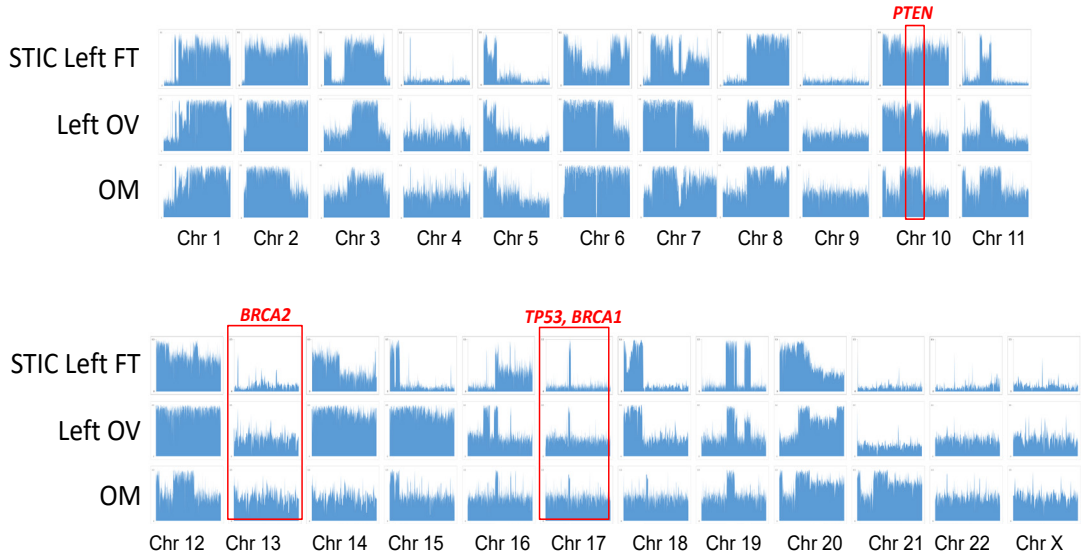

Supplementary Figure 2.5. Loss of heterozygosity analyses for CGOV278. The graphs represent B allele frequencies (BAFs) for the indicated chromosomes. A value of 0.5 indicates a heterozygous genotype (AB) whereas allelic imbalances in tumor samples are observed as a deviation from 0.5. BAF values of 0 typically indicate loss of heterozygosity, although normal contaminating tissue may limit the minimum observed value. Graphs for CGOV278 include STIC of left fallopian tumor, left ovarian tumor, omental metastasis. LOH events that contain *BRACA2*, *TP53* and *BRCA1* genes are indicated by the red boxes, while the LOH region in chromosome 10 of this sample does not overlap with the *PTEN* gene.

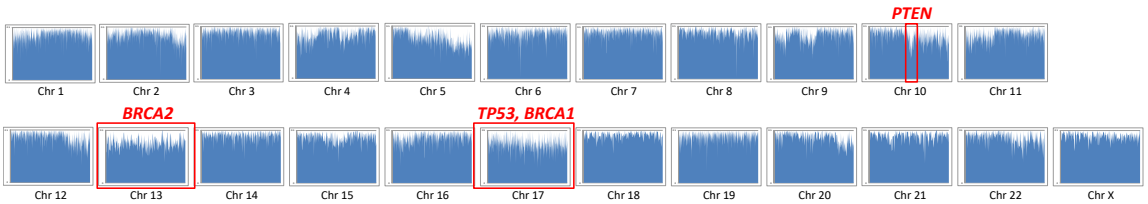

Supplementary Figure 2.6. Loss of heterozygosity analyses for CGOV65. The graphs represent B allele frequencies (BAFs) for the indicated chromosomes for the STIC lesion. A value of 0.5 indicates a heterozygous genotype (AB) whereas allelic imbalances in tumor samples are observed as a deviation from 0.5. BAF values of 0 typically indicate loss of heterozygosity, although normal contaminating tissue may limit the minimum observed value. LOH events that contain *PTEN*, *BRACA2*, *TP53* and *BRCA1* genes are indicated by the red boxes.

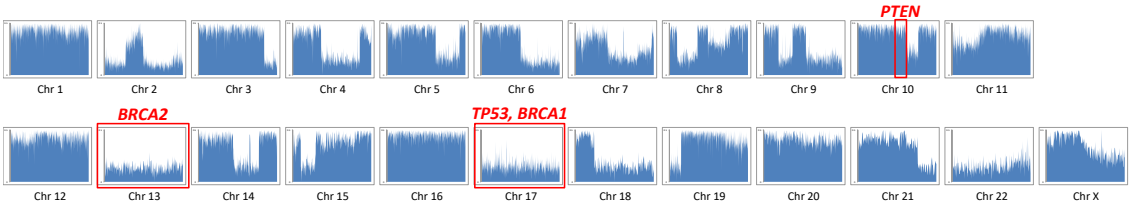

Supplementary Figure 2.7. Loss of heterozygosity analyses for CGOV64. The graphs represent B allele frequencies (BAFs) for the indicated chromosomes for the STIC lesion. A value of 0.5 indicates a heterozygous genotype (AB) whereas allelic imbalances in tumor samples are observed as a deviation from 0.5. BAF values of 0 typically indicate loss of heterozygosity, although normal contaminating tissue may limit the minimum observed value. LOH events that contain *BRACA2*, *TP53* and *BRCA1* genes are indicated by the red boxes, while the LOH region in chromosome 10 of this sample does not overlap with the *PTEN* gene.

Supplementary Figure 2.8. Loss of heterozygosity analyses for CGOV303. The graphs represent B allele frequencies (BAFs) for the indicated chromosomes for the STIC lesion. A value of 0.5 indicates a heterozygous genotype (AB) whereas allelic imbalances in tumor samples are observed as a deviation from 0.5. BAF values of 0 typically indicate loss of heterozygosity, although normal contaminating tissue may limit the minimum observed value. LOH events that contain *BRACA2*, *TP53* and *BRCA1* genes are indicated by the red boxes, while no LOH in chromosome 10 containing *PTEN* was observed.

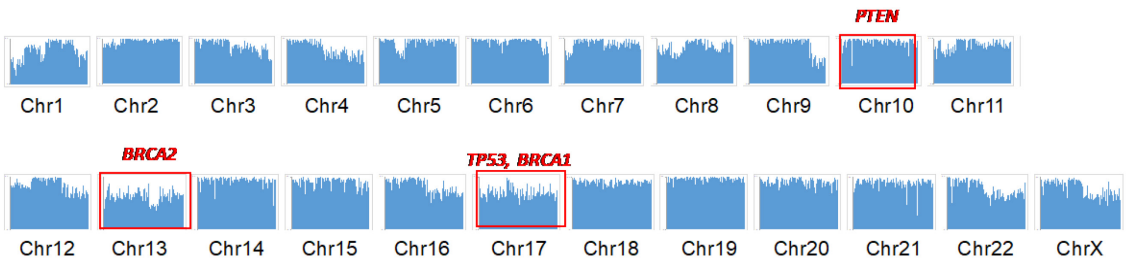

Supplementary Figure 2.9. Loss of heterozygosity analyses for CGOV304. The graphs represent B allele frequencies (BAFs) for the indicated chromosomes for the STIC lesion. A value of 0.5 indicates a heterozygous genotype (AB) whereas allelic imbalances in tumor samples are observed as a deviation from 0.5. BAF values of 0 typically indicate loss of heterozygosity, although normal contaminating tissue may limit the minimum observed value. LOH events that contain *BRACA2*, *TP53* and *BRCA1* genes are indicated by the red boxes, while no LOH in chromosome 10 containing *PTEN* was observed.

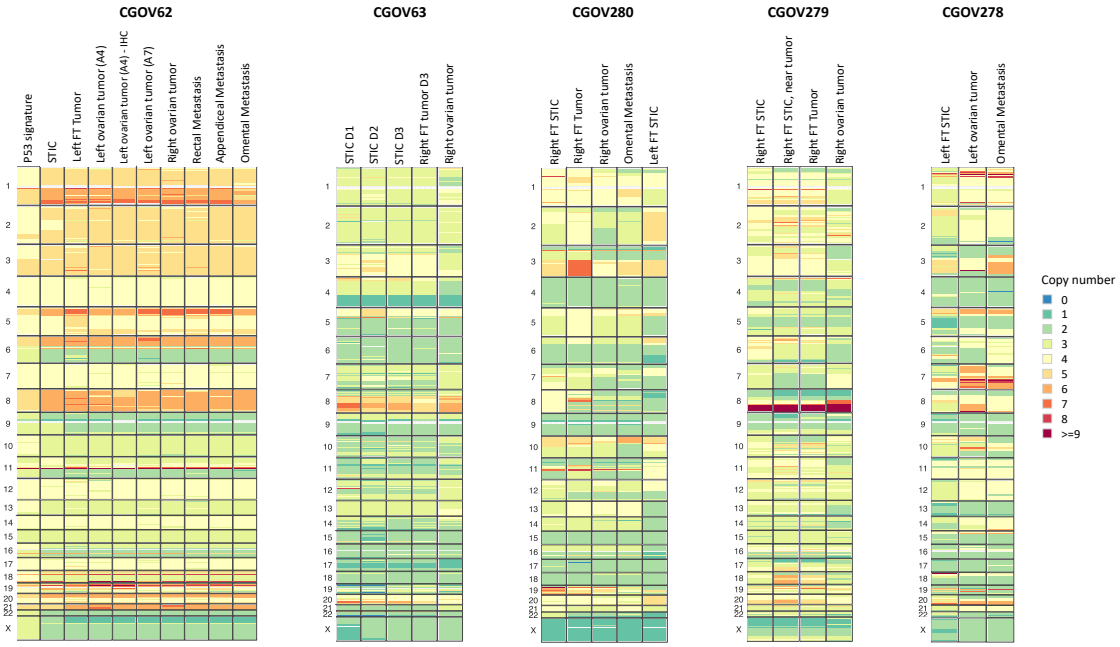

Supplementary Figure 2.10. Genome-wide copy number profile. Copy number ratio of genomic bins were determined based on target and off-target reads from whole exome sequencing. The raw copy ratio were corrected for GC-content, repetitive sequences, and target capture enrichment using CNVKit, and then converted to integer copy levels by accounting for tumor purity and average genome-wide ploidy (Methods, copy number analysis). The resulting copy number profiles suggest a relatively consistent pattern of copy number aberrations across the lesions analyzed from each patient.

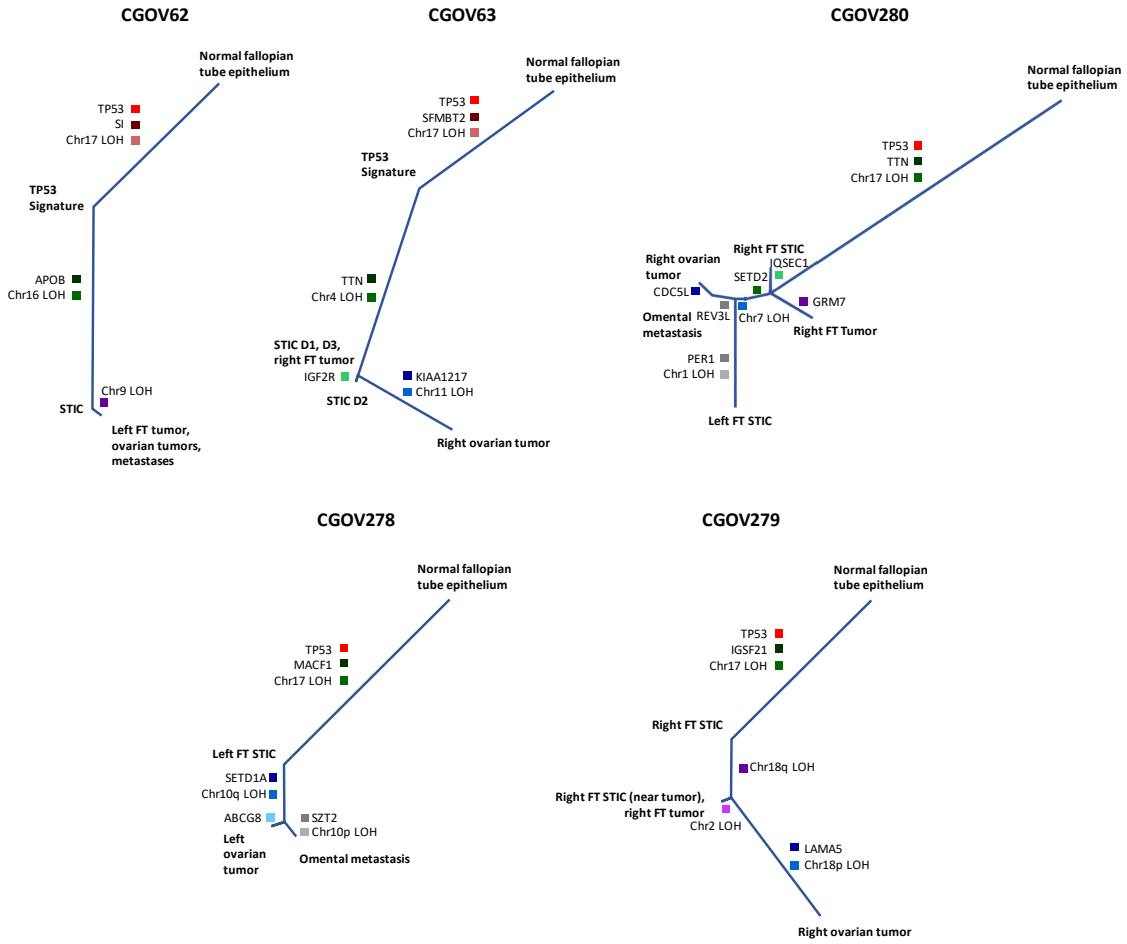

Supplementary Figure 2.11. Schematic of tumor evolution using PHYLIP. Visualization of evolutionary trees from each patient based on mutational and LOH changes. Branch lengths are proportional to the number of somatic alterations.

Supplementary Table 2.1. Summary of Patient and Sample Characteristics

Patient ID	Age Diagnosis	Sample ID	Histopathologic Diagnosis
CGOV62	61	CGOV62N	Blood
		CGOV62T_4	High grade serous ovarian carcinoma
		CGOV62T_3_1	High grade serous ovarian carcinoma
		CGOV62T_2	High grade serous ovarian carcinoma
		CGOV62T	High grade serous ovarian carcinoma
		CGOV62T_10	High grade serous ovarian carcinoma
		CGOV62T_9	High grade serous ovarian carcinoma
		CGOV62T_8	High grade serous ovarian carcinoma
		CGOV62T_1	High grade serous ovarian carcinoma
		CGOV62T_6	High grade serous ovarian carcinoma
		CGOV62T_7	High grade serous ovarian carcinoma
CGOV63	61	CGOV63N	Blood
		CGOV63T_10	High grade serous miliary ovarian carcinoma
		CGOV63T_2_1	High grade serous miliary ovarian carcinoma
		CGOV63T_12	High grade serous miliary ovarian carcinoma
		CGOV63T_14	High grade serous miliary ovarian carcinoma
		CGOV63T_7_1	High grade serous miliary ovarian carcinoma
		CGOV63T_9_1	High grade serous miliary ovarian carcinoma
		CGOV63T_5_1	High grade serous miliary ovarian carcinoma
		CGOV63T_6_1	High grade serous miliary ovarian carcinoma
CGOV280	81	CGOV280N	Normal ovarian stroma
		CGOV280T3	STIC
		CGOV280T4	High grade serous ovarian carcinoma
		CGOV280T5	High grade serous ovarian carcinoma
		CGOV280T2	STIC
		CGOV280T6	High grade serous ovarian carcinoma
CGOV279	55	CGOV279N	Normal cervix
		CGOV279T4	High grade serous ovarian carcinoma
		CGOV279T5	High grade serous ovarian carcinoma
		CGOV279T1	High grade serous ovarian carcinoma
		CGOV279T2	High grade serous ovarian carcinoma
		CGOV279T3	High grade serous ovarian carcinoma
CGOV278	54	CGOV278N	Normal cervix
		CGOV278T2	High grade serous ovarian carcinoma
		CGOV278T3	High grade serous ovarian carcinoma
		CGOV278T4	High grade serous ovarian carcinoma

		CGOV278T1	High grade serous ovarian carcinoma	
CGOV64	41	CGOV64N	Normal ovarian stroma	
		CGOV64T	Serous tubal in situ carcinoma	
CGOV65	56	CGOV65N	Normal ovarian stroma	
		CGOV65T_0	Serous tubal in situ carcinoma	
CGOV303	84	CGOV303N	Normal fallopian tube stroma	
		CGOV303T	Serous tubal in situ carcinoma	b
		CGOV303T1	Serous tubal in situ carcinoma	b
CGOV304	61	CGOV304N	Normal fallopian tube stroma	
		CGOV304T	Serous tubal in situ carcinoma	

Supplementary Data 2.2. Summary of Next-Generation Sequencing Analyses

Sample ID	Analysis Type	Read Length (bp)	Sequenced Bases Mapped to Genome	Bases Mapped to Target Region
CGOV62T	Targeted	150	932,888,250	356,941,707
CGOV62T_1	Targeted	150	894,803,700	338,574,182
CGOV62T_9	Targeted	150	841,124,850	298,377,222
CGOV62T_10	Targeted	150	814,842,450	305,723,970
CGOV62T_2	Targeted	150	857,697,600	361,375,554
CGOV62T_6	Targeted	150	926,878,950	381,400,070
CGOV62T_7	Targeted	150	941,013,600	397,968,603
CGOV62T_8	Targeted	150	942,642,900	388,150,695
CGOV62T_4	Targeted	150	1,078,715,100	557,146,096
CGOV62N	Exome	100	16,477,126,700	8,505,340,214
CGOV62T_4	Exome	100	17,992,865,800	9,690,155,310
CGOV62T_3_1	Exome	100	14,181,614,100	7,937,939,584
CGOV62T_2	Exome	100	14,941,805,600	7,846,722,527
CGOV62T	Exome	100	14,090,629,000	7,391,883,856
CGOV62T_10	Exome	100	14,543,242,100	7,142,842,723
CGOV62T_9	Exome	100	18,353,598,700	9,489,914,649
CGOV62T_8	Exome	100	17,936,056,700	9,267,379,798
CGOV62T_1	Exome	100	13,287,558,000	6,777,868,722
CGOV62T_6	Exome	100	15,954,387,900	8,278,513,630
CGOV62T_7	Exome	100	16,516,806,900	8,688,962,176
CGOV63N	Exome	100	14,725,190,400	7,566,006,080
CGOV63T_10	Exome	100	17,895,736,300	9,647,692,172
CGOV63T_2_1	Exome	100	14,680,242,100	8,150,805,108
CGOV63T_12	Exome	100	19,576,607,700	10,386,204,204
CGOV63T_14	Exome	100	16,788,306,100	8,874,167,120
CGOV63T_7_1	Exome	100	15,236,162,400	7,928,083,568
CGOV63T_9_1	Exome	100	15,167,179,700	8,195,369,998
CGOV63T_5_1	Exome	100	13,415,779,600	7,186,267,032
CGOV63T_6_1	Exome	100	18,104,964,100	9,596,432,258
CGOV280N	Exome	100	9,569,584,300	5,535,308,482
CGOV280T3	Exome	100	19,927,930,700	11,397,858,848
CGOV280T4	Exome	100	18,981,692,300	9,853,972,056
CGOV280T5	Exome	100	19,510,760,800	11,521,903,291
CGOV280T2	Exome	100	19,503,540,000	11,973,304,206
CGOV280T6	Exome	100	19,226,763,300	7,739,355,157
CGOV279N	Exome	100	9,699,560,900	5,291,411,860
CGOV279T4	Exome	100	22,387,574,900	13,805,553,635

CGOV279T5	Exome	100	20,247,027,900	12,575,991,130
CGOV279T1	Exome	100	22,128,038,900	12,237,762,174
CGOV279T2	Exome	100	20,526,235,400	8,335,017,872
CGOV279T3	Exome	100	22,013,047,100	12,909,800,399
CGOV278N	Exome	100	11,346,856,700	7,232,475,712
CGOV278T2	Exome	100	25,449,694,700	15,110,349,424
CGOV278T3	Exome	100	23,961,348,800	13,850,252,057
CGOV278T4	Exome	100	21,574,201,100	12,573,576,783
CGOV278T1	Exome	100	22,534,338,000	13,107,330,003
CGOV64N	Exome	100	18,497,697,200	9,963,890,280
CGOV64T	Exome	100	18,717,312,200	9,900,216,092
CGOV65N	Exome	100	17,918,581,500	9,604,269,218
CGOV65T_0	Exome	100	15,410,288,200	8,241,676,869
CGOV303N	Exome	100	12,512,391,500	7,982,064,286
CGOV303T	Exome	100	20,616,367,500	11,674,202,824
CGOV303T1	Exome	100	22,335,245,900	10,157,940,995
CGOV304N	Exome	100	11,720,312,800	7,112,810,741
CGOV304T	Exome	100	22,857,799,100	13,949,508,352

Supplementary Data 2.3. Targeted Sequencing Panel

Gene Symbol	Gene Description
ABL1	c-abl oncogene 1, non-receptor tyrosine kinase
AKT1	v-akt murine thymoma viral oncogene homolog 1
AKT2	v-akt murine thymoma viral oncogene homolog 2
ALK	anaplastic lymphoma receptor tyrosine kinase
APC	adenomatous polyposis coli
AR	androgen receptor
ARID1A	AT rich interactive domain 1A (SWI-like)
ARID1B	AT rich interactive domain 1B (SWI1-like)
ASXL1	additional sex combs like 1
ATM	ataxia telangiectasia mutated
ATRX	alpha thalassemia/mental retardation syndrome X-linked
BAP1	BRCA1 associated protein-1
BCR	breakpoint cluster region
BRAF	v-raf murine sarcoma viral oncogene homolog B1
BRCA1	breast cancer 1, early onset
BRCA2	breast cancer 2, early onset
CBL	Cas-Br-M (murine) ecotropic retroviral transforming sequence
CCND1	cyclin D1
CCNE1	cyclin E1
CDH1	cadherin 1, type 1, E-cadherin (epithelial)
CDK4	cyclin-dependent kinase 4
CDK6	cyclin-dependent kinase 6
CDKN2A	cyclin-dependent kinase inhibitor 2A
CEBPA	CCAAT/enhancer binding protein (C/EBP), alpha
CREBBP	CREB binding protein
CTNNB1	catenin (cadherin-associated protein), beta 1, 88kDa
DAXX	death-domain associated protein
DNMT3A	DNA (cytosine-5-)-methyltransferase 3 alpha
EGFR	epidermal growth factor receptor
ERBB2	v-erb-b2 erythroblastic leukemia viral oncogene homolog 2
ERBB3	v-erb-b2 erythroblastic leukemia viral oncogene homolog 3
ERBB4	v-erb-a erythroblastic leukemia viral oncogene homolog 4
ETV1	ets variant 1
ETV4	ets variant 4
ETV5	ets variant 5
ETV6	ets variant 6
EWSR1	Ewing sarcoma breakpoint region 1
EZH2	Enhancer of zeste homolog 2
FBXW7	F-box and WD repeat domain containing 7

FGFR2	fibroblast growth factor receptor 2
FGFR3	fibroblast growth factor receptor 3
FGFR4	fibroblast growth factor receptor 4
FLT3	fms-related tyrosine kinase 3
FOXL2	forkhead box L2
GATA1	GATA binding protein 1 (globin transcription factor 1)
GATA2	GATA binding protein 2
GNA11	guanine nucleotide binding protein (G protein), alpha 11
GNAQ	guanine nucleotide binding protein (G protein), q polypeptide
GNAS	GNAS complex locus
HNF1A	HNF1 homeobox A
HRAS	v-Ha-ras Harvey rat sarcoma viral oncogene homolog
IDH1	isocitrate dehydrogenase 1 (NADP+), soluble
IDH2	isocitrate dehydrogenase 2 (NADP+), mitochondrial
IGF1R	insulin-like growth factor 1 receptor
IGF2R	insulin-like growth factor 2 receptor
IKZF1	IKAROS family zinc finger 1 (Ikaros)
JAK1	Janus kinase 1
JAK2	Janus kinase 2
JAK3	Janus kinase 3
KDR	kinase insert domain receptor (a type III receptor tyrosine kinase)
KIT	v-kit Hardy-Zuckerman 4 feline sarcoma viral oncogene homolog
KRAS	v-Ki-ras2 Kirsten rat sarcoma viral oncogene homolog
MAML1	mastermid-like 1
MDM2	Mdm2, p53 E3 ubiquitin protein ligase homolog
MDM4	Mdm4 p53 binding protein homolog
MED12	mediator complex subunit 12
MEN1	multiple endocrine neoplasia I
MET	met proto-oncogene (hepatocyte growth factor receptor)
MLH1	mutL homolog 1, colon cancer, nonpolyposis type 2
MLL	myeloid/lymphoid or mixed-lineage leukemia
MPL	myeloproliferative leukemia virus oncogene
MSH2	mutS homolog 2, colon cancer, nonpolyposis type 1
MSH6	mutS homolog 6
MYC	v-myc myelocytomatosis viral oncogene homolog
MYCN	v-myc myelocytomatosis viral related oncogene, neuroblastoma derived
MYD88	myeloid differentiation primary response gene
NF1	neurofibromin 1
NF2	neurofibromin 2 (merlin)
NOTCH1	notch 1
NOTCH2	notch 2
NOTCH3	notch 3
NOTCH4	notch 4

NPM1	nucleophosmin (nucleolar phosphoprotein B23, numatrin)
NRAS	neuroblastoma RAS viral (v-ras) oncogene homolog
PALB2	partner and localizer of BRCA2
PAX5	paired box 5
PBRM1	polybromo 1
PDGFRA	platelet-derived growth factor receptor, alpha polypeptide
PDGFRB	platelet-derived growth factor receptor, beta polypeptide
PIK3CA	phosphoinositide-3-kinase, catalytic, alpha polypeptide
PIK3R1	phosphoinositide-3-kinase, regulatory subunit 1 (alpha)
PMS2	PMS2 postmeiotic segregation increased 2
PTCH1	patched 1
PTEN	phosphatase and tensin homolog
PTPN11	protein tyrosine phosphatase, non-receptor type 11
RAF1	v-raf-1 murine leukemia viral oncogene homolog 1
RAR-alpha (PML)	retinoic acid receptor, alpha
RB1	retinoblastoma 1
RET	ret proto-oncogene
RNF43	ring finger protein 43
ROS1	c-ros oncogene 1 , receptor tyrosine kinase
RUNX1	runt-related transcription factor 1
SF3B1	splicing factor 3b, subunit 1
SMAD2	SMAD family member 2
SMAD3	SMAD family member 3
SMAD4	SMAD family member 4
SMARCB1	SWI/SNF related, actin dependent regulator of chromatin, subfamily b, member 1
SMO	smoothened, frizzled family receptor
STAG2	stromal antigen 2
STK11	serine/threonine kinase 11
TET2	tet methylcytosine dioxygenase 2
TGFBR2	transforming growth factor, beta receptor II (70/80kDa)
TMPRSS2	transmembrane protease, serine 2
TNFAIP3	tumor necrosis factor, alpha-induced protein 3
TP53	Tumor protein p53
TSC1	tuberous sclerosis 1
TSC2	tuberous sclerosis 2
TSHR	thyroid stimulating hormone receptor
VHL	von Hippel-Lindau tumor suppressor
WT1	Wilms tumor 1

Supplementary Data 2.4. Somatic Sequence Alterations

Case ID	Analysis Type	Gene	Gene description	Tra Acc
CGOV65T_0	Exome	ABI3BP	target of Nesh-SH3 precursor	NM_01
CGOV65T_0	Exome	ADAMTS9	ADAM metallopeptidase with thrombospondin type 1 motif; 9	CCDS2
CGOV65T_0	Exome	ADAMTSL 3	ADAMTS-like 3	CCDS1
CGOV65T_0	Exome	ANKRD5	ankyrin repeat domain 5	CCDS1
CGOV65T_0	Exome	ATP10D	ATPase; class V; type 10D	CCDS3
CGOV65T_0	Exome	BCAS3	breast carcinoma amplified sequence 3	CCDS1
CGOV65T_0	Exome	BCR	breakpoint cluster region	CCDS1
CGOV65T_0	Exome	C1orf116	chromosome 1 open reading frame 116	CCDS1
CGOV65T_0	Exome	C20orf194	chromosome 20 open reading frame 194	CCDS4
CGOV65T_0	Exome	C3orf77	hypothetical protein LOC375337	NM_00
CGOV65T_0	Exome	CAMSAP1 L1	calmodulin regulated spectrin-associated protein 1-like 1	CCDS1
CGOV65T_0	Exome	CCDC69	coiled-coil domain containing 69	CCDS4
CGOV65T_0	Exome	COL4A2	collagen; type IV; alpha 2	CCDS4
CGOV65T_0	Exome	CPA3	carboxypeptidase A3 (mast cell)	CCDS3
CGOV65T_0	Exome	CWC22	CWC22 spliceosome-associated protein homolog (S. cerevisiae)	NM_02
CGOV65T_0	Exome	DMBT1	deleted in malignant brain tumors 1 protein isoform b precursor	NM_00
CGOV65T_0	Exome	DOCK6	dedicator of cytokinesis protein 6	NM_02
CGOV65T_0	Exome	DOCK6	dedicator of cytokinesis protein 6	NM_02
CGOV65T_0	Exome	DUSP27	dual specificity phosphatase 27 (putative)	CCDS3

CGOV65T_0	Exome	EML6	echinoderm microtubule-associated protein-like 6	NM_00
CGOV65T_0	Exome	EXOC7	exocyst complex component 7	CCDS3
CGOV65T_0	Exome	FANCM	Fanconi anemia; complementation group M	CCDS3
CGOV65T_0	Exome	FANCM	Fanconi anemia; complementation group M	CCDS3
CGOV65T_0	Exome	FAT3	protocadherin Fat 3	NM_00
CGOV65T_0	Exome	FBF1	fas-binding factor 1	NM_00
CGOV65T_0	Exome	FBXO38	F-box protein 38	CCDS4
CGOV65T_0	Exome	FLRT2	fibronectin leucine rich transmembrane protein 2	CCDS9
CGOV65T_0	Exome	FOXS1	forkhead box S1	CCDS1
CGOV65T_0	Exome	GPR112	G protein-coupled receptor 112	CCDS3
CGOV65T_0	Exome	GRAMD2	GRAM domain containing 2	CCDS3
CGOV65T_0	Exome	GSR	glutathione reductase	CCDS3
CGOV65T_0	Exome	HEATR7B2	HEAT repeat-containing protein 7B2	NM_17
CGOV65T_0	Exome	HFM1	HFM1; ATP-dependent DNA helicase homolog (S. cerevisiae)	CCDS3
CGOV65T_0	Exome	IL11RA	interleukin 11 receptor; alpha	CCDS6
CGOV65T_0	Exome	INPP5E	inositol polyphosphate-5-phosphatase; 72 kDa	CCDS7
CGOV65T_0	Exome	ITGA5	integrin; alpha 5 (fibronectin receptor; alpha polypeptide)	CCDS8
CGOV65T_0	Exome	KIAA0913	zinc finger SWIM domain-containing protein KIAA0913 isoform 1	NM_01
CGOV65T_0	Exome	KIAA1199	KIAA1199	CCDS1
CGOV65T_0	Exome	KIF9	kinesin family member 9	CCDS2
CGOV65T_0	Exome	KLB	klotho beta	CCDS3
CGOV65T_0	Exome	LRP1B	low density lipoprotein receptor-related protein 1B	CCDS2
CGOV65T_0	Exome	MAP7D2	MAP7 domain containing 2	CCDS1

CGOV65T_0	Exome	MID1IP1	MID1 interacting protein 1 (gastrulation specific G12 homolog (zebrafish))	CCDS1
CGOV65T_0	Exome	MUC16	mucin-16	NM_02
CGOV65T_0	Exome	MUC4	mucin 4; cell surface associated	CCDS3
CGOV65T_0	Exome	MYO1F	myosin IF	CCDS4
CGOV65T_0	Exome	MYO7B	myosin-VIIb	NM_00
CGOV65T_0	Exome	NHS	Nance-Horan syndrome (congenital cataracts and dental anomalies)	CCDS1
CGOV65T_0	Exome	NPR2	natriuretic peptide receptor B/guanylate cyclase B (atrionatriuretic peptide receptor B)	CCDS6
CGOV65T_0	Exome	OR14I1	olfactory receptor; family 14; subfamily I; member 1	CCDS3
CGOV65T_0	Exome	OR4K13	olfactory receptor; family 4; subfamily K; member 13	CCDS3
CGOV65T_0	Exome	OR5P3	olfactory receptor; family 5; subfamily P; member 3	CCDS7
CGOV65T_0	Exome	PAN2	PAN2 poly(A) specific ribonuclease subunit homolog (S. cerevisiae)	CCDS8
CGOV65T_0	Exome	PCNX	pecanex homolog (Drosophila)	CCDS9
CGOV65T_0	Exome	PDGFRB	platelet-derived growth factor receptor; beta polypeptide	CCDS4
CGOV65T_0	Exome	PIK3R5	phosphoinositide-3-kinase; regulatory subunit 5	CCDS1
CGOV65T_0	Exome	PPP1R13L	protein phosphatase 1; regulatory (inhibitor) subunit 13 like	CCDS3
CGOV65T_0	Exome	PRDM10	PR domain containing 10	CCDS8
CGOV65T_0	Exome	PRDM16	PR domain containing 16	CCDS4
CGOV65T_0	Exome	PRKG1	protein kinase; cGMP-dependent; type I	CCDS7
CGOV65T_0	Exome	PTCHD2	patched domain containing 2	CCDS4
CGOV65T_0	Exome	PTPN13	tyrosine-protein phosphatase non-receptor type 13 isoform 4	NM_08
CGOV65T_0	Exome	PTPRH	protein tyrosine phosphatase; receptor type; H	CCDS3

CGOV65T_0	Exome	RAPGEF2	Rap guanine nucleotide exchange factor (GEF) 2	CCDS4
CGOV65T_0	Exome	RASSF5	Ras association (RalGDS/AF-6) domain family member 5	CCDS3
CGOV65T_0	Exome	RUNDC1	RUN domain containing 1	CCDS1
CGOV65T_0	Exome	RYR1	ryanodine receptor 1 (skeletal)	CCDS3
CGOV65T_0	Exome	SCML4	sex comb on midleg-like 4 (Drosophila)	NM_19
CGOV65T_0	Exome	SCUBE2	signal peptide; CUB domain; EGF-like 2	CCDS7
CGOV65T_0	Exome	SLC16A13	solute carrier family 16; member 13 (monocarboxylic acid transporter 13)	CCDS1
CGOV65T_0	Exome	SLC9A3	solute carrier family 9 (sodium/hydrogen exchanger); member 3	CCDS3
CGOV65T_0	Exome	SPG7	spastic paraplegia 7 (pure and complicated autosomal recessive)	CCDS1
CGOV65T_0	Exome	SRPX	sushi-repeat-containing protein; X-linked	CCDS1
CGOV65T_0	Exome	SYNE2	spectrin repeat containing; nuclear envelope 2	CCDS9
CGOV65T_0	Exome	THBS1	thrombospondin 1	CCDS3
CGOV65T_0	Exome	TLX2	T-cell leukemia homeobox 2	CCDS1
CGOV65T_0	Exome	TP53	tumor protein p53	CCDS1
CGOV65T_0	Exome	TRPC5	transient receptor potential cation channel; subfamily C; member 5	CCDS1
CGOV65T_0	Exome	TRPM1	transient receptor potential cation channel; subfamily M; member 1	CCDS1
CGOV65T_0	Exome	TTLL13	tubulin tyrosine ligase-like family; member 13	CCDS3
CGOV65T_0	Exome	TTN	titin	ENST0 38
CGOV65T_0	Exome	UGGT1	UDP-glucose glycoprotein glucosyltransferase 1	CCDS2
CGOV65T_0	Exome	WDFY4	WD repeat- and FYVE domain-containing protein 4	NM_02
CGOV65T_0	Exome	WDR11	WD repeat domain 11	CCDS7
CGOV65T_0	Exome	ZC3H12B	probable ribonuclease ZC3H12B	NM_00

CGOV65T_0	Exome	ZC3H12C	zinc finger CCCH-type containing 12C	NM_03
CGOV65T_0	Exome	ZCCHC6	zinc finger; CCHC domain containing 6	CCDS3
CGOV65T_0	Exome	ZNF446	zinc finger protein 446	CCDS1
CGOV65T_0	Exome	ZNF622	zinc finger protein 622	CCDS3
CGOV65T_0	Exome	ZNF764	zinc finger protein 764	CCDS1
CGOV65T_0	Exome	ZPBP2	zona pellucida binding protein 2	CCDS1
CGOV64T	Exome	ABCA13	ATP-binding cassette; sub-family A (ABC1); member 13	ENST0 79
CGOV64T	Exome	DOCK11	dedicator of cytokinesis 11	CCDS3
CGOV64T	Exome	DPP10	dipeptidyl-peptidase 10 (non-functional)	NM_02
CGOV64T	Exome	IGDCC3	immunoglobulin superfamily; DCC subclass; member 3	CCDS1
CGOV64T	Exome	KIF13A	kinesin-like protein KIF13A isoform a	NM_02
CGOV64T	Exome	KLHL6	kelch-like 6 (Drosophila)	CCDS3
CGOV64T	Exome	LIMK2	LIM domain kinase 2	CCDS3
CGOV64T	Exome	MED14	mediator complex subunit 14	CCDS1
CGOV64T	Exome	MYCBP2	MYC binding protein 2	CCDS3
CGOV64T	Exome	NUP35	nucleoporin 35kDa	CCDS2
CGOV64T	Exome	PAK6	p21 protein (Cdc42/Rac)-activated kinase 6	CCDS1
CGOV64T	Exome	PIK3R5	phosphoinositide-3-kinase; regulatory subunit 5	CCDS1
CGOV64T	Exome	PLS3	plastin 3	CCDS1
CGOV64T	Exome	PTEN	phosphatase and tensin homolog	CCDS3
CGOV64T	Exome	PTH2R	parathyroid hormone 2 receptor	CCDS2
CGOV64T	Exome	RGL2	Ral guanine nucleotide dissociation stimulator-like 2 (RalGDS-like factor) (RAS-associated protein RAB2L).	CCDS4
CGOV64T	Exome	RTKN	rhotekin	CCDS3

CGOV64T	Exome	SLC14A2	solute carrier family 14 (urea transporter); member 2	CCDS1
CGOV64T	Exome	TAB3	TGF-beta activated kinase 1/MAP3K7 binding protein 3	CCDS1
CGOV64T	Exome	TLN1	talin 1	CCDS3
CGOV64T	Exome	TP53	tumor protein p53	CCDS1
CGOV64T	Exome	WDFY4	WD repeat- and FYVE domain-containing protein 4	NM_02
CGOV64T	Exome	XPO7	exportin 7	NM_00
CGOV63T_9_1	Exome	AADACL2	arylacetamide deacetylase-like 2	CCDS3
CGOV63T_9_1	Exome	ABI2	abl-interactor 2	CCDS2
CGOV63T_9_1	Exome	ACVR1C	activin A receptor; type IC	CCDS2
CGOV63T_9_1	Exome	ATP2B3	ATPase; Ca++ transporting; plasma membrane 3	CCDS3
CGOV63T_9_1	Exome	C12orf43	chromosome 12 open reading frame 43	CCDS9
CGOV63T_9_1	Exome	C1orf174	chromosome 1 open reading frame 174	CCDS5
CGOV63T_9_1	Exome	C2orf21	Uncharacterized protein C2orf21.	CCDS2
CGOV63T_9_1	Exome	C7orf62	chromosome 7 open reading frame 62	CCDS3
CGOV63T_9_1	Exome	C9orf152	chromosome 9 open reading frame 152	CCDS3
CGOV63T_9_1	Exome	CA6	carbonic anhydrase VI	ENST0 74
CGOV63T_9_1	Exome	CAPRIN2	caprin family member 2	CCDS3
CGOV63T_9_1	Exome	CAPZA3	capping protein (actin filament) muscle Z-line; alpha 3	CCDS8
CGOV63T_9_1	Exome	CARD8	caspase recruitment domain family; member 8	ENST0 61
CGOV63T_9_1	Exome	CDH5	cadherin 5; type 2 (vascular endothelium)	CCDS1
CGOV63T_9_1	Exome	CEP135	centrosomal protein 135kDa	CCDS3
CGOV63T_9_1	Exome	CLCC1	chloride channel CLIC-like 1	CCDS4
CGOV63T_9_1	Exome	CLSPN	claspin homolog (Xenopus laevis)	CCDS3
CGOV63T_9_1	Exome	CSMD1	CUB and sushi domain-containing protein 1 precursor	NM_03

CGOV63T_9_1	Exome	CSMD1	CUB and sushi domain-containing protein 1 precursor	NM_03
CGOV63T_9_1	Exome	CWC22	CWC22 spliceosome-associated protein homolog (S. cerevisiae)	NM_02
CGOV63T_9_1	Exome	DGKB	diacylglycerol kinase; beta 90kDa	NM_00
CGOV63T_9_1	Exome	DLEC1	deleted in lung and esophageal cancer 1	CCDS2
CGOV63T_9_1	Exome	DNAH3	dynein; axonemal; heavy chain 3	CCDS1
CGOV63T_9_1	Exome	ERBB3	v-erb-b2 erythroblastic leukemia viral oncogene homolog 3 (avian)	CCDS3
CGOV63T_9_1	Exome	FAM135B	family with sequence similarity 135; member B	CCDS6
CGOV63T_9_1	Exome	FAM135B	family with sequence similarity 135; member B	CCDS6
CGOV63T_9_1	Exome	GJB1	gap junction protein; beta 1; 32kDa	CCDS1
CGOV63T_9_1	Exome	HCK	hemopoietic cell kinase	ENST0 52
CGOV63T_9_1	Exome	HTR1E	5-hydroxytryptamine (serotonin) receptor 1E	CCDS5
CGOV63T_9_1	Exome	INTS9	integrator complex subunit 9	CCDS3
CGOV63T_9_1	Exome	KIAA1217	KIAA1217	CCDS3
CGOV63T_9_1	Exome	KIF13A	kinesin-like protein KIF13A isoform a	NM_02
CGOV63T_9_1	Exome	LINGO4	leucine rich repeat and Ig domain containing 4	CCDS3
CGOV63T_9_1	Exome	LRRC15	leucine rich repeat containing 15	CCDS3
CGOV63T_9_1	Exome	MACF1	microtubule-actin crosslinking factor 1	CCDS4
CGOV63T_9_1	Exome	MUC7	mucin 7; secreted	CCDS3
CGOV63T_9_1	Exome	NFS1	Cysteine desulfurase, mitochondrial precursor	CCDS1
CGOV63T_9_1	Exome	NID1	nidogen 1	CCDS1
CGOV63T_9_1	Exome	NPHS2	nephrosis 2; idiopathic; steroid-resistant (podocin)	CCDS1
CGOV63T_9_1	Exome	NRK	nik-related protein kinase	NM_19
CGOV63T_9_1	Exome	OR4F15	olfactory receptor; family 4; subfamily F; member 15	CCDS3
CGOV63T_9_1	Exome	PHOX2B	paired-like homeobox 2b	CCDS3

CGOV63T_9_1	Exome	PTPRJ	protein tyrosine phosphatase; receptor type; J	CCDS7
CGOV63T_9_1	Exome	RDH10	retinol dehydrogenase 10 (all-trans)	CCDS6
CGOV63T_9_1	Exome	RPS6KA5	ribosomal protein S6 kinase; 90kDa; polypeptide 5	CCDS9
CGOV63T_9_1	Exome	SEPT6	septin 6	CCDS1
CGOV63T_9_1	Exome	SFMBT2	Scm-like with four mbt domains 2	CCDS3
CGOV63T_9_1	Exome	SHH	sonic hedgehog homolog (Drosophila)	CCDS5
CGOV63T_9_1	Exome	SILV	silver homolog (mouse)	CCDS8
CGOV63T_9_1	Exome	SLC17A6	solute carrier family 17 (sodium-dependent inorganic phosphate cotransporter); member 6	CCDS7
CGOV63T_9_1	Exome	SLC44A3	solute carrier family 44; member 3	CCDS7
CGOV63T_9_1	Exome	SORCS3	sortilin-related VPS10 domain containing receptor 3	CCDS7
CGOV63T_9_1	Exome	STX11	syntaxin 11	CCDS5
CGOV63T_9_1	Exome	TARBP1	TAR (HIV-1) RNA binding protein 1	CCDS1
CGOV63T_9_1	Exome	TMEM62	transmembrane protein 62	CCDS3
CGOV63T_9_1	Exome	TP53	tumor protein p53	CCDS1
CGOV63T_9_1	Exome	TRIM35	tripartite motif-containing 35	CCDS6
CGOV63T_9_1	Exome	TRIP12	thyroid hormone receptor interactor 12	CCDS3
CGOV63T_9_1	Exome	TTN	titin	ENST0 38
CGOV63T_9_1	Exome	TWISTNB	TWIST neighbor	CCDS3
CGOV63T_9_1	Exome	UNC13A	protein unc-13 homolog A	NM_00
CGOV63T_9_1	Exome	UROC1	urocanase domain containing 1	CCDS3
CGOV63T_9_1	Exome	ZNF345	zinc finger protein 345	CCDS1
CGOV63T_9_1	Exome	ZNF462	zinc finger protein 462	CCDS3
CGOV63T_7_1	Exome	ACVR1C	activin A receptor; type IC	CCDS2

CGOV63T_7_1	Exome	ATP2B3	ATPase; Ca++ transporting; plasma membrane 3	CCDS3
CGOV63T_7_1	Exome	C12orf43	chromosome 12 open reading frame 43	CCDS9
CGOV63T_7_1	Exome	C16orf68	chromosome 16 open reading frame 68	CCDS1
CGOV63T_7_1	Exome	C1orf174	chromosome 1 open reading frame 174	CCDS5
CGOV63T_7_1	Exome	C2orf21	Uncharacterized protein C2orf21.	CCDS2
CGOV63T_7_1	Exome	C9orf152	chromosome 9 open reading frame 152	CCDS3
CGOV63T_7_1	Exome	CA6	carbonic anhydrase VI	ENST0 74
CGOV63T_7_1	Exome	CAPRIN2	caprin family member 2	CCDS3
CGOV63T_7_1	Exome	CAPZA3	capping protein (actin filament) muscle Z-line; alpha 3	CCDS8
CGOV63T_7_1	Exome	CARD8	caspase recruitment domain family; member 8	ENST0 61
CGOV63T_7_1	Exome	CDH5	cadherin 5; type 2 (vascular endothelium)	CCDS1
CGOV63T_7_1	Exome	CEP135	centrosomal protein 135kDa	CCDS3
CGOV63T_7_1	Exome	CLSPN	claspin homolog (Xenopus laevis)	CCDS3
CGOV63T_7_1	Exome	CSMD1	CUB and sushi domain-containing protein 1 precursor	NM_03
CGOV63T_7_1	Exome	CWC22	CWC22 spliceosome-associated protein homolog (S. cerevisiae)	NM_02
CGOV63T_7_1	Exome	DGKB	diacylglycerol kinase; beta 90kDa	NM_00
CGOV63T_7_1	Exome	DLEC1	deleted in lung and esophageal cancer 1	CCDS2
CGOV63T_7_1	Exome	DNAH3	dynein; axonemal; heavy chain 3	CCDS1
CGOV63T_7_1	Exome	ERBB3	v-erb-b2 erythroblastic leukemia viral oncogene homolog 3 (avian)	CCDS3
CGOV63T_7_1	Exome	FAM135B	family with sequence similarity 135; member B	CCDS6
CGOV63T_7_1	Exome	FAM135B	family with sequence similarity 135; member B	CCDS6
CGOV63T_7_1	Exome	GJB1	gap junction protein; beta 1; 32kDa	CCDS1
CGOV63T_7_1	Exome	HCK	hemopoietic cell kinase	ENST0 52

CGOV63T_7_1	Exome	INTS9	integrator complex subunit 9	CCDS3
CGOV63T_7_1	Exome	KIF13A	kinesin-like protein KIF13A isoform a	NM_02
CGOV63T_7_1	Exome	LINGO4	leucine rich repeat and Ig domain containing 4	CCDS3
CGOV63T_7_1	Exome	LRRC15	leucine rich repeat containing 15	CCDS3
CGOV63T_7_1	Exome	MACF1	microtubule-actin crosslinking factor 1	CCDS4
CGOV63T_7_1	Exome	NFS1	Cysteine desulfurase, mitochondrial precursor	CCDS1
CGOV63T_7_1	Exome	NID1	nidogen 1	CCDS1
CGOV63T_7_1	Exome	OR4F15	olfactory receptor; family 4; subfamily F; member 15	CCDS3
CGOV63T_7_1	Exome	PHOX2B	paired-like homeobox 2b	CCDS3
CGOV63T_7_1	Exome	PTPRJ	protein tyrosine phosphatase; receptor type; J	CCDS7
CGOV63T_7_1	Exome	RDH10	retinol dehydrogenase 10 (all-trans)	CCDS6
CGOV63T_7_1	Exome	RPS6KA5	ribosomal protein S6 kinase; 90kDa; polypeptide 5	CCDS9
CGOV63T_7_1	Exome	SEPT6	septin 6	CCDS1
CGOV63T_7_1	Exome	SFMBT2	Scm-like with four mbt domains 2	CCDS3
CGOV63T_7_1	Exome	SHH	sonic hedgehog homolog (Drosophila)	CCDS5
CGOV63T_7_1	Exome	SILV	silver homolog (mouse)	CCDS8
CGOV63T_7_1	Exome	SLC17A6	solute carrier family 17 (sodium-dependent inorganic phosphate cotransporter); member 6	CCDS7
CGOV63T_7_1	Exome	SLC44A3	solute carrier family 44; member 3	CCDS7
CGOV63T_7_1	Exome	SORCS3	sortilin-related VPS10 domain containing receptor 3	CCDS7
CGOV63T_7_1	Exome	STX11	syntaxin 11	CCDS5
CGOV63T_7_1	Exome	TARBP1	TAR (HIV-1) RNA binding protein 1	CCDS1
CGOV63T_7_1	Exome	TP53	tumor protein p53	CCDS1
CGOV63T_7_1	Exome	TTN	titin	ENST0 38

CGOV63T_7_1	Exome	UNC13A	protein unc-13 homolog A	NM_00
CGOV63T_7_1	Exome	UROC1	urocanase domain containing 1	CCDS3
CGOV63T_7_1	Exome	ZNF462	zinc finger protein 462	CCDS3
CGOV63T_2_1	Exome	ACVR1C	activin A receptor; type IC	CCDS2
CGOV63T_2_1	Exome	ATP2B3	ATPase; Ca++ transporting; plasma membrane 3	CCDS3
CGOV63T_2_1	Exome	C12orf43	chromosome 12 open reading frame 43	CCDS9
CGOV63T_2_1	Exome	C16orf68	chromosome 16 open reading frame 68	CCDS1
CGOV63T_2_1	Exome	C1orf174	chromosome 1 open reading frame 174	CCDS5
CGOV63T_2_1	Exome	C2orf21	Uncharacterized protein C2orf21.	CCDS2
CGOV63T_2_1	Exome	C9orf152	chromosome 9 open reading frame 152	CCDS3
CGOV63T_2_1	Exome	CA6	carbonic anhydrase VI	ENST0 74
CGOV63T_2_1	Exome	CAPRIN2	caprin family member 2	CCDS3
CGOV63T_2_1	Exome	CAPZA3	capping protein (actin filament) muscle Z-line; alpha 3	CCDS8
CGOV63T_2_1	Exome	CARD8	caspase recruitment domain family; member 8	ENST0 61
CGOV63T_2_1	Exome	CDH5	cadherin 5; type 2 (vascular endothelium)	CCDS1
CGOV63T_2_1	Exome	CEP135	centrosomal protein 135kDa	CCDS3
CGOV63T_2_1	Exome	CLSPN	claspin homolog (Xenopus laevis)	CCDS3
CGOV63T_2_1	Exome	CSMD1	CUB and sushi domain-containing protein 1 precursor	NM_03
CGOV63T_2_1	Exome	CWC22	CWC22 spliceosome-associated protein homolog (S. cerevisiae)	NM_02
CGOV63T_2_1	Exome	DGKB	diacylglycerol kinase; beta 90kDa	NM_00
CGOV63T_2_1	Exome	DLEC1	deleted in lung and esophageal cancer 1	CCDS2
CGOV63T_2_1	Exome	DNAH3	dynein; axonemal; heavy chain 3	CCDS1
CGOV63T_2_1	Exome	ERBB3	v-erb-b2 erythroblastic leukemia viral oncogene homolog 3 (avian)	CCDS3

CGOV63T_2_1	Exome	FAM135B	family with sequence similarity 135; member B	CCDS6
CGOV63T_2_1	Exome	FAM135B	family with sequence similarity 135; member B	CCDS6
CGOV63T_2_1	Exome	GJB1	gap junction protein; beta 1; 32kDa	CCDS1
CGOV63T_2_1	Exome	HCK	hemopoietic cell kinase	ENST0 52
CGOV63T_2_1	Exome	INTS9	integrator complex subunit 9	CCDS3
CGOV63T_2_1	Exome	KIF13A	kinesin-like protein KIF13A isoform a	NM_02
CGOV63T_2_1	Exome	LINGO4	leucine rich repeat and Ig domain containing 4	CCDS3
CGOV63T_2_1	Exome	LRRC15	leucine rich repeat containing 15	CCDS3
CGOV63T_2_1	Exome	MACF1	microtubule-actin crosslinking factor 1	CCDS4
CGOV63T_2_1	Exome	NFS1	Cysteine desulfurase, mitochondrial precursor	CCDS1
CGOV63T_2_1	Exome	NID1	nidogen 1	CCDS1
CGOV63T_2_1	Exome	OR4F15	olfactory receptor; family 4; subfamily F; member 15	CCDS3
CGOV63T_2_1	Exome	PHOX2B	paired-like homeobox 2b	CCDS3
CGOV63T_2_1	Exome	PTPRJ	protein tyrosine phosphatase; receptor type; J	CCDS7
CGOV63T_2_1	Exome	RDH10	retinol dehydrogenase 10 (all-trans)	CCDS6
CGOV63T_2_1	Exome	RPS6KA5	ribosomal protein S6 kinase; 90kDa; polypeptide 5	CCDS9
CGOV63T_2_1	Exome	SEPT6	septin 6	CCDS1
CGOV63T_2_1	Exome	SFMBT2	Scm-like with four mbt domains 2	CCDS3
CGOV63T_2_1	Exome	SHH	sonic hedgehog homolog (Drosophila)	CCDS5
CGOV63T_2_1	Exome	SILV	silver homolog (mouse)	CCDS8
CGOV63T_2_1	Exome	SLC17A6	solute carrier family 17 (sodium-dependent inorganic phosphate cotransporter); member 6	CCDS7
CGOV63T_2_1	Exome	SLC44A3	solute carrier family 44; member 3	CCDS7
CGOV63T_2_1	Exome	SORCS3	sortilin-related VPS10 domain containing receptor 3	CCDS7

CGOV63T_2_1	Exome	STX11	syntaxin 11	CCDS5
CGOV63T_2_1	Exome	TARBP1	TAR (HIV-1) RNA binding protein 1	CCDS1
CGOV63T_2_1	Exome	TP53	tumor protein p53	CCDS1
CGOV63T_2_1	Exome	TTN	titin	ENST0 38
CGOV63T_2_1	Exome	UNC13A	protein unc-13 homolog A	NM_00
CGOV63T_2_1	Exome	UROC1	urocanase domain containing 1	CCDS3
CGOV63T_2_1	Exome	ZNF462	zinc finger protein 462	CCDS3
CGOV63T_14	Exome	CAPZA3	capping protein (actin filament) muscle Z-line; alpha 3	CCDS8
CGOV63T_14	Exome	MACF1	microtubule-actin crosslinking factor 1	CCDS4
CGOV63T_14	Exome	SILV	silver homolog (mouse)	CCDS8
CGOV63T_14	Exome	TP53	tumor protein p53	CCDS1
CGOV63T_14	Exome	ACVR1C	activin A receptor; type IC	CCDS2
CGOV63T_14	Exome	ATP2B3	ATPase; Ca++ transporting; plasma membrane 3	CCDS3
CGOV63T_14	Exome	C12orf43	chromosome 12 open reading frame 43	CCDS9
CGOV63T_14	Exome	C1orf174	chromosome 1 open reading frame 174	CCDS5
CGOV63T_14	Exome	C2orf21	Uncharacterized protein C2orf21.	CCDS2
CGOV63T_14	Exome	C9orf152	chromosome 9 open reading frame 152	CCDS3
CGOV63T_14	Exome	CA6	carbonic anhydrase VI	ENST0 74
CGOV63T_14	Exome	CAPRIN2	caprin family member 2	CCDS3
CGOV63T_14	Exome	CARD8	caspase recruitment domain family; member 8	ENST0 61
CGOV63T_14	Exome	CDH5	cadherin 5; type 2 (vascular endothelium)	CCDS1
CGOV63T_14	Exome	CEP135	centrosomal protein 135kDa	CCDS3
CGOV63T_14	Exome	CLSPN	claspin homolog (Xenopus laevis)	CCDS3
CGOV63T_14	Exome	CSMD1	CUB and sushi domain-containing protein 1 precursor	NM_03

CGOV63T_14	Exome	CWC22	CWC22 spliceosome-associated protein homolog (S. cerevisiae)	NM_02
CGOV63T_14	Exome	DGKB	diacylglycerol kinase; beta 90kDa	NM_00
CGOV63T_14	Exome	DLEC1	deleted in lung and esophageal cancer 1	CCDS2
CGOV63T_14	Exome	DNAH3	dynein; axonemal; heavy chain 3	CCDS1
CGOV63T_14	Exome	ERBB3	v-erb-b2 erythroblastic leukemia viral oncogene homolog 3 (avian)	CCDS3
CGOV63T_14	Exome	FAM135B	family with sequence similarity 135; member B	CCDS6
CGOV63T_14	Exome	FAM135B	family with sequence similarity 135; member B	CCDS6
CGOV63T_14	Exome	GJB1	gap junction protein; beta 1; 32kDa	CCDS1
CGOV63T_14	Exome	HCK	hemopoietic cell kinase	ENST0 52
CGOV63T_14	Exome	INTS9	integrator complex subunit 9	CCDS3
CGOV63T_14	Exome	KIF13A	kinesin-like protein KIF13A isoform a	NM_02
CGOV63T_14	Exome	LINGO4	leucine rich repeat and Ig domain containing 4	CCDS3
CGOV63T_14	Exome	LRRC15	leucine rich repeat containing 15	CCDS3
CGOV63T_14	Exome	NFS1	Cysteine desulfurase, mitochondrial precursor	CCDS1
CGOV63T_14	Exome	NID1	nidogen 1	CCDS1
CGOV63T_14	Exome	OR4F15	olfactory receptor; family 4; subfamily F; member 15	CCDS3
CGOV63T_14	Exome	PHOX2B	paired-like homeobox 2b	CCDS3
CGOV63T_14	Exome	PTPRJ	protein tyrosine phosphatase; receptor type; J	CCDS7
CGOV63T_14	Exome	RDH10	retinol dehydrogenase 10 (all-trans)	CCDS6
CGOV63T_14	Exome	RPS6KA5	ribosomal protein S6 kinase; 90kDa; polypeptide 5	CCDS9
CGOV63T_14	Exome	SEPT6	septin 6	CCDS1
CGOV63T_14	Exome	SFMBT2	Scm-like with four mbt domains 2	CCDS3
CGOV63T_14	Exome	SHH	sonic hedgehog homolog (Drosophila)	CCDS5
CGOV63T_14	Exome	SLC17A6	solute carrier family 17 (sodium-dependent	CCDS7

CGOV63T_14	Exome	SLC44A3	inorganic phosphate cotransporter); member 6 solute carrier family 44; member 3	CCDS7
CGOV63T_14	Exome	SORCS3	sortilin-related VPS10 domain containing receptor 3	CCDS7
CGOV63T_14	Exome	STX11	syntaxin 11	CCDS5
CGOV63T_14	Exome	TARBP1	TAR (HIV-1) RNA binding protein 1	CCDS1
CGOV63T_14	Exome	TTN	titin	ENST0 38
CGOV63T_14	Exome	UNC13A	protein unc-13 homolog A	NM_00
CGOV63T_14	Exome	UROC1	urocanase domain containing 1	CCDS3
CGOV63T_14	Exome	ZNF462	zinc finger protein 462	CCDS3
CGOV63T_12	Exome	ACVR1C	activin A receptor; type IC	CCDS2
CGOV63T_12	Exome	ATP2B3	ATPase; Ca++ transporting; plasma membrane 3	CCDS3
CGOV63T_12	Exome	C12orf43	chromosome 12 open reading frame 43	CCDS9
CGOV63T_12	Exome	C16orf68	chromosome 16 open reading frame 68	CCDS1
CGOV63T_12	Exome	C1orf174	chromosome 1 open reading frame 174	CCDS5
CGOV63T_12	Exome	C2orf21	Uncharacterized protein C2orf21.	CCDS2
CGOV63T_12	Exome	C9orf152	chromosome 9 open reading frame 152	CCDS3
CGOV63T_12	Exome	CA6	carbonic anhydrase VI	ENST0 74
CGOV63T_12	Exome	CAPRIN2	caprin family member 2	CCDS3
CGOV63T_12	Exome	CAPZA3	capping protein (actin filament) muscle Z-line; alpha 3	CCDS8
CGOV63T_12	Exome	CARD8	caspase recruitment domain family; member 8	ENST0 61
CGOV63T_12	Exome	CDH5	cadherin 5; type 2 (vascular endothelium)	CCDS1
CGOV63T_12	Exome	CEP135	centrosomal protein 135kDa	CCDS3
CGOV63T_12	Exome	CLSPN	claspin homolog (Xenopus laevis)	CCDS3
CGOV63T_12	Exome	CSMD1	CUB and sushi domain-containing protein 1 precursor	NM_03

CGOV63T_12	Exome	CWC22	CWC22 spliceosome-associated protein homolog (S. cerevisiae)	NM_02
CGOV63T_12	Exome	DGKB	diacylglycerol kinase; beta 90kDa	NM_00
CGOV63T_12	Exome	DLEC1	deleted in lung and esophageal cancer 1	CCDS2
CGOV63T_12	Exome	DNAH3	dynein; axonemal; heavy chain 3	CCDS1
CGOV63T_12	Exome	ERBB3	v-erb-b2 erythroblastic leukemia viral oncogene homolog 3 (avian)	CCDS3
CGOV63T_12	Exome	FAM135B	family with sequence similarity 135; member B	CCDS6
CGOV63T_12	Exome	FAM135B	family with sequence similarity 135; member B	CCDS6
CGOV63T_12	Exome	GJB1	gap junction protein; beta 1; 32kDa	CCDS1
CGOV63T_12	Exome	HCK	hemopoietic cell kinase	ENST0 52
CGOV63T_12	Exome	IGF2R	insulin-like growth factor 2 receptor	CCDS5
CGOV63T_12	Exome	INTS9	integrator complex subunit 9	CCDS3
CGOV63T_12	Exome	KIF13A	kinesin-like protein KIF13A isoform a	NM_02
CGOV63T_12	Exome	LINGO4	leucine rich repeat and Ig domain containing 4	CCDS3
CGOV63T_12	Exome	LRRC15	leucine rich repeat containing 15	CCDS3
CGOV63T_12	Exome	MACF1	microtubule-actin crosslinking factor 1	CCDS4
CGOV63T_12	Exome	NFS1	Cysteine desulfurase, mitochondrial precursor	CCDS1
CGOV63T_12	Exome	NID1	nidogen 1	CCDS1
CGOV63T_12	Exome	OR4F15	olfactory receptor; family 4; subfamily F; member 15	CCDS3
CGOV63T_12	Exome	PHOX2B	paired-like homeobox 2b	CCDS3
CGOV63T_12	Exome	PTPRJ	protein tyrosine phosphatase; receptor type; J	CCDS7
CGOV63T_12	Exome	RDH10	retinol dehydrogenase 10 (all-trans)	CCDS6
CGOV63T_12	Exome	RPS6KA5	ribosomal protein S6 kinase; 90kDa; polypeptide 5	CCDS9
CGOV63T_12	Exome	SEPT6	septin 6	CCDS1
CGOV63T_12	Exome	SFMBT2	Scm-like with four mbt domains 2	CCDS3

CGOV63T_12	Exome	SHH	sonic hedgehog homolog (Drosophila)	CCDS5
CGOV63T_12	Exome	SILV	silver homolog (mouse)	CCDS8
CGOV63T_12	Exome	SLC17A6	solute carrier family 17 (sodium-dependent inorganic phosphate cotransporter); member 6	CCDS7
CGOV63T_12	Exome	SLC44A3	solute carrier family 44; member 3	CCDS7
CGOV63T_12	Exome	SORCS3	sortilin-related VPS10 domain containing receptor 3	CCDS7
CGOV63T_12	Exome	STX11	syntaxin 11	CCDS5
CGOV63T_12	Exome	TARBP1	TAR (HIV-1) RNA binding protein 1	CCDS1
CGOV63T_12	Exome	TP53	tumor protein p53	CCDS1
CGOV63T_12	Exome	TTN	titin	ENST0 38
CGOV63T_12	Exome	UNC13A	protein unc-13 homolog A	NM_00
CGOV63T_12	Exome	UROC1	urocanase domain containing 1	CCDS3
CGOV63T_12	Exome	ZNF462	zinc finger protein 462	CCDS3
CGOV63T_10	Exome	ATP2B3	ATPase; Ca++ transporting; plasma membrane 3	CCDS3
CGOV63T_10	Exome	C12orf43	chromosome 12 open reading frame 43	CCDS9
CGOV63T_10	Exome	CAPZA3	capping protein (actin filament) muscle Z-line; alpha 3	CCDS8
CGOV63T_10	Exome	CLSPN	claspin homolog (Xenopus laevis)	CCDS3
CGOV63T_10	Exome	CSMD1	CUB and sushi domain-containing protein 1 precursor	NM_03
CGOV63T_10	Exome	DGKB	diacylglycerol kinase; beta 90kDa	NM_00
CGOV63T_10	Exome	FAM135B	family with sequence similarity 135; member B	CCDS6
CGOV63T_10	Exome	HCK	hemopoietic cell kinase	ENST0 52
CGOV63T_10	Exome	KIF13A	kinesin-like protein KIF13A isoform a	NM_02
CGOV63T_10	Exome	LINGO4	leucine rich repeat and Ig domain containing 4	CCDS3
CGOV63T_10	Exome	LRRC15	leucine rich repeat containing 15	CCDS3

CGOV63T_10	Exome	MACF1	microtubule-actin crosslinking factor 1	CCDS4
CGOV63T_10	Exome	NID1	nidogen 1	CCDS1
CGOV63T_10	Exome	RPS6KA5	ribosomal protein S6 kinase; 90kDa; polypeptide 5	CCDS9
CGOV63T_10	Exome	SEPT6	septin 6	CCDS1
CGOV63T_10	Exome	SFMBT2	Scm-like with four mbt domains 2	CCDS3
CGOV63T_10	Exome	SILV	silver homolog (mouse)	CCDS8
CGOV63T_10	Exome	TP53	tumor protein p53	CCDS1
CGOV62T_9	Exome	ANKFN1	ankyrin-repeat and fibronectin type III domain containing 1	CCDS3
CGOV62T_9	Exome	ANKRD35	ankyrin repeat domain 35	CCDS9
CGOV62T_9	Exome	APOB	apolipoprotein B (including Ag(x) antigen)	CCDS1
CGOV62T_9	Exome	BTNL9	butyrophilin-like 9	CCDS4
CGOV62T_9	Exome	C1S	complement component 1; s subcomponent	CCDS3
CGOV62T_9	Exome	C4orf43	chromosome 4 open reading frame 43	CCDS4
CGOV62T_9	Exome	C5orf25	chromosome 5 open reading frame 25	CCDS4
CGOV62T_9	Exome	C5orf46	chromosome 5 open reading frame 46	CCDS3
CGOV62T_9	Exome	C6	complement component 6	CCDS3
CGOV62T_9	Exome	CDKAL1	CDK5 regulatory subunit associated protein 1-like 1	CCDS4
CGOV62T_9	Exome	DNAH6	dynein heavy chain 6, axonemal	NM_00
CGOV62T_9	Exome	DUSP27	dual specificity phosphatase 27 (putative)	CCDS3
CGOV62T_9	Exome	EPHA5	EPH receptor A5	CCDS3
CGOV62T_9	Exome	FAM5C	family with sequence similarity 5; member C	CCDS1
CGOV62T_9	Exome	KIF17	kinesin family member 17	CCDS2
CGOV62T_9	Exome	KIF3C	kinesin family member 3C	CCDS1
CGOV62T_9	Exome	PRSS23	protease; serine; 23	CCDS4
CGOV62T_9	Exome	RANBP2	RAN binding protein 2	CCDS2

CGOV62T_9	Exome	RHBDD1	rhomboid domain containing 1	CCDS2
CGOV62T_9	Exome	ROBO1	roundabout homolog 1 isoform a precursor	NM_00
CGOV62T_9	Exome	SEMA3F	sema domain; immunoglobulin domain (Ig); short basic domain; secreted; (semaphorin) 3F	CCDS2
CGOV62T_9	Exome	SI	sucrase-isomaltase (alpha-glucosidase)	CCDS3
CGOV62T_9	Exome	SLC1A2	solute carrier family 1 (glial high affinity glutamate transporter); member 2	CCDS3
CGOV62T_9	Exome	SLC25A3	solute carrier family 25 (mitochondrial carrier; phosphate carrier); member 3	CCDS9
CGOV62T_9	Exome	TP53	tumor protein p53	CCDS1
CGOV62T_9	Exome	TRIO	triple functional domain (PTPRF interacting)	CCDS3
CGOV62T_9	Exome	USP34	ubiquitin specific peptidase 34	CCDS4
CGOV62T_9	Exome	WDR11	WD repeat domain 11	CCDS7
CGOV62T_9	Exome	ZBBX	zinc finger; B-box domain containing	CCDS3
CGOV62T_9	Exome	ZNF71	zinc finger protein 71	CCDS1
CGOV62T_8	Exome	ANKFN1	ankyrin-repeat and fibronectin type III domain containing 1	CCDS3
CGOV62T_8	Exome	ANKRD35	ankyrin repeat domain 35	CCDS9
CGOV62T_8	Exome	APOB	apolipoprotein B (including Ag(x) antigen)	CCDS1
CGOV62T_8	Exome	BTNL9	butyrophilin-like 9	CCDS4
CGOV62T_8	Exome	C1S	complement component 1; s subcomponent	CCDS3
CGOV62T_8	Exome	C4orf43	chromosome 4 open reading frame 43	CCDS4
CGOV62T_8	Exome	C5orf25	chromosome 5 open reading frame 25	CCDS4
CGOV62T_8	Exome	C5orf46	chromosome 5 open reading frame 46	CCDS3
CGOV62T_8	Exome	C6	complement component 6	CCDS3
CGOV62T_8	Exome	CDKAL1	CDK5 regulatory subunit associated protein 1-like 1	CCDS4

CGOV62T_8	Exome	DNAH6	dynein heavy chain 6, axonemal	NM_00
CGOV62T_8	Exome	DUSP27	dual specificity phosphatase 27 (putative)	CCDS3
CGOV62T_8	Exome	EPHA5	EPH receptor A5	CCDS3
CGOV62T_8	Exome	FAM5C	family with sequence similarity 5; member C	CCDS1
CGOV62T_8	Exome	KIF17	kinesin family member 17	CCDS2
CGOV62T_8	Exome	KIF3C	kinesin family member 3C	CCDS1
CGOV62T_8	Exome	PRSS23	protease; serine; 23	CCDS4
CGOV62T_8	Exome	RANBP2	RAN binding protein 2	CCDS2
CGOV62T_8	Exome	RHBDD1	rhomboid domain containing 1	CCDS2
CGOV62T_8	Exome	ROBO1	roundabout homolog 1 isoform a precursor	NM_00
CGOV62T_8	Exome	SEMA3F	sema domain; immunoglobulin domain (Ig); short basic domain; secreted; (semaphorin) 3F	CCDS2
CGOV62T_8	Exome	SI	sucrase-isomaltase (alpha-glucosidase)	CCDS3
CGOV62T_8	Exome	SLC1A2	solute carrier family 1 (glial high affinity glutamate transporter); member 2	CCDS3
CGOV62T_8	Exome	SLC25A3	solute carrier family 25 (mitochondrial carrier; phosphate carrier); member 3	CCDS9
CGOV62T_8	Exome	TP53	tumor protein p53	CCDS1
CGOV62T_8	Exome	TRIO	triple functional domain (PTPRF interacting)	CCDS3
CGOV62T_8	Exome	USP34	ubiquitin specific peptidase 34	CCDS4
CGOV62T_8	Exome	WDR11	WD repeat domain 11	CCDS7
CGOV62T_8	Exome	ZBBX	zinc finger; B-box domain containing	CCDS3
CGOV62T_8	Exome	ZNF71	zinc finger protein 71	CCDS1
CGOV62T_7	Exome	ANKFN1	ankyrin-repeat and fibronectin type III domain containing 1	CCDS3
CGOV62T_7	Exome	ANKRD35	ankyrin repeat domain 35	CCDS9

CGOV62T_7	Exome	APOB	apolipoprotein B (including Ag(x) antigen)	CCDS1
CGOV62T_7	Exome	BTNL9	butyrophilin-like 9	CCDS4
CGOV62T_7	Exome	C1S	complement component 1; s subcomponent	CCDS3
CGOV62T_7	Exome	C4orf43	chromosome 4 open reading frame 43	CCDS4
CGOV62T_7	Exome	C5orf25	chromosome 5 open reading frame 25	CCDS4
CGOV62T_7	Exome	C5orf46	chromosome 5 open reading frame 46	CCDS3
CGOV62T_7	Exome	C6	complement component 6	CCDS3
CGOV62T_7	Exome	CDKAL1	CDK5 regulatory subunit associated protein 1-like 1	CCDS4
CGOV62T_7	Exome	DNAH6	dynein heavy chain 6, axonemal	NM_00
CGOV62T_7	Exome	DUSP27	dual specificity phosphatase 27 (putative)	CCDS3
CGOV62T_7	Exome	EPHA5	EPH receptor A5	CCDS3
CGOV62T_7	Exome	FAM5C	family with sequence similarity 5; member C	CCDS1
CGOV62T_7	Exome	KIF17	kinesin family member 17	CCDS2
CGOV62T_7	Exome	KIF3C	kinesin family member 3C	CCDS1
CGOV62T_7	Exome	PRSS23	protease; serine; 23	CCDS4
CGOV62T_7	Exome	RANBP2	RAN binding protein 2	CCDS2
CGOV62T_7	Exome	RHBDD1	rhomboid domain containing 1	CCDS2
CGOV62T_7	Exome	ROBO1	roundabout homolog 1 isoform a precursor	NM_00
CGOV62T_7	Exome	SEMA3F	sema domain; immunoglobulin domain (Ig); short basic domain; secreted; (semaphorin) 3F	CCDS2
CGOV62T_7	Exome	SI	sucrase-isomaltase (alpha-glucosidase)	CCDS3
CGOV62T_7	Exome	SLC1A2	solute carrier family 1 (glial high affinity glutamate transporter); member 2	CCDS3
CGOV62T_7	Exome	SLC25A3	solute carrier family 25 (mitochondrial carrier; phosphate carrier); member 3	CCDS9
CGOV62T_7	Exome	TP53	tumor protein p53	CCDS1

CGOV62T_7	Exome	TRIO	triple functional domain (PTPRF interacting)	CCDS3
CGOV62T_7	Exome	USP34	ubiquitin specific peptidase 34	CCDS4
CGOV62T_7	Exome	WDR11	WD repeat domain 11	CCDS7
CGOV62T_7	Exome	ZBBX	zinc finger; B-box domain containing	CCDS3
CGOV62T_7	Exome	ZNF71	zinc finger protein 71	CCDS1
CGOV62T_6	Exome	ANKFN1	ankyrin-repeat and fibronectin type III domain containing 1	CCDS3
CGOV62T_6	Exome	ANKRD35	ankyrin repeat domain 35	CCDS9
CGOV62T_6	Exome	APOB	apolipoprotein B (including Ag(x) antigen)	CCDS1
CGOV62T_6	Exome	BTNL9	butyrophilin-like 9	CCDS4
CGOV62T_6	Exome	C1S	complement component 1; s subcomponent	CCDS3
CGOV62T_6	Exome	C4orf43	chromosome 4 open reading frame 43	CCDS4
CGOV62T_6	Exome	C5orf25	chromosome 5 open reading frame 25	CCDS4
CGOV62T_6	Exome	C5orf46	chromosome 5 open reading frame 46	CCDS3
CGOV62T_6	Exome	C6	complement component 6	CCDS3
CGOV62T_6	Exome	CDKAL1	CDK5 regulatory subunit associated protein 1-like 1	CCDS4
CGOV62T_6	Exome	DNAH6	dynein heavy chain 6, axonemal	NM_00
CGOV62T_6	Exome	DUSP27	dual specificity phosphatase 27 (putative)	CCDS3
CGOV62T_6	Exome	EPHA5	EPH receptor A5	CCDS3
CGOV62T_6	Exome	FAM5C	family with sequence similarity 5; member C	CCDS1
CGOV62T_6	Exome	KIF17	kinesin family member 17	CCDS2
CGOV62T_6	Exome	KIF3C	kinesin family member 3C	CCDS1
CGOV62T_6	Exome	PRSS23	protease; serine; 23	CCDS4
CGOV62T_6	Exome	RANBP2	RAN binding protein 2	CCDS2
CGOV62T_6	Exome	RHBDD1	rhomboid domain containing 1	CCDS2
CGOV62T_6	Exome	ROBO1	roundabout homolog 1 isoform a precursor	NM_00

CGOV62T_6	Exome	SEMA3F	sema domain; immunoglobulin domain (Ig); short basic domain; secreted; (semaphorin) 3F	CCDS2
CGOV62T_6	Exome	SI	sucrase-isomaltase (alpha-glucosidase)	CCDS3
CGOV62T_6	Exome	SLC1A2	solute carrier family 1 (glial high affinity glutamate transporter); member 2	CCDS3
CGOV62T_6	Exome	SLC25A3	solute carrier family 25 (mitochondrial carrier; phosphate carrier); member 3	CCDS9
CGOV62T_6	Exome	TP53	tumor protein p53	CCDS1
CGOV62T_6	Exome	TRIO	triple functional domain (PTPRF interacting)	CCDS3
CGOV62T_6	Exome	USP34	ubiquitin specific peptidase 34	CCDS4
CGOV62T_6	Exome	WDR11	WD repeat domain 11	CCDS7
CGOV62T_6	Exome	ZBBX	zinc finger; B-box domain containing	CCDS3
CGOV62T_6	Exome	ZNF71	zinc finger protein 71	CCDS1
CGOV62T_4	Exome	ANKFN1	ankyrin-repeat and fibronectin type III domain containing 1	CCDS3
CGOV62T_4	Exome	ANKRD35	ankyrin repeat domain 35	CCDS9
CGOV62T_4	Exome	C5orf25	chromosome 5 open reading frame 25	CCDS4
CGOV62T_4	Exome	C5orf46	chromosome 5 open reading frame 46	CCDS3
CGOV62T_4	Exome	EPHA5	EPH receptor A5	CCDS3
CGOV62T_4	Exome	SI	sucrase-isomaltase (alpha-glucosidase)	CCDS3
CGOV62T_4	Exome	SLC25A3	solute carrier family 25 (mitochondrial carrier; phosphate carrier); member 3	CCDS9
CGOV62T_4	Exome	TP53	tumor protein p53	CCDS1
CGOV62T_4	Exome	TRIO	triple functional domain (PTPRF interacting)	CCDS3
CGOV62T_4	Exome	WDR11	WD repeat domain 11	CCDS7
CGOV62T_4	Exome	ZNF71	zinc finger protein 71	CCDS1

CGOV62T_3_1	Exome	ANKFN1	ankyrin-repeat and fibronectin type III domain containing 1	CCDS3
CGOV62T_3_1	Exome	ANKRD35	ankyrin repeat domain 35	CCDS9
CGOV62T_3_1	Exome	APOB	apolipoprotein B (including Ag(x) antigen)	CCDS1
CGOV62T_3_1	Exome	BTNL9	butyrophilin-like 9	CCDS4
CGOV62T_3_1	Exome	C1S	complement component 1; s subcomponent	CCDS3
CGOV62T_3_1	Exome	C4orf43	chromosome 4 open reading frame 43	CCDS4
CGOV62T_3_1	Exome	C5orf25	chromosome 5 open reading frame 25	CCDS4
CGOV62T_3_1	Exome	C5orf46	chromosome 5 open reading frame 46	CCDS3
CGOV62T_3_1	Exome	C6	complement component 6	CCDS3
CGOV62T_3_1	Exome	CDKAL1	CDK5 regulatory subunit associated protein 1-like 1	CCDS4
CGOV62T_3_1	Exome	DNAH6	dynein heavy chain 6, axonemal	NM_00
CGOV62T_3_1	Exome	DUSP27	dual specificity phosphatase 27 (putative)	CCDS3
CGOV62T_3_1	Exome	EPHA5	EPH receptor A5	CCDS3
CGOV62T_3_1	Exome	FAM5C	family with sequence similarity 5; member C	CCDS1
CGOV62T_3_1	Exome	KIF17	kinesin family member 17	CCDS2
CGOV62T_3_1	Exome	KIF3C	kinesin family member 3C	CCDS1
CGOV62T_3_1	Exome	PRSS23	protease; serine; 23	CCDS4
CGOV62T_3_1	Exome	RANBP2	RAN binding protein 2	CCDS2
CGOV62T_3_1	Exome	RHBDD1	rhomboid domain containing 1	CCDS2
CGOV62T_3_1	Exome	ROBO1	roundabout homolog 1 isoform a precursor	NM_00
CGOV62T_3_1	Exome	SEMA3F	sema domain; immunoglobulin domain (Ig); short basic domain; secreted; (semaphorin) 3F	CCDS2
CGOV62T_3_1	Exome	SI	sucrase-isomaltase (alpha-glucosidase)	CCDS3
CGOV62T_3_1	Exome	SLC1A2	solute carrier family 1 (glial high affinity glutamate transporter); member 2	CCDS3

CGOV62T_3_1	Exome	SLC25A3	solute carrier family 25 (mitochondrial carrier; phosphate carrier); member 3	CCDS9
CGOV62T_3_1	Exome	TP53	tumor protein p53	CCDS1
CGOV62T_3_1	Exome	TRIO	triple functional domain (PTPRF interacting)	CCDS3
CGOV62T_3_1	Exome	USP34	ubiquitin specific peptidase 34	CCDS4
CGOV62T_3_1	Exome	WDR11	WD repeat domain 11	CCDS7
CGOV62T_3_1	Exome	ZBBX	zinc finger; B-box domain containing	CCDS3
CGOV62T_3_1	Exome	ZNF71	zinc finger protein 71	CCDS1
CGOV62T_2	Exome	ANKFN1	ankyrin-repeat and fibronectin type III domain containing 1	CCDS3
CGOV62T_2	Exome	ANKRD35	ankyrin repeat domain 35	CCDS9
CGOV62T_2	Exome	APOB	apolipoprotein B (including Ag(x) antigen)	CCDS1
CGOV62T_2	Exome	BTNL9	butyrophilin-like 9	CCDS4
CGOV62T_2	Exome	C1S	complement component 1; s subcomponent	CCDS3
CGOV62T_2	Exome	C4orf43	chromosome 4 open reading frame 43	CCDS4
CGOV62T_2	Exome	C5orf25	chromosome 5 open reading frame 25	CCDS4
CGOV62T_2	Exome	C5orf46	chromosome 5 open reading frame 46	CCDS3
CGOV62T_2	Exome	C6	complement component 6	CCDS3
CGOV62T_2	Exome	CDKAL1	CDK5 regulatory subunit associated protein 1-like 1	CCDS4
CGOV62T_2	Exome	DNAH6	dynein heavy chain 6, axonemal	NM_00
CGOV62T_2	Exome	DUSP27	dual specificity phosphatase 27 (putative)	CCDS3
CGOV62T_2	Exome	EPHA5	EPH receptor A5	CCDS3
CGOV62T_2	Exome	FAM5C	family with sequence similarity 5; member C	CCDS1
CGOV62T_2	Exome	KIF17	kinesin family member 17	CCDS2
CGOV62T_2	Exome	KIF3C	kinesin family member 3C	CCDS1
CGOV62T_2	Exome	PRSS23	protease; serine; 23	CCDS4

CGOV62T_2	Exome	RANBP2	RAN binding protein 2	CCDS2
CGOV62T_2	Exome	RHBDD1	rhomboid domain containing 1	CCDS2
CGOV62T_2	Exome	ROBO1	roundabout homolog 1 isoform a precursor	NM_00
CGOV62T_2	Exome	SEMA3F	sema domain; immunoglobulin domain (Ig); short basic domain; secreted; (semaphorin) 3F	CCDS2
CGOV62T_2	Exome	SI	sucrase-isomaltase (alpha-glucosidase)	CCDS3
CGOV62T_2	Exome	SLC1A2	solute carrier family 1 (glial high affinity glutamate transporter); member 2	CCDS3
CGOV62T_2	Exome	SLC25A3	solute carrier family 25 (mitochondrial carrier; phosphate carrier); member 3	CCDS9
CGOV62T_2	Exome	TP53	tumor protein p53	CCDS1
CGOV62T_2	Exome	TRIO	triple functional domain (PTPRF interacting)	CCDS3
CGOV62T_2	Exome	USP34	ubiquitin specific peptidase 34	CCDS4
CGOV62T_2	Exome	WDR11	WD repeat domain 11	CCDS7
CGOV62T_2	Exome	ZBBX	zinc finger; B-box domain containing	CCDS3
CGOV62T_2	Exome	ZNF71	zinc finger protein 71	CCDS1
CGOV62T_10	Exome	ANKFN1	ankyrin-repeat and fibronectin type III domain containing 1	CCDS3
CGOV62T_10	Exome	ANKRD35	ankyrin repeat domain 35	CCDS9
CGOV62T_10	Exome	APOB	apolipoprotein B (including Ag(x) antigen)	CCDS1
CGOV62T_10	Exome	BTNL9	butyrophilin-like 9	CCDS4
CGOV62T_10	Exome	C1S	complement component 1; s subcomponent	CCDS3
CGOV62T_10	Exome	C4orf43	chromosome 4 open reading frame 43	CCDS4
CGOV62T_10	Exome	C5orf25	chromosome 5 open reading frame 25	CCDS4
CGOV62T_10	Exome	C5orf46	chromosome 5 open reading frame 46	CCDS3
CGOV62T_10	Exome	C6	complement component 6	CCDS3

CGOV62T_10	Exome	CDKAL1	CDK5 regulatory subunit associated protein 1-like 1	CCDS4
CGOV62T_10	Exome	DNAH6	dynein heavy chain 6, axonemal	NM_00
CGOV62T_10	Exome	DUSP27	dual specificity phosphatase 27 (putative)	CCDS3
CGOV62T_10	Exome	EPHA5	EPH receptor A5	CCDS3
CGOV62T_10	Exome	FAM5C	family with sequence similarity 5; member C	CCDS1
CGOV62T_10	Exome	KIF17	kinesin family member 17	CCDS2
CGOV62T_10	Exome	KIF3C	kinesin family member 3C	CCDS1
CGOV62T_10	Exome	PRSS23	protease; serine; 23	CCDS4
CGOV62T_10	Exome	RANBP2	RAN binding protein 2	CCDS2
CGOV62T_10	Exome	RHBDD1	rhomboid domain containing 1	CCDS2
CGOV62T_10	Exome	ROBO1	roundabout homolog 1 isoform a precursor	NM_00
CGOV62T_10	Exome	SEMA3F	sema domain; immunoglobulin domain (Ig); short basic domain; secreted; (semaphorin) 3F	CCDS2
CGOV62T_10	Exome	SI	sucrase-isomaltase (alpha-glucosidase)	CCDS3
CGOV62T_10	Exome	SLC1A2	solute carrier family 1 (glial high affinity glutamate transporter); member 2	CCDS3
CGOV62T_10	Exome	SLC25A3	solute carrier family 25 (mitochondrial carrier; phosphate carrier); member 3	CCDS9
CGOV62T_10	Exome	TP53	tumor protein p53	CCDS1
CGOV62T_10	Exome	TRIO	triple functional domain (PTPRF interacting)	CCDS3
CGOV62T_10	Exome	USP34	ubiquitin specific peptidase 34	CCDS4
CGOV62T_10	Exome	WDR11	WD repeat domain 11	CCDS7
CGOV62T_10	Exome	ZBBX	zinc finger; B-box domain containing	CCDS3
CGOV62T_10	Exome	ZNF71	zinc finger protein 71	CCDS1
CGOV62T_1	Exome	ANKFN1	ankyrin-repeat and fibronectin type III domain containing 1	CCDS3

CGOV62T_1	Exome	ANKRD35	ankyrin repeat domain 35	CCDS9
CGOV62T_1	Exome	APOB	apolipoprotein B (including Ag(x) antigen)	CCDS1
CGOV62T_1	Exome	BTNL9	butyrophilin-like 9	CCDS4
CGOV62T_1	Exome	C1S	complement component 1; s subcomponent	CCDS3
CGOV62T_1	Exome	C4orf43	chromosome 4 open reading frame 43	CCDS4
CGOV62T_1	Exome	C5orf25	chromosome 5 open reading frame 25	CCDS4
CGOV62T_1	Exome	C5orf46	chromosome 5 open reading frame 46	CCDS3
CGOV62T_1	Exome	C6	complement component 6	CCDS3
CGOV62T_1	Exome	CDKAL1	CDK5 regulatory subunit associated protein 1-like 1	CCDS4
CGOV62T_1	Exome	DNAH6	dynein heavy chain 6, axonemal	NM_00
CGOV62T_1	Exome	DUSP27	dual specificity phosphatase 27 (putative)	CCDS3
CGOV62T_1	Exome	EPHA5	EPH receptor A5	CCDS3
CGOV62T_1	Exome	FAM5C	family with sequence similarity 5; member C	CCDS1
CGOV62T_1	Exome	KIF17	kinesin family member 17	CCDS2
CGOV62T_1	Exome	KIF3C	kinesin family member 3C	CCDS1
CGOV62T_1	Exome	PRSS23	protease; serine; 23	CCDS4
CGOV62T_1	Exome	RANBP2	RAN binding protein 2	CCDS2
CGOV62T_1	Exome	RHBDD1	rhomboid domain containing 1	CCDS2
CGOV62T_1	Exome	ROBO1	roundabout homolog 1 isoform a precursor	NM_00
CGOV62T_1	Exome	SEMA3F	sema domain; immunoglobulin domain (Ig); short basic domain; secreted; (semaphorin) 3F	CCDS2
CGOV62T_1	Exome	SI	sucrase-isomaltase (alpha-glucosidase)	CCDS3
CGOV62T_1	Exome	SLC1A2	solute carrier family 1 (glial high affinity glutamate transporter); member 2	CCDS3
CGOV62T_1	Exome	SLC25A3	solute carrier family 25 (mitochondrial carrier; phosphate carrier); member 3	CCDS9

CGOV62T_1	Exome	TP53	tumor protein p53	CCDS1
CGOV62T_1	Exome	TRIO	triple functional domain (PTPRF interacting)	CCDS3
CGOV62T_1	Exome	USP34	ubiquitin specific peptidase 34	CCDS4
CGOV62T_1	Exome	WDR11	WD repeat domain 11	CCDS7
CGOV62T_1	Exome	ZBBX	zinc finger; B-box domain containing	CCDS3
CGOV62T_1	Exome	ZNF71	zinc finger protein 71	CCDS1
CGOV62T	Exome	ANKFN1	ankyrin-repeat and fibronectin type III domain containing 1	CCDS3
CGOV62T	Exome	ANKRD35	ankyrin repeat domain 35	CCDS9
CGOV62T	Exome	APOB	apolipoprotein B (including Ag(x) antigen)	CCDS1
CGOV62T	Exome	BTNL9	butyrophilin-like 9	CCDS4
CGOV62T	Exome	C1S	complement component 1; s subcomponent	CCDS3
CGOV62T	Exome	C4orf43	chromosome 4 open reading frame 43	CCDS4
CGOV62T	Exome	C5orf25	chromosome 5 open reading frame 25	CCDS4
CGOV62T	Exome	C5orf46	chromosome 5 open reading frame 46	CCDS3
CGOV62T	Exome	C6	complement component 6	CCDS3
CGOV62T	Exome	CDKAL1	CDK5 regulatory subunit associated protein 1-like 1	CCDS4
CGOV62T	Exome	DNAH6	dynein heavy chain 6, axonemal	NM_00
CGOV62T	Exome	DUSP27	dual specificity phosphatase 27 (putative)	CCDS3
CGOV62T	Exome	EPHA5	EPH receptor A5	CCDS3
CGOV62T	Exome	FAM5C	family with sequence similarity 5; member C	CCDS1
CGOV62T	Exome	KIF17	kinesin family member 17	CCDS2
CGOV62T	Exome	KIF3C	kinesin family member 3C	CCDS1
CGOV62T	Exome	PRSS23	protease; serine; 23	CCDS4
CGOV62T	Exome	RANBP2	RAN binding protein 2	CCDS2
CGOV62T	Exome	RHBDD1	rhomboid domain containing 1	CCDS2

CGOV62T	Exome	ROBO1	roundabout homolog 1 isoform a precursor	NM_00
CGOV62T	Exome	SEMA3F	sema domain; immunoglobulin domain (Ig); short basic domain; secreted; (semaphorin) 3F	CCDS2
CGOV62T	Exome	SI	sucrase-isomaltase (alpha-glucosidase)	CCDS3
CGOV62T	Exome	SLC1A2	solute carrier family 1 (glial high affinity glutamate transporter); member 2	CCDS3
CGOV62T	Exome	SLC25A3	solute carrier family 25 (mitochondrial carrier; phosphate carrier); member 3	CCDS9
CGOV62T	Exome	TP53	tumor protein p53	CCDS1
CGOV62T	Exome	TRIO	triple functional domain (PTPRF interacting)	CCDS3
CGOV62T	Exome	USP34	ubiquitin specific peptidase 34	CCDS4
CGOV62T	Exome	WDR11	WD repeat domain 11	CCDS7
CGOV62T	Exome	ZBBX	zinc finger; B-box domain containing	CCDS3
CGOV62T	Exome	ZNF71	zinc finger protein 71	CCDS1
CGOV304T	Exome	ANKRD62	ankyrin repeat domain 62	NM_00
CGOV304T	Exome	ANXA1	annexin A1	CCDS6
CGOV304T	Exome	ARFGAP3	ADP-ribosylation factor GTPase activating protein 3	CCDS1
CGOV304T	Exome	ASPM	asp (abnormal spindle) homolog, microcephaly associated (Drosophila)	CCDS1
CGOV304T	Exome	ATF6	activating transcription factor 6	CCDS1
CGOV304T	Exome	BMP2K	BMP2 inducible kinase	CCDS4
CGOV304T	Exome	CDH26	cadherin 26	CCDS1
CGOV304T	Exome	CDK18	cyclin-dependent kinase 18	CCDS1
CGOV304T	Exome	COL17A1	collagen, type XVII, alpha 1	CCDS7
CGOV304T	Exome	DAPK1	death-associated protein kinase 1	CCDS4
CGOV304T	Exome	DDX47	DEAD (Asp-Glu-Ala-Asp) box polypeptide 47	CCDS8

CGOV304T	Exome	DOCK8	dedicator of cytokinesis 8	CCDS6
CGOV304T	Exome	DUSP27	dual specificity phosphatase 27 (putative)	CCDS3
CGOV304T	Exome	FA2H	fatty acid 2-hydroxylase	CCDS1
CGOV304T	Exome	FAM186B	family with sequence similarity 186, member B	CCDS8
CGOV304T	Exome	FCER2	Fc fragment of IgE, low affinity II, receptor for (CD23)	CCDS1
CGOV304T	Exome	FOLR1	folate receptor 1 (adult)	CCDS8
CGOV304T	Exome	GALNT3	UDP-N-acetyl-alpha-D-galactosamine:polypeptide N-acetylgalactosaminyltransferase 3 (GalNAc-T3)	CCDS2
CGOV304T	Exome	GLCE	glucuronic acid epimerase	CCDS3
CGOV304T	Exome	GP9	glycoprotein IX (platelet)	CCDS3
CGOV304T	Exome	HECW1	HECT, C2 and WW domain containing E3 ubiquitin protein ligase 1	CCDS5
CGOV304T	Exome	JMJD7-PLA2G4B	JMJD7-PLA2G4B readthrough	CCDS3
CGOV304T	Exome	KBTBD8	kelch repeat and BTB (POZ) domain containing 8	CCDS2
CGOV304T	Exome	KIAA1462	KIAA1462	CCDS4
CGOV304T	Exome	LRRC16B	leucine rich repeat containing 16B	CCDS3
CGOV304T	Exome	LRRFIP2	leucine rich repeat (in FLII) interacting protein 2	CCDS2
CGOV304T	Exome	LYNX1	Ly6/neurotoxin 1	CCDS3
CGOV304T	Exome	MAEA	macrophage erythroblast attacher	CCDS3
CGOV304T	Exome	MUC19	mucin 19, oligomeric	NM_17
CGOV304T	Exome	NPDC1	neural proliferation, differentiation and control, 1	CCDS7
CGOV304T	Exome	PAPPA	pregnancy-associated plasma protein A, pappalysin 1	CCDS6
CGOV304T	Exome	PDE1C	phosphodiesterase 1C, calmodulin-dependent 70kDa	CCDS5
CGOV304T	Exome	PLCE1	phospholipase C, epsilon 1	CCDS4

CGOV304T	Exome	R3HDML	R3H domain containing-like	CCDS1
CGOV304T	Exome	SALL3	sal-like 3 (Drosophila)	CCDS1
CGOV304T	Exome	SCN2A	sodium channel, voltage-gated, type II, alpha subunit	CCDS3
CGOV304T	Exome	SPPL3	signal peptide peptidase like 3	CCDS9
CGOV304T	Exome	SULT1B1	sulfotransferase family, cytosolic, 1B, member 1	CCDS3
CGOV304T	Exome	TAF1L	TAF1 RNA polymerase II, TATA box binding protein (TBP)-associated factor, 210kDa-like	CCDS3
CGOV304T	Exome	TINF2	TERF1 (TRF1)-interacting nuclear factor 2	CCDS4
CGOV304T	Exome	TLR10	toll-like receptor 10	CCDS3
CGOV304T	Exome	TMEM215	transmembrane protein 215	CCDS6
CGOV304T	Exome	TP53	tumor protein p53	CCDS1
CGOV304T	Exome	ZMYM3	zinc finger, MYM-type 3	CCDS1
CGOV304T	Exome	ZNF292	zinc finger protein 292	CCDS4
CGOV304T	Exome	ZNF41	zinc finger protein 41	CCDS1
CGOV303T1	Exome	AGXT2	alanine--glyoxylate aminotransferase 2	CCDS3
CGOV303T1	Exome	BATF	basic leucine zipper transcription factor, ATF-like	CCDS9
CGOV303T1	Exome	CDH23	cadherin-related 23	NM_00
CGOV303T1	Exome	DMD	dystrophin	CCDS1
CGOV303T1	Exome	EMP3	epithelial membrane protein 3	CCDS1
CGOV303T1	Exome	IGSF9	immunoglobulin superfamily, member 9	CCDS4
CGOV303T1	Exome	KIF1A	kinesin family member 1A	CCDS5
CGOV303T1	Exome	KIF1A	kinesin family member 1A	CCDS5
CGOV303T1	Exome	NOTCH3	notch 3	CCDS1
CGOV303T1	Exome	OFD1	oral-facial-digital syndrome 1	CCDS1

CGOV303T1	Exome	PIK3CA	phosphatidylinositol-4,5-bisphosphate 3-kinase, catalytic subunit alpha	CCDS4
CGOV303T1	Exome	R3HDM1	R3H domain containing 1	CCDS2
CGOV303T1	Exome	RAP1GAP	RAP1 GTPase activating protein	CCDS5
CGOV303T1	Exome	RASL12	RAS-like, family 12	CCDS1
CGOV303T1	Exome	SLC38A10	solute carrier family 38, member 10	CCDS1
CGOV303T1	Exome	SLCO4C1	solute carrier organic anion transporter family, member 4C1	CCDS3
CGOV303T1	Exome	SOX6	SRY (sex determining region Y)-box 6	CCDS7
CGOV303T1	Exome	SPPL2C	signal peptide peptidase like 2C	CCDS3
CGOV303T1	Exome	TEP1	telomerase-associated protein 1	CCDS9
CGOV303T1	Exome	TM4SF20	transmembrane 4 L six family member 20	CCDS2
CGOV303T1	Exome	TP53	tumor protein p53	CCDS1
CGOV303T1	Exome	VAV3	vav 3 guanine nucleotide exchange factor	CCDS7
CGOV303T	Exome	ABCB6	ATP-binding cassette, sub-family B (MDR/TAP), member 6	CCDS2
CGOV303T	Exome	AGXT2	alanine--glyoxylate aminotransferase 2	CCDS3
CGOV303T	Exome	AGXT2	alanine--glyoxylate aminotransferase 2	CCDS3
CGOV303T	Exome	ASAP1	ArfGAP with SH3 domain, ankyrin repeat and PH domain 1	CCDS6
CGOV303T	Exome	BATF	basic leucine zipper transcription factor, ATF-like	CCDS9
CGOV303T	Exome	CDH23	cadherin-related 23	NM_00
CGOV303T	Exome	DMD	dystrophin	CCDS1
CGOV303T	Exome	GTPBP2	GTP binding protein 2	CCDS4
CGOV303T	Exome	HTR5A	5-hydroxytryptamine (serotonin) receptor 5A, G protein-coupled	CCDS5
CGOV303T	Exome	HUWE1	HECT, UBA and WWE domain containing 1, E3 ubiquitin protein ligase	CCDS3

CGOV303T	Exome	KIF1A	kinesin family member 1A	CCDS5
CGOV303T	Exome	KMT2C	lysine (K)-specific methyltransferase 2C	CCDS5
CGOV303T	Exome	NOTCH3	notch 3	CCDS1
CGOV303T	Exome	OR13A1	olfactory receptor, family 13, subfamily A, member 1	CCDS3
CGOV303T	Exome	PIK3CA	phosphatidylinositol-4,5-bisphosphate 3-kinase, catalytic subunit alpha	CCDS4
CGOV303T	Exome	PRRC2C	proline-rich coiled-coil 2C	CCDS1
CGOV303T	Exome	PYGM	phosphorylase, glycogen, muscle	CCDS8
CGOV303T	Exome	R3HDM1	R3H domain containing 1	CCDS2
CGOV303T	Exome	RAP1GAP	RAP1 GTPase activating protein	CCDS5
CGOV303T	Exome	RASL12	RAS-like, family 12	CCDS1
CGOV303T	Exome	SASS6	spindle assembly 6 homolog (C. elegans)	CCDS7
CGOV303T	Exome	SLCO4C1	solute carrier organic anion transporter family, member 4C1	CCDS3
CGOV303T	Exome	SOX6	SRY (sex determining region Y)-box 6	CCDS7
CGOV303T	Exome	SPPL2C	signal peptide peptidase like 2C	CCDS3
CGOV303T	Exome	SYNE1	spectrin repeat containing, nuclear envelope 1	CCDS5
CGOV303T	Exome	TCTE1	t-complex-associated-testis-expressed 1	CCDS4
CGOV303T	Exome	TEP1	telomerase-associated protein 1	CCDS9
CGOV303T	Exome	TM4SF20	transmembrane 4 L six family member 20	CCDS2
CGOV303T	Exome	TP53	tumor protein p53	CCDS1
CGOV303T	Exome	UHRF1	ubiquitin-like with PHD and ring finger domains 1	NM_01
CGOV303T	Exome	USP29	ubiquitin specific peptidase 29	CCDS3
CGOV303T	Exome	VAV3	vav 3 guanine nucleotide exchange factor	CCDS7
CGOV303T	Exome	ZMYND15	zinc finger, MYND-type containing 15	CCDS5
CGOV280T6	Exome	ADAMTSL 4	ADAMTS-like 4	CCDS9

CGOV280T6	Exome	C1orf173	chromosome 1 open reading frame 173	CCDS3
CGOV280T6	Exome	FLG2	filaggrin family member 2	CCDS3
CGOV280T6	Exome	FOXG1	forkhead box G1	CCDS9
CGOV280T6	Exome	GPR25	G protein-coupled receptor 25	CCDS1
CGOV280T6	Exome	INPP5E		CCDS7
CGOV280T6	Exome	ISM1		CCDS4
CGOV280T6	Exome	LPIN3		CCDS3
CGOV280T6	Exome	LRP1		CCDS8
CGOV280T6	Exome	MRPS12	mitochondrial ribosomal protein S12	CCDS1
CGOV280T6	Exome	MS4A14		CCDS5
CGOV280T6	Exome	NALCN	sodium leak channel, non-selective	CCDS9
CGOV280T6	Exome	NOS1AP	nitric oxide synthase 1 (neuronal) adaptor protein	CCDS1
CGOV280T6	Exome	NPAP1	nuclear pore associated protein 1	CCDS1
CGOV280T6	Exome	REV3L	REV3-like, polymerase (DNA directed), zeta, catalytic subunit	CCDS5
CGOV280T6	Exome	RHBDL3	rhomboid, veinlet-like 3 (Drosophila)	CCDS3
CGOV280T6	Exome	SETBP1		CCDS4
CGOV280T6	Exome	SLX4	SLX4 structure-specific endonuclease subunit	CCDS1
CGOV280T6	Exome	XIRP2	xin actin-binding repeat containing 2	CCDS4
CGOV280T6	Exome	ZMYM6	zinc finger, MYM-type 6	CCDS3
CGOV280T5	Exome	ABCA13	ATP-binding cassette, sub-family A (ABC1), member 13	CCDS4
CGOV280T5	Exome	ADAMTSL 4	ADAMTS-like 4	CCDS9
CGOV280T5	Exome	ASB15	ankyrin repeat and SOCS box containing 15	CCDS3
CGOV280T5	Exome	C1orf173	chromosome 1 open reading frame 173	CCDS3
CGOV280T5	Exome	CACNA1C	calcium channel, voltage-dependent, L type, alpha 1C subunit	CCDS4

CGOV280T5	Exome	CCR2	chemokine (C-C motif) receptor 2	CCDS4
CGOV280T5	Exome	CDC5L	cell division cycle 5-like	CCDS4
CGOV280T5	Exome	DNAH3	dynein, axonemal, heavy chain 3	CCDS1
CGOV280T5	Exome	DUSP27	dual specificity phosphatase 27 (putative)	CCDS3
CGOV280T5	Exome	FLG2	filaggrin family member 2	CCDS3
CGOV280T5	Exome	FOXG1	forkhead box G1	CCDS9
CGOV280T5	Exome	GPR158	G protein-coupled receptor 158	CCDS3
CGOV280T5	Exome	GPR25	G protein-coupled receptor 25	CCDS1
CGOV280T5	Exome	INPP5E		CCDS7
CGOV280T5	Exome	ISM1		CCDS4
CGOV280T5	Exome	LPIN3		CCDS3
CGOV280T5	Exome	LRP1		CCDS8
CGOV280T5	Exome	MRPS12	mitochondrial ribosomal protein S12	CCDS1
CGOV280T5	Exome	MS4A14		CCDS5
CGOV280T5	Exome	MTA3	metastasis associated 1 family, member 3	CCDS4
CGOV280T5	Exome	NALCN	sodium leak channel, non-selective	CCDS9
CGOV280T5	Exome	NOS1AP	nitric oxide synthase 1 (neuronal) adaptor protein	CCDS1
CGOV280T5	Exome	NPAP1	nuclear pore associated protein 1	CCDS1
CGOV280T5	Exome	PCDHGB4	protocadherin gamma subfamily B, 4	CCDS5
CGOV280T5	Exome	PDE2A	phosphodiesterase 2A, cGMP-stimulated	CCDS8
CGOV280T5	Exome	PPP1CC	protein phosphatase 1, catalytic subunit, gamma isozyme	CCDS5
CGOV280T5	Exome	PREX1	phosphatidylinositol-3,4,5-trisphosphate-dependent Rac exchange factor 1	CCDS1
CGOV280T5	Exome	REV3L	REV3-like, polymerase (DNA directed), zeta, catalytic subunit	CCDS5
CGOV280T5	Exome	RHBDL3	rhomboid, veinlet-like 3 (Drosophila)	CCDS3

CGOV280T5	Exome	SETBP1		CCDS4
CGOV280T5	Exome	SETD2	SET domain containing 2	CCDS2
CGOV280T5	Exome	SHPRH	SNF2 histone linker PHD RING helicase, E3 ubiquitin protein ligase	CCDS4
CGOV280T5	Exome	SLX4	SLX4 structure-specific endonuclease subunit	CCDS1
CGOV280T5	Exome	ST18	suppression of tumorigenicity 18 (breast carcinoma) (zinc finger protein)	CCDS6
CGOV280T5	Exome	TMEM64	transmembrane protein 64	CCDS3
CGOV280T5	Exome	TP53	tumor protein p53	CCDS1
CGOV280T5	Exome	TRHR	thyrotropin-releasing hormone receptor	CCDS6
CGOV280T5	Exome	TRIML1	tripartite motif family-like 1	CCDS3
CGOV280T5	Exome	TTN	titin	CCDS5
CGOV280T5	Exome	XIRP2	xin actin-binding repeat containing 2	CCDS4
CGOV280T5	Exome	ZMIZ2	zinc finger, MIZ-type containing 2	CCDS4
CGOV280T5	Exome	ZMYM6	zinc finger, MYM-type 6	CCDS3
CGOV280T4	Exome	ABCA13	ATP-binding cassette, sub-family A (ABC1), member 13	CCDS4
CGOV280T4	Exome	ADAMTSL 4	ADAMTS-like 4	CCDS9
CGOV280T4	Exome	ASB15	ankyrin repeat and SOCS box containing 15	CCDS3
CGOV280T4	Exome	C1orf173	chromosome 1 open reading frame 173	CCDS3
CGOV280T4	Exome	CACNA1C	calcium channel, voltage-dependent, L type, alpha 1C subunit	CCDS4
CGOV280T4	Exome	CCR2	chemokine (C-C motif) receptor 2	CCDS4
CGOV280T4	Exome	DNAH3	dynein, axonemal, heavy chain 3	CCDS1
CGOV280T4	Exome	DUSP27	dual specificity phosphatase 27 (putative)	CCDS3
CGOV280T4	Exome	EFCAB4B	EF-hand calcium binding domain 4B	CCDS4
CGOV280T4	Exome	FLG2	filaggrin family member 2	CCDS3

CGOV280T4	Exome	GPR158	G protein-coupled receptor 158	CCDS3
CGOV280T4	Exome	GPR25	G protein-coupled receptor 25	CCDS1
CGOV280T4	Exome	GRM7	glutamate receptor, metabotropic 7	CCDS4
CGOV280T4	Exome	INPP5E		CCDS7
CGOV280T4	Exome	ISM1		CCDS4
CGOV280T4	Exome	LPIN3		CCDS3
CGOV280T4	Exome	LRP1		CCDS8
CGOV280T4	Exome	MS4A14		CCDS5
CGOV280T4	Exome	MTA3	metastasis associated 1 family, member 3	CCDS4
CGOV280T4	Exome	NALCN	sodium leak channel, non-selective	CCDS9
CGOV280T4	Exome	PARN	poly(A)-specific ribonuclease	CCDS4
CGOV280T4	Exome	PCDHGB4	protocadherin gamma subfamily B, 4	CCDS5
CGOV280T4	Exome	PDE2A	phosphodiesterase 2A, cGMP-stimulated	CCDS8
CGOV280T4	Exome	PREX1	phosphatidylinositol-3,4,5-trisphosphate-dependent Rac exchange factor 1	CCDS1
CGOV280T4	Exome	SETBP1		CCDS4
CGOV280T4	Exome	SETD2	SET domain containing 2	CCDS2
CGOV280T4	Exome	SHPRH	SNF2 histone linker PHD RING helicase, E3 ubiquitin protein ligase	CCDS4
CGOV280T4	Exome	SLX4	SLX4 structure-specific endonuclease subunit	CCDS1
CGOV280T4	Exome	ST18	suppression of tumorigenicity 18 (breast carcinoma) (zinc finger protein)	CCDS6
CGOV280T4	Exome	STK36	serine/threonine kinase 36	CCDS2
CGOV280T4	Exome	TMEM64	transmembrane protein 64	CCDS3
CGOV280T4	Exome	TP53	tumor protein p53	CCDS1
CGOV280T4	Exome	TRHR	thyrotropin-releasing hormone receptor	CCDS6

CGOV280T4	Exome	TRIML1	tripartite motif family-like 1	CCDS3
CGOV280T4	Exome	TTN	titin	CCDS5
CGOV280T4	Exome	XIRP2	xin actin-binding repeat containing 2	CCDS4
CGOV280T4	Exome	ZFHX4	zinc finger homeobox 4	CCDS4
CGOV280T4	Exome	ZMIZ2	zinc finger, MIZ-type containing 2	CCDS4
CGOV280T4	Exome	ZMYM6	zinc finger, MYM-type 6	CCDS3
CGOV280T4	Exome	ZNF804B	zinc finger protein 804B	CCDS5
CGOV280T3	Exome	ABCA13	ATP-binding cassette, sub-family A (ABC1), member 13	CCDS4
CGOV280T3	Exome	ADAMTSL 4	ADAMTS-like 4	CCDS9
CGOV280T3	Exome	ASB15	ankyrin repeat and SOCS box containing 15	CCDS3
CGOV280T3	Exome	C1orf173	chromosome 1 open reading frame 173	CCDS3
CGOV280T3	Exome	CACNA1C	calcium channel, voltage-dependent, L type, alpha 1C subunit	CCDS4
CGOV280T3	Exome	CCR2	chemokine (C-C motif) receptor 2	CCDS4
CGOV280T3	Exome	DNAH3	dynein, axonemal, heavy chain 3	CCDS1
CGOV280T3	Exome	DUSP27	dual specificity phosphatase 27 (putative)	CCDS3
CGOV280T3	Exome	FLG2	filaggrin family member 2	CCDS3
CGOV280T3	Exome	FOXG1	forkhead box G1	CCDS9
CGOV280T3	Exome	GPR158	G protein-coupled receptor 158	CCDS3
CGOV280T3	Exome	GPR25	G protein-coupled receptor 25	CCDS1
CGOV280T3	Exome	INPP5E		CCDS7
CGOV280T3	Exome	IQSEC1	IQ motif and Sec7 domain 1	CCDS3
CGOV280T3	Exome	ISM1		CCDS4
CGOV280T3	Exome	LPIN3		CCDS3
CGOV280T3	Exome	LRP1		CCDS8

CGOV280T3	Exome	MS4A14		CCDS5
CGOV280T3	Exome	MTA3	metastasis associated 1 family, member 3	CCDS4
CGOV280T3	Exome	NALCN	sodium leak channel, non-selective	CCDS9
CGOV280T3	Exome	NOS1AP	nitric oxide synthase 1 (neuronal) adaptor protein	CCDS1
CGOV280T3	Exome	NPAP1	nuclear pore associated protein 1	CCDS1
CGOV280T3	Exome	PCDHGB4	protocadherin gamma subfamily B, 4	CCDS5
CGOV280T3	Exome	PDE2A	phosphodiesterase 2A, cGMP-stimulated	CCDS8
CGOV280T3	Exome	POU3F2	POU class 3 homeobox 2	CCDS5
CGOV280T3	Exome	PREX1	phosphatidylinositol-3,4,5-trisphosphate-dependent Rac exchange factor 1	CCDS1
CGOV280T3	Exome	SETBP1		CCDS4
CGOV280T3	Exome	SHPRH	SNF2 histone linker PHD RING helicase, E3 ubiquitin protein ligase	CCDS4
CGOV280T3	Exome	SLX4	SLX4 structure-specific endonuclease subunit	CCDS1
CGOV280T3	Exome	ST18	suppression of tumorigenicity 18 (breast carcinoma) (zinc finger protein)	CCDS6
CGOV280T3	Exome	TMEM64	transmembrane protein 64	CCDS3
CGOV280T3	Exome	TP53	tumor protein p53	CCDS1
CGOV280T3	Exome	TRHR	thyrotropin-releasing hormone receptor	CCDS6
CGOV280T3	Exome	TRIML1	tripartite motif family-like 1	CCDS3
CGOV280T3	Exome	TTN	titin	CCDS5
CGOV280T3	Exome	XIRP2	xin actin-binding repeat containing 2	CCDS4
CGOV280T3	Exome	ZMIZ2	zinc finger, MIZ-type containing 2	CCDS4
CGOV280T3	Exome	ZMYM6	zinc finger, MYM-type 6	CCDS3
CGOV280T2	Exome	ABCA13	ATP-binding cassette, sub-family A (ABC1), member 13	CCDS4
CGOV280T2	Exome	ASB15	ankyrin repeat and SOCS box containing 15	CCDS3

CGOV280T2	Exome	C1orf173	chromosome 1 open reading frame 173	CCDS3
CGOV280T2	Exome	CACNA1C	calcium channel, voltage-dependent, L type, alpha 1C subunit	CCDS4
CGOV280T2	Exome	CACNB4	calcium channel, voltage-dependent, beta 4 subunit	CCDS4
CGOV280T2	Exome	CCR2	chemokine (C-C motif) receptor 2	CCDS4
CGOV280T2	Exome	DNAH3	dynein, axonemal, heavy chain 3	CCDS1
CGOV280T2	Exome	DNAH6	dynein, axonemal, heavy chain 6	CCDS4
CGOV280T2	Exome	DUSP27	dual specificity phosphatase 27 (putative)	CCDS3
CGOV280T2	Exome	EYA3	eyes absent homolog 3 (Drosophila)	CCDS3
CGOV280T2	Exome	FLG2	filaggrin family member 2	CCDS3
CGOV280T2	Exome	GALNT16	UDP-N-acetyl-alpha-D-galactosamine:polypeptide N-acetylgalactosaminyltransferase 16	CCDS3
CGOV280T2	Exome	GP6	glycoprotein VI (platelet)	CCDS4
CGOV280T2	Exome	GPR158	G protein-coupled receptor 158	CCDS3
CGOV280T2	Exome	GPR25	G protein-coupled receptor 25	CCDS1
CGOV280T2	Exome	GPRC5B	G protein-coupled receptor, family C, group 5, member B	CCDS1
CGOV280T2	Exome	INPP5E		CCDS7
CGOV280T2	Exome	ISM1		CCDS4
CGOV280T2	Exome	LPIN3		CCDS3
CGOV280T2	Exome	LRP1		CCDS8
CGOV280T2	Exome	MS4A14		CCDS5
CGOV280T2	Exome	MTA3	metastasis associated 1 family, member 3	CCDS4
CGOV280T2	Exome	PCDHGB4	protocadherin gamma subfamily B, 4	CCDS5
CGOV280T2	Exome	PDE2A	phosphodiesterase 2A, cGMP-stimulated	CCDS8
CGOV280T2	Exome	PER1	period circadian clock 1	CCDS1

CGOV280T2	Exome	PREX1	phosphatidylinositol-3,4,5-trisphosphate-dependent Rac exchange factor 1	CCDS1
CGOV280T2	Exome	SAMD4B	sterile alpha motif domain containing 4B	CCDS3
CGOV280T2	Exome	SETBP1		CCDS4
CGOV280T2	Exome	SETD2	SET domain containing 2	CCDS2
CGOV280T2	Exome	SHPRH	SNF2 histone linker PHD RING helicase, E3 ubiquitin protein ligase	CCDS4
CGOV280T2	Exome	ST18	suppression of tumorigenicity 18 (breast carcinoma) (zinc finger protein)	CCDS6
CGOV280T2	Exome	STK36	serine/threonine kinase 36	CCDS2
CGOV280T2	Exome	TMEM64	transmembrane protein 64	CCDS3
CGOV280T2	Exome	TP53	tumor protein p53	CCDS1
CGOV280T2	Exome	TRHR	thyrotropin-releasing hormone receptor	CCDS6
CGOV280T2	Exome	TRIML1	tripartite motif family-like 1	CCDS3
CGOV280T2	Exome	TTN	titin	CCDS5
CGOV280T2	Exome	XIRP2	xin actin-binding repeat containing 2	CCDS4
CGOV280T2	Exome	ZKSCAN8	zinc finger with KRAB and SCAN domains 8	CCDS4
CGOV280T2	Exome	ZMIZ2	zinc finger, MIZ-type containing 2	CCDS4
CGOV280T2	Exome	ZMYM6	zinc finger, MYM-type 6	CCDS3
CGOV280T6	Exome	ABCA13	ATP-binding cassette, sub-family A (ABC1), member 13	CCDS4
CGOV280T6	Exome	ASB15	ankyrin repeat and SOCS box containing 15	CCDS3
CGOV280T6	Exome	CACNA1C	calcium channel, voltage-dependent, L type, alpha 1C subunit	CCDS4
CGOV280T6	Exome	CCR2	chemokine (C-C motif) receptor 2	CCDS4
CGOV280T6	Exome	DNAH3	dynein, axonemal, heavy chain 3	CCDS1
CGOV280T6	Exome	DUSP27	dual specificity phosphatase 27 (putative)	CCDS3

CGOV280T6	Exome	GPR158	G protein-coupled receptor 158	CCDS3
CGOV280T6	Exome	MTA3	metastasis associated 1 family, member 3	CCDS4
CGOV280T6	Exome	PCDHGB4	protocadherin gamma subfamily B, 4	CCDS5
CGOV280T6	Exome	PDE2A	phosphodiesterase 2A, cGMP-stimulated	CCDS8
CGOV280T6	Exome	PREX1	phosphatidylinositol-3,4,5-trisphosphate-dependent Rac exchange factor 1	CCDS1
CGOV280T6	Exome	TMEM64	transmembrane protein 64	CCDS3
CGOV280T6	Exome	TP53	tumor protein p53	CCDS1
CGOV280T6	Exome	TRHR	thyrotropin-releasing hormone receptor	CCDS6
CGOV280T6	Exome	TRIML1	tripartite motif family-like 1	CCDS3
CGOV280T6	Exome	TTN	titin	CCDS5
CGOV280T6	Exome	ZMIZ2	zinc finger, MIZ-type containing 2	CCDS4
CGOV279T4	Exome	ARAP3	ArfGAP with RhoGAP domain, ankyrin repeat and PH domain 3	CCDS4
CGOV279T4	Exome	ATN1	atrophin 1	CCDS3
CGOV279T4	Exome	ATP13A3	ATPase type 13A3	CCDS4
CGOV279T4	Exome	C20orf194	chromosome 20 open reading frame 194	CCDS4
CGOV279T4	Exome	CD14	CD14 molecule	CCDS4
CGOV279T4	Exome	DLG5	discs, large homolog 5 (Drosophila)	CCDS7
CGOV279T4	Exome	EVC2	Ellis van Creveld syndrome 2	CCDS3
CGOV279T4	Exome	IGSF21	immunoglobin superfamily, member 21	CCDS1
CGOV279T4	Exome	KCNJ10	potassium inwardly-rectifying channel, subfamily J, member 10	CCDS1
CGOV279T4	Exome	KCNQ2	potassium voltage-gated channel, KQT-like subfamily, member 2	CCDS1
CGOV279T4	Exome	KIAA1614	KIAA1614	CCDS4
CGOV279T4	Exome	LAMA5	laminin, alpha 5	CCDS3

CGOV279T4	Exome	MB	myoglobin	CCDS1
CGOV279T4	Exome	MCL1	myeloid cell leukemia sequence 1 (BCL2-related)	CCDS9
CGOV279T4	Exome	NOL4	nucleolar protein 4	CCDS1
CGOV279T4	Exome	OR8S1	olfactory receptor, family 8, subfamily S, member 1	CCDS3
CGOV279T4	Exome	SLC13A3	solute carrier family 13 (sodium-dependent dicarboxylate transporter), member 3	CCDS1
CGOV279T4	Exome	SLC41A3	solute carrier family 41, member 3	CCDS3
CGOV279T4	Exome	SP9	Sp9 transcription factor	CCDS4
CGOV279T4	Exome	SV2C	synaptic vesicle glycoprotein 2C	CCDS4
CGOV279T4	Exome	TP53	tumor protein p53	CCDS1
CGOV279T4	Exome	TRPC7	transient receptor potential cation channel, subfamily C, member 7	CCDS4
CGOV279T4	Exome	VPS16	vacuolar protein sorting 16 homolog (S. cerevisiae)	CCDS1
CGOV279T3	Exome	ATN1	atrophin 1	CCDS3
CGOV279T3	Exome	ATP13A3	ATPase type 13A3	CCDS4
CGOV279T3	Exome	CD14	CD14 molecule	CCDS4
CGOV279T3	Exome	GRIN2B	glutamate receptor, ionotropic, N-methyl D-aspartate 2B	CCDS8
CGOV279T3	Exome	IGSF21	immunoglobin superfamily, member 21	CCDS1
CGOV279T3	Exome	KCNJ10	potassium inwardly-rectifying channel, subfamily J, member 10	CCDS1
CGOV279T3	Exome	KIAA1614	KIAA1614	CCDS4
CGOV279T3	Exome	NOL4	nucleolar protein 4	CCDS1
CGOV279T3	Exome	OR10W1	olfactory receptor, family 10, subfamily W, member 1	CCDS7
CGOV279T3	Exome	OR8S1	olfactory receptor, family 8, subfamily S, member 1	CCDS3
CGOV279T3	Exome	SLC13A3	solute carrier family 13 (sodium-dependent dicarboxylate transporter), member 3	CCDS1

CGOV279T3	Exome	SLC41A3	solute carrier family 41, member 3	CCDS3
CGOV279T3	Exome	SV2C	synaptic vesicle glycoprotein 2C	CCDS4
CGOV279T3	Exome	TP53	tumor protein p53	CCDS1
CGOV279T3	Exome	TRPC7	transient receptor potential cation channel, subfamily C, member 7	CCDS4
CGOV279T2	Exome	ATN1	atrophin 1	CCDS3
CGOV279T2	Exome	ATP13A3	ATPase type 13A3	CCDS4
CGOV279T2	Exome	CD14	CD14 molecule	CCDS4
CGOV279T2	Exome	GRIN2B	glutamate receptor, ionotropic, N-methyl D-aspartate 2B	CCDS8
CGOV279T2	Exome	IGSF21	immunoglobin superfamily, member 21	CCDS1
CGOV279T2	Exome	KCNJ10	potassium inwardly-rectifying channel, subfamily J, member 10	CCDS1
CGOV279T2	Exome	KIAA1614	KIAA1614	CCDS4
CGOV279T2	Exome	NOL4	nucleolar protein 4	CCDS1
CGOV279T2	Exome	OR10W1	olfactory receptor, family 10, subfamily W, member 1	CCDS7
CGOV279T2	Exome	OR8S1	olfactory receptor, family 8, subfamily S, member 1	CCDS3
CGOV279T2	Exome	SLC13A3	solute carrier family 13 (sodium-dependent dicarboxylate transporter), member 3	CCDS1
CGOV279T2	Exome	SLC41A3	solute carrier family 41, member 3	CCDS3
CGOV279T2	Exome	TP53	tumor protein p53	CCDS1
CGOV279T2	Exome	TRPC7	transient receptor potential cation channel, subfamily C, member 7	CCDS4
CGOV279T1	Exome	ATN1	atrophin 1	CCDS3
CGOV279T1	Exome	ATP13A3	ATPase type 13A3	CCDS4
CGOV279T1	Exome	CD14	CD14 molecule	CCDS4
CGOV279T1	Exome	GRIN2B	glutamate receptor, ionotropic, N-methyl D-aspartate 2B	CCDS8

CGOV279T1	Exome	IGSF21	immunoglobin superfamily, member 21	CCDS1
CGOV279T1	Exome	KCNJ10	potassium inwardly-rectifying channel, subfamily J, member 10	CCDS1
CGOV279T1	Exome	KIAA1614	KIAA1614	CCDS4
CGOV279T1	Exome	NOL4	nucleolar protein 4	CCDS1
CGOV279T1	Exome	OR10W1	olfactory receptor, family 10, subfamily W, member 1	CCDS7
CGOV279T1	Exome	OR8S1	olfactory receptor, family 8, subfamily S, member 1	CCDS3
CGOV279T1	Exome	SLC13A3	solute carrier family 13 (sodium-dependent dicarboxylate transporter), member 3	CCDS1
CGOV279T1	Exome	SLC41A3	solute carrier family 41, member 3	CCDS3
CGOV279T1	Exome	SV2C	synaptic vesicle glycoprotein 2C	CCDS4
CGOV279T1	Exome	TP53	tumor protein p53	CCDS1
CGOV279T1	Exome	TRPC7	transient receptor potential cation channel, subfamily C, member 7	CCDS4
CGOV278T4	Exome	ACTL10	actin-like 10	CCDS3
CGOV278T4	Exome	AHDC1	AT hook, DNA binding motif, containing 1	CCDS3
CGOV278T4	Exome	BAHCC1	BAH domain and coiled-coil containing 1	NM_00
CGOV278T4	Exome	COL6A5	collagen, type VI, alpha 5	NM_00
CGOV278T4	Exome	CREB3L1	cAMP responsive element binding protein 3-like 1	CCDS5
CGOV278T4	Exome	CTNND2	catenin (cadherin-associated protein), delta 2	CCDS3
CGOV278T4	Exome	ELL		CCDS1
CGOV278T4	Exome	EPPIN-WFDC6		CCDS5
CGOV278T4	Exome	GPATCH1	G patch domain containing 1	CCDS1
CGOV278T4	Exome	HKDC1	hexokinase domain containing 1	CCDS7
CGOV278T4	Exome	IGHMBP2	immunoglobulin mu binding protein 2	CCDS8
CGOV278T4	Exome	KCNAB1	potassium voltage-gated channel, shaker-related subfamily, beta member 1	CCDS3

CGOV278T4	Exome	KRT3	keratin 3	CCDS4
CGOV278T4	Exome	LCK	lymphocyte-specific protein tyrosine kinase	CCDS3
CGOV278T4	Exome	LMAN2	lectin, mannose-binding 2	CCDS4
CGOV278T4	Exome	MACF1	microtubule-actin crosslinking factor 1	CCDS4
CGOV278T4	Exome	MAGEC1	melanoma antigen family C, 1	CCDS3
CGOV278T4	Exome	METAP2	methionyl aminopeptidase 2	CCDS9
CGOV278T4	Exome	MPZ	myelin protein zero	CCDS1
CGOV278T4	Exome	NLRP5	NLR family, pyrin domain containing 5	CCDS1
CGOV278T4	Exome	NPFFR1		CCDS5
CGOV278T4	Exome	PTPRN	protein tyrosine phosphatase, receptor type, N	CCDS2
CGOV278T4	Exome	RAD9A		CCDS8
CGOV278T4	Exome	RNF148	ring finger protein 148	CCDS4
CGOV278T4	Exome	SERINC2	serine incorporator 2	CCDS5
CGOV278T4	Exome	SETD1A	SET domain containing 1A	CCDS3
CGOV278T4	Exome	SH3PXD2B	SH3 and PX domains 2B	CCDS3
CGOV278T4	Exome	SMARCA4		CCDS1
CGOV278T4	Exome	SYT12		CCDS8
CGOV278T4	Exome	SZT2	seizure threshold 2 homolog (mouse)	CCDS3
CGOV278T4	Exome	TMPPE	transmembrane protein with metallophosphoesterase domain	CCDS3
CGOV278T4	Exome	TP53	tumor protein p53	CCDS1
CGOV278T2	Exome	ABCG8	ATP-binding cassette, sub-family G (WHITE), member 8	CCDS1
CGOV278T2	Exome	ACTL10	actin-like 10	CCDS3
CGOV278T2	Exome	AHDC1	AT hook, DNA binding motif, containing 1	CCDS3
CGOV278T2	Exome	BAHCC1	BAH domain and coiled-coil containing 1	NM_00

CGOV278T2	Exome	COL6A5	collagen, type VI, alpha 5	NM_00
CGOV278T2	Exome	CREB3L1	cAMP responsive element binding protein 3-like 1	CCDS5
CGOV278T2	Exome	CTNND2	catenin (cadherin-associated protein), delta 2	CCDS3
CGOV278T2	Exome	ELL		CCDS1
CGOV278T2	Exome	EPPIN-WFDC6		CCDS5
CGOV278T2	Exome	GPATCH1	G patch domain containing 1	CCDS1
CGOV278T2	Exome	HKDC1	hexokinase domain containing 1	CCDS7
CGOV278T2	Exome	IGHMBP2	immunoglobulin mu binding protein 2	CCDS8
CGOV278T2	Exome	KCNAB1	potassium voltage-gated channel, shaker-related subfamily, beta member 1	CCDS3
CGOV278T2	Exome	KRT3	keratin 3	CCDS4
CGOV278T2	Exome	LCK	lymphocyte-specific protein tyrosine kinase	CCDS3
CGOV278T2	Exome	LMAN2	lectin, mannose-binding 2	CCDS4
CGOV278T2	Exome	MACF1	microtubule-actin crosslinking factor 1	CCDS4
CGOV278T2	Exome	MAGEC1	melanoma antigen family C, 1	CCDS3
CGOV278T2	Exome	METAP2	methionyl aminopeptidase 2	CCDS9
CGOV278T2	Exome	MPZ	myelin protein zero	CCDS1
CGOV278T2	Exome	NLRP5	NLR family, pyrin domain containing 5	CCDS1
CGOV278T2	Exome	NPFFR1		CCDS5
CGOV278T2	Exome	PCK2		CCDS9
CGOV278T2	Exome	PTPRN	protein tyrosine phosphatase, receptor type, N	CCDS2
CGOV278T2	Exome	RAD9A		CCDS8
CGOV278T2	Exome	RNF148	ring finger protein 148	CCDS4
CGOV278T2	Exome	SERINC2	serine incorporator 2	CCDS5
CGOV278T2	Exome	SETD1A	SET domain containing 1A	CCDS3

CGOV278T2	Exome	SH3PXD2B	SH3 and PX domains 2B	CCDS3
CGOV278T2	Exome	SMARCA4		CCDS1
CGOV278T2	Exome	SYT12		CCDS8
CGOV278T2	Exome	TMPPE	transmembrane protein with metallophosphoesterase domain	CCDS3
CGOV278T2	Exome	TP53	tumor protein p53	CCDS1
CGOV278T1	Exome	AHDC1	AT hook, DNA binding motif, containing 1	CCDS3
CGOV278T1	Exome	BAHCC1	BAH domain and coiled-coil containing 1	NM_00
CGOV278T1	Exome	COL6A5	collagen, type VI, alpha 5	NM_00
CGOV278T1	Exome	CREB3L1	cAMP responsive element binding protein 3-like 1	CCDS5
CGOV278T1	Exome	CTNND2	catenin (cadherin-associated protein), delta 2	CCDS3
CGOV278T1	Exome	ELL		CCDS1
CGOV278T1	Exome	EPPIN-WFDC6		CCDS5
CGOV278T1	Exome	GPATCH1	G patch domain containing 1	CCDS1
CGOV278T1	Exome	IGHMBP2	immunoglobulin mu binding protein 2	CCDS8
CGOV278T1	Exome	KCNAB1	potassium voltage-gated channel, shaker-related subfamily, beta member 1	CCDS3
CGOV278T1	Exome	KRT3	keratin 3	CCDS4
CGOV278T1	Exome	LMAN2	lectin, mannose-binding 2	CCDS4
CGOV278T1	Exome	MACF1	microtubule-actin crosslinking factor 1	CCDS4
CGOV278T1	Exome	METAP2	methionyl aminopeptidase 2	CCDS9
CGOV278T1	Exome	MPZ	myelin protein zero	CCDS1
CGOV278T1	Exome	NLRP5	NLR family, pyrin domain containing 5	CCDS1
CGOV278T1	Exome	PTPRN	protein tyrosine phosphatase, receptor type, N	CCDS2
CGOV278T1	Exome	RAD9A		CCDS8
CGOV278T1	Exome	SERINC2	serine incorporator 2	CCDS5

CGOV278T1	Exome	SMARCA4		CCDS1
CGOV278T1	Exome	TMPPE	transmembrane protein with metallophosphoesterase domain	CCDS3
CGOV278T1	Exome	TP53	tumor protein p53	CCDS1

Supplementary Data 2.5. Somatic Sequence Alterations used for Evolutionary Cluster Analyses

Case ID	Gene symbol	Nucleotide (genomic)	Amino Acid (protein)	Mutation T
CGOV62	TP53	chr17_7519279-7519279_A_T	126Y>N	Substitution
CGOV62	C5orf25	chr5_175681953-175681953_C_T	635T>M	Substitution
CGOV62	EPHA5	chr4_65872430-65872430_C_A	1037L>F	Substitution
CGOV62	SI	chr3_166199018-166199018_T_C	_ISV+4>	Substitution
CGOV62	SLC25A3	chr12_97515945-97515945_G_A	_ISV+1>	Substitution
CGOV62	WDR11	chr10_122616187-122616187_G_A	371A>T	Substitution
CGOV62	ZNF71	chr19_61825541-61825541_G_T	358E>D	Substitution
CGOV62	ANKFN1	chr17_51786312-51786312_C_T	172S>S	Substitution
CGOV62	ANKRD35	chr1_144274393-144274393_G_C	908T>T	Substitution
CGOV62	TRIO	chr5_14333529-14333529_C_T	111L>L	Substitution
CGOV62	C5orf46	chr5_147261489-147261489_C_G	37S>S	Substitution
CGOV62	APOB	chr2_21082355-21082355_C_G	3630K>N	Substitution
CGOV62	BTNL9	chr5_180407550-180407550_C_T	43P>S	Substitution
CGOV62	DNAH6	chr2_84686181-84686181_G_A	1043R>H	Substitution
CGOV62	FAM5C	chr1_188334053-188334053_C_A	673M>I	Substitution
CGOV62	KIF17	chr1_20881891-20881891_G_A	769R>W	Substitution
CGOV62	KIF3C	chr2_26057741-26057741_C_T	184V>I	Substitution
CGOV62	PRSS23	chr6_84290919-84290919_G_T	347G>V	Substitution
CGOV62	RANBP2	chr2_108746226-108746226_G_T	933M>I	Substitution
CGOV62	SEMA3F	chr3_50186311-50186311_A_G	65D>G	Substitution
CGOV62	SLC1A2	chr11_35279729-35279729_C_T	257G>E	Substitution
CGOV62	USP34	chr2_61369447-61369447_C_G	1540D>H	Substitution
CGOV62	ZBBX	chr3_168482852-168482852_C_A	669A>S	Substitution
CGOV62	RHBDD1	chr2_227437667-227437667_C_G	5S>X	Substitution
CGOV62	C4orf43	chr4_164656017-164656017_G_C	114K>N	Substitution
CGOV62	C6	chr5_41212475-41212475_T_C	343N>D	Substitution
CGOV62	DUSP27	chr1_165353281-165353281_G_A	100V>I	Substitution
CGOV62	C1S	chr12_7042822-7042822_G_A	225V>V	Substitution
CGOV62	ROBO1	chr3_78783747-78783747_T_A	879S>S	Substitution
CGOV62	CDKAL1	chr6_20889473-20889473_C_T	212T>T	Substitution
CGOV63	TP53	chr17_7518915-7518915_T_C	220Y>C	Substitution
CGOV63	CAPZA3	chr12_18783119-18783119_A_T	217N>I	Substitution
CGOV63	CLSPN	chr1_35975230-35975230_C_A	1261A>S	Substitution
CGOV63	HCK	chr20_30135444-30135444_G_A	186G>S	Substitution
CGOV63	LINGO4	chr1_150041185-150041185_A_G	207V>A	Substitution
CGOV63	ATP2B3	chrX_152468932-152468932_T_C	606L>S	Substitution
CGOV63	C12orf43	chr12_119926461-119926461_A_C	223S>A	Substitution
CGOV63	CSMD1	chr8_3002824-3002824_A_T	NA	Substitution
CGOV63	LRRC15	chr3_195562695-195562695_C_T	125D>N	Substitution

CGOV63	NID1	chr1_234268097-234268097_G_T	405D>E	Substitution
CGOV63	SFMBT2	chr10_7270604-7270604_G_A	599T>M	Substitution
CGOV63	KIF13A	chr6_17902580-17902580_G_A	1034T>M	Substitution
CGOV63	SEPT6	chrX_118634735-118634735_T_G	NA	Substitution
CGOV63	RPS6KA5	chr14_90408176-90408176_C_G	802A>P	Substitution
CGOV63	SILV	chr12_54641402-54641402_C_A	100G>G	Substitution
CGOV63	MACF1	chr1_39556802-39556802_C_G	1296A>A	Substitution
CGOV63	FAM135B	chr8_139222687-139222687_C_T	1242T>T	Substitution
CGOV63	DGKB	chr7_14847378-14847378_A_T	12P>P	Substitution
CGOV63	CA6	chr1_8934113-8934113_G_A	102G>R	Substitution
CGOV63	CAPRIN2	chr12_30775683-30775683_T_G	307K>N	Substitution
CGOV63	CDH5	chr16_64979793-64979793_G_C	189V>L	Substitution
CGOV63	CWC22	chr2_180527216-180527216_C_A	550M>I	Substitution
CGOV63	ACVR1C	chr2_158107536-158107536_C_T	343G>E	Substitution
CGOV63	CARD8	chr19_53427033-53427033_T_C	13I>V	Substitution
CGOV63	SLC17A6	chr11_22355858-22355858_C_G	582S>X	Substitution
CGOV63	SORCS3	chr10_106889224-106889224_C_T	431S>L	Substitution
CGOV63	SHH	chr7_155291969-155291969_T_A	115N>I	Substitution
CGOV63	SLC44A3	chr1_95062777-95062777_A_T	44K>N	Substitution
CGOV63	CEP135	chr4_56526612-56526612_C_T	292R>X	Substitution
CGOV63	PHOX2B	chr4_41445374-41445374_A_G	4M>T	Substitution
CGOV63	STX11	chr6_144549963-144549963_G_C	169G>A	Substitution
CGOV63	TTN	chr2_179152719-179152719_A_T	18465I>N	Substitution
CGOV63	DNAH3	chr16_20906631-20906631_C_T	2256R>K	Substitution
CGOV63	UROC1	chr3_127709522-127709522_C_T	173R>Q	Substitution
CGOV63	C1orf174	chr1_3799395-3799395_G_T	14A>E	Substitution
CGOV63	C2orf21	chr2_210349005-210349005_A_T	97N>Y	Substitution
CGOV63	NFS1	chr20_33724100-33724100_C_G	434R>P	Substitution
CGOV63	PTPRJ	chr11_48115265-48115265_G_T	670A>S	Substitution
CGOV63	RDH10	chr8_74395748-74395748_G_C	218V>L	Substitution
CGOV63	UNC13A	chr19_17602058-17602058_C_T	1277V>M	Substitution
CGOV63	ERBB3	chr12_54765120-54765120_C_T	103R>R	Substitution
CGOV63	OR4F15	chr15_100175930-100175930_C_T	6H>H	Substitution
CGOV63	TARBP1	chr1_232631902-232631902_A_G	918F>F	Substitution
CGOV63	DLEC1	chr3_38079117-38079117_A_G	305L>L	Substitution
CGOV63	FAM135B	chr8_139234202-139234202_A_G	566A>A	Substitution
CGOV63	ZNF462	chr9_108731027-108731027_G_T	1671T>T	Substitution
CGOV63	C9orf152	chr9_112003385-112003385_T_C	107Q>Q	Substitution
CGOV63	INTS9	chr8_28694344-28694344_G_A	395T>T	Substitution
CGOV63	GJB1	chrX_70360789-70360789_C_T	169D>D	Substitution
CGOV63	C16orf68	chr16_8630324-8630324_G_A	124V>M	Substitution
CGOV63	IGF2R	chr6_160402544-160402544_C_T	1094Y>Y	Substitution
CGOV63	C7orf62	chr7_88261610-88261610_C_A	195G>X	Substitution

CGOV63	CLCC1	chr1_109287998-109287998_G_C	182P>A	Substitution
CGOV63	CSMD1	chr8_3002856-3002856_G_A	1962P>L	Substitution
CGOV63	KIAA1217	chr10_24871693-24871693_G_C	1200M>I	Substitution
CGOV63	MUC7	chr4_71381361-71381361_C_	NA	Deletion
CGOV63	NPHS2	chr1_177792953-177792953_A_T	190D>E	Substitution
CGOV63	HTR1E	chr6_87782039-87782039_C_G	90L>V	Substitution
CGOV63	TMEM62	chr15_41263804-41263804_C_T	554R>W	Substitution
CGOV63	TWISTNB	chr7_19704504-19704504_T_C	326K>R	Substitution
CGOV63	AADACL2	chr3_152957546-152957546_C_G	205S>C	Substitution
CGOV63	ABI2	chr2_203975666-203975666_C_A	319Q>K	Substitution
CGOV63	NRK	chrX_105040120-105040120_C_T	611P>S	Substitution
CGOV63	TRIM35	chr8_27207719-27207719_C_T	186R>Q	Substitution
CGOV63	ZNF345	chr19_42059738-42059738_C_T	56H>Y	Substitution
CGOV63	TRIP12	chr2_230378721-230378721_T_C	798R>R	Substitution
CGOV280	TP53	chr17_7577608-7577609_CC_AG	CC>AG	Substitution
CGOV280	TTN	chr2_179485244-179485244_G_C	15335T>S	Substitution
CGOV280	MTA3	chr2_42806274-42806274_G_T	42V>L	Substitution
CGOV280	GPR158	chr10_25887561-25887561_C_A	1002D>E	Substitution
CGOV280	ZMIZ2	chr7_44800129-44800129_G_T	393V>F	Substitution
CGOV280	CACNA1C	chr12_2721166-2721166_C_A	1292A>D	Substitution
CGOV280	PDE2A	chr11_72300794-72300794_C_T	873+1G>A	Substitution
CGOV280	PREX1	chr20_47317360-47317360_G_A	283A>V	Substitution
CGOV280	DUSP27	chr1_167097006-167097006_G_A	880D>N	Substitution
CGOV280	ABCA13	chr7_48311895-48311895_C_T	878H>Y	Substitution
CGOV280	ASB15	chr7_123270086-123270086_G_T	503D>Y	Substitution
CGOV280	DNAH3	chr16_20976175-20976175_C_T	3011A>T	Substitution
CGOV280	CCR2	chr3_46399061-46399061_G_T	15E>X	Substitution
CGOV280	TMEM64	chr8_91637909-91637909_T_C	378N>S	Substitution
CGOV280	TRIML1	chr4_189068417-189068417_C_T	433P>L	Substitution
CGOV280	PCDHGB4	chr5_140768673-140768673_C_A	408L>I	Substitution
CGOV280	TRHR	chr8_110131470-110131470_G_A	328R>H	Substitution
CGOV280	SHPRH	chr6_146264286-146264286_C_T	744R>Q	Substitution
CGOV280	ZMYM6	chr1_35454118-35454118_T_C	855P>P	Substitution
CGOV280	C1orf173	chr1_75038703-75038703_C_T	897Q>Q	Substitution
CGOV280	FLG2	chr1_152330070-152330070_A_G	64D>D	Substitution
CGOV280	GPR25	chr1_200842228-200842228_G_A	21L>L	Substitution
CGOV280	XIRP2	chr2_168105159-168105159_G_A	2419L>L	Substitution
CGOV280	INPP5E	chr9_139324785-139324785_G_A	582S>S	Substitution
CGOV280	MS4A14	chr11_60165354-60165354_T_A	56I>I	Substitution
CGOV280	LRP1	chr12_57588868-57588868_C_T	2764D>D	Substitution
CGOV280	SETBP1	chr18_42456670-42456670_C_T	227L>L	Substitution
CGOV280	ISM1	chr20_13279761-13279761_C_T	350D>D	Substitution
CGOV280	LPIN3	chr20_39985745-39985745_C_A	623G>G	Substitution

CGOV280	ADAMTSL4	chr1_150532645-150532645_G_A	1066L>L	Substitution
CGOV280	NALCN	chr13_101795467-101795467_G_A	694R>R	Substitution
CGOV280	SLX4	chr16_3641293-3641293_G_C	782L>L	Substitution
CGOV280	ST18	chr8_53084937-53084937_C_T	162D>N	Substitution
CGOV280	SETD2	chr3_47163976-47163976_G_A	717S>L	Substitution
CGOV280	TTN	chr2_179485244-179485244_G_C	15335T>S	Substitution
CGOV280	NOS1AP	chr1_162337128-162337128_G_A	464S>S	Substitution
CGOV280	FOXG1	chr14_29237277-29237277_G_C	264V>V	Substitution
CGOV280	NPAP1	chr15_24922100-24922100_T_G	362V>V	Substitution
CGOV280	IQSEC1	chr3_12983221-12983221_C_T	70S>S	Substitution
CGOV280	POU3F2	chr6_99283727-99283727_T_A	326P>P	Substitution
CGOV280	STK36	chr2_219561851-219561851_C_T	892P>P	Substitution
CGOV280	GRM7	chr3_6903534-6903534_G_C	153V>V	Substitution
CGOV280	ZNF804B	chr7_88964426-88964426_C_G	710S>S	Substitution
CGOV280	ZFHX4	chr8_77767608-77767608_C_T	2817D>D	Substitution
CGOV280	EFCAB4B	chr12_3789435-3789435_A_G	103Y>Y	Substitution
CGOV280	PARN	chr16_14676132-14676132_A_G	366F>F	Substitution
CGOV280	REV3L	chr6_111696849-111696849_C_T	903T>T	Substitution
CGOV280	RHBDL3	chr17_30615900-30615900_G_A	128G>G	Substitution
CGOV280	MRPS12	chr19_39423121-39423121_T_C	66F>F	Substitution
CGOV280	CDC5L	chr6_44413454-44413454_A_G	718K>K	Substitution
CGOV280	PPP1CC	chr12_111160453-111160453_G_T	191R>R	Substitution
CGOV280	EYA3	chr1_28339722-28339722_A_C	223T>T	Substitution
CGOV280	DNAH6	chr2_84931424-84931424_C_G	2821A>A	Substitution
CGOV280	CACNB4	chr2_152717295-152717295_A_T	266A>A	Substitution
CGOV280	ZKSCAN8	chr6_28121474-28121474_G_A	472R>R	Substitution
CGOV280	GALNT16	chr14_69813784-69813784_C_T	433G>G	Substitution
CGOV280	GPRC5B	chr16_19883244-19883244_G_A	308F>F	Substitution
CGOV280	PER1	chr17_8052080-8052080_C_T	310G>G	Substitution
CGOV280	SAMD4B	chr19_39868415-39868415_C_T	465P>P	Substitution
CGOV280	GP6	chr19_55543619-55543619_T_G	71A>A	Substitution
CGOV279	TP53	chr17_7577120-7577120_C_T	273R>H	Substitution
CGOV279	KCNJ10	chr1_160011319-160011319_T_G	335K>T	Substitution
CGOV279	ATP13A3	chr3_194126806-194126806_C_A	1175A>S	Substitution
CGOV279	CD14	chr5_140011816-140011820_GGGCT_	Q250Pfs*17	Deletion
CGOV279	TRPC7	chr5_135692883-135692883_C_A	65E>X	Substitution
CGOV279	SLC13A3	chr20_45242320-45242320_C_T	52W>X	Substitution
CGOV279	IGSF21	chr1_18691928-18691928_C_A	251T>N	Substitution
CGOV279	OR8S1	chr12_48920186-48920186_C_T	258R>C	Substitution
CGOV279	SLC41A3	chr3_125786851-125786851_A_G	71V>A	Substitution
CGOV279	KIAA1614	chr1_180885486-180885486_C_G	83L>V	Substitution
CGOV279	ATN1	chr12_7045885-7045885_A_G	485Q>Q	Substitution
CGOV279	NOL4	chr18_31803134-31803134_C_T	28V>V	Substitution

CGOV279	OR10W1	chr11_58034983-58034983_G_T	116A>A	Substitution
CGOV279	GRIN2B	chr12_14019002-14019002_C_T	47E>E	Substitution
CGOV279	SV2C	chr5_75428010-75428010_C_T	145C>C	Substitution
CGOV279	ARAP3	chr5_141041269-141041269_A_T	1034L>H	Substitution
CGOV279	EVC2	chr4_5642363-5642363_T_C	450K>E	Substitution
CGOV279	LAMA5	chr20_60885984-60885984_G_C	3419R>G	Substitution
CGOV279	MCL1	chr1_150551505-150551505_C_G	168E>Q	Substitution
CGOV279	SP9	chr2_175201323-175201323_C_A	170G>G	Substitution
CGOV279	DLG5	chr10_79581731-79581731_C_T	837Q>Q	Substitution
CGOV279	VPS16	chr20_2841211-2841211_C_G	162L>L	Substitution
CGOV279	C20orf194	chr20_3297403-3297403_C_T	502L>L	Substitution
CGOV279	KCNQ2	chr20_62071011-62071011_G_A	289N>N	Substitution
CGOV279	MB	chr22_36007027-36007027_A_G	74G>G	Substitution
CGOV278	TP53	chr17_7579420-7579420__G	S90Lfs*59	Insertion
CGOV278	TMPPE	chr3_33134370-33134370_T_A	440S>C	Substitution
CGOV278	BAHCC1	chr17_79409990-79409990_C_G	484Q>E	Substitution
CGOV278	NLRP5	chr19_56538687-56538687_G_T	363G>V	Substitution
CGOV278	CTNND2	chr5_11159773-11159773_C_G	692G>R	Substitution
CGOV278	METAP2	chr12_95876989-95876989_A_T	260-2A>T	Substitution
CGOV278	KCNAB1	chr3_156009832-156009832_A_G	46I>V	Substitution
CGOV278	IGHMBP2	chr11_68701367-68701367_C_G	508S>W	Substitution
CGOV278	GPATCH1	chr19_33617638-33617638_C_T	922R>W	Substitution
CGOV278	AHDC1	chr1_27874973-27874973_G_C	1218N>K	Substitution
CGOV278	COL6A5	chr3_130095274-130095274_A_G	88K>E	Substitution
CGOV278	LMAN2	chr5_176764224-176764224_C_A	235E>X	Substitution
CGOV278	KRT3	chr12_53189429-53189429_C_T	133G>E	Substitution
CGOV278	CREB3L1	chr11_46334423-46334423_G_C	328E>D	Substitution
CGOV278	SERINC2	chr1_31905910-31905910_A_G	379A>A	Substitution
CGOV278	MPZ	chr1_161275904-161275904_C_A	213G>G	Substitution
CGOV278	PTPRN	chr2_220161170-220161170_G_A	793D>D	Substitution
CGOV278	RAD9A	chr11_67163393-67163393_C_G	190A>A	Substitution
CGOV278	SMARCA4	chr19_11129684-11129684_G_A	830V>V	Substitution
CGOV278	ELL	chr19_18632830-18632830_C_A	12L>L	Substitution
CGOV278	EPPIN-WFDC6	chr20_44174372-44174372_T_C	43Q>Q	Substitution
CGOV278	MACF1	chr1_39748874-39748874_G_T	242D>Y	Substitution
CGOV278	ACTL10	chr20_32255958-32255958_C_A	219L>M	Substitution
CGOV278	HKDC1	chr10_71016879-71016879_A_G	642R>G	Substitution
CGOV278	LCK	chr1_32740686-32740686_T_G	278+2T>G	Substitution
CGOV278	MAGEC1	chrX_140995655-140995655_C_A	822S>X	Substitution
CGOV278	RNF148	chr7_122342318-122342318_T_C	163I>V	Substitution
CGOV278	SETD1A	chr16_30970105-30970105_G_A	18R>Q	Substitution
CGOV278	SH3PXD2B	chr5_171765653-171765653_C_T	819R>Q	Substitution
CGOV278	SYT12	chr11_66812066-66812066_C_T	280A>A	Substitution

CGOV278	NPFFR1	chr10_72015016-72015016_G_C	330G>G	Substitution
CGOV278	ABCG8	chr2_44102365-44102365_A_C	523P>P	Substitution
CGOV278	PCK2	chr14_24567871-24567871_G_A	216Q>Q	Substitution
CGOV278	SZT2	chr1_43902903-43902903_C_G	1975V>V	Substitution

Supplementary Data 2.6. Recurrent Somatic Sequence Alterations

Case ID	Gene Symbol	Name
CGOV65	ABCA13	ATP-binding cassette; sub-family A (ABC1); member 13
CGOV280	ABCA13	ATP-binding cassette, sub-family A (ABC1), member 13
CGOV64	CWC22	CWC22 spliceosome-associated protein homolog (S. cerevisiae)
CGOV63	CWC22	CWC22 spliceosome-associated protein homolog (S. cerevisiae)
CGOV63	DNAH3	dynein; axonemal; heavy chain 3
CGOV280	DNAH3	dynein, axonemal, heavy chain 3
CGOV64	DUSP27	dual specificity phosphatase 27 (putative)
CGOV62	DUSP27	dual specificity phosphatase 27 (putative)
CGOV280	DUSP27	dual specificity phosphatase 27 (putative)
CGOV65	KIF13A	kinesin-like protein KIF13A isoform a
CGOV63	KIF13A	kinesin-like protein KIF13A isoform a
CGOV65	PIK3R5	phosphoinositide-3-kinase; regulatory subunit 5
CGOV64	PIK3R5	phosphoinositide-3-kinase; regulatory subunit 5
CGOV65	TP53	tumor protein p53
CGOV64	TP53	tumor protein p53
CGOV62	TP53	tumor protein p53
CGOV63	TP53	tumor protein p53
CGOV279	TP53	tumor protein p53
CGOV278	TP53	tumor protein p53
CGOV280	TP53	tumor protein p53
CGOV303	TP53	tumor protein p53
CGOV304	TP53	tumor protein p53
CGOV64	TTN	titin
CGOV63	TTN	titin

CGOV280	TTN	titin
CGOV65	WDFY4	WD repeat- and FYVE domain-containing protein 4
CGOV64	WDFY4	WD repeat- and FYVE domain-containing protein 4
CGOV62	WDR11	WD repeat domain 11
CGOV64	WDR11	WD repeat domain 11

Supplementary Data 2.7. Regions of Allelic Imbalance in CGOV62

Chromosome	Start (hg18)	End (hg18)	Segment Length	SNP Count	Normal MAF	TP53 Signature		STIC		Left FT tumor		Left ovarian tumor (A4)		Left ovarian tumor (A4) IHC		Left Ovarian Tumor (A7)		Right Ovarian Tumor		Rectal Metastasis		Appendiceal Metastasis		Omental Metastasis	
						MAF	LOH	MAF	LOH	MAF	LOH	MAF	LOH	MAF	LOH	MAF	LOH	MAF	LOH	MAF	LOH	MAF	LOH	MAF	LOH
	15521105	21352192	55959627	3	0.46	0		0		0		0		0		0		0		0		0		0	
chr1	691	218		96		.35	1	.27	1	.23	1	.17	1	.19	1	.19	1	.18	1	.19	1	.16	1	.22	1
	11600304	12129840	40161	58	0.47	0		0		0		0		0		0		0		0		0		0	
chr10	4	5		7		.36	1	.24	1	.16	1	.04	1	.06	1	.05	1	.05	1	.06	1	.03	1	.06	1
	82322418	10272341	20184125	71	0.47	0		0		0		0		0		0		0		0		0		0	
chr11	24127	23718		71		.36	1	.33	1	.19	1	.06	1	.07	1	.07	1	.07	1	.08	1	.05	1	.09	1
	10670281	12950187	22907956	1	0.47	0		0		0		0		0		0		0		0		0		0	
chr11	816	872		79		.41	0	.33	1	.19	1	.06	1	.07	1	.07	1	.07	1	.08	1	.05	1	.09	1
	20841173	11402303	93170856	3	0.46	0		0		0		0		0		0		0		0		0		0	
chr13	7361	7		08		.34	1	.24	1	.15	1	.04	1	.05	1	.05	1	.05	1	.05	1	.03	1	.06	1
	19285077	10479350	85507634	6	0.47	0		0		0		0		0		0		0		0		0		0	
chr14	6138	771		34		.33	1	.21	1	.12	1	.03	1	.04	1	.04	1	.04	1	.04	1	.03	1	.05	1
	45160392	84927664	39762687	2	0.47	0		.0		0		.0		.0		.0		.0		.0		.0		.0	
chr16	0320	0787		12		.39	0	.33	1	.21	1	.06	1	.08	1	.08	1	.07	1	.09	1	.07	1	.09	1

		70	70			0		0		0		0		0		0		0		0		0					
	29	63	34	7	0.	.		.		.		.		.		.		.		.		.					
chr	60	62	02	1	4	3		2		1		0		0		0		0		0		0					
17	05	87	82	4	7	2	1	1	1	2	1	3	1	5	1	5	1	4	1	5	1	3	1	5	1		
	29	66	36			0		0		0		0		0		0		0		0		0					
	57	14	56	1	0.	.		.		.		.		.		.		.		.		.					
chr	42	36	94	0	4	3		2		1		0		0		0		0		0		0					
18	27	64	37	6	6	3	1	2	1	5	1	4	1	5	1	5	1	4	1	5	1	3	1	7	1		
	31	54	23			0				0		0		0		0		0		0		0					
	08	64	55	1	0.	.		0		.		.		.		.		.		.		.					
chr	64	26	62	6	4	3		.		1		0		0		0		0		0		0					
20	29	64	35	6	7	1	1	2	1	2	1	3	1	4	1	4	1	4	1	5	1	2	1	5	1		
	16	39	22			0		0				0		0		0		0		0		0					
	58	13	54	2	0.	.		.		0		.		.		.		.		.		.					
chr	99	04	05	3	4	3		2		.		0		0		0		0		0		0					
22	20	90	70	1	7	7	1	9	1	2	1	6	1	9	1	8	1	7	1	8	1	4	1	9	1		
	86	17 07	84					0				0		0		0		0		0		0					
	25	04	44	3	0.	0		.		0		.		.		.		.		.		.					
chr	59	22	82	3	4	.		2		.		0		0		0		0		0		0					
6	52	5	73	9	6	4	0	9	1	2	1	5	1	7	1	7	1	7	1	8	1	4	1	9	1		
		38	38									0		0		0		0		0		0					
	27	38	10	1	0.	0		0		0		.		.		.		.		.		.					
chr	65	60	94	2	4	.		.		.		0		0		0		0		0		0					
9	93	65	72	9	7	4	0	3	1	2	1	5	1	7	1	7	1	7	1	8	1	9	1	9	1		
	98	40	30					0		0		0		0		0				0		0		0			
	19	39	58		0.	0		.		.		.		.		.		0		.		.					
chr	09	92	01	5	4	.		2		2		0		1		1		.		1		0		1			
X	8	66	68	6	6	4	0	9	1	8	1	9	1	2	1	1	1	1	1	3	1	5	1	4	1		
	44	15 41	10 92			0		0		0		0		0		0		0		0		0					
	93	60	24	1	0.	.		.		.		.		.		.		.		.		.					
chr	60	36	31	6	4	3		2		1		0		0		0		0		0		0					
X	55	7	2	5	6	6	1	9	1	8	1	5	1	7	1	7	1	6	1	7	1	5	1	9	1		
chr 9	70 81 80 27	13 17 02 60 7	60 ,8 84 ,5 80	3 8 8	0. 4 7	0 . 4	0	0 . 3 9	0	0 . 2	1	0 . 0 5	1	0 . 0 7	1	0 . 0 7	1	0 . 0 7	1	0 . 0 8	1	0 . 1 7	1	0 . 0 9	1		

Supplementary Data 2.8. Regions of Allelic Imbalance in CGOV63

Chromosome	Start (hg18)	End (hg18)	Segment Length	SNP Count	Nor MA
chr16	17110302	65503448	48,393,146	229	0.4
chr16	70561453	87429777	16,868,324	178	0.4
chr17	37533817	59374080	21,840,263	156	0.4
chr5	57790608	180601976	122,811,368	564	0.4
chr14	60517415	72510617	11,993,202	57	0.4
chr14	90953252	101877424	10,924,172	100	0.4
chr4	120643177	154733172	34,089,995	67	0.4
chr4	154733172	177319063	22,585,891	42	0.4
chr4	178499778	189259414	10,759,636	39	0.4
chr10	18997653	31174220	12,176,567	54	0.4
chr10	42926693	93658090	50,731,397	167	0.4
chr11	65395295	105129105	39,733,810	153	0.4

Supplementary Data 2.9. Regions of Allelic Imbalance in CGOV280

Chromosome	Start (hg19)	End (hg19)	Segment Length	SNP Count	No M
chr15	22925851	102264304	79,338,453	529	0
chr17	131516	20914635	20,783,119	328	0
chr17	26676135	72889676	46,213,541	409	0
chr18	196829	77918221	77,721,392	271	0
chr19	30314666	41386171	11,071,505	194	0
chr4	8608634	189061036	180,452,402	545	0
chr6	348906	29798083	29,449,177	187	0
chr6	39864730	51732807	11,868,077	86	0
chr6	62390916	121629167	59,238,251	221	0
chr6	122766138	168459845	45,693,707	202	0
chr7	1132153	18788589	17,656,436	112	0
chr9	117877	140865989	140,748,112	679	0
chrX	3021798	23898946	20,877,148	43	0
chrX	23928489	153694187	129,765,698	250	0
chr7	112724417	158902567	46,178,150	278	0
chr1	1663861	28209366	26,545,505	294	0
chr13	21063524	102367888	81,304,364	237	0
chr13	103346659	115047305	11,700,646	72	0
chr22	17264904	32579559	15,314,655	215	0

Supplementary Data 2.10. Regions of Allelic Imbalance in CGOV279

Chromosome	Start (hg19)	End (hg19)	Segment Length	SNP Count	Norı MA
chr16	56362725	70817982	14,455,257	155	0.4
chr16	77769897	90095597	12,325,700	226	0.4
chr17	9764531	21075343	11,310,812	120	0.4
chr17	29852092	72959000	43,106,908	573	0.4
chr8	41525914	66517486	24,991,572	44	0.4
chr8	120744349	144895553	24,151,204	171	0.4
chr18	50683691	77896308	27,212,617	127	0.4
chr2	98277090	109106381	10,829,291	66	0.4
chr3	391100	13368892	12,977,792	88	0.4
chr8	75924820	95531419	19,606,599	48	0.4
chr9	286593	21007935	20,721,342	123	0.4
chr9	71098987	100995721	29,896,734	190	0.4
chr2	135180550	153514583	18,334,033	62	0.4
chr2	69659126	96780986	27,121,860	124	0.4
chr11	16133413	46406767	30,273,354	135	0.4
chr18	7044887	19345932	12,301,045	37	0.4

Supplementary Data 2.11. Regions of Allelic Imbalance in CGOV278

Chromosome	Start (hg19)	End (hg19)	Segment Length	SNP Count	Nor M
chr1	1226102	16385250	15,159,148	185	0
chr11	67051857	134244123	67,192,266	311	0
chr13	22255167	53422553	31,167,386	108	0
chr13	67800935	115091399	47,290,464	103	0
chr15	38988760	101924546	62,935,786	402	0
chr16	53262964	70818759	17,555,795	109	0
chr17	648186	19729495	19,081,309	297	0
chr17	26676135	81050982	54,374,847	531	0
chr18	20953720	34850846	13,897,126	33	0
chr18	43310415	77896242	34,585,827	119	0
chr19	308662	12186761	11,878,099	422	0
chr2	224919	11924950	11,700,031	41	0
chr21	11098626	47970581	36,871,955	233	0
chr22	17264904	48940644	31,675,740	274	0
chr3	29529907	51971382	22,441,475	147	0
chr4	4249297	190862155	186,612,858	414	0
chr5	74651084	135692575	61,041,491	149	0
chr5	137426447	178419288	40,992,841	235	0
chr8	196274	33416222	33,219,948	168	0
chr9	214864	20765097	20,550,233	63	0
chr9	27455095	140786516	113,331,421	476	0
chrX	2825403	154020114	151,194,711	155	0
chr6	156275691	170871046	14,595,355	49	0
chr10	97116219	134145166	37,028,947	227	0
chr20	4776445	14830596	10,054,151	25	0
chr10	15106441	26505822	11,399,381	39	0
chr2	201342616	230841074	29,498,458	114	0

CHAPTER 3:

INTEGRATED GENOMIC, EPIGENOMIC, AND EXPRESSION ANALYSES OF OVARIAN CANCER CELL LINES

METHODS

Cell Lines and Growth Analyses

All samples were obtained under Institutional Review Board–approved protocols with informed consent for research use or were publicly available. Cells were plated into 24-well tissue culture plates at a density of 2×105 to 5×105 cells per well and grown in cell line-specific medium without or with increasing concentrations of their respective drugs (ranging between 0.001 and 10 μm/L). Cells were counted on day 7 using an automated cell viability assay (Vi-CELL XR Cell Viability Analyzer; Beckman Coulter, Fullerton, CA), a video imaging system that uses an automated trypan blue exclusion protocol. Both adherent and floating viable cells were counted for treatment and control wells. Growth inhibition (GI) was calculated as a percentage of untreated controls. The log of the fractional GI was then plotted against the log of the drug concentration and the IC50 values were interpolated from the resulting linear regression curve fit (CalcuSyn; Biosoft, Ferguson, MO). Experiments were performed thrice in duplicate for each cell line.

STR Analyses

Genomic DNA from all cell lines was PCR amplified using a Geneprint 10 System (Promega, Madison, WI) that contains eight STR loci plus Amelogenin, a gender-determining marker. The PCR amplification was carried out in a GeneAmp PCR System 9700 following the manufacturer's protocol. The PCR products were electrophoresed on a ABI Prism 3730xl Genetic Analyzer using Internal Lane Standard 600 (Promega) for sizing. Data were analyzed using GeneMapper v. 4.0 software (Applied Biosystems, Foster City, CA). We compared our STR profiles (Johns Hopkins University [JHU]) for these cell lines to external STR profiles, including Korch et al[59], COSMIC (v83; https://cancer.sanger.ac.uk/cosmic), the RIKEN BioResource Center

(https://www.jove.com/institutions/AS-asia/JP-japan/20278-riken-bioresource-center), or Yu et al.[60] The average percent similarity between JHU STRs and external STRs was 98%. An external STR was not available for five cell lines.

Whole-Genome Next-Generation Sequencing

DNA was extracted from cell lines using a QIAamp DNA Blood Mini QIAcube Kit (QIAGEN, Valencia, CA). In brief, the samples were incubated in proteinase K for 16 hr before DNA extraction. DNA purification was performed using the QIAamp DNA Blood Mini QIAcube kit following the manufacturer's instructions (QIAGEN, Valencia, CA). Genomic DNA from tumor samples were used for Illumina TruSeq library construction (Illumina, San Diego, CA) according to the manufacturer's instructions. Paired-end sequencing resulting in 100 bases from each end of the fragments was performed using Illumina HiSeq2000 instrumentation.

PCR and Sanger Sequencing

PCR and Sanger sequencing confirmed the presence of fusion candidates generated by Trellis. Primers were designed 200 bp on either side of the junction. Primers were purchased from IDT (Coralville, IA) and purified by desalting. Primers and probes were resuspended to 100 μM in IDTE (10 mM Tris, pH 8.0; 0.1 mM EDTA) buffer and stored at −20∘C. Using the primers specific for each fusion, PCR amplification was performed in a 50-μL reaction volume in quadruplicate, consisting of 10 μL of 5X Phusion buffer, 1 μL of 10 mM dNTP, 2.5 μL of each primer at 10 μM, 0.5 μL of HotStart Phusion, and 10 ng of cell line DNA. PCR was performed using a Bio-Rad S1000 Thermal Cycler. The thermal cycle was programmed for 30 s at 98∘C for initial denaturation, followed by 34 cycles of 10 s at 98∘C for denaturation, 30 s at 59∘C for annealing, 30 s at 72∘C for extension, and 5 min at 72∘C for final extension. Human mixed

genomic DNA (Promega, Madison, WI) and no template were used as negative controls. PCR products were purified using Nucleospin Gel and PCR cleanup as per the manufacturer's instructions (Macherey-Nagel, Duren, Germany). PCR products were then subjected to Sanger sequencing using the Applied Biosystems 3730xl DNA Analyzer as per manufacturer's instructions (Thermo Fisher, Waltham, MA). Output was compared to original candidate fusion sequence and confirmed.

Droplet Digital PCR

The translocation primers were designed on both sides of the translocation. One of these primers was used as a common primer for both the translocation and the control. A third primer was designed to be used in combination with the common primer to amplify the wild-type sequence of one of the two translocation partners. The hydrolysis probes labeled with the FAM-fluorochrome at the 5′ end were designed to bind specifically to the translocation PCR product, while the probes labeled with the HEX-fluorochrome were designed to bind specifically to the control PCR product. As quenchers, a ZEN quencher was used as an internal quencher, while the Iowa Black FQ-quencher was added to the 3′ end of the probes. Probes were designed to have a higher melting temperature than the primers. The primers and hydrolysis probes were purchased from IDT (Coralville, IA). The primers were purified by desalting, while the hydrolysis probes were purified using high-performance liquid chromatography. Upon arrival, primers and probes were resuspended to 100 μM in IDTE (10 mM Tris, pH 8.0; 0.1 mM EDTA) buffer and stored at −20∘C. 20-μL droplet digital PCR (ddPCR) reactions were prepared, using 10 μL of 2× ddPCR SuperMix for Probes (No dUTP) (Bio-Rad, Hercules, CA), 5–30 ng of gDNA, as quantified by the Qubit dsDNA high-sensitivity assay kit (Thermo Fisher Scientific, Waltham, MA), primers (each at a final concentration of 900 nM), probes (each at a final concentration of 250 nM), and nuclease-free water. Human mixed genomic DNA (Promega) was used as negative control. Droplets were

generated using the QX200 droplet generator (Bio-Rad) by loading the DG8 cartridge (Bio-Rad) with 20μL of the reaction mixture and 70μL of droplet generation oil for probes (Bio-Rad). 40μL of droplet/oil mixture was transferred to a ddPCR 96-well plate (Bio-Rad). The plate was heat-sealed with a pierceable foil heat seal (Bio-Rad). A S1000 Thermal Cycler (Bio-Rad) was used with the following amplification protocol: enzyme activation at 95∘C for 10 min, followed by six cycles: denaturation at 54∘C for 30 s; annealing/extension at 60∘C for 1 min, followed by 34 cycles: denaturation at 58°C for 30 s; and annealing/extension at 60∘C for 1 min. Following cycling, the samples were held at 98∘C for 10 min. Upon completion of the PCR protocol, the plate was read using the QX200 droplet reader (Bio-Rad). Droplet counts and amplitudes were analyzed with QuantaSoft software (v1.7) (Bio-Rad).

Alignment and Identification of Sequence Alterations

Prior to mutation calling, primary processing of sequence data for samples was performed using Illumina CASAVA software (v1.8.2), including masking of adaptor sequences. Sequence reads were aligned against the hg19 human reference genome using ELAND. Candidate somatic mutations in the exome, consisting of point mutations, insertions, and deletions were identified using VariantDx[30]. To detect mutations that were more likely to be somatic, we excluded mutations that appeared in >10% of the distinct reads and mutations tagged as COMMON or MULT in dbSNP VCF files. Additionally, we excluded mutations without a record in COSMIC as well as in-frame deletions (COSMIC v72). Exceptions to the COSMIC requirement were mutations that predicted truncations in relevant pathways or tumor suppressor genes (Table S3.1e). SNPs flagged as clinically associated or reported in COSMIC were not excluded regardless of heterozygosity or percentage of distinct reads. All candidate somatic mutations were confirmed by visual inspection. Samples with more than 2,000 alterations after dbSNP filtering were considered hypermutators. Mutational signatures were based on the fraction

of mutations in each of the 96 trinucleotide contexts[61]. The contribution of each signature to each tumor sample was estimated using the deconstructSigs R package (Table S3.1n for R package versions).

Implementation of DELLY and LUMPY

Identifying probable somatic structural variants in tumor-only experimental designs is a major challenge. False positives arise from germline variants incorrectly reported as somatic and spurious alignments misinterpreted as biological variation. We considered two established tools, DELLY and LUMPY, for detection of structural variants[62,63]. Reads were aligned to the hg19 reference genome using BWA-MEM (version 0.7.10)[64] as recommended by these methods. DELLY (version 0.7.7) and LUMPY (version 0.2.13) were implemented using default parameters.

A simple leave-one-out cross-validation experiment was implemented using 10 lymphoblastoid controls to evaluate the specificity of these methods for identifying somatic structural variants in a tumor-only experimental design. Specifically, we treated the held out sample as a *tumor* and identified germline structural alterations in the training set. Excluding structural variants identified in the training set, we considered any alteration identified in the held-out sample as a false positive.

Implementation of Trellis

Germline Filters

Using 10 lymphoblastoid cell lines and 8 normal ovarian samples, we developed sequence and germline filters for the hg19 reference genome to flag regions prone to alignment artifacts and/or germline structural variation. Sequence filters for the hg19 reference genome that were masked prior to copy number analyses comprised 326.4 Mb of the genome and included non-overlapping

1-kb genomic intervals (bins) with average mappability less than 0.75 or GC percentage less than 10%, as well as the gaps track from the University of California, Santa Cruz (UCSC) genome browser that includes heterochromatin, centromeric, and subtelomeric regions[65]. After removing these sequence filters as well as chrY (all cell lines were derived from women), we normalized the read depth for the remaining 2,680,222 bins. For each bin, we computed the GC-adjusted, log2-transformed count of aligned reads. GC normalization was implemented using a loess smoother with span 1/3 fitted to a scatterplot of the bin-level GC and log2 count. We denote the GC-adjusted log2 ratios (the residuals from the loess correction) by *R*, the mean *R* for a genomic region by $\bar{R}$, and the median absolute deviation of the autosomal *R*s by *S*. Because some bins had an unusually high or low number of aligned reads in multiple controls, we defined bin *i* in normal control *j* as an outlier if $|Ri|>(3\times Sj)$. Bins identified as an outlier in two or more normal controls were flagged. These analyses flagged 55,764 genomic regions totaling 75.9 Mb of sequence. To identify somatic copy number alterations, we segmented the *R*s using circular binary segmentation implemented in the R package DNAcopy with settings alpha = 0.001, undo.splits = 'sdundo', and undo.SD = 2[66,67]. To exclude regions that were either copy number altered in the lymphoblastoid cell lines as well as segments that span difficult regions to genotype, we flagged segments having $|\bar{R}|>1$. We flagged a total of 919 segments (46.8 Mb) across the 18 normal controls.

To characterize copy neutral rearrangements including inversions and translocations in the normal controls, we extracted all read pairs from the BAM file that were *improperly* paired and for which the intra-mate distance between paired reads was at least 10 kb. We defined a cluster of improper read pairs as a genomic region where at least one base is spanned by five or more improper reads and for which the union of the aligned regions is at least 115 bp. Next, we linked these clusters by the mates of the constituent reads. Clusters that could not be linked by at least five read pairs were excluded from further analysis. For all linked clusters, we required at least 90% of the linking read

pairs to support the same structural variant group (Table S3.1l). Linked clusters for which the type of rearrangement was not consistent among the linking read pairs were excluded from further analysis. For the remaining linked clusters, we realigned all the reads supporting the link using the local aligner BLAT (Kent, 2002). A command-line version of BLAT was utilized for this step (Standalone BLAT v. 35). Confirmation by BLAT required that the reads only align to one location with a BLAT score $\geq 90\%$ in the hg19 reference genome. These germline rearrangements were used to screen candidate somatic rearrangements as described in greater detail below.

Somatic Deletions

Putative focal homozygous and hemizygous deletions greater than 2 kb and less than 3 Mb in the ovarian cell lines were identified by $\bar{R}<-3$ and $\bar{R}\in(-3,-0.75]$, respectively. We excluded focal deletions in tumor samples if $\geq 75\%$ of the region was identified as a deletion in a control sample. For each deletion, we investigated whether any improperly paired reads were aligned within 5 kb of the segmentation boundaries. When five or more rearranged read pairs were aligned near the segmentation boundaries, the distribution of the improper read pair alignments was used to further resolve the genomic coordinates of the deletion boundaries. Resolution of the deletion breakpoints using this approach depends on the intra-mate distance of the improperly paired reads. On average, the intra-mate distance in the ovarian tumors was 262 bp (5th and 95th percentiles, 183 and 353). With multiple rearranged read pairs, we expect that the resolution of the deletion breakpoints was generally less than 100 bp. As previously described, realignment by BLAT was used to confirm that the rearranged read pairs supporting the deletion mapped uniquely and with high fidelity to this region of the genome. Hemizygous and homozygous deletions supported by rearranged read pairs were indicated by hemizygous+ or homozygous+, respectively. Any deletion for which the outlier bins or germline CNVs occupied 75% or more of the width were excluded. Hemizygous deletions not supported by rearranged read pairs were also excluded. All deletions were confirmed by visual inspection.

Somatic Amplifications

To identify focal amplicons and establish how these amplicons were linked in the tumor genome, we seeded a graph with high-copy focal amplicons. Specifically, putative amplifications were identified as segments with $\bar{R}>1.46$, or a 2.75-fold increase from the mean ploidy of the cell line, and between 2 kb and 3 Mb in length. Properly paired reads were used to link seed amplicons to adjacent low-copy duplications (segments with $\bar{R}>0.81$ or fold change of 1.75). When five or more links were established, the low-copy segments were added as nodes to the graph with an edge indicating the connection between the high- and low-copy amplicons. Similarly, we established links between the low- and high-copy amplicons that were non-adjacent with respect to the reference genome by analysis of improperly paired reads as previously described.

Somatic Copy-Neutral Intra- and Inter-chromosomal Translocations and Inversions

Candidate somatic copy-neutral rearrangements were identified as previously described in the control samples. However, rearrangements in the ovarian tumor cell lines that overlapped any rearrangement identified in the controls samples were excluded. In addition to improperly paired reads, we required at least one split read supporting the rearrangement. To identify split read alignments, we extracted all read pairs for which only one read in the pair was aligned within 5 kb of the candidate rearrangement. For all such read pairs, we re-aligned the unmapped mate using BLAT[68]. A read aligned by BLAT to both ends of the candidate sequence junction with a combined score ≥90% constituted a split read (e.g., Figure S3.6).

In-Frame Gene Fusions

To report candidate gene fusions, we identified all candidate somatic rearrangements for which both ends of the novel adjacency in the tumor genome was in a coding region of the genome or a promoter of a gene defined as within 5 kb of the transcription start site. Rearrangements in which

both ends resided in the same gene were excluded as these may represent alternative isoforms. For each candidate fusion, we evaluated two possible orientations of the regions joined in the tumor genome, and for each orientation we extracted the full amino acid sequence of both the 5′ and 3′ transcripts as well as the candidate amino acid sequence that would be created by the fusion. We considered the fusion to be in-frame if the amino acid sequence of the 3′ partner was a subsequence of the reference amino acid sequence.

Genome-wide Methylation Analyses

We pre-processed and normalized raw IDAT files from the Infinimum MethylationEPIC array using the preprocess Funnorm function in the R package minfi Aryee et al.[69]. Probes on chromosomes X or Y, probes with detection p value greater than 0.5, or probes overlapping a SNP with dbSNP minor allele frequency greater than 10% were excluded. In order to understand the similarity of ovarian cells lines with human ovarian cancer, we compared the ovarian cells lines with human ovarian cancer samples available from Genomic Data Commons (https://gdc.cancer.gov/). The Genomic Data Commons contained 533 human methylation profiles of ovarian cancer and eight normal fallopian tissue samples. Methylation of TCGA ovarian cancers was assessed using Infinium HumanMethylation27 BeadChip array (27,578 probes). The number of probes in common between the HumanMethylation27 platforms and the MethylationEPIC platform was 18,016. On the common set of 18,016 probes, we quantified overall methylation in the TCGA samples and the ovarian cell lines as the fraction of CpG sites with $\beta>0.3$. To identify differentially methylated CpG sites comparing normal fallopian tissue to TCGA ovarian cancers, we selected probes from the common set of 18,016 that were hyper-methylated in TCGA ovarian cancer (average $\beta>0.4$) and unmethylated in normal fallopian tissue (average $\beta<0.2$). In addition, we also selected probes that were hypo-methylated in TCGA ovarian cancer (average $\beta<0.1$) and hyper-methylated in normal fallopian (average $\beta>0.3$).

Gene Expression Analyses

Pre-processing and normalization of the 44k Agilent microarray for the ovarian cell lines has been previously described, and normalized expression data were available for 44 of the 45 tumors[70]. For copy number altered genes with known clinical relevance to cancer, we assessed whether amplified genes were overexpressed and whether deleted genes were underexpressed. The probability that a gene was overexpressed or underexpressed was estimated by a two-component pooled variance mixture model implemented in the R package CNPBayes (https://bioconductor.org/packages/release/bioc/html/CNPBayes.html). The location of the non-differentially expressed mixture component was fixed at the median log2 expression of unmethylated cell lines without copy number alterations. A gene was considered differentially expressed if the posterior probability of membership in the overexpressed or underexpressed mixture component exceeded 0.5.

Dose Response Models

Bayesian Model Averaging

We considered models of the formlogCi=γ1xi,1+…+γpxi,p,+εi,whereCi denotes the logIC50 and xi,j is an indicator for the alteration status (0, not altered; 1, altered) of feature *j* in cell line *i*. The regression coefficient for feature *j* is the product of a binary indicator zj and a real number hj. We used a modified *g*-prior for γ such that γj was zero whenever zj was zero[71]. For the vector of γ's with non-zero *z*'s, we used a multivariate normal prior. We explored the space of the possible 2p models using a Gibbs sampler. The binary features comprising the x's included somatic mutations, somatic structural variants (deletions, amplifications, in-frame fusions), methylation, and underexpression or overexpression. For the PARP inhibitor, we additionally considered the

number of intra-chromosomal rearrangements and the HRD score as potential markers for HRD. For rearrangements, we computed the mean of the square-root-transformed frequency across all cell lines and defined a binary covariate for whether the square-root-transformed statistic was greater than the mean. We used the HRD score without transformation for Bayesian model averaging. For the univariate analyses described in the next section, we defined a binary covariate for HRD according to whether the score was larger than the mean. We obtained qualitatively similar inferences using the continuous HRD score (data not shown). For the inhibitor of the MEK pathway, one of the logIC50 concentrations was missing. For this cell line, we used the posterior mean from the imputation described in greater detail below.

Univariate Analysis of Selected Features

For a given feature, our sampling model for the length-3 vector of inhibitor concentrations inducing 20%, 50%, and 80% cell death is logCi, altered=$\mu+\delta+\epsilon i$,a lteredfor a cell line with an alteration in this feature and logCi,WT=$\mu-\delta+\epsilon i$,WT for a cell line without an alteration. With inhibitor concentrations on the log scale, the residuals are approximately multivariate-normal:$\epsilon i,j \sim$i.i.d. MVN(0,Σ).Computationally convenient conjugate priors for the unknown parameters in this model are p(μ,δ,Σ)=p(μ)p(δ)p(Σ),$\mu\sim$MVN(μ0,Σ0), $\delta\sim$MVN(δ0,Ψ0), and $\Sigma-1\sim$W(ν0,S0$-$1). For some cell lines, inhibitor concentrations were incomplete. As the logC were highly correlated across cell lines, we imputed missing observations from the observed data using a Gibbs sampler. Inference regarding differences in mean logC, given by the posterior distribution of 2δ, was based on the marginal probability of the observed data integrating over the missing data. We reported 90% highest posterior density (HPD) intervals for the difference in the mean logIC50.

RESULTS

Overall Approach

We aimed to assemble a collection of ovarian cancer cell lines that would be representative of the different histological subtypes. These encompassed both publicly available as well as newly generated cell lines, ultimately comprising 19 serous, 9 clear-cell, 3 mucinous, 2 undifferentiated, 2 endometrioid, 1 mixed, and 9 unclassified subtypes (Table S3.1a). Information related to the original description and classification of these cell lines is indicated in Table S3.1a, and the origin of the lines was confirmed using unique short tandem repeat (STR) analyses. To identify sequence and structural changes in these ovarian cancer cell lines, we performed next-generation whole-genome analyses at an average coverage of 32x and 116.6 Gb per sample (Table S3.1c). As matched normal DNA was not available for these samples, we also sequenced a set of 18 unmatched DNA samples from normal blood or lymphoblastoid cell lines from individuals of various ethnicities. We developed approaches to focus on likely tumor-specific sequence and genome-wide structural changes, including amplifications, deletions, and rearrangements. In parallel, genome-wide methylation analyses were performed and integrated with genomic and expression data in order to obtain a comprehensive molecular profile of these samples (Figure 3.1).

Sequence analyses

A high-sensitivity analysis of sequence alterations, including single-base substitutions and small insertions and deletions, was performed for the exomes of these samples. Given the challenges of characterizing tumor-specific (somatic) changes in tumor samples without matched normal tissue [30], we developed stringent bioinformatic approaches to determine likely somatic mutations. Removal of common germline variants resulted in an average of 928 alterations per cell line exome,

comprising 41,768 changes that included rare germline and somatic alterations. Six cell lines (two clear cell and one each of endometrioid, serous, unclassified, and mixed lineage) were hypermutated, having alterations in mismatch repair (MMR) genes MLH1, MSH2, MSH6, or PMS2, and six times as many sequence changes compared to those tumors that were MMR proficient (Table S3.1d). To focus on likely somatic alterations involved in tumorigenesis, we analyzed the sequence alterations in each cell line and identified changes that have been previously detected in the coding genomes of other cancer patients[72]. We also identified nonsense or frameshift inactivating mutations in a panel of tumor suppressor genes (Table S3.1e). Through these analyses, we discovered 659 putative driver somatic mutations across 45 ovarian cell lines (Table S3.1f).

The most frequently mutated gene was the TP53 tumor suppressor gene (altered in 25 non-hypermutated and 3 hypermutated tumors). Excluding hypermutated samples, other genes frequently mutated included ARID1A (14 cancer cell lines), PIK3CA (6), SMAD4 (4), KRAS (4), APC (3), CREBBP (3), and PPP2R1A (3). Mutations were predominantly CpG transitions CT or GA (48%) followed by non-CpG transitions AG or CT (25%). These observations are consistent with mutations in TP53 in a high fraction of serous ovarian cancers[16], and PIK3CA, ARID1A, and PPP2R1A in clear-cell tumors [31]. Analysis of mutation signatures aggregated by ovarian cancer subtypes revealed that serous, mucinous, and undifferentiated tumor cell lines had an age-related signature previously reported in ovarian adenocarcinomas[61]. Clear-cell and serous ovarian cancers also had a profile consistent with a MMR-associated mutation signature, likely due to the subset of tumors with MMR defects in the cell lines[17]. Overall, both the compendium of mutated genes as well as mutation-associated signatures were representative of previous ovarian cancer genome analyses (Table S3.1f).

Structural variant analyses

Given the importance of structural alterations in the development of ovarian cancer[16,17,32 13], we used whole-genome sequence data to characterize copy number changes as well as rearrangements that may affect key driver genes. We first considered existing approaches for whole-genome analyses, including DELLY and LUMPY, but these typically use matched normal sequences to accurately identify tumor-specific rearrangements[62,63]. Given the multitude of tumor cell lines and other cancer specimens where matched normal DNA is not available, we developed a framework for structural variant detection called Trellis that could be used with tumor genome sequence data directly. Additionally, because many structural changes are linked genomically (i.e., an amplified gene has both copy number changes and rearrangements that can be located in multiple locations of the genome), we aimed to connect the multiple changes that were related to individual genetic targets. The features of this approach include (1) detection of tumor-only structural changes through removal of germline and artifactual changes, (2) distinction of focal homozygous deletions and amplifications from larger structural changes, (3) connection of apparently disparate copy number regions using paired sequences in the same amplicons, (4) detection of homozygous and hemizygous deletions through copy number and rearrangement data, (5) confirmation of rearrangements using a stringent local re-alignment to detect and remove spurious paired read and split alignments, and (6) identification of in-frame rearrangements that would likely lead to gene fusions.

To implement the Trellis approach, we excluded low complexity sequences by mappability, as well as regions of germline copy number variants (CNVs) and rearrangements detected in the genomes of 18 samples derived from normal blood cells. We divided the remaining 2.7 Gb of the genome into 1-kb bins and examined areas of increased read density (2.75-fold) to identify copy number gains, and regions of decreased read density (0.6-fold) to detect hemizygous or homozygous deletions greater than 2 kb using approaches similar to digital karyotyping[73,74]. We identified rearrangements from atypical orientation or spacing of paired reads as well as split read alignments.

To evaluate the specificity of our approach in a set of non-tumor samples where we expected very few somatic structural changes, we used a leave-one-out cross-validation analysis among the 10 unmatched normal blood samples. Using Trellis, these analyses identified no focal high copy gains. On average, we identified 5 hemizygous deletions (interquartile range, 2–15) and 1 homozygous deletion (interquartile range, 0–8) in the normal samples (Figure 3.2). Likewise, the average number of rearrangements observed per sample was 3 (interquartile range, 0–6). These observations are consistent with previous descriptions of germline structural changes in normal DNA, in particular in lymphoblastoid DNA[75], and suggest a high specificity of our approach for detection of bona fide somatic alterations (mean specificity, 0.97).

By contrast, analysis of normal samples with DELLY or LUMPY detected hundreds to thousands of structural changes in each normal DNA sample (Figure 3.2). With DELLY and LUMPY, the average numbers of focal high-quality copy number alterations were 13 and 21, respectively. The average numbers of intra- and inter-chromosomal rearrangements identified by DELLY were 297 and 433, respectively, and for LUMPY these were higher, at 511 and 2203, respectively. The number of alterations observed by DELLY using low-stringency settings was higher yet (Figure 3.2). False positives for copy number changes appeared to largely be due to inclusion of single-copy gains and losses, with neither DELLY nor LUMPY distinguishing hemizygous from homozygous losses or single-copy gains from high-copy amplifications. The source of the rearrangement false positives appeared to be largely the result of mapping artifacts due to low sequence complexity in putative rearrangements.

To assess the sensitivity of this approach, we sequenced 16 cell lines using high-coverage next-generation sequencing of 111 genes comprising 585,216 bp. Computing the fold change of read depth at these targeted regions, we found four high-copy amplifications with fold change 6, nine

low-copy amplifications with fold change and 6, and nine homozygous deletions. Trellis detected all four high-copy amplifications, including amplifications of AKT2, CCNE1, and KRAS. All nine regions identified as low-copy amplifications by targeted sequencing were also determined to be low-copy amplifications by Trellis, corroborating quantitative and qualitative characteristics of the amplifications. Similarly, all nine deletions discovered by targeted sequencing, comprising CDKN2A (8) and NF1 (1), were also characterized as homozygous deletions by Trellis. Overall, these analyses established that the Trellis approach had both high specificity and sensitivity for detection of structural alterations that are currently not possible with tumor-only samples using existing approaches.

Linked amplicons

We focused our analysis of amplifications to regions smaller than 3 Mb that were present at 2.75-fold compared to the modal genome copy number, as such alterations have historically been linked to amplified driver genes[74]. An analysis of the 45 ovarian cancer samples identified 538 focal amplicons, or an average of 12 amplicons per tumor. As multiple amplicons within the same tumor may be derived from an amplification of a single target gene localized to different chromosomal regions[74,76,77], we examined the possibility that amplicons may be linked. Using our paired read whole-genome analyses, we found that reads at the edges of many amplicons were linked with aberrant spacing and/or orientation with respect to the reference genome. In order to identify links between apparently distant amplicons, we visualized these as undirected graphs where the nodes were amplicons and edges between amplicons were defined by multiple paired reads aligned to both genomic locations (e.g., Figures 3.3A and 3.3B). Our analyses discovered 57 amplicon groups from the 538 amplicons across the ovarian tumor cell lines. Among tumors with at least one amplicon, the median number of amplicon groups was 2 and the median number of amplicons within an amplicon group was 4 (interquartile range, 2–9). The majority of cell lines (15/28) with

an amplicon group contained known driver genes. As an example, cell line ES-2 had 41 apparent amplicons, but through this approach we determined that 38 of the amplicons were linked to a single group that contained the CCND1 driver gene (Figure S4). Both the copy number ($t = 3.3$, $p = 0.003$) and number of connections between amplicons ($t = 5.3$, p 0.001) was significantly higher for amplicon groups containing known drivers compared to amplicon groups without known drivers (Figure 3C).

Driver genes that were amplified in two or more cell lines as part of amplicon groups that have previously been observed in ovarian cancer included well-known oncogenes such as MYC (4), ERBB2 (2), CCND1 (2), CCNE1 (2), FGFR4 (2), and KRAS (2). Interestingly, we identified amplifications of cancer driver genes that have not been previously appreciated in ovarian cancer, including epigenetic regulator ASXL1 (2), H3 histone family member H3F3B (2), NOTCH family receptor NOTCH4 (1), repair and recombination paralog RAD51C (1), and ubiquitin ligase RNF43 (1). ASXL1 amplification and overexpression have been previously identified in cervical cancer[78], and overexpression of H3F3B has been reported in several tumor types but not ovarian cancer[79]. Several of these genes have been observed as being part of larger structural alterations in recent TCGA high-grade serous ovarian carcinoma analyses[16] but have not been identified as target genes in those cases.

Overall, these analyses greatly simplified the observed amplification events and revealed that many focal amplicons would not have been associated with driver genes had they not been linked in specific amplicon groups. The observed amplicons were consistent with previously detected genes in ovarian cancer, but we also identified genes not previously implicated in this disease.

Deletions

We used a combination of stringent analyses of segmented read depth and aberrant read pair spacing to identify homozygous and hemizygous deletions. As deletions may occur in the germline, we removed deletions that were in or near structural alterations observed in the normal controls in order to identify those deletions that were most likely to be somatic. These analyses revealed 674 hemizygous^{+}, 41 overlapping hemizygous^{+}, 286 homozygous, and 263 homozygous^{+} deletions, where "+" denotes evidence for deletion supported by rearranged read pairs in addition to read depth (Figures 3.3D; Table S3.1h). Deletion breakpoints with rearranged read pairs were more precise (typically within 100 bp), while deletions without rearranged read pairs had a resolution of 1–5 kb. We included homozygous deletions from segmentation analyses even if these were without rearranged read pairs as these could have been missed in read pair analyses due to the limited mappability at one or both deletion breakpoints. The median number of homozygous and hemizygous deletions per tumor was 10.5 (interquartile range, 8–16) and 11.0 (interquartile range, 6–18), respectively. Genes that were recurrently deleted included cell cycle regulators CDKN2A (9) and CDKN2B (8), tyrosine kinase receptor ERBB4 (5), neurofibromin genes NF1 (3) and NF2 (3), transcriptional regulator CDC73 (2), polycomb-group repressor EZH2 (2), and serine/threonine kinase STK11 (2) (Table S1h), of which CDKN2A, NF1, NF2, and STK11 have been previously reported to be altered in high-grade serous ovarian carcinomas[16,80]. Genes that have been implicated through somatic deletion in other tumors but that had not been previously implicated in ovarian cancer include CDC73, ERBB4, EZH2, MLH1, as well as TGF-beta pathway members TGFBR2, SMAD3, and SMAD4, estrogen receptor ESR1, cell cycle kinase CDK6, notch receptor NOTCH1, cohesin member STAG2, and epigenetic regulator ATRX (Table S3.1h). In a fashion similar to amplifications, several of these genes have been observed as being part of larger structural alterations in recent TCGA high-grade serous ovarian carcinoma analyses[16] but have not been identified as target genes in those cases or other histologic subtypes. The absence or low frequency of such alterations in previous studies may in part reflect the challenges of identifying bona fide deletions through existing approaches in primary tumors.

Other recurrent deletions occurred in genes encompassing large genomic regions (>1 Mb) that were more likely to be affected by structural alterations, including a member of the low-density lipoprotein receptor family LRP1B (7), fragile histidine triad involved in purine metabolism FHIT (11), a member of the short-chain dehydrogenases/reductases protein family WWOX (15), and the deacetylase MACROD2 (7). FHIT and WWOX occur in fragile sites and are often deleted in cancers, and some evidence suggests they encode putative tumor suppressors [81-84]. LRP1B deletion has been associated with chemotherapy resistance in high-grade serous ovarian cancers and is a putative tumor suppressor[85]. Because of their proximity to CDKN2A, the methylthioadenosine phosphorylase MTAP and the transcription factor DMRT1 are commonly co-deleted with CDKN2A[86], and use of compounds exploiting the loss of MTAP has been proposed as a potential therapeutic avenue[87] for tumors with CDKN2A deletions.

Rearrangements and fusions

We next examined structural rearrangements that were not associated with segmental copy number changes. We detected 834 inter-chromosomal and 2,277 intra-chromosomal rearrangements (Table S3.1i). The median per sample of inter- and intra-chromosomal rearrangements was 16 (interquartile range, 5–31) and 37 (interquartile range, 17–62), respectively, with many of these rearrangements involving inversions (median of 8 and 6, respectively).

Among rearrangements for which the sequence junction was within the intron or exon of a gene, we detected 128 in-frame fusions of two genes (Table S3.1j). Several of these in-frame fusions have not been observed in ovarian cancer but have been previously reported in other cancers. For example, YAP1-MAML2 has been reported in nasopharyngeal carcinoma and salivary cancers [88-90], IKZF2-ERBB4 has been reported in T cell lymphomas[91], and fusions involving CCND1 were

identified in a patient with leukemic mantle cell lymphoma[92]. Our study discovered the YAP1-MAML2 fusion in cell line ES-2 after exon 6 of YAP1 and before exon 2 of MAML2, preserving the transactivation domain of MAML2 and its likely role in Notch signaling. The predicted amino acid sequence of the affected MAML2 gene is the same as reported in nasopharyngeal carcinoma and salivary gland cancers (amino acid 172) [88-90].

The IKZF2-ERBB4 fusion we identified in ovarian tumor KK involves the first three exons of IKZF2 and exons 2–27 of ERBB4, a member of the epidermal growth factor receptor (EGFR) family. This IKZF2-ERBB4 junction is nearly identical to that reported by Boddicker et al.[91] in T cell lymphoma and mucinous lung adenocarcinoma, involving the same exons of ERBB4 and leaving the ERBB4 kinase domain intact. Gene expression analyses indicated that the ERBB4 transcript, including the fusion transcript, was overexpressed. ERBB4 overexpression has been associated with resistance to platinum-based therapy in ovarian serous carcinomas[93], suggesting a potentially important role for this translocation event for therapeutic selection. In ovarian tumor ES-2, CCND1 was amplified and also participated in a fusion where the promoter of SHANK2 was linked to the coding region of CCND1. An amplification and fusion involving CCND1 has been previously identified in a patient with leukemic mantle cell lymphoma[92]. Additional gene fusions not previously observed in ovarian cancer involved the negative regulator of the RAS pathway NF1, the tumor suppressor regulating mTORC1 signaling TSC2, and the member of the F-box protein family FBXW7. The fusion of NF1 (NF1-MYO1D) occurred after the first exon of this gene and would be expected to disrupt its function, consistent with its tumor-suppressive role Cancer Genome Atlas Research Network[16]. Similarly, the fusion of MLST8-TSC2 would be expected to result in a TSC2 protein lacking the first 373 aa, disrupting the key region of interaction with TSC1[94]. As detailed below, the fusion of full-length FBXW7 to the promoter of FAM160A1 was also likely deleterious due to decreased expression under the new promoter. For each of the nine predicted fusions involving at least one gene previously identified in other cancer fusions, we

independently validated the novel sequence junction using PCR and Sanger sequencing and a recently developed droplet digital PCR approach[95].

Epigenetic and expression analyses

We next examined genome-wide methylation profiles in order to evaluate the role of epigenetic alterations in these ovarian cancer cell lines. Analyses of over 850,000 methylation sites were performed using Infinium MethylationEPIC arrays. Methylation levels were evaluated at individual CpG sites within gene promoter regions (1,500 bp upstream of the transcription start site) or within individual genes. We compared methylation levels in the ovarian cell lines to methylation levels in the normal lymphoblastoid cells, as well as to 8 TCGA normal fallopian tissue and 533 TCGA ovarian cancers. Among the 18,619 CpG probes shared by the Infinium HumanMethylation27 BeadChip array (27,578 probes) and the MethylationEPIC array, we estimated the proportion of methylated CpG sites as the fraction of CpG probes with beta > 0.3 . Consistent with previous studies[96-98], we found that the overall proportion of methylated CpG sites in the lymphoblastoid (median, 0.35) and ovarian cell lines (median, 0.41) was higher than the proportion in fallopian tissues (median, 0.30) and ovarian cancers (median, 0.29) (Figure 3.4A). Previous studies have suggested that differences in methylation between cell cultures and primary tumors often occur at genes involved in cell cycle regulation[98], and may also result from contamination of normal cells in the primary tissues. To examine methylation profiles of the cell lines at individual CpG sites in the broader context of ovarian cancer methylation profiles, we identified 96 genes that were differentially methylated between normal fallopian tissue and 100 randomly sampled TCGA ovarian tumors (Figure 3.4B). While we excluded both the lymphoblastoid cell lines and the ovarian cancer cell lines from the probe selection procedure, the normal lymphoblastoid cell lines were more highly correlated to the normal fallopian tissues while the ovarian cancer cell lines were more correlated to the TCGA ovarian cancers. Taken together, these analyses indicate that the

ovarian cell lines retain epigenetic profiles of genes commonly methylated in ovarian cancer and that the methylation of these genes is unlikely to be related to growth in culture.

We integrated our genomic and epigenetic analyses with expression data previously obtained for these cell lines through the Agilent 44K array[70]. We assessed whether specific genes affected by deletions or other structural changes in some tumors may be silenced through methylation and low expression in others. Among genes that were methylated or deleted, expression analyses revealed lower expression for many of these genes. Cell lines RMG-I and IGROV-1 both had hemizygous deletion and loss of expression of CDC73. Of the 13 drivers homozygously deleted in at least one tumor, five genes, including CDKN2A and ESR1, displayed loss of expression and concomitant promoter methylation in additional ovarian cancers (Figures 3.4C). When promoter methylation and underexpression were considered, the fraction of tumors with alterations in CDKN2A more than doubled from 23% to 55%, highlighting the multiple mechanisms by which CDKN2A function can be compromised. Similarly, MLH1 was mutated in a single case, but was mutated and/or underexpressed in an additional seven cancers. For ESR1, the inactivating methylation is thought to be associated with age and has been previously observed in both ovarian cancers and ovarian cancer cell lines[99,100]. Lower expression also resulted from abnormal fusion of non-adjacent promoters to the full coding sequence of target genes. In OVCAR-8, the fusion of the promoter of FAM160A1 with the full-length FBXW7 gene resulted in dramatically decreased expression of FBXW7, consistent with the tumor-suppressive function of this protein and inactivating mutations observed in other tumor types[101].

We also examined the possibility of increased expression for genes with structural changes. We identified 17 genes with focal amplification in one or more cancer cell lines and evidence of bimodal expression across the samples analyzed. For these genes, 20 of the 22 tumors (91%) with focal amplification also had increased expression. Genes associated with amplification and fusion

had particularly high expression, suggesting that the combination of genetic alterations led to increased overall transcription of these genes. The amplification of CCND1 and its fusion to SHANK2 in sample ES-2 increased the expression of CCND1 relative to other ovarian cell lines without the amplification and fusion. The YAP1-MAML2 fusion, which was also duplicated in the same sample, resulted in expression of MAML2 that was higher than 85% of the other ovarian cancer cell lines. For driver genes that were amplified, we examined whether additional tumors may be identified with increased expression of these genes. We found increased expression of CCNE1, ERBB2, KRAS, and AKT2 in eight additional cases without genomic alterations in these genes (Figure 3.5). These analyses indicate the importance of integrated genomic, epigenetic, and expression analyses and have resulted in an expansion of the number of tumors with alterations in key driver genes. These observations also highlight the functional consequences of genomic and epigenomic alterations in human cancer at the RNA level.

Combining sequence and structural variants with methylation and differential gene expression, we found that nearly all ovarian cancer subtypes had alterations in cell cycle, chromatin remodeling, DNA repair, RAS, Notch, PI3K, or TGFB signaling pathways (Figure 3.5). Alterations in the cell cycle pathway genes, including CDKN2A, were the most common with one or more alterations in 60%–70% of the three most represented subtypes (serous, adenocarcinoma, and clear cell). Chromatin modifications occur in 5/7 (71%) of the clear-cell subtypes but in only 2/21 (11%) of the serous samples. We see evidence of mutual exclusivity between CDKN2A, CCNE1, and RB1 within the cell cycle pathway, but not mutual exclusivity between cell cycle and KRAS pathways, underscoring that clonal selection often involves multiple drivers regulating distinct molecular processes.

Sensitivity and resistance to pathway inhibitors

To begin to understand the relationship between genomic, epigenetic, and expression alterations and response to pathway inhibitors, we developed a screening platform for evaluating cellular proliferation in the presence of candidate therapeutic agents. As an example of the analyses that can be performed and the genotype-phenotype connections that can be obtained, we measured IC20, IC50, and IC80 after 7 days of incubation for three inhibitors, GNE-493, BMN673, and MEK162, targeting PI3K, PARP, and MEK proteins, respectively (Table S3.1k). Aggregating the molecular information from multiple platforms to the gene level, we limited our analyses to genes that were altered in 3 or more of the 45 cell lines. Alterations that tend to be mutually exclusive between cell lines were combined, including genes in the PI3K pathway (PIK3CA and PPP2R1A) and the genes in the TGFBR pathway (SMAD3 and SMAD4). As tumors with homologous recombination deficiencies (HRDs) have been known to be sensitive to PARP inhibitors, we additionally added covariates summarizing the extent of genome-wide structural alterations for the PARP inhibitor BMN673. A priori, we hypothesized that most alterations would not modulate response to the targeted inhibitors. Implementing a Bayesian model averaging approach to variable selection as has been previously considered for other biomarkers[102-104], we specified a positive prior probability that the coefficient for each gene is exactly zero. Given the genes or combination of genes and structural variant summaries, we explored the space of possible single and multi-variate models for logIC50 by Markov chain Monte Carlo. Relevant posterior summaries available for each inhibitor include the probability that the regression coefficient is non-zero and the posterior distribution of the regression coefficients. We used this approach to focus on those features that were present in at least half of the models as these had a higher probability of being predictive for drug response (Figure 3.6A).

For PARP inhibition by BMN673, our analyses revealed that the number of genome-wide rearrangements and amplification of MYC were important predictors of drug sensitivity (Figure 3.6). Importantly, the two cell lines with inactivating BRCA1/2 mutations, as well as the HRD

score as defined by Abkevich et al. or Swisher et al. and applied through our whole-genome analyses, and PARP1 expression showed a trend toward increased sensitivity to PARP inhibition but were not statistically significant (Figure 3.6). We found that amplification of MYC or an increase in the number of genome-wide rearrangements, including inversions and intra-chromosomal rearrangements, were significantly associated with sensitivity to this therapy, appearing in 94% of the single-variate and multi-variate models. We estimated the difference of the mean log IC_{50} between the group of tumors with alterations in these features and the group of tumors without such changes, revealing a 93% (90% confidence interval [CI], 99%–64%) and 86% (90% CI, 96%–43%) increased sensitivity to PARP inhibition for cell lines with MYC amplification and increased rearrangements, respectively (Figure 3.6). Although other genomic signatures and PARP1 expression have been suggested as biomarkers for PARP sensitivity[105], MYC amplification and rearrangements have not been previously identified as markers of PARP sensitivity in serous and endometrioid ovarian cancers. Taken together, these observations suggest that alterations of common drivers along with large-scale structural alterations in ovarian cancer may identify tumors with high sensitivity to this therapy.

For inhibition of the PI3K pathway by GNE-493, mutations of PPP2R1A or PIK3CA appeared in more than 75% of the models evaluated. Cancer cell lines with mutations in PARP1 or PPP2R1A had a 66% increased sensitivity to GNE-493 (Figure 3.6). PPP2R1A is a subunit of protein phosphatase 2A (PP2A), a known tumor suppressor and regulator of PI3K signaling through AKT inhibition[106]. Somatic mutations in PIK3CA and PPP2R1 have been previously reported in ovarian and uterine cancers[13,30,107,108]. Our observations suggest that PI3K inhibitors counter the loss of PI3K pathway regulation from inactivating mutations of PPP2R1A and activating mutations of PIK3CA.

For the MEK pathway, mutations or deletions in SMAD3 or SMAD4 were predictive of IC_{50} levels in response to the inhibitor MEK-162. These were selected in more than 85% of the models and resulted in an increased sensitivity of 89% to this therapy. SMAD3 and SMAD4 form a complex that activates transcription of TGF-beta-regulated genes important in cellular growth control[109]. Our results are consistent with previous observations showing that loss of SMAD4 can lead to activation of Smad-independent MEK/ERK pathway signaling and that inhibition of this pathway with MEK inhibitors can reverse tumorigenic effects[110].

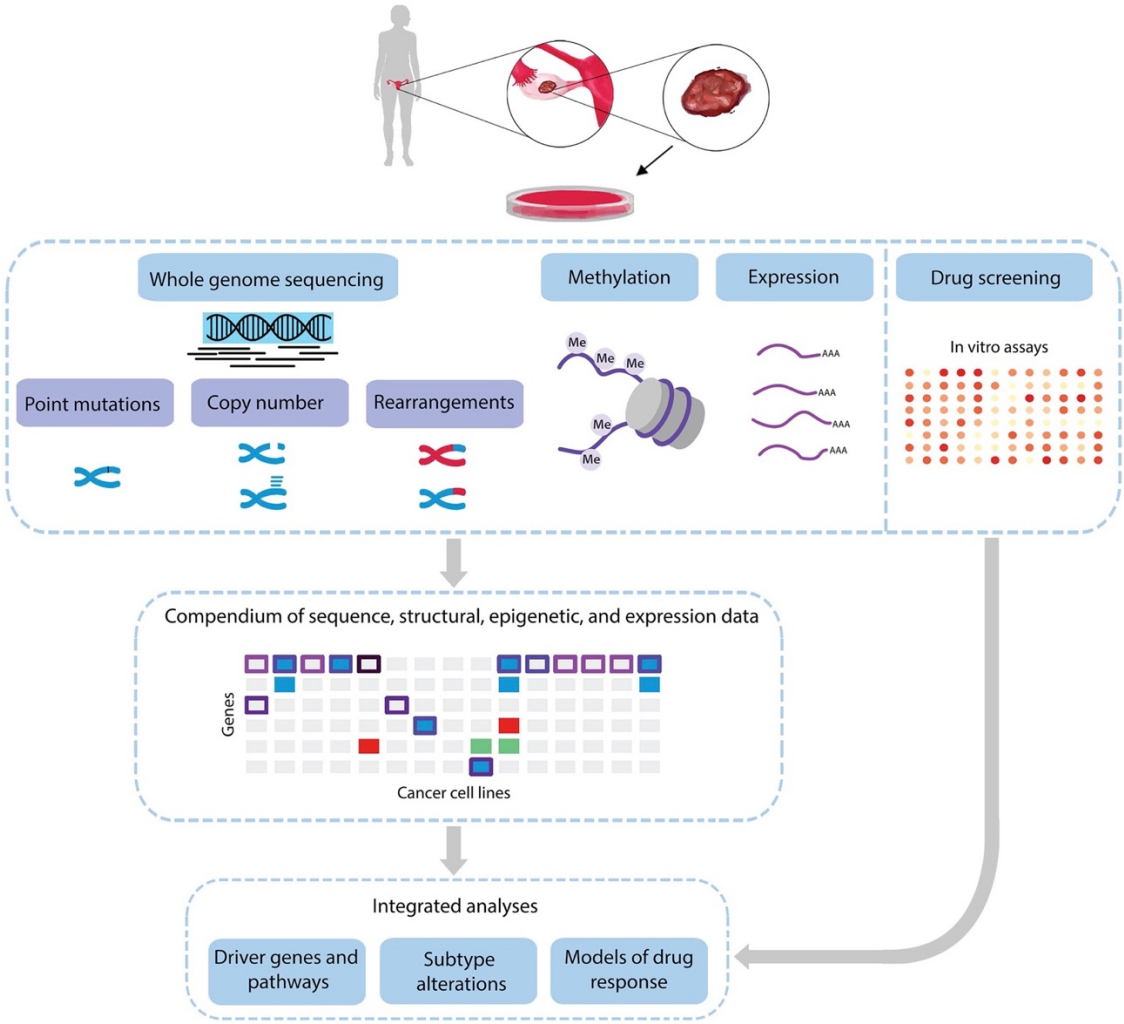

Figure 3.1. Overview of Genomic, Epigenomic, Expression, and Therapeutic Analyses of Ovarian Cancer Cell Lines

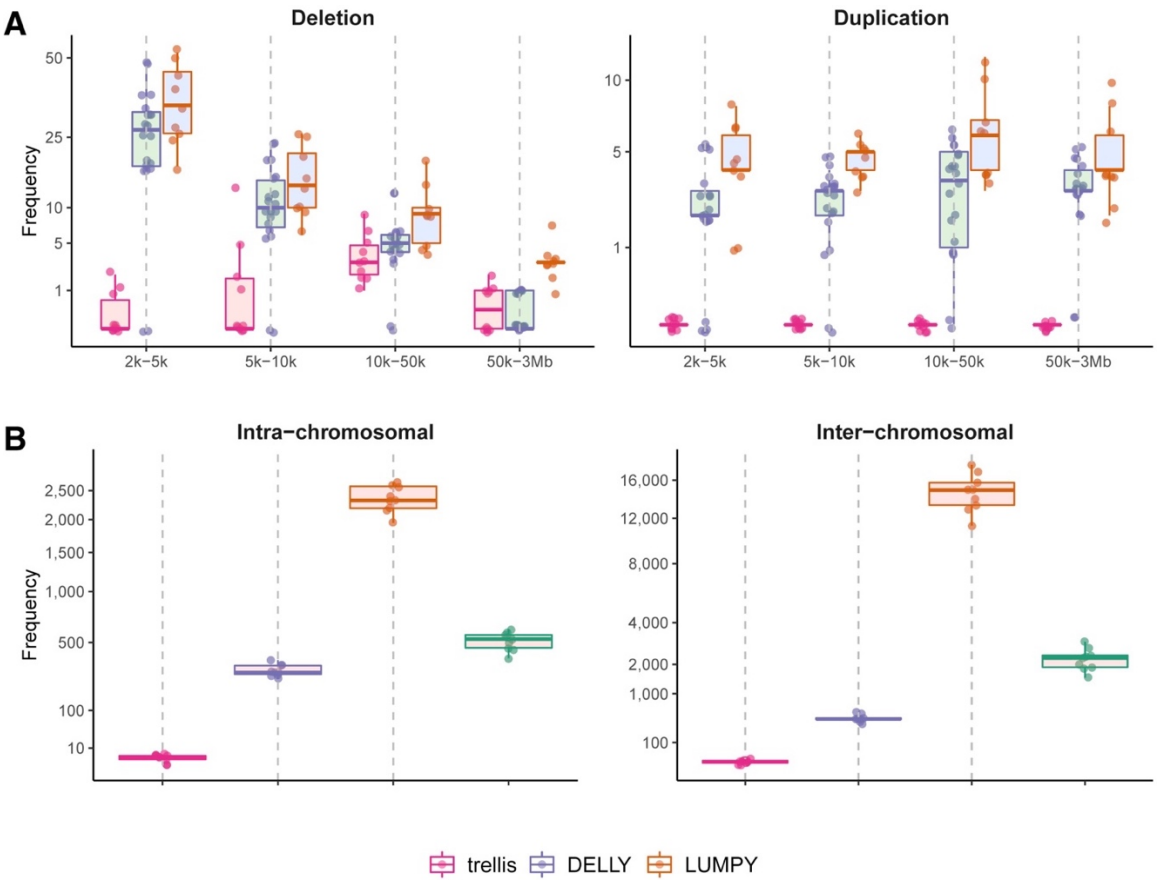

Figure 3.2. Number of False-Positive Somatic Structural Variant Identifications in Lymphoblastoid Cell Lines. (A and B) Estimated number of false-positive somatic deletions and duplications (A) and somatic intra-chromosomal and inter-chromosomal rearrangements (B).

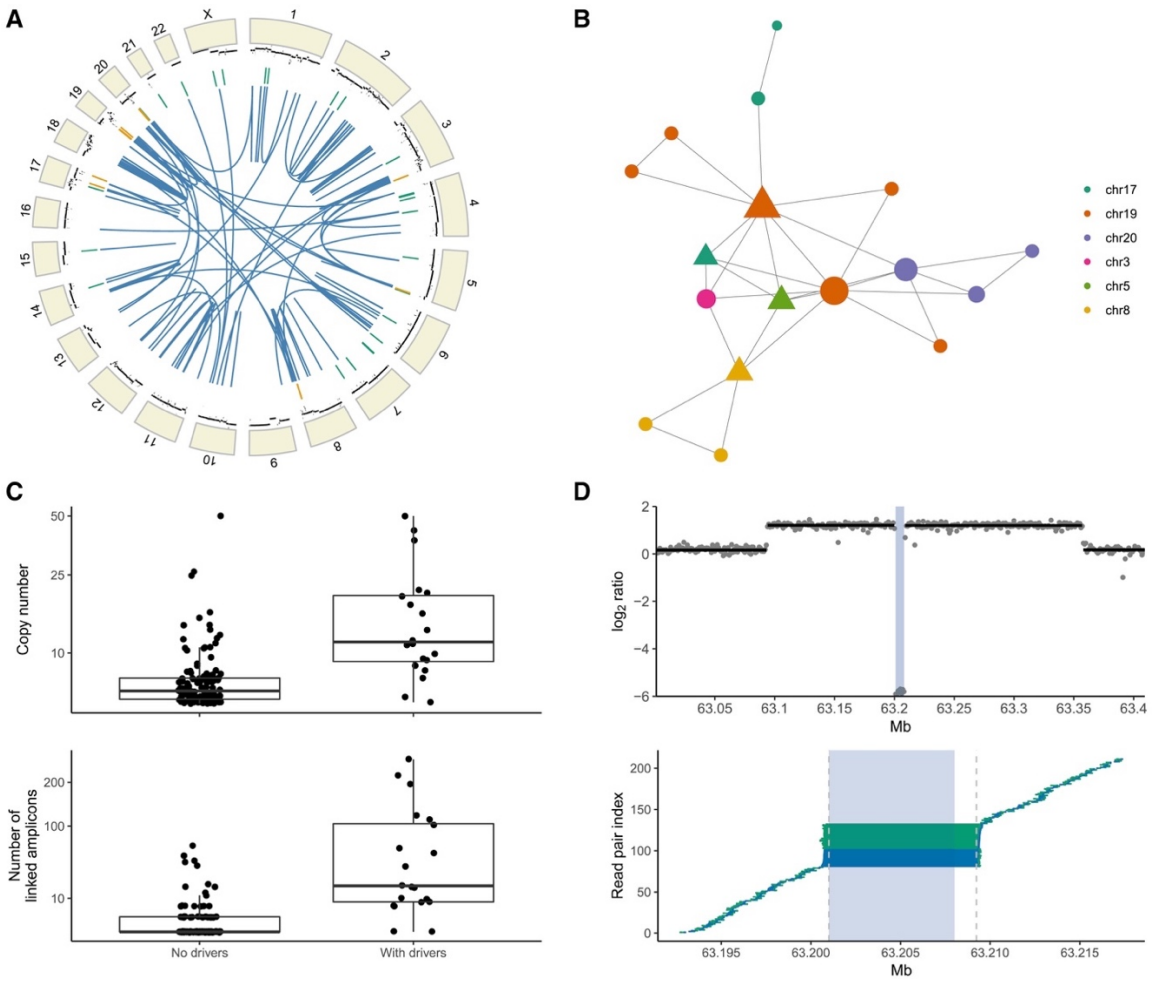

Figure 3.3. Trellis Approach for Characterization of Genomic Structural Alterations. (A) Circos plot displaying focal deletions (green), amplifications (orange), and intra- and inter-chromosomal rearrangements (blue) for cell line FU-OV-1. (B) Improperly paired reads established connections (edges) between distant amplicons (nodes) visualized as a graph. The size of the plotting symbols is proportional to the number of sites in which the amplicon was inserted, and the triangle shape indicates an amplicon involving a known driver. (C) The average maximum copy number (top) and mean number of amplicon links (bottom) for amplicon groups with and without drivers. (D) Top: Segmented normalized coverage identified a homozygous deletion (shaded). Bottom: Rearranged read pairs improved the precision of the deletion breakpoints. Lines connecting the read pairs indicate whether the positive or negative strand was sequenced (blue, positive; green, negative).

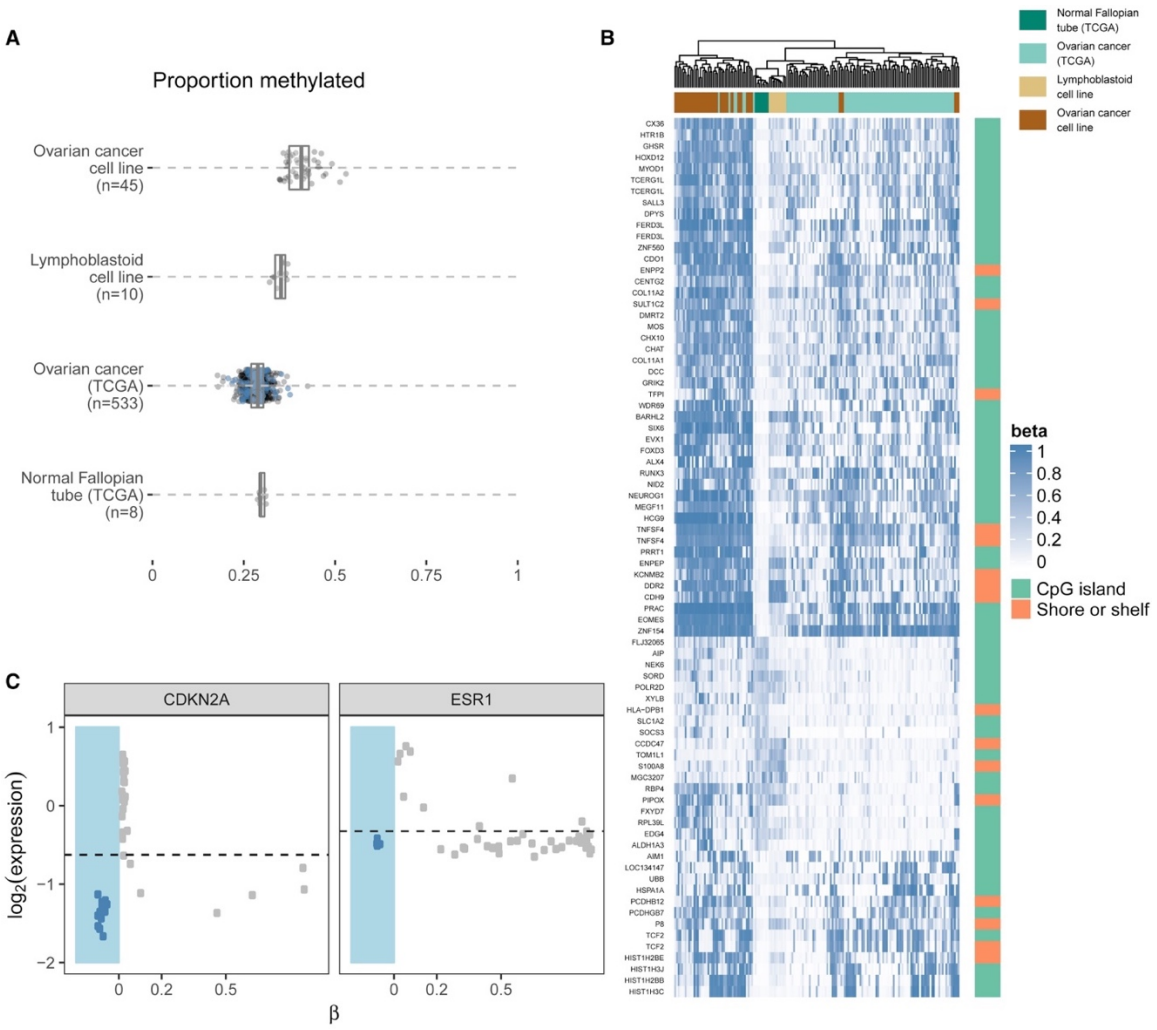

Figure 3.4. Methylation of CpG Sites in Ovarian Cancers and Normal Fallopian Tissue. (A) The proportion of methylated CpG sites (mean) in the lymphoblastoid cell lines, ovarian cell lines, TCGA ovarian cancers, and TCGA normal fallopian tissues. (B) Plotted are 96 probes that were differentially methylated between normal TCGA fallopian tissue and 100 randomly selected TCGA ovarian tumors (blue points, A). Among these probes, the lymphoblastoid cell lines were most correlated with normal fallopian tissue and the ovarian cell lines were most correlated with TCGA ovarian tumors, suggesting that the cell line effect does not dominate among probes that were differentially methylated in these tissues. Among probes that were methylated in TCGA ovarian and unmethylated in TCGA fallopian, the ovarian cell lines were predominantly methylated and have quantitatively higher β values. While copy number analyses suggested that the purity in the ovarian cell lines was , the median tumor purity of TCGA ovarian tumors was 85% (interquartile range, 78%–88%). (C) Genes CDKN2A and ESR1 exhibit bimodal gene expression explained by homozygous copy number deletions (blue points in x-axis margin) or methylation levels above 0.2.

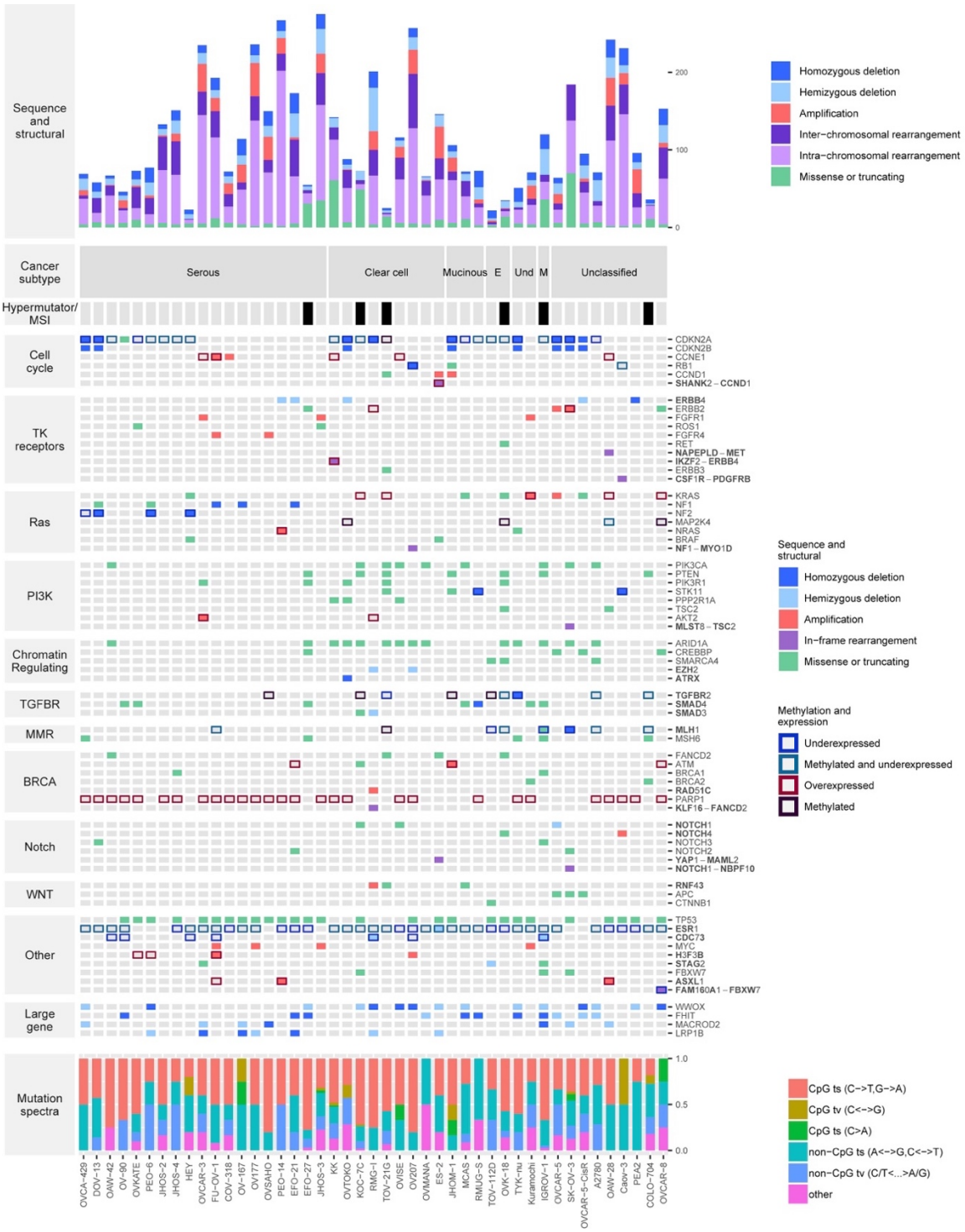

Figure 3.5. Sequence, Structural, Epigenomic, and Expression Alterations in Ovarian Cancer Cell Lines. Cell lines were grouped by tumor subtype (E, endometrioid; Und, undifferentiated; M, mixed). For many of the pathways, mutual exclusivity of genomic alterations within the pathway is evident (e.g., cell cycle, TK receptors, TGFBR, BRCA, and WNT). The group indicated as Other contains genes that are clinically relevant for ovarian cancer but cannot be easily categorized by a single molecular process. Methylation and expression were not evaluated for the Large Gene group.

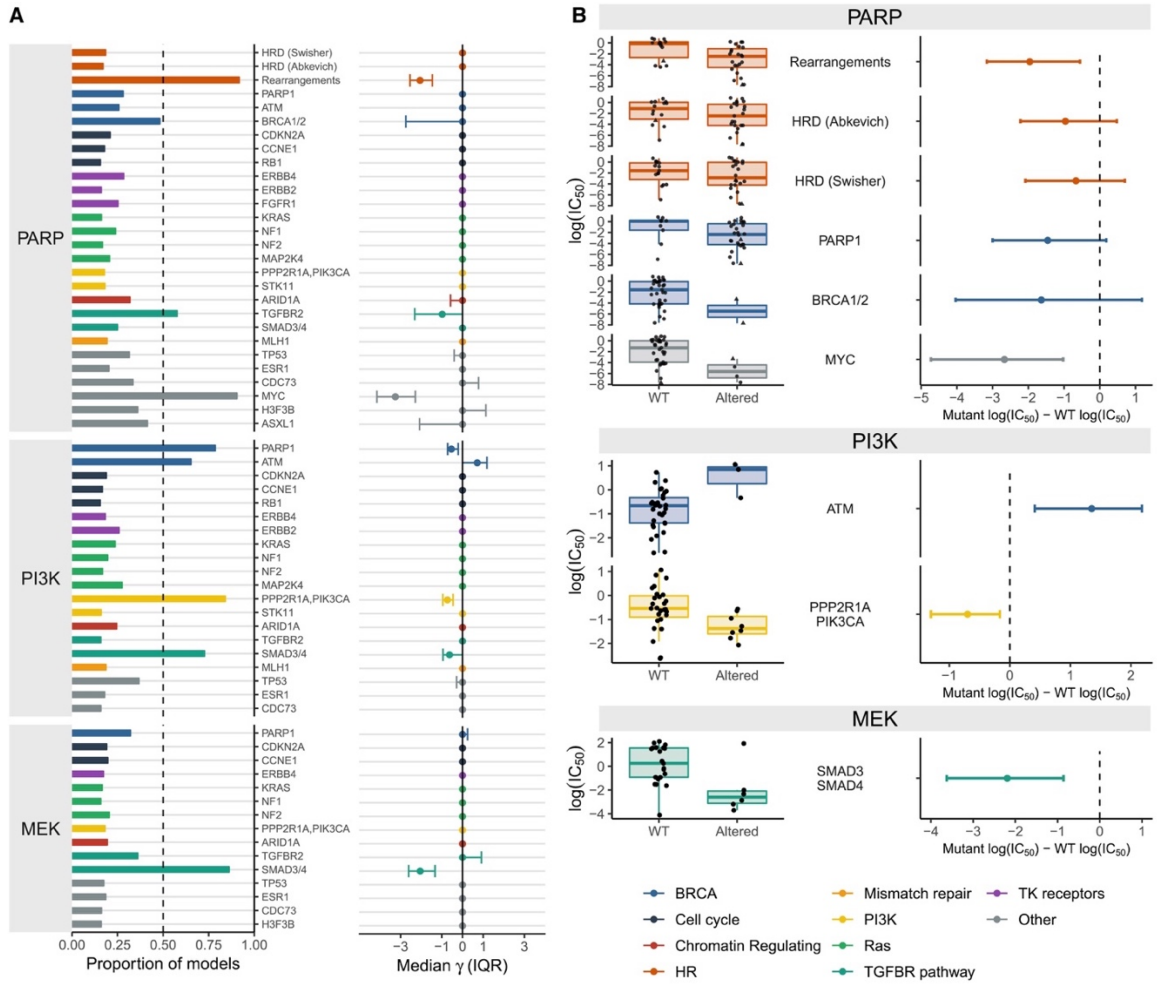

Figure 3.6. Sensitivity and Resistance to Pathway Inhibitors. (A) Bayesian model averaging was used to identify features associated with response to drug. Features selected in fewer than half of the multi-variate models have a posterior probability of being non-zero ≤ 0.5 (vertical dashed line, left) and a posterior median of zero (right). (B) Boxplots of inhibitor concentrations for features selected by this approach, as well as HRD, *PARP1*, and *BRCA1/2* (left). The two cell lines with *BRCA1/2* mutations are indicated by triangles in the PARP pathway. Right: The difference in mean logIC50 concentrations by alteration status and the 90% highest posterior density (HPD) interval for the difference.

Table S3.1a. Summary of ovarian cancer cell lines analyzed

Lab ID	Cell line	Tissue	Subtype	D
CGOV16T	OAW42	ovarian	serous	Unlikely
CGOV17T	OV167	ovarian	serous	Possibly
CGOV18T	OV177	ovarian	serous	Possibly
CGOV21T	OV-90	ovarian	serous	Possibly
CGOV23T	OVCA429	ovarian	serous	Unlikely
CGOV25T	OVCAR3	ovarian	serous	Possibly
CGOV28T	OVKATE	ovarian	serous	Likely h
CGOV30T	OVSAHO	ovarian	serous	Likely h
CGOV32T	PE014	ovarian	serous	Possibly
CGOV34T	PEO6	ovarian	serous	Possibly
CGOV44T	FUOV1	ovarian	serous	Possibly
CGOV45T	COV318	ovarian	serous	Likely h
CGOV46T	JHOS-2	ovarian	serous	Likely h
CGOV47T	JHOS-4	ovarian	serous	Likely h
CGOV4T	DOV13	ovarian	serous	Unlikely
CGOV5T	EFO-21	ovarian	serous	Unlikely
CGOV6T	EFO-27	ovarian	serous	Hy
CGOV8T	HEY	ovarian	serous	Unlikely
CGOV92T	JHOS-3	ovarian	serous	Unlikely
CGOV12T	KOC-7C	ovarian	clear cell	Hy
CGOV20T	OV207	ovarian	clear cell	Possibly
CGOV27T	OVISE	ovarian	clear cell	Unlikely
CGOV29T	OVMANA	ovarian	clear cell	Unlikely
CGOV31T	OVTOKO	ovarian	clear cell	Unlikely
CGOV35T	RMG-1	ovarian	clear cell	Unlikely
CGOV39T	TOV-21G	ovarian	clear cell	Hy
CGOV7T	ES-2	ovarian	clear cell	Possibly
CGOV11T_1	KK	ovarian	clear cell	Unlikely
CGOV14T	MCAS	ovarian	mucinous	Unlikely
CGOV36T	RMUG-S	ovarian	mucinous	Unlikely
CGOV48T	JHOM-1	ovarian	mucinous	Possibly
CGOV38T	TOV-112D	ovarian	endometrioid	Possibly
CGOV49T	OVK-18	ovarian	endometrioid	Hy
CGOV10T	IGROV1	ovarian	mixed	Hy

CGOV13T	Kuramochi	ovarian	undifferentiated	Likely h
CGOV40T	TYK-nu	ovarian	undifferentiated	Likely h
CGOV15T	OAW28	ovarian	unclassified	Likely h
CGOV1T	A2780	ovarian	unclassified	Unlikely
CGOV26T	OVCAR5	ovarian	unclassified	Unlikely
CGOV2T	CAOV-3	ovarian	unclassified	Likely h
CGOV33T	PEA2	ovarian	unclassified	Possibly
CGOV3T	COLO-704	ovarian	unclassified	Hy
CGOV42T	OVCAR8	ovarian	unclassified	Possibly
CGOV53T	OVCAR5-CisR	ovarian	unclassified	Unlikely
CGOV37T_3	SKOV-3	ovarian	unclassified	Possibly
CGH8N	GM10847	lymphoblast culture	NA	Ut
CGH7N	GM12878	lymphoblast culture	NA	Ut
CGH3N	GM17981	lymphoblast culture	NA	Chinese in M Co
CGH4N	GM17982	lymphoblast culture	NA	Chinese in M Co
CGH5N	GM19573	lymphoblast culture	NA	Japanese
CGH6N	GM19574	lymphoblast culture	NA	Japanese
CGH10N	GM19734	lymphoblast culture	NA	Chinese in M Co
CGH9N	GM19737	lymphoblast culture	NA	Chinese in M Co
CGH1N	GM19901	lymphoblast culture	NA	African Ance
CGH2N	GM19902	lymphoblast culture	NA	African Ance

* Tomioka Y. Establishment and characterization of human ovarian clear cell carcinoma cell lines KOC-4c, KOC

** The original score of 0.33 reported by Domcke et al. was revised to reflect a frameshift TP53 mutation in this

Table S3.1c. Summary of genomic analyses

Lab ID	Cell line	Mapped to genome (# bases)	Mapped to exome (# bases)
CGOV16T	OAW-42	127,314,031,800	2,120,021,711
CGOV17T	OV-167	126,889,722,400	2,082,988,874
CGOV18T	OV177	120,683,161,500	2,007,052,935
CGOV21T	OV-90	111,726,115,300	1,928,309,879
CGOV23T	OVCA-429	99,277,561,900	1,612,676,165
CGOV25T	OVCAR-3	107,345,406,200	1,777,448,826
CGOV28T	OVKATE	120,111,997,200	1,933,406,773
CGOV30T	OVSAHO	109,589,203,500	1,837,664,083
CGOV32T	PEO-14	104,155,218,200	1,757,681,426
CGOV34T	PEO-6	118,543,121,800	1,985,859,928
CGOV44T	FU-OV-1	120,329,213,000	2,014,874,040
CGOV45T	COV-318	119,963,006,000	2,062,539,382
CGOV46T	JHOS-2	114,896,903,700	1,856,445,593
CGOV47T	JHOS-4	92,656,405,000	1,512,549,230
CGOV4T	DOV-13	115,247,452,900	1,890,926,588
CGOV5T	EFO-21	131,659,499,000	2,236,327,562
CGOV6T	EFO-27	100,169,989,700	1,636,428,682
CGOV8T	HEY	119,823,556,000	2,063,329,007
CGOV92T	JHOS-3	130,481,536,800	1,799,381,383
CGOV12T	KOC-7C	126,543,652,000	1,880,665,950
CGOV20T	OV207	133,869,300,700	2,256,556,953
CGOV27T	OVISE	93,368,716,800	1,663,322,332
CGOV29T	OVMANA	102,777,959,400	1,744,487,916

CGOV31T	OVTOKO	101,813,930,300	1,606,105,297
CGOV35T	RMG-I	97,702,225,700	1,610,003,898
CGOV39T	TOV-21G	117,004,545,400	1,961,829,335
CGOV7T	ES-2	111,500,740,800	1,851,794,498
CGOV11T_1	KK	140,084,001,800	2,210,022,872
CGOV14T	MCAS	124,679,677,000	1,992,307,537
CGOV36T	RMUG-S	108,068,457,700	1,800,235,062
CGOV48T	JHOM-1	135,333,315,800	2,076,589,350
CGOV38T	TOV-112D	104,131,023,100	1,792,121,233
CGOV49T	OVK-18	90,482,755,900	1,448,721,569
CGOV10T	IGROV-1	121,519,271,300	2,045,216,061
CGOV13T	Kuramochi	127,510,600,400	2,118,335,846
CGOV40T	TYK-nu	112,725,891,000	1,852,556,701
CGOV15T	OAW-28	124,074,985,900	2,048,299,245
CGOV1T	A2780	117,451,750,500	1,944,777,962
CGOV26T	OVCAR-5	99,897,404,200	1,619,448,579
CGOV2T	Caov-3	131,306,959,000	2,270,780,071
CGOV33T	PEA2	120,977,572,400	1,896,767,863
CGOV3T	COLO-704	118,365,148,800	1,992,816,003
CGOV42T	OVCAR-8	115,593,426,900	1,814,448,925
CGOV53T	OVCAR-5-CisR	97,823,176,800	1,558,538,741
CGOV37T_3	SK-OV-3	132,514,663,700	2,071,847,943

Table S3.1d. Summary of sequence alterations

Lab ID	Cell line	Subtype	Total sequence alterations	Puta al
CGOV16T	OAW42	serous	615	
CGOV17T	OV167	serous	489	
CGOV18T	OV177	serous	466	
CGOV21T	OV-90	serous	553	
CGOV23T	OVCA429	serous	667	
CGOV25T	OVCAR3	serous	419	
CGOV28T	OVKATE	serous	539	
CGOV30T	OVSAHO	serous	588	
CGOV32T	PE014	serous	503	
CGOV34T	PEO6	serous	510	
CGOV44T	FUOV1	serous	1108	
CGOV45T	COV318	serous	574	
CGOV46T	JHOS-2	serous	537	
CGOV47T	JHOS-4	serous	655	
CGOV4T	DOV13	serous	778	
CGOV5T	EFO-21	serous	744	
CGOV6T	EFO-27	serous	2417	
CGOV8T	HEY	serous	638	
CGOV92T	JHOS-3	serous	367	
CGOV12T	KOC-7C	clear cell	3930	
CGOV20T	OV207	clear cell	566	
CGOV27T	OVISE	clear cell	596	
CGOV29T	OVMANA	clear cell	644	
CGOV31T	OVTOKO	clear cell	609	
CGOV35T	RMG-1	clear cell	516	
CGOV39T	TOV-21G	clear cell	2292	
CGOV7T	ES-2	clear cell	1016	
CGOV11T_1	KK	clear cell	423	
CGOV14T	MCAS	mucinous	844	
CGOV36T	RMUG-S	mucinous	584	
CGOV48T	JHOM-1	mucinous	564	
CGOV38T	TOV-112D	endometrioid	404	
CGOV49T	OVK-18	endometrioid	2643	
CGOV10T	IGROV1	mixed	4075	
CGOV13T	Kuramochi	undifferentiated	627	
CGOV40T	TYK-nu	undifferentiated	575	

CGOV15T	OAW28	unclassified	507
CGOV1T	A2780	unclassified	1225
CGOV26T	OVCAR5	unclassified	483
CGOV2T	CAOV-3	unclassified	606
CGOV33T	PEA2	unclassified	511
CGOV3T	COLO-704	unclassified	2009
CGOV42T	OVCAR8	unclassified	619
CGOV53T	OVCAR5-CisR	unclassified	987
CGOV37T_3	SKOV-3	unclassified	746

* Hypermutated cell lines have mutations in one or more MMR genes and more than 2000 alterations after exclu

Table S3.1e. Driver genes evaluated for inactivating mutations

Gene symbol	Gene name
POLL	polymerase (DNA directed), lambda
RPA1	replication protein A1, 70kDa
NEIL1	nei endonuclease VIII-like 1 (E. coli)
NEIL2	nei endonuclease VIII-like 2 (E. coli)
NTHL1	nth endonuclease III-like 1 (E. coli)
PNKP	polynucleotide kinase 3'-phosphatase
APTX	aprataxin
TDP1	tyrosyl-DNA phosphodiesterase 1
OGG1	8-oxoguanine DNA glycosylase
AGPAT9	1-acylglycerol-3-phosphate O-acyltransferase
UNG	uracil-DNA glycosylase
APEX1	APEX nuclease (multifunctional DNA repair enzy
APEX2	APEX nuclease (apurinic/apyrimidinic endonuclea
POLB	polymerase (DNA directed), beta
FEN1	flap structure-specific endonuclease 1
ALKBH2	alkB, alkylation repair homolog 2 (E. coli)
ALKBH3	alkB, alkylation repair homolog 3 (E. coli)
XAB2	XPA binding protein 2
CCNH	cyclin H
CDK7	cyclin-dependent kinase 7
CETN2	centrin, EF-hand protein, 2
DDB1	damage-specific DNA binding protein 1, 127kD
ERCC6	excision repair cross-complementation group 6
ERCC7	excision repair cross-complementation group 7
ERCC8	excision repair cross-complementation group 8
LIG1	ligase I, DNA, ATP-dependent
MNAT1	MNAT CDK-activating kinase assembly factor
MMS19	MMS19 nucleotide excision repair homolog (S. cere
RAD23A	RAD23 homolog A (S. cerevisiae)
RAD23B	RAD23 homolog B (S. cerevisiae)
RPA2	replication protein A2, 32kDa
GTF2H5	general transcription factor IIH, polypeptide 5
RAD51B	RAD51 paralog B
RAD51D	RAD51 paralog D
XRCC2	X-ray repair complementing defective repair in Chinese ha
XRCC3	X-ray repair complementing defective repair in Chinese ha
MUS81	MUS81 structure-specific endonuclease subun
EME1	essential meiotic structure-specific endonuclease

ATR	ATR serine/threonine kinase
BARD1	BRCA1 associated RING domain 1
MRE11A	MRE11 meiotic recombination 11 homolog A (S. cer
RAD50	RAD50 homolog (S. cerevisiae)
RAD51	RAD51 recombinase
DCLRE1C	DNA cross-link repair 1C
XRCC6	X-ray repair complementing defective repair in Chinese ha
XRCC5	X-ray repair complementing defective repair in Chinese hamster cells 5 (d
XRCC4	X-ray repair complementing defective repair in Chinese ha
PRKDC	protein kinase, DNA-activated, catalytic polypep
HELQ	helicase, POLQ-like
POLG	polymerase (DNA directed), gamma
POLI	polymerase (DNA directed) iota
POLK	polymerase (DNA directed) kappa
POLM	polymerase (DNA directed), mu
POLN	polymerase (DNA directed) nu
POLQ	polymerase (DNA directed), theta
SLX4	SLX4 structure-specific endonuclease subunit
H2AFX	H2A histone family, member X
CHAF1A	chromatin assembly factor 1, subunit A (p150
RECQL	RecQ helicase-like
RECQL5	RecQ protein-like 5
MSH3	mutS homolog 3
MLH3	mutL homolog 3
EXO1	exonuclease 1
CHEK1	checkpoint kinase 1
MDC1	mediator of DNA-damage checkpoint 1
TP53BP1	tumor protein p53 binding protein 1
C11orf30	chromosome 11 open reading frame 30
ERCC4	excision repair cross-complementation group 4
RAD51C	RAD51 paralog C
RAD51C	RAD51 homolog C (S. cerevisiae)
BRIP1	BRCA1 interacting protein C-terminal helicase
BRCA2	breast cancer 2, early onset
PALB2	partner and localizer of BRCA2
PALB2	partner and localizer of BRCA2
FANCL	Fanconi anemia, complementation group L
XRCC1	X-ray repair complementing defective repair in Chinese ha
DDB2	damage-specific DNA binding protein 2, 48kD
ERCC1	excision repair cross-complementation group 1

ERCC2	excision repair cross-complementation group 2
ERCC3	excision repair cross-complementation group 3
ERCC5	excision repair cross-complementation group 5
ATM	ATM serine/threonine kinase
CHEK2	checkpoint kinase 2
TP53	tumor protein p53
BRCA1	breast cancer 1, early onset
NBN	nibrin
POLE	polymerase (DNA directed), epsilon, catalytic sub
POLH	polymerase (DNA directed), eta
FANCC	Fanconi anemia, complementation group C
FANCD2	Fanconi anemia, complementation group D2
FANCB	Fanconi anemia, complementation group B
FANCA	Fanconi anemia, complementation group A
FANCE	Fanconi anemia, complementation group E
FANCF	Fanconi anemia, complementation group F
FANCG	Fanconi anemia, complementation group G
FANCI	Fanconi anemia, complementation group I
FANCM	Fanconi anemia, complementation group M
ATRX	alpha thalassemia/mental retardation syndrome X-l
RECQL4	RecQ protein-like 4
MSH2	mutS homolog 2
MSH6	mutS homolog 6
MLH1	mutL homolog 1
PMS1	PMS1 postmeiotic segregation increased 1 (S. cerev
PMS2	PMS2 postmeiotic segregation increased 2 (S. cerev
PTEN	phosphatase and tensin homolog
PIK3R1	phosphoinositide-3-kinase, regulatory subunit 1 (a
MAX	MYC associated factor X
ARID1A	AT rich interactive domain 1A (SWI-like)
ARID1B	AT rich interactive domain 1B (SWI1-like)
SMARCA4	SWI/SNF related, matrix associated, actin dependent regulator of chroma
SMARCA2	SWI/SNF related, matrix associated, actin dependent regulator of chroma
NF1	neurofibromin 1
CREBBP	CREB binding protein
mTOR	mechanistic target of rapamycin (serine/threonine k
MLL	myeloid/lymphoid or mixed-lineage leukemia (trithorax homo
MLL2	myeloid/lymphoid or mixed-lineage leukemia
MLL3	myeloid/lymphoid or mixed-lineage leukemia
NBS1	Nijmegen Breakage Syndrome 1

ATXN1	ataxin 1
AR	androgen receptor
ARMC4	armadillo repeat containing 4
DRD4	dopamine receptor D4
EP300	E1A binding protein p300
ERBB2	v-erb-b2 erythroblastic leukemia viral oncogene homolog 2, neuro/glioblastoma
ANK3	ankyrin 3, node of Ranvier (ankyrin G)
APC	adenomatous polyposis coli
CACNA1S	calcium channel, voltage-dependent, L type, alpha 1S
FCGBP	Fc fragment of IgG binding protein
FLG	filaggrin
GRM8	glutamate receptor, metabotropic 8
HYDIN	HYDIN, axonemal central pair apparatus protei
KIAA1217	uncharacterized protein
KIF3A	kinesin family member 3A
NAA16	N(alpha)-acetyltransferase 16, NatA auxiliary sub
NFE2L2	nuclear factor (erythroid-derived 2)-like 2
OR52B4	olfactory receptor, family 52, subfamily B, memb
PPP2R1A	protein phosphatase 2, regulatory subunit A, alp
RAB17	RAB17, member RAS oncogene family
RELN	reelin
REST	RE1-silencing transcription factor
RET	ret proto-oncogene
RIPK1	receptor (TNFRSF)-interacting serine-threonine kin
SIGLEC10	sialic acid binding Ig-like lectin 10
SLC2A7	solute carrier family 2 (facilitated glucose transporter),
SMAD4	SMAD family member 4
SPEF2	sperm flagellar 2
USH2A	Usher syndrome 2A (autosomal recessive, mild
VPS13A	vacuolar protein sorting 13 homolog A (S. cerevis
ZFHX4	zinc finger homeobox 4
ZNF426	zinc finger protein 426
ABL1	c-abl oncogene 1, non-receptor tyrosine kinase
ACVR1C	activin A receptor, type IC
ACVR1B	activin A receptor, type IB
ALK	anaplastic lymphoma receptor tyrosine kinase
ASXL1	additional sex combs like 1 (Drosophila)
AURKA	aurora kinase A
AXIN2	axin 2
BAP1	BRCA1 associated protein-1 (ubiquitin carboxy-terminal

BCL2	apoptosis regulator
BCR	breakpoint cluster region
BLM	Bloom syndrome, RecQ helicase-like
BMPR1A	bone morphogenetic protein receptor, type IA
BTK	Bruton agammaglobulinemia tyrosine kinase
CALR	calreticulin
CBL	Cbl proto-oncogene, E3 ubiquitin protein ligas
CCND1	cyclin D1
CCNE1	cyclin E1
CDC73	cell division cycle 73
CDH1	cadherin 1
CDK4	cyclin-dependent kinase 4
CDK6	cyclin dependent kinase 6
CDKN1B	cyclin-dependent kinase inhibitor 1B (p27, Kip
CDKN2A	cyclin-dependent kinase inhibitor 2A
CDKN2C	cyclin-dependent kinase inhibitor 2C (p18, inhibits C
CEBPA	CCAAT/enhancer binding protein (C/EBP), alp
CIC	capicua homolog (Drosophila)
CSF1R	colony stimulating factor 1 receptor
CYLD	cylindromatosis (turban tumor syndrome)
DAXX	death-domain associated protein
DDR2	discoidin domain receptor tyrosine kinase 2
DICER1	dicer 1, ribonuclease type III
DNMT3A	DNA (cytosine-5-)-methyltransferase 3 alpha
EGFR	epidermal growth factor receptor
ERBB3	v-erb-b2 erythroblastic leukemia viral oncogene homolo
ERBB4	v-erb-a erythroblastic leukemia viral oncogene homolog
ESR1	estrogen receptor 1
ETV1	ets variant 1
ETV5	ETS variant 5
EWSR1	Ewing sarcoma breakpoint region 1
EXT1	exostosin 1
EXT2	exostosin 2
EZH2	enhancer of zeste homolog 2 (Drosophila)
FGFR1	fibroblast growth factor receptor 1
FGFR2	fibroblast growth factor receptor 2
FGFR3	fibroblast growth factor receptor 3
FGFR4	fibroblast growth factor receptor 4
FH	fumarate hydratase
FLCN	folliculin

FLT3	fms-related tyrosine kinase 3
FLT4	fms-related tyrosine kinase 4
FOXL2	forkhead box L2
GATA1	GATA binding protein 1
GATA2	GATA binding protein 2
GNA11	guanine nucleotide binding protein (G protein), alpha 11
GNAQ	guanine nucleotide binding protein (G protein), q poly
GNAS	GNAS complex locus
GPC3	glypican 3
H3F3A	H3 histone family member 3A
H3F3B	H3 histone family member 3B
HNF1A	HNF1 homeobox A
IDH1	isocitrate dehydrogenase 1 (NADP+), soluble
IDH2	isocitrate dehydrogenase 2 (NADP+), mitochond
IGF1R	insulin-like growth factor 1 receptor
IGF2R	insulin-like growth factor 2 receptor
IKZF1	IKAROS family zinc finger 1 (Ikaros)
JAK1	Janus kinase 1
JAK2	Janus kinase 2
JAK3	Janus kinase 3
KDR	kinase insert domain receptor (a type III receptor tyrosi
KIT	v-kit Hardy-Zuckerman 4 feline sarcoma viral oncogene
MAML1	mastermind-like 1 (Drosophila)
MAP2K1	mitogen-activated protein kinase kinase 1
MAP2K4	mitogen-activated protein kinase kinase 4
MDM2	Mdm2, p53 E3 ubiquitin protein ligase homolog (m
MDM4	Mdm4 p53 binding protein homolog (mouse)
MED12	mediator complex subunit 12
MEN1	multiple endocrine neoplasia I
MET	met proto-oncogene (hepatocyte growth factor rece
MPL	myeloproliferative leukemia virus oncogene
MUTYH	mutY DNA glycosylase
MYC	v-myc myelocytomatosis viral oncogene homolog (
MYCL1	v-myc myelocytomatosis viral oncogene homolog 1, lung carcino
MYCN	v-myc myelocytomatosis viral related oncogene, neuroblastom
MYD88	myeloid differentiation primary response 88
NCOA3	nuclear receptor coactivator 3
NF2	neurofibromin 2 (merlin)
NKX2-1	NK2 homeobox 1
NOTCH1	notch 1

NOTCH3	notch 3
NOTCH4	notch 4
NPM1	nucleophosmin (nucleolar phosphoprotein B23, nun
NTRK1	neurotrophic tyrosine kinase, receptor, type 1
PALB2	partner and localizer of BRCA2
PALB2	partner and localizer of BRCA2
PAX5	paired box 5
PBRM1	polybromo 1
PDGFRA	platelet-derived growth factor receptor, alpha polyp
PHOX2B	paired-like homeobox 2b
POLD1	polymerase (DNA directed), delta 1, catalytic sub
POT1	protection of telomeres 1
PRKAR1A	protein kinase, cAMP-dependent, regulatory, type I,
PRSS1	serine protease 1
PTCH1	patched 1
PTPN11	protein tyrosine phosphatase, non-receptor type
RAD51C	RAD51 paralog C
RAD51C	RAD51 homolog C (S. cerevisiae)
RAF1	v-raf-1 murine leukemia viral oncogene homolog
RNF43	ring finger protein 43
RUNX1	runt-related transcription factor 1
SBDS	SBDS, ribosome maturation factor
SDHAF2	succinate dehydrogenase complex assembly facto
SDHB	succinate dehydrogenase complex, subunit B, iron su
SDHC	succinate dehydrogenase complex subunit C
SDHD	succinate dehydrogenase complex, subunit D, integral mem
SF3B1	splicing factor 3b, subunit 1, 155kDa
SMAD2	SMAD family member 2
SMAD3	SMAD family member 3
SMARCB1	SWI/SNF related, matrix associated, actin dependent regulator of chroma
SMO	smoothened, frizzled family receptor
SRC	SRC proto-oncogene, non-receptor tyrosine kina
STAG2	stromal antigen 2
SUFU	suppressor of fused homolog (Drosophila)
TERT	telomerase reverse transcriptase
TET2	tet methylcytosine dioxygenase 2
TGFBR2	transforming growth factor, beta receptor II (70/80
TNFAIP3	tumor necrosis factor, alpha-induced protein 3
TOP1	topoisomerase (DNA) I
TSC1	tuberous sclerosis 1

TSC2	tuberous sclerosis 2
TSHR	thyroid stimulating hormone receptor
WAS	Wiskott-Aldrich syndrome
WRN	Werner syndrome, RecQ helicase-like
WT1	Wilms tumor 1
XPA	DNA damage recognition and repair factor
XPC	xeroderma pigmentosum, complementation grou
DNAJB1	DnaJ heat shock protein family (Hsp40) member
ETV4	ets variant 4
ETV6	ETS variant 6
PDGFRB	platelet-derived growth factor receptor, beta polype
PRKACA	protein kinase, cAMP-dependent, catalytic, alp
RARA	retinoic acid receptor, alpha
TACC3	transforming, acidic coiled-coil containing protei
TMPRSS2	transmembrane protease, serine 2
AKT2	AKT serine/threonine kinase 2
CTNNB1	catenin (cadherin-associated protein), beta 1, 88k
ACVR1	activin A receptor type 1
AKT1	v-akt murine thymoma viral oncogene homolog
BUB1B	BUB1 mitotic checkpoint serine/threonine kinas
CDKN2B	cyclin dependent kinase inhibitor 2B
VHL	von Hippel-Lindau tumor suppressor, E3 ubiquitin prot
SMARCC1	SWI/SNF related, matrix associated, actin dependent regulator of chroma
SMARCD2	SWI/SNF related, matrix associated, actin dependent regulator of chroma
SMARCE1	SWI/SNF related, matrix associated, actin dependent regulator of chroma
FBXW7	F-box and WD repeat domain containing 7, E3 ubiquitin p
NOTCH2	notch 2
AXIN1	axin 1
PARP1	poly (ADP-ribose) polymerase 1
STK11	serine/threonine kinase 11
ROS1	c-ros oncogene 1 , receptor tyrosine kinase

Table S3.1f. Sequence alterations

Lab ID	Cell line	Gene symbol	
CGOV1T	A2780	ARID1A	AT
CGOV1T	A2780	ARID1A	AT
CGOV1T	A2780	DRD4	
CGOV1T	A2780	FCGBP	
CGOV1T	A2780	MAX	
CGOV1T	A2780	PIK3CA	phosphatidylinosit
CGOV1T	A2780	SMARCA4	SWI/SNF related, matrix associa
CGOV1T	A2780	WRN	W
CGOV10T	IGROV-1	ABL1	c-abl
CGOV10T	IGROV-1	AKAP6	
CGOV10T	IGROV-1	AMBRA1	
CGOV10T	IGROV-1	ARHGAP27	
CGOV10T	IGROV-1	ARID1A	AT
CGOV10T	IGROV-1	ARID1A	AT
CGOV10T	IGROV-1	ATXN1	
CGOV10T	IGROV-1	AXIN2	
CGOV10T	IGROV-1	BRCA1	
CGOV10T	IGROV-1	CHEK1	
CGOV10T	IGROV-1	DIABLO	diab
CGOV10T	IGROV-1	DICER1	
CGOV10T	IGROV-1	ERCC5	excision repair cross-comp
CGOV10T	IGROV-1	FAM160A2	family
CGOV10T	IGROV-1	FAM46C	family

CGOV10T	IGROV-1	FBN2	
CGOV10T	IGROV-1	FBXW7	F-box and WD rep
CGOV10T	IGROV-1	FLG	
CGOV10T	IGROV-1	GLI3	
CGOV10T	IGROV-1	GRB14	gro
CGOV10T	IGROV-1	GRM8	
CGOV10T	IGROV-1	IGHMBP2	in
CGOV10T	IGROV-1	ITPR3	inos
CGOV10T	IGROV-1	JAK1	
CGOV10T	IGROV-1	KIAA0100	
CGOV10T	IGROV-1	KIAA1217	
CGOV10T	IGROV-1	MED12	
CGOV10T	IGROV-1	MLH1	mutL homolo
CGOV10T	IGROV-1	MLH3	
CGOV10T	IGROV-1	MLL	myeloid/lymphoid or
CGOV10T	IGROV-1	MLL2	myelo
CGOV10T	IGROV-1	MLL3	myelo
CGOV10T	IGROV-1	MSH2	mutS homolo
CGOV10T	IGROV-1	MSH3	
CGOV10T	IGROV-1	MSH6	
CGOV10T	IGROV-1	NCOR2	
CGOV10T	IGROV-1	NOTCH3	
CGOV10T	IGROV-1	OR1S2	olfactory
CGOV10T	IGROV-1	PDE4DIP	pho
CGOV10T	IGROV-1	PDGFRB	platelet-der
CGOV10T	IGROV-1	PIK3CA	phosphatidylinosit
CGOV10T	IGROV-1	PIK3CA	phosphatidylinosit

CGOV10T	IGROV-1	PMS1	PMS1 postr
CGOV10T	IGROV-1	PMS1	PMS1 postr
CGOV10T	IGROV-1	POLN	
CGOV10T	IGROV-1	POLQ	
CGOV10T	IGROV-1	PPP5C	pr
CGOV10T	IGROV-1	PTEN	
CGOV10T	IGROV-1	PTEN	
CGOV10T	IGROV-1	RAD50	
CGOV10T	IGROV-1	RSPH6A	radial sp
CGOV10T	IGROV-1	SCN8A	sodium ch
CGOV10T	IGROV-1	SHPRH	SNF2 histone lin
CGOV10T	IGROV-1	SIM1	sir
CGOV10T	IGROV-1	SLC43A3	
CGOV10T	IGROV-1	SMAD4	
CGOV10T	IGROV-1	SPEF2	
CGOV10T	IGROV-1	STAG2	
CGOV10T	IGROV-1	TASP1	
CGOV10T	IGROV-1	TOP1	
CGOV10T	IGROV-1	VHL	von Hippel-Lin
CGOV10T	IGROV-1	WDR62	
CGOV10T	IGROV-1	ZBTB4	zinc
CGOV10T	IGROV-1	ZDHHC6	z
CGOV10T	IGROV-1	ZFHX4	
CGOV10T	IGROV-1	ZFHX4	
CGOV10T	IGROV-1	ZFHX4	

CGOV11T_1	KK	ACAA2	
CGOV11T_1	KK	ADAMTSL1	
CGOV11T_1	KK	AFF2	
CGOV11T_1	KK	ANKRD11	
CGOV11T_1	KK	ANKRD13C	
CGOV11T_1	KK	ARID1A	AT
CGOV11T_1	KK	BAZ2A	bromod
CGOV11T_1	KK	BBX	
CGOV11T_1	KK	CLCN1	c
CGOV11T_1	KK	CLEC4E	C-t
CGOV11T_1	KK	COL11A1	
CGOV11T_1	KK	COL4A6	
CGOV11T_1	KK	CRB1	
CGOV11T_1	KK	CSTF1	cleavage sti
CGOV11T_1	KK	DDX39A	DEAD
CGOV11T_1	KK	DNAH1	
CGOV11T_1	KK	DOCK5	
CGOV11T_1	KK	DSG1	
CGOV11T_1	KK	DTNA	
CGOV11T_1	KK	FBN2	
CGOV11T_1	KK	FLG2	
CGOV11T_1	KK	FTCD	for
CGOV11T_1	KK	GAD2	glutamate dec
CGOV11T_1	KK	GCSAML	germinal
CGOV11T_1	KK	GRM3	

CGOV11T_1	KK	HOMEZ	ho
CGOV11T_1	KK	KRT3	
CGOV11T_1	KK	KRTAP12-2	
CGOV11T_1	KK	LAIR2	leukocyte
CGOV11T_1	KK	LAMP5	lysosomal-a
CGOV11T_1	KK	LRRC8E	leucine
CGOV11T_1	KK	LZTS1	leuc
CGOV11T_1	KK	MEGF11	
CGOV11T_1	KK	MUC20	
CGOV11T_1	KK	MYH11	my
CGOV11T_1	KK	MYOM1	
CGOV11T_1	KK	NCKAP5	
CGOV11T_1	KK	NPC1L1	
CGOV11T_1	KK	NR2C2AP	nu
CGOV11T_1	KK	NUP153	
CGOV11T_1	KK	OR10J1	olfactory
CGOV11T_1	KK	PCMTD1	protein-L-isoaspartate
CGOV11T_1	KK	PLXNB2	
CGOV11T_1	KK	PNMA3	
CGOV11T_1	KK	PPP2R1A	protein
CGOV11T_1	KK	PRSS3	
CGOV11T_1	KK	PRSS53	
CGOV11T_1	KK	QRICH2	
CGOV11T_1	KK	RHBDF2	r
CGOV11T_1	KK	RTFDC1	replicatio

CGOV11T_1	KK	SELENBP1	
CGOV11T_1	KK	SLC1A6	solute carrier family 1
CGOV11T_1	KK	SLC22A8	solute carrier
CGOV11T_1	KK	SLC39A14	solute car
CGOV11T_1	KK	SLC4A10	solute carrier fa
CGOV11T_1	KK	SORCS1	sortilin-r
CGOV11T_1	KK	TBC1D8B	TBC1 dom
CGOV11T_1	KK	TCF3	
CGOV11T_1	KK	UNC13C	
CGOV11T_1	KK	USH2A	Usher
CGOV11T_1	KK	WNK4	W
CGOV11T_1	KK	ZNF382	
CGOV12T	KOC-7C	ABCB11	ATP-binding
CGOV12T	KOC-7C	ADAM20	A
CGOV12T	KOC-7C	ANK2	
CGOV12T	KOC-7C	ARID1A	AT
CGOV12T	KOC-7C	ARID1A	AT
CGOV12T	KOC-7C	ARID1A	AT
CGOV12T	KOC-7C	ARID1B	AT
CGOV12T	KOC-7C	ATM	
CGOV12T	KOC-7C	BAP1	BRCA1 associat
CGOV12T	KOC-7C	BCL9L	
CGOV12T	KOC-7C	BLM	B
CGOV12T	KOC-7C	CCDC93	
CGOV12T	KOC-7C	CHIT1	
CGOV12T	KOC-7C	CORIN	

CGOV12T	KOC-7C	COX10	cytochro
CGOV12T	KOC-7C	FAT1	FAT t
CGOV12T	KOC-7C	FBXW7	F-box and WD rep
CGOV12T	KOC-7C	FLG	
CGOV12T	KOC-7C	GRIK3	glu
CGOV12T	KOC-7C	HAO1	hyd
CGOV12T	KOC-7C	IDH2	isocitrate
CGOV12T	KOC-7C	IGF2BP3	insulin-li
CGOV12T	KOC-7C	KCND1	potassium voltag
CGOV12T	KOC-7C	KCNH7	potassium voltage
CGOV12T	KOC-7C	KRT34	
CGOV12T	KOC-7C	L1CAM	
CGOV12T	KOC-7C	MEN1	
CGOV12T	KOC-7C	MLL2	myelo
CGOV12T	KOC-7C	MNS1	r
CGOV12T	KOC-7C	MSH2	mutS homolo
CGOV12T	KOC-7C	MSH2	mutS homolo
CGOV12T	KOC-7C	MSH3	
CGOV12T	KOC-7C	MYCN	v-myc myelocytomato
CGOV12T	KOC-7C	MYOM1	
CGOV12T	KOC-7C	NAA16	N(alpha)-
CGOV12T	KOC-7C	NETO2	neu
CGOV12T	KOC-7C	NFE2L2	nuc
CGOV12T	KOC-7C	NOTCH1	
CGOV12T	KOC-7C	NUTF2	

CGOV12T	KOC-7C	PCCA	propio
CGOV12T	KOC-7C	PIK3CA	phosphatidylinosit
CGOV12T	KOC-7C	PMS1	PMS1 postr
CGOV12T	KOC-7C	PREX2	phosphatidylinosito
CGOV12T	KOC-7C	PSMD6	proteasome (p
CGOV12T	KOC-7C	PTEN	
CGOV12T	KOC-7C	PTEN	
CGOV12T	KOC-7C	PTPRS	prote
CGOV12T	KOC-7C	RAD23A	
CGOV12T	KOC-7C	RAD50	
CGOV12T	KOC-7C	RPA1	
CGOV12T	KOC-7C	RSG1	R
CGOV12T	KOC-7C	SAMD9L	steri
CGOV12T	KOC-7C	SDHAF2	succinate
CGOV12T	KOC-7C	SIGLEC10	
CGOV12T	KOC-7C	SLC24A1	solute carrier family
CGOV12T	KOC-7C	SLC7A8	solute carrier family 7
CGOV12T	KOC-7C	SLIT2	
CGOV12T	KOC-7C	SMAD3	
CGOV12T	KOC-7C	SNX13	
CGOV12T	KOC-7C	TBX18	
CGOV12T	KOC-7C	TGM2	transglutaminase 2 (C p
CGOV12T	KOC-7C	TMEM2	
CGOV12T	KOC-7C	TMIGD1	transmembr
CGOV12T	KOC-7C	TP53	

CGOV12T	KOC-7C	TUSC3	
CGOV12T	KOC-7C	VPS13A	vacuolar
CGOV12T	KOC-7C	VPS13A	vacuolar
CGOV12T	KOC-7C	ZNF415	
CGOV13T	Kuramochi	BRCA2	
CGOV13T	Kuramochi	CDH18	
CGOV13T	Kuramochi	EWSR1	
CGOV13T	Kuramochi	SMAD4	
CGOV13T	Kuramochi	SMO	s
CGOV13T	Kuramochi	TP53	
CGOV14T	MCAS	C1orf168	ch
CGOV14T	MCAS	ENPP4	ectonucleotide
CGOV14T	MCAS	KRAS	v-Ki-ras2
CGOV14T	MCAS	PIK3CA	phosphatidylinosit
CGOV14T	MCAS	PPP3CA	protein ph
CGOV14T	MCAS	RIMS1	regu
CGOV14T	MCAS	RNF43	
CGOV14T	MCAS	SMAD4	
CGOV14T	MCAS	SPG11	spas
CGOV14T	MCAS	SYT16	
CGOV14T	MCAS	USH2A	Usher
CGOV14T	MCAS	USP21	
CGOV15T	OAW-28	ALDH16A1	aldehy
CGOV15T	OAW-28	ERCC2	excision repair cross-comp
CGOV15T	OAW-28	TP53	

CGOV15T	OAW-28	TSC2	
CGOV16T	OAW-42	ARID1A	AT
CGOV16T	OAW-42	ARID1A	AT
CGOV16T	OAW-42	FAM129C	family
CGOV16T	OAW-42	FANCD2	Fanc
CGOV16T	OAW-42	PIK3CA	phosphatidylinosit
CGOV16T	OAW-42	SLC14A2	solute ca
CGOV16T	OAW-42	SUSD3	
CGOV17T	OV-167	ARMC4	
CGOV17T	OV-167	TP53	
CGOV17T	OV-167	USH2A	Usher
CGOV18T	OV177	ASCC3	activati
CGOV18T	OV177	TP53	
CGOV2T	Caov-3	ARMC4	
CGOV2T	Caov-3	TP53	
CGOV20T	OV207	ARID1A	AT
CGOV20T	OV207	KIF3A	
CGOV20T	OV207	NID1	
CGOV20T	OV207	SLC2A7	solute carrier fa
CGOV20T	OV207	SPEF2	
CGOV20T	OV207	TP53	
CGOV21T	OV-90	CDKN2A	c
CGOV21T	OV-90	EPHA1	
CGOV21T	OV-90	HNF1A	
CGOV21T	OV-90	IFIT1	interferon-i
CGOV21T	OV-90	KIAA1958	

CGOV21T	OV-90	SMAD4	
CGOV21T	OV-90	TP53	
CGOV23T	OVCA-429	DAAM2	dishevel
CGOV23T	OVCA-429	MSH6	
CGOV23T	OVCA-429	PCDHA5	
CGOV23T	OVCA-429	REST	
CGOV25T	OVCAR-3	ADCY1	
CGOV25T	OVCAR-3	MAMDC4	
CGOV25T	OVCAR-3	PIK3R1	phosphoin
CGOV25T	OVCAR-3	POLK	
CGOV25T	OVCAR-3	STAG2	
CGOV25T	OVCAR-3	TP53	
CGOV26T	OVCAR-5	ANK3	an
CGOV26T	OVCAR-5	APC	
CGOV26T	OVCAR-5	CREBBP	
CGOV26T	OVCAR-5	EP300	
CGOV26T	OVCAR-5	KRAS	v-Ki-ras2
CGOV26T	OVCAR-5	RIPK1	receptor (T
CGOV27T	OVISE	ARID1A	AT
CGOV27T	OVISE	ARID1A	AT
CGOV27T	OVISE	ARID1B	AT
CGOV27T	OVISE	FCGBP	
CGOV27T	OVISE	GRM8	
CGOV27T	OVISE	KIF1A	
CGOV27T	OVISE	NOTCH1	

CGOV27T	OVISE	PIK3CA	phosphatidylinosit
CGOV27T	OVISE	PPP2R1A	protein
CGOV28T	OVKATE	CNTNAP2	
CGOV28T	OVKATE	DNMT3A	DNA
CGOV28T	OVKATE	DNMT3A	DNA
CGOV28T	OVKATE	GPR17	
CGOV28T	OVKATE	GXYLT1	
CGOV28T	OVKATE	PLA2G12B	
CGOV28T	OVKATE	ROS1	c-ro
CGOV28T	OVKATE	SMAD4	
CGOV28T	OVKATE	TM4SF4	tra
CGOV28T	OVKATE	TP53	
CGOV29T	OVMANA	ARID1A	AT
CGOV29T	OVMANA	ARID1A	AT
CGOV29T	OVMANA	PIK3CA	phosphatidylinosit
CGOV3T	COLO-704	ALKBH2	alkB
CGOV3T	COLO-704	ALKBH2	alkB
CGOV3T	COLO-704	AR	
CGOV3T	COLO-704	AR	
CGOV3T	COLO-704	BLM	B
CGOV3T	COLO-704	BMS1	BMS1 h
CGOV3T	COLO-704	BRCA2	
CGOV3T	COLO-704	COL1A1	
CGOV3T	COLO-704	DBC1	
CGOV3T	COLO-704	EP300	

CGOV3T	COLO-704	GRM8	
CGOV3T	COLO-704	HNF1A	
CGOV3T	COLO-704	INTS1	
CGOV3T	COLO-704	MLL2	myelo
CGOV3T	COLO-704	MSH3	
CGOV3T	COLO-704	MSH6	
CGOV3T	COLO-704	MYCL1	v-myc myelocytomatosis
CGOV3T	COLO-704	NRP2	
CGOV3T	COLO-704	PTEN	
CGOV3T	COLO-704	SHROOM4	
CGOV3T	COLO-704	WRN	W
CGOV3T	COLO-704	WRN	W
CGOV3T	COLO-704	ZFHX2	
CGOV3T	COLO-704	ZFHX4	
CGOV3T	COLO-704	ZFHX4	
CGOV30T	OVSAHO	NSD1	nuclea
CGOV30T	OVSAHO	PIAS4	pi
CGOV30T	OVSAHO	SH3PXD2B	
CGOV30T	OVSAHO	TP53	
CGOV30T	OVSAHO	ZNF556	
CGOV31T	OVTOKO	ARID1A	AT
CGOV31T	OVTOKO	ARID1A	AT
CGOV31T	OVTOKO	BCAS1	br
CGOV31T	OVTOKO	EBF3	
CGOV31T	OVTOKO	PIK3R1	phosphoin

CGOV31T	OVTOKO	PNPLA3	patatin
CGOV31T	OVTOKO	PPP2R1A	protein
CGOV31T	OVTOKO	SYCP1	
CGOV32T	PEO-14	SLC22A14	s
CGOV32T	PEO-14	TP53	
CGOV33T	PEA2	BARD1	
CGOV33T	PEA2	CACNA1S	calcium chan
CGOV33T	PEA2	RECQL5	
CGOV33T	PEA2	TLL2	
CGOV33T	PEA2	TP53	
CGOV34T	PEO-6	LSS	lanosterol s
CGOV34T	PEO-6	NF1	
CGOV34T	PEO-6	RELN	
CGOV34T	PEO-6	TP53	
CGOV35T	RMG-I	FANCL	Fanc
CGOV35T	RMG-I	MORN3	
CGOV35T	RMG-I	TRIM37	
CGOV35T	RMG-I	TRUB1	TruB pseu
CGOV36T	RMUG-S	BUB1B	BUB1 m
CGOV36T	RMUG-S	CCDC54	
CGOV36T	RMUG-S	SEMA5B	sema domain, seven thrombospondin repeat
CGOV37T_3	SK-OV-3	ABCD1	ATP-bind
CGOV37T_3	SK-OV-3	ANK3	an
CGOV37T_3	SK-OV-3	APC	
CGOV37T_3	SK-OV-3	ARID1A	AT
CGOV37T_3	SK-OV-3	ATF6	

CGOV37T_3	SK-OV-3	B4GALNT2	beta-1
CGOV37T_3	SK-OV-3	BCL11B	B-cell
CGOV37T_3	SK-OV-3	C11orf30	ch
CGOV37T_3	SK-OV-3	C1QTNF9	C1q a
CGOV37T_3	SK-OV-3	C7orf26	cl
CGOV37T_3	SK-OV-3	CCDC15	
CGOV37T_3	SK-OV-3	CD5L	
CGOV37T_3	SK-OV-3	CDAN1	
CGOV37T_3	SK-OV-3	CDC25B	
CGOV37T_3	SK-OV-3	CHIA	
CGOV37T_3	SK-OV-3	COL4A5	
CGOV37T_3	SK-OV-3	CSPP1	centros
CGOV37T_3	SK-OV-3	DOCK2	
CGOV37T_3	SK-OV-3	EEF1A2	eukary
CGOV37T_3	SK-OV-3	ELMSAN1	ELM2
CGOV37T_3	SK-OV-3	FBXW7	F-box and WD re
CGOV37T_3	SK-OV-3	FCRL1	
CGOV37T_3	SK-OV-3	FMO3	f
CGOV37T_3	SK-OV-3	GNMT	
CGOV37T_3	SK-OV-3	GPR34	
CGOV37T_3	SK-OV-3	GSDMA	
CGOV37T_3	SK-OV-3	GUCY2F	
CGOV37T_3	SK-OV-3	ILVBL	ilv
CGOV37T_3	SK-OV-3	IRS4	
CGOV37T_3	SK-OV-3	KANSL1	KA

CGOV37T_3	SK-OV-3	KDM8	
CGOV37T_3	SK-OV-3	LINGO4	leucin
CGOV37T_3	SK-OV-3	LOXHD1	
CGOV37T_3	SK-OV-3	LRRN4	
CGOV37T_3	SK-OV-3	MEF2D	
CGOV37T_3	SK-OV-3	MEIS3	
CGOV37T_3	SK-OV-3	NADSYN1	
CGOV37T_3	SK-OV-3	NDST4	N-deacetyla
CGOV37T_3	SK-OV-3	NEDD4	neural precursor cell expresse
CGOV37T_3	SK-OV-3	NOTCH2	
CGOV37T_3	SK-OV-3	NTSR2	
CGOV37T_3	SK-OV-3	OR51L1	olfactory
CGOV37T_3	SK-OV-3	PHEX	phosphate
CGOV37T_3	SK-OV-3	PHIP	plecks
CGOV37T_3	SK-OV-3	PI4KA	phosp
CGOV37T_3	SK-OV-3	PIGN	phosphatid
CGOV37T_3	SK-OV-3	PIK3CA	phosphatidylinosit
CGOV37T_3	SK-OV-3	POLD1	polymera
CGOV37T_3	SK-OV-3	PPFIA2	protein tyrosine phosphatase, rece
CGOV37T_3	SK-OV-3	PPFIBP2	PTPRF inte
CGOV37T_3	SK-OV-3	PRLR	
CGOV37T_3	SK-OV-3	PSKH1	
CGOV37T_3	SK-OV-3	PTGER4	pro
CGOV37T_3	SK-OV-3	RASGEF1A	R
CGOV37T_3	SK-OV-3	RBM47	

CGOV37T_3	SK-OV-3	RHBDF2	r
CGOV37T_3	SK-OV-3	RPTOR	regulato
CGOV37T_3	SK-OV-3	SELENBP1	
CGOV37T_3	SK-OV-3	SIK1	
CGOV37T_3	SK-OV-3	SLC12A9	
CGOV37T_3	SK-OV-3	SLC2A6	solute carrier fa
CGOV37T_3	SK-OV-3	SMARCC1	SWI/SNF related, matrix associa
CGOV37T_3	SK-OV-3	SSC5D	scavenger rece
CGOV37T_3	SK-OV-3	STRA6	
CGOV37T_3	SK-OV-3	TBC1D2	
CGOV37T_3	SK-OV-3	TOX3	TOX h
CGOV37T_3	SK-OV-3	TP53	
CGOV37T_3	SK-OV-3	TP63	
CGOV37T_3	SK-OV-3	TP63	
CGOV37T_3	SK-OV-3	TSHZ3	
CGOV37T_3	SK-OV-3	TYK2	
CGOV37T_3	SK-OV-3	USP26	
CGOV37T_3	SK-OV-3	VWCE	von
CGOV37T_3	SK-OV-3	WNK1	W
CGOV37T_3	SK-OV-3	WRNIP1	W
CGOV37T_3	SK-OV-3	ZNF30	
CGOV37T_3	SK-OV-3	ZNF831	
CGOV38T	TOV-112D	CTNNB1	catenin (
CGOV38T	TOV-112D	SMARCA4	SWI/SNF related, matrix associa
CGOV38T	TOV-112D	TP53	

CGOV38T	TOV-112D	ZAN	
CGOV39T	TOV-21G	ABCC1	ATP-binding
CGOV39T	TOV-21G	ARID1A	AT
CGOV39T	TOV-21G	ARID1A	AT
CGOV39T	TOV-21G	ARID1B	AT r
CGOV39T	TOV-21G	AXIN1	
CGOV39T	TOV-21G	CCND1	
CGOV39T	TOV-21G	CSF2RA	colony stimulating facto
CGOV39T	TOV-21G	ERBB3	v-erb-b2 erythro
CGOV39T	TOV-21G	FANCD2	Fanc
CGOV39T	TOV-21G	FGFR3	
CGOV39T	TOV-21G	JAK1	
CGOV39T	TOV-21G	JAK1	
CGOV39T	TOV-21G	KIAA1161	
CGOV39T	TOV-21G	KRAS	v-Ki-ras2
CGOV39T	TOV-21G	MCCC1	meth
CGOV39T	TOV-21G	MEN1	
CGOV39T	TOV-21G	MLL3	myelo
CGOV39T	TOV-21G	NBN	
CGOV39T	TOV-21G	NUP50	
CGOV39T	TOV-21G	NXF5	
CGOV39T	TOV-21G	PDGFRB	platelet-de
CGOV39T	TOV-21G	PIK3CA	phosphatidylinosit
CGOV39T	TOV-21G	PIK3R1	phosphoin
CGOV39T	TOV-21G	PTEN	

CGOV39T	TOV-21G	PTEN	
CGOV39T	TOV-21G	RNF43	
CGOV39T	TOV-21G	SHMT2	serine h
CGOV39T	TOV-21G	SLC24A2	solute carrier family
CGOV39T	TOV-21G	STK11	
CGOV39T	TOV-21G	USH2A	Usher
CGOV39T	TOV-21G	VGLL4	
CGOV4T	DOV-13	KRTAP12-1	
CGOV4T	DOV-13	NF1	
CGOV4T	DOV-13	NF1	
CGOV4T	DOV-13	NOTCH3	
CGOV4T	DOV-13	OGG1	
CGOV4T	DOV-13	SLC22A10	s
CGOV4T	DOV-13	SPTA1	spectr
CGOV4T	DOV-13	TRPM8	transient recepto
CGOV40T	TYK-nu	ARID1A	AT
CGOV40T	TYK-nu	MSH6	
CGOV40T	TYK-nu	NRAS	neurobla
CGOV40T	TYK-nu	NRAS	neurobla
CGOV40T	TYK-nu	SIGLEC10	
CGOV40T	TYK-nu	TP53	
CGOV40T	TYK-nu	ZDHHC1	z
CGOV42T	OVCAR-8	CREBBP	
CGOV42T	OVCAR-8	EP300	
CGOV42T	OVCAR-8	ERBB2	v-erb-b2 erythroblastic leukemia viral or

CGOV42T	OVCAR-8	NCOA2	
CGOV42T	OVCAR-8	TP53	
CGOV44T	FU-OV-1	ADCYAP1	adenylate
CGOV44T	FU-OV-1	BTRC	beta-transduc
CGOV44T	FU-OV-1	DNER	de
CGOV44T	FU-OV-1	MLL	myeloid/lymphoid or
CGOV44T	FU-OV-1	MYO10	
CGOV44T	FU-OV-1	POLG	p
CGOV44T	FU-OV-1	PPM1D	protein
CGOV44T	FU-OV-1	PRKDC	protein k
CGOV44T	FU-OV-1	PROZ	protein Z
CGOV44T	FU-OV-1	SPEF2	
CGOV44T	FU-OV-1	TP53	
CGOV44T	FU-OV-1	TP53	
CGOV45T	COV-318	CD209	
CGOV45T	COV-318	KBTBD6	kelch re
CGOV45T	COV-318	KIF16B	
CGOV45T	COV-318	OGG1	
CGOV45T	COV-318	REST	
CGOV45T	COV-318	TP53	
CGOV45T	COV-318	ZNF45	
CGOV46T	JHOS-2	AR	
CGOV46T	JHOS-2	EPSTI1	ep
CGOV46T	JHOS-2	GPR158	
CGOV46T	JHOS-2	HYDIN	HYDIN

CGOV46T	JHOS-2	NLRP10	NL
CGOV46T	JHOS-2	ZNF426	
CGOV47T	JHOS-4	BRCA1	
CGOV47T	JHOS-4	KCTD6	potassium
CGOV47T	JHOS-4	SLC2A7	solute carrier fa
CGOV47T	JHOS-4	TP53	
CGOV48T	JHOM-1	ANKRD33	
CGOV48T	JHOM-1	PTEN	
CGOV48T	JHOM-1	RB1	
CGOV48T	JHOM-1	STK11	
CGOV48T	JHOM-1	STK11	
CGOV48T	JHOM-1	TP53	
CGOV48T	JHOM-1	TRIM65	
CGOV49T	OVK-18	ALDH1L1	aldehy
CGOV49T	OVK-18	ARID1A	AT
CGOV49T	OVK-18	ARID1A	AT
CGOV49T	OVK-18	BLM	B
CGOV49T	OVK-18	C2CD2L	
CGOV49T	OVK-18	FANCD2	Fanc
CGOV49T	OVK-18	GBF1	golgi brefeldin
CGOV49T	OVK-18	GBP6	guan
CGOV49T	OVK-18	IGF2R	i
CGOV49T	OVK-18	JAK2	
CGOV49T	OVK-18	KIAA1109	
CGOV49T	OVK-18	KRAS	v-Ki-ras2
CGOV49T	OVK-18	MDC1	me

CGOV49T	OVK-18	MLL3	myelo
CGOV49T	OVK-18	MNAT1	menage a trois ho
CGOV49T	OVK-18	MYCL1	v-myc myelocytomatosis
CGOV49T	OVK-18	NEIL1	n
CGOV49T	OVK-18	NOTCH4	
CGOV49T	OVK-18	PIK3R1	phosphoin
CGOV49T	OVK-18	POLG	p
CGOV49T	OVK-18	POU4F1	
CGOV49T	OVK-18	PTEN	
CGOV49T	OVK-18	PTEN	
CGOV49T	OVK-18	RET	
CGOV49T	OVK-18	SMAD2	
CGOV49T	OVK-18	SMARCA4	SWI/SNF related, matrix associa
CGOV49T	OVK-18	SMARCA4	SWI/SNF related, matrix associa
CGOV49T	OVK-18	TP53	
CGOV49T	OVK-18	TSC2	
CGOV49T	OVK-18	WRN	W
CGOV49T	OVK-18	ZFHX4	
CGOV49T	OVK-18	ZFHX4	
CGOV49T	OVK-18	ZFHX4	
CGOV5T	EFO-21	ANK3	an
CGOV5T	EFO-21	CYP11B1	cytochrom
CGOV5T	EFO-21	FER1L6	
CGOV5T	EFO-21	NOTCH2	
CGOV5T	EFO-21	TP53	
CGOV53T	OVCAR-5-CisR	ANK3	an
CGOV53T	OVCAR-5-CisR	APC	

CGOV53T	OVCAR-5-CisR	CREBBP	
CGOV53T	OVCAR-5-CisR	KRAS	v-Ki-ras2
CGOV53T	OVCAR-5-CisR	RIPK1	receptor (T
CGOV6T	EFO-27	ARID1A	AT
CGOV6T	EFO-27	ARID1A	AT
CGOV6T	EFO-27	ARID1B	AT
CGOV6T	EFO-27	ARID1B	AT
CGOV6T	EFO-27	AXIN1	
CGOV6T	EFO-27	CNGA3	cy
CGOV6T	EFO-27	CREBBP	
CGOV6T	EFO-27	DCDC5	
CGOV6T	EFO-27	DCP1B	DCP1 de
CGOV6T	EFO-27	EIF2D	euk
CGOV6T	EFO-27	ELMO2	
CGOV6T	EFO-27	EPHX1	epoxi
CGOV6T	EFO-27	ERBB2	v-erb-b2 erythroblastic leukemia viral or
CGOV6T	EFO-27	ERCC2	excision repair cross-comp
CGOV6T	EFO-27	ERCC3	excision repair cross-comp
CGOV6T	EFO-27	ERCC6	excision repair cross-comp
CGOV6T	EFO-27	EYA2	e
CGOV6T	EFO-27	FLCN	
CGOV6T	EFO-27	GDF6	
CGOV6T	EFO-27	GPR50	
CGOV6T	EFO-27	LACTB	
CGOV6T	EFO-27	MLL2	myelo
CGOV6T	EFO-27	MSH2	mutS homolo

CGOV6T	EFO-27	MSH2	mutS homolo
CGOV6T	EFO-27	MSH6	
CGOV6T	EFO-27	MTMR6	
CGOV6T	EFO-27	MUC6	mu
CGOV6T	EFO-27	NAA35	N(alpha)-
CGOV6T	EFO-27	NES	
CGOV6T	EFO-27	PER1	
CGOV6T	EFO-27	PIK3R1	phosphoin
CGOV6T	EFO-27	PMS1	PMS1 postı
CGOV6T	EFO-27	POU3F4	
CGOV6T	EFO-27	PTEN	
CGOV6T	EFO-27	RAB17	RA
CGOV6T	EFO-27	RD3	
CGOV6T	EFO-27	RFX2	regulatory fa
CGOV6T	EFO-27	RFX5	regulatory fa
CGOV6T	EFO-27	ROBO2	roundabout, a
CGOV6T	EFO-27	SEMA3D	sema domain, immunoglobu
CGOV6T	EFO-27	SLC7A14	solute carr
CGOV6T	EFO-27	SMAD4	
CGOV6T	EFO-27	TP53	
CGOV6T	EFO-27	USH2A	Usher
CGOV6T	EFO-27	VPS13A	vacuolar
CGOV7T	ES-2	BRAF	v-raf m
CGOV7T	ES-2	CYP11A1	cytochrom
CGOV7T	ES-2	FANCD2	Fanc

CGOV7T	ES-2	FANCM	Fanc
CGOV7T	ES-2	FASTKD2	
CGOV7T	ES-2	GRM8	
CGOV7T	ES-2	HOXD12	
CGOV7T	ES-2	HYDIN	HYDIN
CGOV7T	ES-2	NRD1	narc
CGOV7T	ES-2	POLM	
CGOV7T	ES-2	TEX14	
CGOV7T	ES-2	TP53	
CGOV7T	ES-2	TRRAP	transforma
CGOV8T	HEY	ANKRD40	
CGOV8T	HEY	ARMC4	
CGOV8T	HEY	BRAF	v-raf m
CGOV8T	HEY	KRAS	v-Ki-ras2
CGOV8T	HEY	STARD10	StAR-relate
CGOV8T	HEY	TP53BP1	t
CGOV92T	JHOS-3	ACAT2	
CGOV92T	JHOS-3	ADAM21	A
CGOV92T	JHOS-3	CCDC141	
CGOV92T	JHOS-3	CD96	
CGOV92T	JHOS-3	CPA4	
CGOV92T	JHOS-3	DCC	
CGOV92T	JHOS-3	EXTL3	e
CGOV92T	JHOS-3	FBXO2	
CGOV92T	JHOS-3	FNDC3B	fibr

CGOV92T	JHOS-3	IQCJ-SCHIP1	
CGOV92T	JHOS-3	LAIR1	leukocyte
CGOV92T	JHOS-3	MISP	
CGOV92T	JHOS-3	MMP12	matrix m
CGOV92T	JHOS-3	NCSTN	
CGOV92T	JHOS-3	OR6C6	olfactory
CGOV92T	JHOS-3	PIK3CG	phosphatidylinositc
CGOV92T	JHOS-3	PPAPDC3	phosphatidi
CGOV92T	JHOS-3	RAD1	
CGOV92T	JHOS-3	RHBDF2	r
CGOV92T	JHOS-3	RNF152	
CGOV92T	JHOS-3	RNF175	
CGOV92T	JHOS-3	ROBO2	roundabout, a
CGOV92T	JHOS-3	ROS1	c-ro
CGOV92T	JHOS-3	RSBN1	
CGOV92T	JHOS-3	SLC4A10	solute carrier fa
CGOV92T	JHOS-3	SON	
CGOV92T	JHOS-3	TAS1R2	
CGOV92T	JHOS-3	TAS1R2	
CGOV92T	JHOS-3	TENM1	
CGOV92T	JHOS-3	TP53	
CGOV92T	JHOS-3	USP34	
CGOV92T	JHOS-3	ZBTB7C	zinc
CGOV92T	JHOS-3	ZIK1	zinc fi
CGOV92T	JHOS-3	ZNF229	

CGOV92T	JHOS-3	ZNF248
CGOV92T	JHOS-3	ZNF280A

Table S3.1h. Deletions*

Lab id	Chr	Deletion	Width
CGOV16T	chr2	g.(215426360_215426460)_(215959491_215959591)	533232
CGOV16T	chr5	g.(33324914_33325014)_(33330942_33331042)	6129
CGOV16T	chr5	g.(97047904_97048004)_(97095995_97096095)	48192
CGOV16T	chr6	g.(26343903_26344003)_(26351413_26351513)	7611
CGOV16T	chr9	g.(90817091_90817191)_(90821828_90821928)	4838
CGOV16T	chr12	g.(866873_866973)_(874651_874751)	7879
CGOV16T	chr13	g.(69244759_69244859)_(69268602_69268702)	23944
CGOV16T	chr13	g.(71912501_71913501)_(71920501_71921501)	8001
CGOV16T	chr16	g.(73344503_73344603)_(73352006_73352106)	7604
CGOV16T	chr18	g.(7588958_7589058)_(7906687_7906787)	317830
CGOV16T	chr18	g.(42868944_42869044)_(43173129_43173229)	304286
CGOV16T	chr22	g.(37744469_37744569)_(37749862_37749962)	5494
CGOV17T	chr1	g.(49410038_49410138)_(49497764_49497864)	87827
CGOV17T	chr1	g.(191661486_191661586)_(191674499_191674599)	13114
CGOV17T	chr2	g.(109689949_109690049)_(109695076_109695176)	5228
CGOV17T	chr2	g.(126814885_126814985)_(126819929_126820029)	5145
CGOV17T	chr2	g.(141314638_141314738)_(141475895_141475995)	161358
CGOV17T	chr2	g.(141782591_141782691)_(142026688_142026788)	244198
CGOV17T	chr2	g.(141965917_141966917)_(142026288_142027288)	60372
CGOV17T	chr2	g.(213716368_213717368)_(213892174_213893174)	175807
CGOV17T	chr2	g.(227832551_227832651)_(227836940_227837040)	4490
CGOV17T	chr3	g.(20311501_20312501)_(20315501_20316501)	4001
CGOV17T	chr4	g.(20386477_20386577)_(20705675_20705775)	319299
CGOV17T	chr4	g.(151957497_151957597)_(152147129_152147229)	189733
CGOV17T	chr4	g.(161046501_161047501)_(161071501_161072501)	25001
CGOV17T	chr6	g.(54846454_54846554)_(54851295_54851395)	4942
CGOV17T	chr6	g.(69687219_69688219)_(69691315_69692315)	4097
CGOV17T	chr6	g.(167142424_167142524)_(167222835_167222935)	80512
CGOV17T	chr8	g.(89809161_89809261)_(90083591_90083691)	274531
CGOV17T	chr9	g.(44232501_44233501)_(44264501_44265501)	32001
CGOV17T	chr10	g.(90940586_90940686)_(90947863_90947963)	7378
CGOV17T	chr11	g.(23454678_23455678)_(23479800_23480800)	25123
CGOV17T	chr11	g.(85234699_85234799)_(85542725_85542825)	308127
CGOV17T	chr13	g.(80343605_80343705)_(80346833_80346933)	3329
CGOV17T	chr13	g.(85200001_85200101)_(85260901_85261001)	61001
CGOV17T	chr13	g.(110822820_110822920)_(110835741_110835841)	13022

CGOV17T	chr13	g.(110838244_110839244)_(111046054_111047054)	207811
CGOV17T	chr14	g.(67389152_67389252)_(67395409_67395509)	6358
CGOV17T	chr15	g.(24055436_24055536)_(24061479_24061579)	6144
CGOV17T	chr17	g.(29590319_29590419)_(29666366_29666466)	76148
CGOV17T	chr19	g.(12039036_12040036)_(12045477_12046477)	6442
CGOV17T	chr20	g.(15031714_15031814)_(15079252_15079352)	47639
CGOV17T	chr22	g.(46321088_46321188)_(46482539_46482639)	161552
CGOV17T	chrX	g.(127145414_127145514)_(127250834_127250934)	105521
CGOV17T	chrX	g.(127630674_127630774)_(128669484_128669584)	103891
CGOV17T	chrX	g.(139495001_139495101)_(139501901_139502001)	7001
CGOV18T	chr1	g.(101774312_101774412)_(101780700_101780800)	6489
CGOV18T	chr1	g.(162575449_162575549)_(162592605_162592705)	17257
CGOV18T	chr2	g.(141923625_141923725)_(141982074_141982174)	58550
CGOV18T	chr2	g.(142325365_142325465)_(142328863_142328963)	3599
CGOV18T	chr2	g.(164640715_164641715)_(164645557_164646557)	4843
CGOV18T	chr3	g.(75423501_75424501)_(75639501_75640501)	216001
CGOV18T	chr3	g.(116318845_116318945)_(116388047_116388147)	69303
CGOV18T	chr3	g.(116483786_116483886)_(116588167_116588267)	104482
CGOV18T	chr3	g.(149585200_149585300)_(149588754_149588854)	3655
CGOV18T	chr3	g.(168898366_168898466)_(169084656_169084756)	186391
CGOV18T	chr4	g.(90559345_90559445)_(90563418_90563518)	4174
CGOV18T	chr4	g.(181992235_181992335)_(182175918_182176018)	183784
CGOV18T	chr7	g.(141744316_141744416)_(141865034_141865134)	120819
CGOV18T	chr8	g.(94955418_94955518)_(94960757_94960857)	5440
CGOV18T	chr8	g.(114040518_114040618)_(114046603_114046703)	6186
CGOV18T	chr9	g.(9541307_9541407)_(9698897_9698997)	157691
CGOV18T	chr11	g.(3238797_3238897)_(3243910_3244010)	5214
CGOV18T	chr14	g.(84183968_84184068)_(84477397_84477497)	293530
CGOV18T	chr18	g.(41976805_41976905)_(41981953_41982053)	5249
CGOV18T	chr20	g.(52647133_52647233)_(52657827_52657927)	10795
CGOV18T	chrX	g.(30470501_30471501)_(30480501_30481501)	10001
CGOV18T	chrX	g.(30728384_30728484)_(31382222_31382322)	653939
CGOV18T	chrX	g.(53513501_53514501)_(53518501_53519501)	5001
CGOV18T	chrX	g.(96345362_96345462)_(96491606_96491706)	146345
CGOV21T	chr1	g.(26460207_26460307)_(26464652_26464752)	4546
CGOV21T	chr3	g.(60372339_60372439)_(60725881_60725981)	353643
CGOV21T	chr7	g.(118292669_118292769)_(118304100_118304200)	11532
CGOV21T	chr8	g.(97551060_97551160)_(97742085_97742185)	191126
CGOV21T	chr8	g.(106653250_106653350)_(106956785_106956885)	303636

CGOV21T	chr9	g.(44248501_44249501)_(44790501_44791501)	542001
CGOV21T	chr14	g.(98030843_98030943)_(99417216_99417316)	138647
CGOV21T	chr16	g.(83920397_83920497)_(84074537_84074637)	154241
CGOV21T	chr16	g.(87265770_87265870)_(87272506_87272606)	6837
CGOV21T	chr18	g.(40054143_40054243)_(40057497_40057597)	3455
CGOV21T	chr20	g.(7398773_7398873)_(7403434_7403534)	4762
CGOV23T	chr3	g.(15049874_15049974)_(15135111_15135211)	85338
CGOV23T	chr4	g.(3895501_3896501)_(4153501_4154501)	258001
CGOV23T	chr4	g.(5615038_5615138)_(5644533_5644633)	29596
CGOV23T	chr4	g.(152204141_152204241)_(152569648_152569748)	365608
CGOV23T	chr4	g.(164612926_164613026)_(164619107_164619207)	6282
CGOV23T	chr4	g.(164872420_164872520)_(165055066_165055166)	182747
CGOV23T	chr6	g.(2568234_2568334)_(2571823_2571923)	3690
CGOV23T	chr6	g.(137069374_137069474)_(137549475_137549575)	480202
CGOV23T	chr9	g.(21958656_21958756)_(22063510_22063610)	104955
CGOV23T	chr9	g.(21958156_21959156)_(21992501_21993501)	34346
CGOV23T	chr9	g.(78004351_78004451)_(78011639_78011739)	7389
CGOV23T	chr9	g.(97451386_97451486)_(97465908_97466008)	14623
CGOV23T	chr10	g.(53665015_53665115)_(53863090_53863190)	198176
CGOV23T	chr11	g.(49709850_49709950)_(49757566_49757666)	47817
CGOV23T	chr11	g.(93020222_93020322)_(93029805_93029905)	9684
CGOV23T	chr12	g.(866868_866968)_(874636_874736)	7869
CGOV23T	chr15	g.(74016851_74017851)_(74025774_74026774)	8924
CGOV23T	chr16	g.(78686083_78686183)_(79072508_79072608)	386526
CGOV23T	chr17	g.(75038653_75038753)_(75158148_75158248)	119596
CGOV23T	chr19	g.(4008434_4008534)_(4084764_4084864)	76431
CGOV23T	chr20	g.(7398765_7398865)_(7403432_7403532)	4768
CGOV23T	chr20	g.(14781484_14781584)_(14827331_14827431)	45948
CGOV25T	chr1	g.(30479718_30479818)_(30489321_30489421)	9704
CGOV25T	chr1	g.(72377134_72377234)_(72471536_72471636)	94503
CGOV25T	chr2	g.(14704234_14704334)_(14709948_14710048)	5815
CGOV25T	chr2	g.(141878286_141878386)_(142041589_142041689)	163404
CGOV25T	chr2	g.(141974556_141974656)_(142139672_142139772)	165217
CGOV25T	chr2	g.(141974056_141975056)_(142041189_142042189)	67134

CGOV25T	chr3	g.(4385597_4385697)_(4455795_4455895)	70299
CGOV25T	chr3	g.(116153523_116153623)_(116250118_116250218)	96696
CGOV25T	chr3	g.(116376722_116376822)_(116970205_116970305)	593584
CGOV25T	chr4	g.(181802859_181802959)_(182463377_182463477)	660619
CGOV25T	chr6	g.(75600365_75600465)_(75606987_75607087)	6723
CGOV25T	chr7	g.(42019946_42020046)_(42162089_42162189)	142244
CGOV25T	chr7	g.(153920400_153920500)_(154109738_154109838)	189439
CGOV25T	chr8	g.(3662157_3662257)_(3730050_3730150)	67994
CGOV25T	chr10	g.(56263776_56263876)_(56332079_56332179)	68404
CGOV25T	chr10	g.(97027671_97027771)_(97044788_97044888)	17218
CGOV25T	chr12	g.(99695055_99695155)_(99927923_99928023)	232969
CGOV25T	chr12	g.(99694555_99695555)_(99727384_99728384)	32830
CGOV25T	chr12	g.(99793970_99794070)_(99802652_99802752)	8783
CGOV25T	chr12	g.(99917238_99918238)_(99927523_99928523)	10286
CGOV25T	chr13	g.(35558501_35559501)_(35562501_35563501)	4001
CGOV25T	chr14	g.(33502125_33502225)_(33806675_33806775)	304651
CGOV25T	chr16	g.(81175878_81175978)_(81188246_81188346)	12469
CGOV25T	chr20	g.(6589166_6589266)_(6614154_6614254)	25089
CGOV25T	chr20	g.(14920162_14920262)_(15024789_15024889)	104728
CGOV25T	chrX	g.(6725420_6725520)_(7140011_7140111)	414692
CGOV25T	chrX	g.(34043060_34043160)_(34072729_34072829)	29770
CGOV28T	chr3	g.(160355949_160356049)_(160366031_160366131)	10183
CGOV28T	chr4	g.(175961671_175961771)_(175986690_175986790)	25120
CGOV28T	chr6	g.(14494026_14494126)_(14499739_14499839)	5814
CGOV28T	chr6	g.(155135096_155135196)_(155172208_155172308)	37213
CGOV28T	chr7	g.(133260013_133260113)_(133702135_133702235)	442223
CGOV28T	chr7	g.(151590831_151590931)_(151599609_151599709)	8879
CGOV28T	chr7	g.(157591843_157591943)_(157598292_157598392)	6550
CGOV28T	chr8	g.(2440119_2440219)_(2470609_2470709)	30591
CGOV28T	chr8	g.(9862648_9862748)_(9880889_9880989)	18342
CGOV28T	chr9	g.(7827533_7827633)_(7846534_7846634)	19102
CGOV28T	chr9	g.(23289601_23290601)_(23299358_23300358)	9758
CGOV28T	chr9	g.(136396620_136396720)_(136428109_136428209)	31590
CGOV28T	chr10	g.(37020375_37020475)_(37030380_37030480)	10106
CGOV28T	chr10	g.(90543987_90544987)_(90571212_90572212)	27226
CGOV28T	chr10	g.(105715355_105716355)_(105720256_105721256)	4902
CGOV28T	chr11	g.(42252030_42252130)_(42266836_42266936)	14907
CGOV28T	chrX	g.(46468558_46469558)_(46471706_46472706)	3149
CGOV28T	chrX	g.(136185614_136186614)_(136193754_136194754)	8141

CGOV28T	chrX	g.(154392501_154393501)_(154409501_154410501)	17001
CGOV30T	chr2	g.(186644331_186644431)_(186957966_186958066)	313736
CGOV30T	chr3	g.(7634615_7634715)_(7830256_7830356)	195742
CGOV30T	chr3	g.(153599268_153599368)_(153613832_153613932)	14665
CGOV30T	chr4	g.(16043746_16043846)_(16051820_16051920)	8175
CGOV30T	chr4	g.(31463501_31464501)_(31467501_31468501)	4001
CGOV30T	chr4	g.(106418218_106418318)_(106513846_106513946)	95729
CGOV30T	chr4	g.(148274180_148274280)_(148907570_148907670)	633491
CGOV30T	chr6	g.(73345273_73345373)_(73521299_73521399)	176127
CGOV30T	chr6	g.(122159169_122159269)_(122168780_122168880)	9712
CGOV30T	chr7	g.(8118612_8118712)_(8192039_8192139)	73528
CGOV30T	chr8	g.(20101643_20101743)_(20114694_20114794)	13152
CGOV30T	chr8	g.(142927661_142927761)_(142934110_142934210)	6550
CGOV30T	chr9	g.(72832227_72832327)_(73061137_73061237)	229011
CGOV30T	chr9	g.(129753263_129754263)_(130059501_130060501)	306239
CGOV30T	chr9	g.(130243462_130243562)_(130323641_130323741)	80280
CGOV30T	chr9	g.(130595085_130596085)_(130635960_130636960)	40876
CGOV30T	chr9	g.(132442256_132443256)_(132454263_132455263)	12008
CGOV30T	chr12	g.(122155247_122155347)_(122376876_122376976)	221730
CGOV30T	chr14	g.(80803045_80803145)_(80914933_80915033)	111989
CGOV30T	chr15	g.(63697036_63698036)_(63701360_63702360)	4325
CGOV30T	chr15	g.(75029360_75029460)_(75172915_75173015)	143656
CGOV30T	chr20	g.(14134326_14134426)_(14142623_14142723)	8398
CGOV30T	chr21	g.(44023501_44024501)_(44038501_44039501)	15001
CGOV30T	chr22	g.(30882816_30882916)_(30885793_30885893)	3078
CGOV30T	chr22	g.(40883801_40884801)_(40894559_40895559)	10759
CGOV30T	chr22	g.(50683538_50684538)_(50690839_50691839)	7302
CGOV30T	chr22	g.(50706820_50707820)_(50714143_50715143)	7324
CGOV30T	chr22	g.(50974351_50975351)_(50977749_50978749)	3399
CGOV30T	chrX	g.(23266755_23266855)_(23330923_23331023)	64269
CGOV30T	chrX	g.(31837277_31837377)_(31894267_31894367)	57091
CGOV30T	chrX	g.(128154820_128154920)_(128610714_128610814)	455995
CGOV30T	chrX	g.(130731297_130731397)_(130746355_130746455)	15159
CGOV30T	chrX	g.(138263632_138263732)_(138267768_138267868)	4237
CGOV32T	chr2	g.(153796005_153796105)_(153799568_153799668)	3664
CGOV32T	chr2	g.(213184021_213184121)_(213191846_213191946)	7926

CGOV32T	chr2	g.(226832018_226832118)_(226838239_226838339)	6322
CGOV32T	chr3	g.(115736880_115736980)_(115879326_115879426)	142547
CGOV32T	chr3	g.(175887258_175887358)_(175914744_175914844)	27587
CGOV32T	chr5	g.(87378945_87379045)_(87381902_87382002)	3058
CGOV32T	chr6	g.(14712629_14712729)_(16058481_16058581)	134595
CGOV32T	chr6	g.(39068610_39068710)_(39072708_39072808)	4199
CGOV32T	chr6	g.(57284962_57285062)_(57289212_57289312)	4351
CGOV32T	chr6	g.(101934624_101934724)_(101938894_101938994)	4371
CGOV32T	chr6	g.(110396120_110396220)_(110414160_110414260)	18141
CGOV32T	chr6	g.(128432727_128432827)_(128437441_128437541)	4815
CGOV32T	chr6	g.(159212184_159212284)_(159318039_159318139)	105956
CGOV32T	chr7	g.(101724549_101724649)_(101727392_101727492)	2944
CGOV32T	chr9	g.(121861410_121861510)_(121878416_121878516)	17107
CGOV32T	chr11	g.(107231501_107232501)_(107242501_107243501)	11001
CGOV32T	chr11	g.(117923302_117923402)_(117942777_117942877)	19576
CGOV32T	chr12	g.(27648190_27648290)_(27655003_27655103)	6914
CGOV32T	chr14	g.(85454792_85454892)_(85547158_85547258)	92467
CGOV32T	chr14	g.(91810963_91811063)_(91987467_91987567)	176605
CGOV32T	chr18	g.(40054133_40054233)_(40057514_40057614)	3482
CGOV32T	chrX	g.(26543501_26544501)_(29198501_29199501)	265500
CGOV32T	chrX	g.(150707112_150707212)_(150712157_150712257)	5146
CGOV34T	chr1	g.(21845729_21845829)_(21849090_21849190)	3462
CGOV34T	chr2	g.(9925548_9925648)_(9928862_9928962)	3415
CGOV34T	chr2	g.(128197626_128197726)_(128292743_128292843)	95218
CGOV34T	chr2	g.(142114370_142114470)_(142423709_142423809)	309440
CGOV34T	chr3	g.(160680335_160680435)_(160685849_160685949)	5615
CGOV34T	chr4	g.(83913482_83914482)_(83918930_83919930)	5449
CGOV34T	chr4	g.(92280214_92280314)_(92285052_92285152)	4939
CGOV34T	chr4	g.(93124501_93125501)_(93142501_93143501)	18001
CGOV34T	chr4	g.(112237002_112238002)_(112241890_112242890)	4889
CGOV34T	chr5	g.(17600501_17601501)_(17643501_17644501)	43001
CGOV34T	chr6	g.(2568252_2568352)_(2571823_2571923)	3672
CGOV34T	chr6	g.(41442616_41442716)_(41447949_41448049)	5434
CGOV34T	chr6	g.(142237501_142238501)_(142242501_142243501)	5001
CGOV34T	chr6	g.(146869348_146869448)_(146875743_146875843)	6496
CGOV34T	chr7	g.(85044501_85045501)_(85046501_85047501)	2001
CGOV34T	chr7	g.(132136647_132136747)_(132146427_132146527)	9881
CGOV34T	chr8	g.(2508866_2508966)_(2526090_2526190)	17325
CGOV34T	chr8	g.(16262079_16262179)_(16274536_16274636)	12558

CGOV34T	chr9	g.(20919501_20920501)_(23847501_23848501)	292800
CGOV34T	chr9	g.(115661708_115661808)_(115667530_115667630)	5923
CGOV34T	chr10	g.(24147354_24147454)_(24156837_24156937)	9584
CGOV34T	chr10	g.(88380446_88380546)_(88402375_88402475)	22030
CGOV34T	chr11	g.(46819792_46819892)_(46835963_46836063)	16272
CGOV34T	chr11	g.(47612771_47612871)_(47635915_47636015)	23245
CGOV34T	chr11	g.(49116350_49116450)_(49119531_49119631)	3282
CGOV34T	chr11	g.(49709847_49709947)_(49757556_49757656)	47810
CGOV34T	chr11	g.(105612470_105612570)_(105619182_105619282)	6813
CGOV34T	chr11	g.(106551771_106551871)_(106584954_106585054)	33284
CGOV34T	chr11	g.(116255656_116255756)_(116267686_116267786)	12131
CGOV34T	chr12	g.(129405278_129405378)_(129455069_129455169)	49892
CGOV34T	chr13	g.(35558501_35559501)_(35562501_35563501)	4001
CGOV34T	chr15	g.(78637775_78637875)_(78648422_78648522)	10748
CGOV34T	chr16	g.(78144600_78144700)_(78869655_78869755)	725156
CGOV34T	chr17	g.(73458567_73459567)_(73492918_73493918)	34352
CGOV34T	chr22	g.(29993607_29993707)_(30009861_30009961)	16355
CGOV34T	chrX	g.(143628747_143628847)_(143637610_143637710)	8964
CGOV44T	chr1	g.(60525683_60525783)_(60534852_60534952)	9270
CGOV44T	chr1	g.(72824099_72824199)_(72927841_72927941)	103843
CGOV44T	chr2	g.(60525347_60525447)_(60532673_60532773)	7427
CGOV44T	chr2	g.(95730268_95731268)_(95736462_95737462)	6195
CGOV44T	chr3	g.(117122100_117122200)_(117284577_117284677)	162578
CGOV44T	chr4	g.(22602001_22602101)_(22605901_22606001)	4001
CGOV44T	chr4	g.(26289989_26290989)_(26294876_26295876)	4888
CGOV44T	chr4	g.(40377081_40377181)_(40440094_40440194)	63114
CGOV44T	chr4	g.(92857501_92858501)_(92945501_92946501)	88001
CGOV44T	chr5	g.(41226856_41226956)_(41243798_41243898)	17043
CGOV44T	chr5	g.(180590874_180591874)_(180595940_180596940)	5067
CGOV44T	chr6	g.(77016759_77016859)_(77028997_77029097)	12339
CGOV44T	chr6	g.(169506347_169506447)_(169520999_169521099)	14753

CGOV44T	chr7	g.(2902501_2903501)_(5191501_5192501)	228900
CGOV44T	chr7	g.(5205501_5206501)_(5291501_5292501)	86001
CGOV44T	chr7	g.(5337501_5338501)_(5512501_5513501)	175001
CGOV44T	chr7	g.(97635501_97636501)_(97874501_97875501)	239001
CGOV44T	chr7	g.(152251843_152252843)_(152276201_152277201)	24359
CGOV44T	chr14	g.(72805851_72805951)_(72810773_72810873)	5023
CGOV44T	chr15	g.(63201003_63201103)_(63209143_63209243)	8241
CGOV44T	chr17	g.(29447326_29448326)_(29705997_29706997)	258672
CGOV44T	chr20	g.(37008042_37009042)_(37014845_37015845)	6804
CGOV44T	chr21	g.(17874424_17874524)_(17891690_17891790)	17367
CGOV44T	chr22	g.(24873967_24874067)_(24886524_24886624)	12658
CGOV44T	chrX	g.(56811501_56812501)_(56861501_56862501)	50001
CGOV44T	chrX	g.(92796360_92796460)_(92801380_92801480)	5121
CGOV45T	chr1	g.(72755761_72755861)_(72763911_72764011)	8251
CGOV45T	chr4	g.(29035847_29035947)_(29140721_29140821)	104975
CGOV45T	chr4	g.(134385737_134385837)_(134392731_134392831)	7095
CGOV45T	chr4	g.(148551875_148551975)_(148888647_148888747)	336873
CGOV45T	chr5	g.(58400155_58400255)_(58878623_58878723)	478569
CGOV45T	chr6	g.(77438501_77439501)_(77452501_77453501)	14001
CGOV45T	chr6	g.(161817300_161817400)_(162361689_162361789)	544490
CGOV45T	chr9	g.(112048997_112049097)_(112191979_112192079)	143083
CGOV45T	chr13	g.(19449094_19450094)_(19641121_19642121)	192028
CGOV45T	chr13	g.(19651825_19652825)_(20754429_20755429)	110260
CGOV45T	chr15	g.(45153623_45154623)_(45159015_45160015)	5393
CGOV45T	chr19	g.(40329972_40330072)_(40334288_40334388)	4417
CGOV45T	chr22	g.(40812967_40813067)_(40960092_40960192)	147226
CGOV45T	chrX	g.(32250501_32251501)_(32254501_32255501)	4001
CGOV45T	chrX	g.(79977350_79977450)_(80201290_80201390)	224041
CGOV46T	chr1	g.(39128575_39128675)_(39137102_39137202)	8628
CGOV46T	chr5	g.(11128325_11128425)_(11135083_11135183)	6859
CGOV46T	chr5	g.(58845780_58845880)_(59135606_59135706)	289927

CGOV46T	chr6	g.(77016750_77016850)_(77028996_77029096)	12347
CGOV46T	chr9	g.(19770501_19771501)_(20340501_20341501)	570001
CGOV46T	chr9	g.(20341501_20342501)_(21806501_21807501)	146500
CGOV46T	chr9	g.(21806526_21807526)_(26655233_26656233)	4848708
CGOV46T	chr14	g.(72805866_72805966)_(72810765_72810865)	5000
CGOV46T	chr14	g.(100733823_100733923)_(100739919_100740019)	6197
CGOV46T	chr16	g.(60081157_60081257)_(60098400_60098500)	17344
CGOV46T	chr18	g.(66745661_66745761)_(66756849_66756949)	11289
CGOV46T	chr20	g.(37008031_37009031)_(37014845_37015845)	6815
CGOV46T	chr21	g.(48092501_48093501)_(48099501_48100501)	7001
CGOV46T	chrX	g.(143628756_143628856)_(143637615_143637715)	8960
CGOV47T	chr1	g.(78884355_78884455)_(78889914_78890014)	5660
CGOV47T	chr2	g.(119527185_119527285)_(119559322_119559422)	32238
CGOV47T	chr2	g.(189800635_189800735)_(189817521_189817621)	16987
CGOV47T	chr3	g.(34707050_34707150)_(34728997_34729097)	22048
CGOV47T	chr3	g.(34855905_34856005)_(36213991_36214091)	135818
CGOV47T	chr3	g.(153599185_153599285)_(153613832_153613932)	14748
CGOV47T	chr4	g.(24488790_24488890)_(24510302_24510402)	21613
CGOV47T	chr4	g.(177728919_177729019)_(177733206_177733306)	4388
CGOV47T	chr5	g.(9519086_9519186)_(9541565_9541665)	22580
CGOV47T	chr5	g.(19809241_19809341)_(19814977_19815077)	5837
CGOV47T	chr5	g.(41226884_41226984)_(41243801_41243901)	17018
CGOV47T	chr5	g.(96247341_96248341)_(96257220_96258220)	9880
CGOV47T	chr5	g.(170760162_170760262)_(170765955_170766055)	5894
CGOV47T	chr6	g.(71648501_71649501)_(71652501_71653501)	4001
CGOV47T	chr7	g.(128857006_128858006)_(128860706_128861706)	3701
CGOV47T	chr8	g.(42397231_42397331)_(42402702_42402802)	5572

CGOV47T	chr9	g.(21879213_21880213)_(30059468_30060468)	818025
CGOV47T	chr9	g.(119016898_119016998)_(119020684_119020784)	3887
CGOV47T	chr10	g.(77463909_77464009)_(78040863_78040963)	577055
CGOV47T	chr10	g.(83901865_83901965)_(85290509_85290609)	138874
CGOV47T	chr14	g.(41552735_41552835)_(41579743_41579843)	27109
CGOV47T	chr15	g.(73858030_73858130)_(73922322_73922422)	64393
CGOV47T	chr15	g.(77451538_77451638)_(77462213_77462313)	10776
CGOV47T	chr16	g.(60081169_60081269)_(60098425_60098525)	17357
CGOV47T	chr17	g.(58239224_58239324)_(58250351_58250451)	11228
CGOV47T	chr17	g.(62686931_62687031)_(62691831_62691931)	5001
CGOV47T	chr18	g.(66745583_66745683)_(66756838_66756938)	11356
CGOV47T	chr19	g.(15985069_15985169)_(16017239_16017339)	32271
CGOV47T	chr20	g.(37008082_37009082)_(37014795_37015795)	6714
CGOV47T	chrX	g.(14209295_14209395)_(14253155_14253255)	43961
CGOV4T	chr1	g.(157986802_157986902)_(158076357_158076457)	89656
CGOV4T	chr1	g.(207841132_207841232)_(207845666_207845766)	4635
CGOV4T	chr1	g.(246294852_246294952)_(246330154_246330254)	35403
CGOV4T	chr3	g.(116679538_116679638)_(116715479_116715579)	36042
CGOV4T	chr4	g.(91433300_91433400)_(91895466_91895566)	462267
CGOV4T	chr5	g.(16974890_16974990)_(16979126_16979226)	4337
CGOV4T	chr6	g.(55341703_55341803)_(55345507_55345607)	3905
CGOV4T	chr8	g.(16321297_16321397)_(16326435_16326535)	5239
CGOV4T	chr9	g.(21792496_21793496)_(21881429_21882429)	88934
CGOV4T	chr9	g.(21920364_21920464)_(22468845_22468945)	548582
CGOV4T	chr9	g.(21919864_21920864)_(22384501_22385501)	464638
CGOV4T	chr9	g.(22428152_22429152)_(22468445_22469445)	40294
CGOV4T	chr9	g.(26365138_26366138)_(26423261_26424261)	58124
CGOV4T	chr12	g.(44348174_44349174)_(44553448_44554448)	205275
CGOV4T	chr12	g.(45790501_45791501)_(47514501_47515501)	172400

CGOV4T	chr14	g.(70017049_70017149)_(70022314_70022414)	5366
CGOV4T	chr19	g.(46956435_46957435)_(46962402_46963402)	5968
CGOV4T	chr22	g.(30039501_30040501)_(30093501_30094501)	54001
CGOV4T	chr22	g.(33755264_33756264)_(33759554_33760554)	4291
CGOV4T	chr22	g.(49709664_49709764)_(49713003_49713103)	3440
CGOV4T	chrX	g.(62577501_62578501)_(62585501_62586501)	8001
CGOV5T	chr1	g.(67391182_67391282)_(67414068_67414168)	22987
CGOV5T	chr2	g.(26489459_26489559)_(26535565_26535665)	46207
CGOV5T	chr2	g.(116622904_116623004)_(117153250_117153350)	530447
CGOV5T	chr2	g.(141909501_141910501)_(141979501_141980501)	70001
CGOV5T	chr2	g.(149085501_149086501)_(149203501_149204501)	118001
CGOV5T	chr2	g.(153796001_153796101)_(153799582_153799682)	3682
CGOV5T	chr2	g.(212342019_212342119)_(212423262_212423362)	81344
CGOV5T	chr2	g.(225364116_225364216)_(225419013_225419113)	54998
CGOV5T	chr2	g.(238549106_238549206)_(238661611_238661711)	112606
CGOV5T	chr3	g.(59887527_59888527)_(60109181_60110181)	221655
CGOV5T	chr3	g.(114799749_114799849)_(114812218_114812318)	12570
CGOV5T	chr3	g.(117321313_117321413)_(117747515_117747615)	426303
CGOV5T	chr3	g.(148963434_148963534)_(148969548_148969648)	6215
CGOV5T	chr4	g.(64134424_64134524)_(64154373_64154473)	20050
CGOV5T	chr4	g.(101975478_101975578)_(102031399_102031499)	56022
CGOV5T	chr4	g.(114603947_114604047)_(114631283_114631383)	27437
CGOV5T	chr4	g.(149252909_149253009)_(149391931_149392031)	139123
CGOV5T	chr4	g.(162525115_162525215)_(162530651_162530751)	5637
CGOV5T	chr4	g.(168869625_168869725)_(168878642_168878742)	9118
CGOV5T	chr4	g.(172645223_172646223)_(172651274_172652274)	6052
CGOV5T	chr5	g.(56103139_56103239)_(56136450_56136550)	33412
CGOV5T	chr5	g.(56119617_56120617)_(56136050_56137050)	16434
CGOV5T	chr5	g.(112331964_112332064)_(112432489_112432589)	100626
CGOV5T	chr6	g.(2568260_2568360)_(2571821_2571921)	3662
CGOV5T	chr6	g.(90121181_90121281)_(90213196_90213296)	92116
CGOV5T	chr6	g.(123817241_123817341)_(123825556_123825656)	8416
CGOV5T	chr7	g.(32533101_32533201)_(32547986_32548086)	14986
CGOV5T	chr7	g.(76886077_76887077)_(76928048_76929048)	41972
CGOV5T	chr7	g.(113870135_113870235)_(113900868_113900968)	30834
CGOV5T	chr7	g.(115931734_115931834)_(115941083_115941183)	9450
CGOV5T	chr7	g.(132564147_132564247)_(132725544_132725644)	161498
CGOV5T	chr8	g.(26131921_26132021)_(26172032_26172132)	40212
CGOV5T	chr8	g.(61619114_61619214)_(61694530_61694630)	75517

CGOV5T	chr9	g.(6700069_6701069)_(6710134_6711134)	10066
CGOV5T	chr9	g.(33885970_33886070)_(34014974_34015074)	129105
CGOV5T	chr10	g.(54537328_54537428)_(54554716_54554816)	17489
CGOV5T	chr10	g.(78833359_78833459)_(79049403_79049503)	216145
CGOV5T	chr11	g.(14093330_14093430)_(14333554_14333654)	240325
CGOV5T	chr12	g.(11156098_11157098)_(11182501_11183501)	26404
CGOV5T	chr12	g.(11183501_11184501)_(11198501_11199501)	15001
CGOV5T	chr12	g.(11199501_11200501)_(11248501_11249501)	49001
CGOV5T	chr12	g.(89533079_89534079)_(89541612_89542612)	8534
CGOV5T	chr12	g.(114599607_114599707)_(115017948_115018048)	418442
CGOV5T	chr12	g.(121268792_121268892)_(121348605_121348705)	79914
CGOV5T	chr13	g.(96153185_96153285)_(96169361_96169461)	16277
CGOV5T	chr14	g.(67139489_67139589)_(67217879_67217979)	78491
CGOV5T	chr14	g.(70017053_70017153)_(70022328_70022428)	5376
CGOV5T	chr15	g.(64675677_64675777)_(64711628_64711728)	36052
CGOV5T	chr16	g.(19945646_19945746)_(19967505_19967605)	21960
CGOV5T	chr16	g.(58566092_58566192)_(58640891_58640991)	74900
CGOV5T	chr17	g.(29663521_29663621)_(29675526_29675626)	12106
CGOV5T	chr17	g.(29663031_29664031)_(29671895_29672895)	8865
CGOV5T	chr18	g.(45971240_45971340)_(46052073_46052173)	80934
CGOV5T	chr19	g.(1873871_1873971)_(1895073_1895173)	21303
CGOV5T	chr19	g.(55265501_55266501)_(55286501_55287501)	21001
CGOV5T	chr19	g.(56594560_56595560)_(56612790_56613790)	18231
CGOV5T	chr21	g.(38745983_38746083)_(38834317_38834417)	88435
CGOV5T	chrX	g.(7010785_7010885)_(7018229_7018329)	7545
CGOV5T	chrX	g.(34043034_34043134)_(34072726_34072826)	29793
CGOV6T	chr1	g.(72755752_72755852)_(72763911_72764011)	8260
CGOV6T	chr3	g.(60169866_60169966)_(60399371_60399471)	229606
CGOV6T	chr3	g.(60378753_60379753)_(60398971_60399971)	20219
CGOV6T	chr9	g.(133030714_133030814)_(133034653_133034753)	4040
CGOV6T	chr16	g.(78745605_78745705)_(78776539_78776639)	31035
CGOV6T	chr20	g.(7398784_7398884)_(7403433_7403533)	4750
CGOV6T	chr20	g.(52647132_52647232)_(52657841_52657941)	10810
CGOV6T	chrX	g.(6946313_6946413)_(7200948_7201048)	254736
CGOV8T	chr3	g.(165041002_165041102)_(165083203_165083303)	42302
CGOV8T	chr7	g.(8826562_8826662)_(8866118_8866218)	39657
CGOV8T	chr8	g.(40182911_40183011)_(40189654_40189754)	6844

CGOV8T	chr9	g.(21513318_21513418)_(23236722_23236822)	172350
CGOV8T	chr9	g.(133382642_133383642)_(133386900_133387900)	4259
CGOV8T	chr12	g.(96674843_96674943)_(96797912_96798012)	123170
CGOV8T	chr13	g.(105680183_105680283)_(105690552_105690652)	10470
CGOV8T	chr18	g.(41976771_41976871)_(41981913_41982013)	5243
CGOV8T	chr18	g.(63906673_63907673)_(63911231_63912231)	4559
CGOV8T	chr20	g.(59111694_59111794)_(59124714_59124814)	13121
CGOV8T	chr22	g.(27220819_27220919)_(27224406_27224506)	3688
CGOV8T	chr22	g.(30066862_30066962)_(30100486_30100586)	33725
CGOV92T	chr1	g.(39679839_39679939)_(39788784_39788884)	109046
CGOV92T	chr1	g.(41464636_41464736)_(41566388_41566488)	101853
CGOV92T	chr1	g.(48191487_48191587)_(48202675_48202775)	11289
CGOV92T	chr2	g.(7060501_7061501)_(7074501_7075501)	14001
CGOV92T	chr2	g.(23999810_23999910)_(24149156_24149256)	149447
CGOV92T	chr2	g.(43450966_43451066)_(43569072_43569172)	118207
CGOV92T	chr2	g.(153339700_153339800)_(153502769_153502869)	163170
CGOV92T	chr3	g.(19045992_19046992)_(19050838_19051838)	4847
CGOV92T	chr3	g.(88468267_88468367)_(88479958_88480058)	11792
CGOV92T	chr3	g.(114827592_114827692)_(114847752_114847852)	20261
CGOV92T	chr4	g.(113208974_113209074)_(113392305_113392405)	183432
CGOV92T	chr5	g.(36938427_36938527)_(37036434_37036534)	98108
CGOV92T	chr5	g.(108446283_108446383)_(108732196_108732296)	286014
CGOV92T	chr6	g.(47052279_47052379)_(47057840_47057940)	5662
CGOV92T	chr6	g.(123102293_123102393)_(123133958_123134058)	31766
CGOV92T	chr6	g.(144601606_144602606)_(145042912_145043912)	441307
CGOV92T	chr6	g.(152766491_152766591)_(152781341_152781441)	14951
CGOV92T	chr7	g.(15912386_15912486)_(15928765_15928865)	16480
CGOV92T	chr7	g.(15912501_15913501)_(15926501_15927501)	14001
CGOV92T	chr7	g.(36949872_36949972)_(37130059_37130159)	180288
CGOV92T	chr7	g.(73183508_73183608)_(73272055_73272155)	88648
CGOV92T	chr7	g.(95823219_95823319)_(95827392_95827492)	4274
CGOV92T	chr7	g.(109821953_109822053)_(110121835_110121935)	299983
CGOV92T	chr7	g.(119297676_119298676)_(119302120_119303120)	4445
CGOV92T	chr8	g.(11666494_11666594)_(11701747_11701847)	35354
CGOV92T	chr8	g.(56690639_56690739)_(56720755_56720855)	30217
CGOV92T	chr8	g.(61327681_61327781)_(61536789_61536889)	209209

CGOV92T	chr8	g.(61613200_61613300)_(61772127_61772227)	159028
CGOV92T	chr10	g.(58894847_58894947)_(58936981_58937081)	42235
CGOV92T	chr10	g.(74507435_74507535)_(74530685_74530785)	23351
CGOV92T	chr11	g.(27380143_27380243)_(27397690_27397790)	17648
CGOV92T	chr11	g.(59056058_59056158)_(59567931_59568031)	511974
CGOV92T	chr11	g.(78691152_78691252)_(79000488_79000588)	309437
CGOV92T	chr12	g.(24067469_24067569)_(24550505_24550605)	483137
CGOV92T	chr12	g.(99573589_99573689)_(99956476_99956576)	382988
CGOV92T	chr12	g.(99573501_99574501)_(99584501_99585501)	11001
CGOV92T	chr12	g.(99585501_99586501)_(99954501_99955501)	369001
CGOV92T	chr13	g.(96621899_96621999)_(96643785_96643885)	21987
CGOV92T	chr14	g.(50921928_50922928)_(51230510_51231510)	308583
CGOV92T	chr16	g.(18821410_18821510)_(18838772_18838872)	17463
CGOV92T	chr16	g.(19332935_19333035)_(19397623_19397723)	64789
CGOV92T	chr16	g.(23317517_23317617)_(23370413_23370513)	52997
CGOV92T	chr17	g.(15043969_15044069)_(15058563_15058663)	14695
CGOV92T	chr17	g.(61226501_61227501)_(61374501_61375501)	148001
CGOV92T	chr17	g.(61381501_61382501)_(61453501_61454501)	72001
CGOV92T	chr20	g.(40698580_40698680)_(40703597_40703697)	5118
CGOV92T	chr21	g.(29653613_29653713)_(29786849_29786949)	133337
CGOV92T	chr22	g.(46985937_46986037)_(46989975_46990075)	4139
CGOV92T	chr22	g.(50722482_50722582)_(50778127_50778227)	55746
CGOV92T	chrX	g.(63686350_63686450)_(63965597_63965697)	279348
CGOV92T	chrX	g.(83236456_83236556)_(83429572_83429672)	193217
CGOV92T	chrX	g.(127300220_127300320)_(127495502_127495602)	195383
CGOV92T	chrX	g.(128236172_128236272)_(128348866_128348966)	112795
CGOV12T	chr1	g.(16751245_16751345)_(16754940_16755040)	3796
CGOV12T	chr1	g.(203919144_203919244)_(203932932_203933032)	13889
CGOV12T	chr3	g.(173422155_173422255)_(173641993_173642093)	219939
CGOV12T	chr3	g.(174446190_174446290)_(174483754_174483854)	37665
CGOV12T	chr4	g.(151883961_151884061)_(151910604_151910704)	26744
CGOV12T	chr7	g.(111020069_111020169)_(111198263_111198363)	178295
CGOV12T	chr8	g.(79746431_79746531)_(79902820_79902920)	156490
CGOV12T	chr9	g.(11947435_11947535)_(12188439_12188539)	241105
CGOV12T	chr11	g.(83965068_83965168)_(84000318_84000418)	35351
CGOV12T	chr16	g.(72078972_72079072)_(72157134_72157234)	78263
CGOV12T	chr16	g.(78194275_78194375)_(78260423_78260523)	66249

CGOV12T	chr21	g.(27184281_27184381)_(27236785_27236885)	52605
CGOV20T	chr1	g.(111748043_111748143)_(111758616_111758716)	10674
CGOV20T	chr1	g.(154691759_154691859)_(154835131_154835231)	143473
CGOV20T	chr2	g.(4116305_4117305)_(4125389_4126389)	9085
CGOV20T	chr2	g.(191754503_191754603)_(191774080_191774180)	19678
CGOV20T	chr3	g.(142055351_142055451)_(142074299_142074399)	19049
CGOV20T	chr4	g.(30738167_30738267)_(30880428_30880528)	142362
CGOV20T	chr5	g.(3957872_3957972)_(3970555_3970655)	12784
CGOV20T	chr5	g.(17342810_17342910)_(17357022_17357122)	14313
CGOV20T	chr5	g.(180632057_180632157)_(180641742_180641842)	9786
CGOV20T	chr7	g.(101724584_101724684)_(101727384_101727484)	2901
CGOV20T	chr7	g.(111024561_111024661)_(111048560_111048660)	24100
CGOV20T	chr7	g.(130607267_130607367)_(130646248_130646348)	39082
CGOV20T	chr7	g.(148427284_148427384)_(148500744_148500844)	73561
CGOV20T	chr8	g.(16262122_16262222)_(16274520_16274620)	12499
CGOV20T	chr9	g.(24502136_24502236)_(24518938_24519038)	16903
CGOV20T	chr11	g.(132992254_132992354)_(133004295_133004395)	12142
CGOV20T	chr12	g.(13356624_13356724)_(13436104_13436204)	79581
CGOV20T	chr13	g.(48899250_48899350)_(48953887_48953987)	54738
CGOV20T	chr14	g.(38133163_38133263)_(38137648_38137748)	4586
CGOV20T	chr15	g.(54883501_54884501)_(54886501_54887501)	3001
CGOV20T	chr16	g.(74376501_74377501)_(74390501_74391501)	14001
CGOV20T	chr16	g.(78552722_78552822)_(78569810_78569910)	17189
CGOV20T	chr16	g.(89516738_89516838)_(89526411_89526511)	9774
CGOV20T	chr18	g.(37355778_37355878)_(37371489_37371589)	15812
CGOV20T	chr18	g.(40054149_40054249)_(40057502_40057602)	3454
CGOV20T	chr18	g.(54339023_54339123)_(54493894_54493994)	154972
CGOV20T	chr20	g.(12147980_12148080)_(13150916_13151016)	100303
CGOV20T	chrX	g.(133082255_133082355)_(133121130_133121230)	38976
CGOV27T	chr1	g.(105832867_105832967)_(105844203_105844303)	11437
CGOV27T	chr2	g.(223865143_223865243)_(223869740_223869840)	4698
CGOV27T	chr3	g.(53267005_53267105)_(53283225_53283325)	16321
CGOV27T	chr3	g.(115663498_115663598)_(116209139_116209239)	545742
CGOV27T	chr7	g.(3882244_3882344)_(3905752_3905852)	23609

CGOV27T	chr8	g.(7224501_7225501)_(8085501_8086501)	861001
CGOV27T	chr12	g.(117005397_117005497)_(117007669_117007769)	2373
CGOV27T	chr13	g.(113514115_113514215)_(113526001_113526101)	11987
CGOV27T	chr14	g.(24264965_24265065)_(24271869_24271969)	7005
CGOV27T	chr16	g.(78762005_78762105)_(78772346_78772446)	10442
CGOV27T	chr18	g.(66745659_66745759)_(66756846_66756946)	11288
CGOV27T	chrX	g.(143628749_143628849)_(143637602_143637702)	8954
CGOV29T	chr3	g.(60415943_60416043)_(60462114_60462214)	46272
CGOV29T	chr3	g.(60676489_60676589)_(60727657_60727757)	51269
CGOV29T	chr3	g.(72779769_72780769)_(72784558_72785558)	4790
CGOV29T	chr13	g.(23640718_23640818)_(23643958_23644058)	3341
CGOV29T	chr13	g.(108947081_108947181)_(108951658_108951758)	4678
CGOV31T	chr2	g.(212283626_212283726)_(212361477_212361577)	77952
CGOV31T	chr4	g.(25712067_25712167)_(25735734_25735834)	23768
CGOV31T	chr4	g.(161013866_161013966)_(161019488_161019588)	5723
CGOV31T	chr5	g.(51466747_51466847)_(51471207_51471307)	4561
CGOV31T	chr9	g.(20799110_20800110)_(20804125_20805125)	5016
CGOV31T	chr9	g.(21952605_21952705)_(22006797_22006897)	54293
CGOV31T	chr9	g.(43503501_43504501)_(43658501_43659501)	155001
CGOV31T	chr9	g.(119016894_119016994)_(119020687_119020787)	3894
CGOV31T	chr11	g.(97818282_97818382)_(97877935_97878035)	59754
CGOV31T	chr13	g.(110928407_110928507)_(110993965_110994065)	65659
CGOV31T	chr22	g.(42519278_42519378)_(42531382_42531482)	12205
CGOV31T	chrX	g.(76764950_76765050)_(76769316_76769416)	4467
CGOV31T	chrX	g.(137045303_137046303)_(137054389_137055389)	9087
CGOV35T	chr1	g.(16751232_16751332)_(16754942_16755042)	3811
CGOV35T	chr1	g.(82317730_82317830)_(82356590_82356690)	38961
CGOV35T	chr1	g.(162054321_162054421)_(162114665_162114765)	60445
CGOV35T	chr1	g.(192931990_192932090)_(192976607_192976707)	44718
CGOV35T	chr1	g.(193211752_193211852)_(193310082_193310182)	98431

CGOV35T	chr1	g.(193412100_193412200)_(193625361_193625461)	213362
CGOV35T	chr1	g.(236232977_236233077)_(236238818_236238918)	5942
CGOV35T	chr2	g.(34991190_34991290)_(35024397_35024497)	33308
CGOV35T	chr2	g.(58119113_58119213)_(58266111_58266211)	147099
CGOV35T	chr2	g.(141529999_141530099)_(141711725_141711825)	181827
CGOV35T	chr2	g.(186750647_186750747)_(186794045_186794145)	43499
CGOV35T	chr2	g.(213880087_213880187)_(213975706_213975806)	95720
CGOV35T	chr2	g.(236733493_236733593)_(236950305_236950405)	216913
CGOV35T	chr3	g.(6191068_6191168)_(6220739_6220839)	29772
CGOV35T	chr3	g.(67537842_67537942)_(67584362_67584462)	46621
CGOV35T	chr3	g.(70199247_70200247)_(70315743_70316743)	116497
CGOV35T	chr3	g.(71104703_71104803)_(71551796_71551896)	447194
CGOV35T	chr3	g.(116214454_116214554)_(116777983_116778083)	563630
CGOV35T	chr3	g.(178284052_178284152)_(178363289_178363389)	79338
CGOV35T	chr4	g.(67379750_67379850)_(67393459_67393559)	13810
CGOV35T	chr4	g.(151272601_151272701)_(151495680_151495780)	223180
CGOV35T	chr4	g.(181823765_181823865)_(182062343_182062443)	238679
CGOV35T	chr4	g.(182200049_182200149)_(182440492_182440592)	240544
CGOV35T	chr5	g.(12276683_12276783)_(12292247_12292347)	15665
CGOV35T	chr5	g.(59265559_59265659)_(59546661_59546761)	281203
CGOV35T	chr5	g.(59266501_59267501)_(59404501_59405501)	138001
CGOV35T	chr5	g.(59405340_59406340)_(59546297_59547297)	140958
CGOV35T	chr5	g.(59781013_59781113)_(59967067_59967167)	186155
CGOV35T	chr5	g.(60681576_60681676)_(60770103_60770203)	88628
CGOV35T	chr5	g.(130851788_130851888)_(130943070_130943170)	91383
CGOV35T	chr5	g.(162521084_162521184)_(162805032_162805132)	284049
CGOV35T	chr5	g.(173061278_173061378)_(173096490_173096590)	35313
CGOV35T	chr6	g.(77016777_77016877)_(77029005_77029105)	12329
CGOV35T	chr6	g.(100940693_100940793)_(101193380_101193480)	252788
CGOV35T	chr6	g.(109042913_109043013)_(109229211_109229311)	186399
CGOV35T	chr6	g.(162726253_162726353)_(162791582_162791682)	65430
CGOV35T	chr7	g.(16269984_16270084)_(16459393_16459493)	189510
CGOV35T	chr7	g.(35858815_35858915)_(35881925_35882025)	23211
CGOV35T	chr7	g.(110787147_110787247)_(110894630_110894730)	107584
CGOV35T	chr7	g.(148516934_148517034)_(148544440_148544540)	27607
CGOV35T	chr9	g.(10977771_10977871)_(11039577_11039677)	61907
CGOV35T	chr9	g.(21908449_21908549)_(21992673_21992773)	84325
CGOV35T	chr9	g.(21907949_21908949)_(21989501_21990501)	81553

CGOV35T	chr9	g.(108101838_108101938)_(108840089_108840189)	738352
CGOV35T	chr10	g.(556290_556390)_(582581_582681)	26392
CGOV35T	chr10	g.(20228769_20228869)_(20377976_20378076)	149308
CGOV35T	chr10	g.(35698356_35698456)_(35785482_35785582)	87227
CGOV35T	chr10	g.(60186785_60186885)_(60333223_60333323)	146539
CGOV35T	chr10	g.(77573487_77573587)_(77592952_77593052)	19566
CGOV35T	chr10	g.(112019953_112020053)_(112027567_112027667)	7715
CGOV35T	chr11	g.(9944084_9944184)_(10058832_10058932)	114849
CGOV35T	chr11	g.(29021852_29021952)_(29214082_29214182)	192331
CGOV35T	chr11	g.(93586244_93586344)_(93710286_93710386)	124143
CGOV35T	chr12	g.(15927615_15927715)_(16072744_16072844)	145230
CGOV35T	chr12	g.(32688373_32688473)_(32804685_32804785)	116413
CGOV35T	chr12	g.(32790562_32791562)_(32804285_32805285)	13724
CGOV35T	chr12	g.(32791062_32791162)_(32824460_32824560)	33499
CGOV35T	chr12	g.(79959640_79959740)_(79995899_79995999)	36360
CGOV35T	chr14	g.(46127209_46127309)_(46162996_46163096)	35888
CGOV35T	chr14	g.(64490205_64490305)_(64553115_64553215)	63011
CGOV35T	chr15	g.(25601425_25601525)_(25665725_25665825)	64401
CGOV35T	chr15	g.(49410612_49410712)_(49589004_49589104)	178493
CGOV35T	chr15	g.(64774738_64774838)_(64819881_64819981)	45244
CGOV35T	chr15	g.(67418598_67418698)_(67476818_67476918)	58321
CGOV35T	chr16	g.(20632787_20632887)_(20671284_20671384)	38598
CGOV35T	chr16	g.(72686200_72686300)_(72875566_72875666)	189467
CGOV35T	chr16	g.(78531906_78532006)_(78717421_78717521)	185616
CGOV35T	chr16	g.(78561196_78562196)_(78717021_78718021)	155826
CGOV35T	chr16	g.(79029196_79029296)_(79077123_79077223)	48028
CGOV35T	chr17	g.(9924658_9924758)_(9927853_9927953)	3296
CGOV35T	chr18	g.(8035157_8035257)_(8041215_8041315)	6159
CGOV35T	chr21	g.(38792673_38792773)_(38834029_38834129)	41457
CGOV35T	chr22	g.(47201644_47201744)_(47323642_47323742)	122099
CGOV35T	chrX	g.(6748902_6749002)_(6922726_6922826)	173925
CGOV35T	chrX	g.(6978933_6979033)_(7010753_7010853)	31921
CGOV35T	chrX	g.(9619187_9619287)_(9903884_9903984)	284798
CGOV35T	chrX	g.(10115127_10115227)_(10546593_10546693)	431567
CGOV35T	chrX	g.(28520819_28520919)_(28525862_28525962)	5144
CGOV35T	chrX	g.(56145982_56146082)_(56242433_56242533)	96552
CGOV35T	chrX	g.(93695433_93696433)_(93953334_93954334)	257902

CGOV35T	chrX	g.(96475496_96475596)_(96487316_96487416)	11921
CGOV35T	chrX	g.(120275502_120275602)_(120280297_120280397)	4896
CGOV39T	chr1	g.(26459605_26460605)_(26464273_26465273)	4669
CGOV39T	chr2	g.(185166764_185166864)_(185180947_185181047)	14284
CGOV39T	chr4	g.(112236956_112237956)_(112241890_112242890)	4935
CGOV39T	chr5	g.(27606207_27606307)_(27633232_27633332)	27126
CGOV39T	chr9	g.(43503501_43504501)_(43658501_43659501)	155001
CGOV39T	chr12	g.(6241499_6241599)_(6247972_6248072)	6574
CGOV7T	chr2	g.(141801123_141801223)_(141845756_141845856)	44734
CGOV7T	chr3	g.(175887255_175887355)_(175914747_175914847)	27593
CGOV7T	chr4	g.(29355881_29355981)_(29436257_29436357)	80477
CGOV7T	chr6	g.(152282226_152282326)_(152298780_152298880)	16655
CGOV7T	chr7	g.(101724536_101724636)_(101727432_101727532)	2997
CGOV7T	chr8	g.(7224501_7225501)_(8085501_8086501)	861001
CGOV7T	chr8	g.(81990694_81990794)_(81993860_81993960)	3267
CGOV7T	chr10	g.(57932452_57932552)_(57954488_57954588)	22137
CGOV7T	chr12	g.(79980150_79980250)_(80293410_80293510)	313361
CGOV7T	chr13	g.(36129417_36129517)_(36140362_36140462)	11046
CGOV7T	chr16	g.(78548743_78548843)_(78556729_78556829)	8087
CGOV7T	chr16	g.(78646020_78646120)_(78695574_78695674)	49655
CGOV7T	chr18	g.(6103935_6104035)_(6109267_6109367)	5433
CGOV7T	chr18	g.(55093038_55093138)_(55124573_55124673)	31636
CGOV7T	chr18	g.(66745650_66745750)_(66756847_66756947)	11298
CGOV7T	chrX	g.(29655863_29655963)_(29825683_29825783)	169921
CGOV11T_1	chr1	g.(43460100_43460200)_(43464195_43464295)	4196
CGOV11T_1	chr2	g.(179573984_179574084)_(179820766_179820866)	246883
CGOV11T_1	chr4	g.(53825244_53825344)_(54132027_54132127)	306884
CGOV11T_1	chr6	g.(6948886_6948986)_(6953333_6953433)	4548
CGOV11T_1	chr6	g.(53924871_53924971)_(53934671_53934771)	9901
CGOV11T_1	chr11	g.(80306216_80306316)_(80312975_80313075)	6860
CGOV11T_1	chr11	g.(81089108_81089208)_(81138743_81138843)	49736
CGOV11T_1	chr12	g.(100453239_100453339)_(100630303_100630403)	177165

CGOV11T_1	chr13	g.(58589205_58589305)_(58599626_58599726)	10522
CGOV11T_1	chr13	g.(110930279_110930379)_(111152795_111152895)	222617
CGOV11T_1	chr18	g.(7888970_7889070)_(8246655_8246755)	357786
CGOV11T_1	chr18	g.(31655160_31655260)_(31686013_31686113)	30954
CGOV11T_1	chrX	g.(120768859_120768959)_(121017533_121017633)	248775
CGOV14T	chr1	g.(193777526_193777626)_(193794588_193794688)	17163
CGOV14T	chr1	g.(231535433_231535533)_(231545846_231545946)	10514
CGOV14T	chr3	g.(60273501_60274501)_(60444501_60445501)	171001
CGOV14T	chr3	g.(60561988_60562088)_(60675475_60675575)	113588
CGOV14T	chr3	g.(60591926_60592926)_(60675075_60676075)	83150
CGOV14T	chr3	g.(60831480_60831580)_(61223873_61223973)	392494
CGOV14T	chr3	g.(61652007_61652107)_(61805810_61805910)	153904
CGOV14T	chr4	g.(30193251_30193351)_(30199442_30199542)	6292
CGOV14T	chr5	g.(67438096_67438196)_(67470485_67470585)	32490
CGOV14T	chr7	g.(18550890_18550990)_(18567966_18568066)	17177
CGOV14T	chr7	g.(106639172_106639272)_(106647605_106647705)	8534
CGOV14T	chr9	g.(18045835_18045935)_(18048938_18049038)	3204
CGOV14T	chr16	g.(78627527_78627627)_(78639492_78639592)	12066
CGOV36T	chr1	g.(217854654_217854754)_(218003578_218003678)	149025
CGOV36T	chr2	g.(153796026_153796126)_(153799612_153799712)	3687
CGOV36T	chr2	g.(236906617_236906717)_(237028180_237028280)	121664
CGOV36T	chr3	g.(37978429_37978529)_(37986777_37986877)	8449
CGOV36T	chr3	g.(45920231_45920331)_(45924147_45924247)	4017
CGOV36T	chr3	g.(60546038_60546138)_(60807141_60807241)	261204
CGOV36T	chr4	g.(477193_477293)_(483925_484025)	6833
CGOV36T	chr4	g.(64134366_64134466)_(64154377_64154477)	20112
CGOV36T	chr4	g.(156457596_156457696)_(156909170_156909270)	451675
CGOV36T	chr4	g.(181616277_181616377)_(182320440_182320540)	704264
CGOV36T	chr6	g.(130482079_130483079)_(132397929_132398929)	191585
CGOV36T	chr6	g.(169247518_169248518)_(169255233_169256233)	7716
CGOV36T	chr6	g.(169272099_169273099)_(169745980_169746980)	473882
CGOV36T	chr6	g.(169760688_169761688)_(170269060_170270060)	508373
CGOV36T	chr7	g.(16348899_16348999)_(16402033_16402133)	53235
CGOV36T	chr9	g.(28514890_28514990)_(28521597_28521697)	6808
CGOV36T	chr9	g.(29414314_29415314)_(29493663_29494663)	79350

CGOV36T	chr11	g.(98822208_98822308)_(98896885_98896985)	74778
CGOV36T	chr13	g.(67464318_67464418)_(68397963_68398063)	933746
CGOV36T	chr15	g.(68750329_68750429)_(68763974_68764074)	13746
CGOV36T	chr16	g.(47544078_47544178)_(47550398_47550498)	6421
CGOV36T	chr16	g.(60081171_60081271)_(60098411_60098511)	17341
CGOV36T	chr18	g.(13337272_13337372)_(13368161_13368261)	30990
CGOV36T	chr18	g.(30081909_30082909)_(30323322_30324322)	241414
CGOV36T	chr18	g.(48110088_48111088)_(48636743_48637743)	526656
CGOV36T	chr18	g.(48646704_48647704)_(48924002_48925002)	277299
CGOV36T	chr18	g.(48969198_48969298)_(49587451_49587551)	618354
CGOV36T	chr18	g.(54734501_54735501)_(54737501_54738501)	3001
CGOV36T	chr18	g.(64557877_64558877)_(65001416_65002416)	443540
CGOV36T	chr18	g.(66745649_66745749)_(66756842_66756942)	11294
CGOV36T	chr19	g.(1194869_1194969)_(1208881_1208981)	14113
CGOV36T	chrX	g.(33662265_33662365)_(33675743_33675843)	13579
CGOV36T	chrX	g.(41454974_41455074)_(41560090_41560190)	105217
CGOV36T	chrX	g.(78679335_78679435)_(78708145_78708245)	28911
CGOV36T	chrX	g.(80088296_80088396)_(80174822_80174922)	86627
CGOV36T	chrX	g.(81166475_81166575)_(81569724_81569824)	403350
CGOV36T	chrX	g.(83721783_83721883)_(84144376_84144476)	422694
CGOV48T	chr2	g.(129456302_129456402)_(129463002_129463102)	6801
CGOV48T	chr2	g.(221011506_221011606)_(221369811_221369911)	358406
CGOV48T	chr2	g.(233905717_233905817)_(233984309_233984409)	78693
CGOV48T	chr4	g.(31463462_31463562)_(31469423_31469523)	6062
CGOV48T	chr4	g.(161013855_161013955)_(161019485_161019585)	5731
CGOV48T	chr4	g.(169825579_169825679)_(169878880_169878980)	53402
CGOV48T	chr9	g.(21814704_21814804)_(22523689_22523789)	709086
CGOV48T	chr9	g.(113604657_113604757)_(113610039_113610139)	5483
CGOV48T	chr9	g.(115777752_115777852)_(115782052_115782152)	4401
CGOV48T	chr10	g.(87337803_87337903)_(87353880_87353980)	16178
CGOV48T	chr12	g.(85756813_85756913)_(86225814_86225914)	469102
CGOV48T	chr18	g.(9743935_9744035)_(9754335_9754435)	10501
CGOV48T	chr19	g.(4988019_4989019)_(4993797_4994797)	5779
CGOV48T	chr19	g.(49183621_49183721)_(49206388_49206488)	22868
CGOV48T	chr22	g.(33755272_33756272)_(33759555_33760555)	4284
CGOV48T	chrX	g.(143628747_143628847)_(143637624_143637724)	8978
CGOV38T	chr1	g.(6437685_6438685)_(6445386_6446386)	7702

CGOV38T	chr1	g.(43445793_43446793)_(43452756_43453756)	6964
CGOV38T	chr1	g.(151980225_151980325)_(152000455_152000555)	20331
CGOV38T	chr2	g.(153796000_153796100)_(153799581_153799681)	3682
CGOV38T	chr6	g.(77438501_77439501)_(77452501_77453501)	14001
CGOV38T	chr6	g.(101934600_101934700)_(101938866_101938966)	4367
CGOV38T	chr9	g.(27777159_27777259)_(27798066_27798166)	21008
CGOV38T	chr13	g.(35558501_35559501)_(35562501_35563501)	4001
CGOV38T	chr15	g.(71474475_71474575)_(71477776_71477876)	3402
CGOV38T	chr18	g.(63906636_63907636)_(63911257_63912257)	4622
CGOV38T	chr19	g.(28294496_28294596)_(28318752_28318852)	24357
CGOV38T	chrX	g.(6501878_6502878)_(6506061_6507061)	4184
CGOV38T	chrX	g.(123104860_123104960)_(123121780_123121880)	17021
CGOV49T	chr3	g.(20311501_20312501)_(20315501_20316501)	4001
CGOV49T	chr3	g.(153599278_153599378)_(153613833_153613933)	14656
CGOV49T	chr4	g.(178821252_178821352)_(178872143_178872243)	50992
CGOV49T	chr6	g.(162322953_162323053)_(162440273_162440373)	117421
CGOV49T	chr9	g.(22599342_22599442)_(22606500_22606600)	7259
CGOV49T	chr9	g.(133030683_133030783)_(133034655_133034755)	4073
CGOV49T	chr10	g.(105715870_105715970)_(105720595_105720695)	4826
CGOV49T	chr15	g.(72016688_72016788)_(72104337_72104437)	87750
CGOV49T	chr18	g.(66784036_66784136)_(66807797_66807897)	23862
CGOV49T	chr19	g.(55266691_55266791)_(55281325_55281425)	14735
CGOV10T	chr1	g.(26460210_26460310)_(26464644_26464744)	4535
CGOV10T	chr1	g.(98168988_98169088)_(98176058_98176158)	7171
CGOV10T	chr1	g.(192945596_192945696)_(193418417_193418517)	472922
CGOV10T	chr2	g.(78565959_78566059)_(78666645_78666745)	100787
CGOV10T	chr2	g.(176203347_176203447)_(176210931_176211031)	7685
CGOV10T	chr2	g.(180411501_180412501)_(180420501_180421501)	9001
CGOV10T	chr3	g.(59811733_59811833)_(60140716_60140816)	329084
CGOV10T	chr3	g.(60246710_60246810)_(60435013_60435113)	188404
CGOV10T	chr3	g.(60318539_60318639)_(60632927_60633027)	314489
CGOV10T	chr3	g.(60318039_60319039)_(60433501_60434501)	115463
CGOV10T	chr3	g.(60866915_60867015)_(60958337_60958437)	91523
CGOV10T	chr3	g.(97293289_97293389)_(97440831_97440931)	147643
CGOV10T	chr3	g.(175026820_175026920)_(175166253_175166353)	139534
CGOV10T	chr3	g.(175026320_175027320)_(175158501_175159501)	132182

CGOV10T	chr4	g.(12677485_12677585)_(12711162_12711262)	33778
CGOV10T	chr4	g.(13119160_13119260)_(13208066_13208166)	89007
CGOV10T	chr4	g.(19084501_19085501)_(19169501_19170501)	85001
CGOV10T	chr5	g.(59161500_59161600)_(59534753_59534853)	373354
CGOV10T	chr5	g.(59850099_59850199)_(60140400_60140500)	290402
CGOV10T	chr5	g.(60314810_60314910)_(60417192_60417292)	102483
CGOV10T	chr5	g.(65288688_65288788)_(65294084_65294184)	5497
CGOV10T	chr5	g.(96372415_96372515)_(96417202_96417302)	44888
CGOV10T	chr5	g.(97047921_97048021)_(97095986_97096086)	48166
CGOV10T	chr5	g.(161893168_161893268)_(162058723_162058823)	165656
CGOV10T	chr5	g.(165767447_165767547)_(165779810_165779910)	12464
CGOV10T	chr6	g.(77438501_77439501)_(77452501_77453501)	14001
CGOV10T	chr6	g.(162769012_162769112)_(162803405_162803505)	34494
CGOV10T	chr7	g.(40115044_40115144)_(40240948_40241048)	126005
CGOV10T	chr7	g.(90013231_90013331)_(90142691_90142791)	129561
CGOV10T	chr7	g.(104662593_104662693)_(104713698_104713798)	51206
CGOV10T	chr7	g.(109632363_109632463)_(110037416_110037516)	405154
CGOV10T	chr7	g.(110768465_110768565)_(110780452_110780552)	12088
CGOV10T	chr7	g.(133518916_133519016)_(133761517_133761617)	242702
CGOV10T	chr8	g.(40182947_40183047)_(40189649_40189749)	6803
CGOV10T	chr9	g.(9053905_9054005)_(9259998_9260098)	206194
CGOV10T	chr9	g.(9990197_9990297)_(10379332_10379432)	389236
CGOV10T	chr9	g.(74827975_74828075)_(74915865_74915965)	87991
CGOV10T	chr11	g.(29027686_29027786)_(29457684_29457784)	430099
CGOV10T	chr11	g.(70155057_70155157)_(70238991_70239091)	84035
CGOV10T	chr12	g.(93178251_93178351)_(94329770_94329870)	115162
CGOV10T	chr14	g.(70017062_70017162)_(70022324_70022424)	5363
CGOV10T	chr16	g.(78162775_78162875)_(78352369_78352469)	189695
CGOV10T	chr16	g.(78609922_78610022)_(78626990_78627090)	17169
CGOV10T	chr16	g.(78741639_78741739)_(78811297_78811397)	69759
CGOV10T	chr16	g.(78847865_78847965)_(78955560_78955660)	107796
CGOV10T	chr17	g.(22060527_22060627)_(22066595_22066695)	6169
CGOV10T	chr20	g.(14676042_14676142)_(15296859_15296959)	620918
CGOV10T	chr20	g.(14723501_14724501)_(14754501_14755501)	31001
CGOV10T	chr20	g.(14724034_14724134)_(14934392_14934492)	210459

CGOV10T	chr20	g.(14755501_14756501)_(14778501_14779501)	23001
CGOV10T	chr20	g.(14876501_14877501)_(14933990_14934990)	57490
CGOV10T	chr20	g.(14939501_14940501)_(14984501_14985501)	45001
CGOV10T	chr20	g.(15096346_15096446)_(15139610_15139710)	43365
CGOV10T	chr20	g.(15155501_15156501)_(15214501_15215501)	59001
CGOV10T	chr20	g.(15255748_15256748)_(15296459_15297459)	40712
CGOV10T	chrX	g.(6686876_6686976)_(6987973_6988073)	301198
CGOV10T	chrX	g.(6686376_6687376)_(6736501_6737501)	50126
CGOV10T	chrX	g.(7022694_7022794)_(7044555_7044655)	21962
CGOV13T	chr2	g.(212321097_212321197)_(213408760_213408860)	108776
CGOV13T	chr3	g.(80863479_80863579)_(80972333_80972433)	108955
CGOV13T	chr4	g.(21900075_21900175)_(21910945_21911045)	10971
CGOV13T	chr5	g.(128926970_128927070)_(128929826_128929926)	2957
CGOV13T	chr7	g.(1388847_1388947)_(1462551_1462651)	73805
CGOV13T	chr7	g.(51816029_51816129)_(51828512_51828612)	12584
CGOV13T	chr12	g.(23123501_23124501)_(23153501_23154501)	30001
CGOV13T	chr12	g.(27648223_27648323)_(27654963_27655063)	6841
CGOV13T	chr12	g.(120577774_120577874)_(120599725_120599825)	22052
CGOV13T	chr13	g.(84820374_84820474)_(84999433_84999533)	179160
CGOV13T	chr14	g.(72805874_72805974)_(72810762_72810862)	4989
CGOV13T	chr18	g.(41325958_41326958)_(41330769_41331769)	4812
CGOV13T	chr18	g.(54021489_54022489)_(54026036_54027036)	4548
CGOV13T	chr18	g.(69591274_69591374)_(69607621_69607721)	16448
CGOV13T	chrX	g.(8017546_8017646)_(8459534_8459634)	442089
CGOV13T	chrX	g.(8017501_8018501)_(8206501_8207501)	189001
CGOV13T	chrX	g.(8207501_8208501)_(8430501_8431501)	223001
CGOV13T	chrX	g.(71532361_71533361)_(71608180_71609180)	75820
CGOV40T	chr3	g.(30109860_30110860)_(30448241_30449241)	338382
CGOV40T	chr3	g.(30476177_30477177)_(30518460_30519460)	42284
CGOV40T	chr3	g.(30664108_30665108)_(30702536_30703536)	38429
CGOV40T	chr3	g.(60322103_60322203)_(60462343_60462443)	140341
CGOV40T	chr3	g.(60365451_60365551)_(60580322_60580422)	214972
CGOV40T	chr3	g.(60364959_60365959)_(60461943_60462943)	96985
CGOV40T	chr3	g.(60467710_60467810)_(60555646_60555746)	88037
CGOV40T	chr4	g.(176779205_176779305)_(176950653_176950753)	171549
CGOV40T	chr6	g.(12478890_12478990)_(12483270_12483370)	4481
CGOV40T	chr6	g.(142237501_142238501)_(142243028_142244028)	5528
CGOV40T	chr8	g.(83693267_83693367)_(83703040_83703140)	9874

CGOV40T	chr9	g.(21879264_21880264)_(22014155_22015155)	134892
CGOV40T	chr9	g.(43503501_43504501)_(43658501_43659501)	155001
CGOV40T	chr9	g.(107361193_107362193)_(107367012_107368012)	5820
CGOV40T	chr9	g.(115777732_115777832)_(115782089_115782189)	4458
CGOV40T	chr10	g.(67905425_67906425)_(67915416_67916416)	9992
CGOV40T	chr13	g.(69244761_69244861)_(69268614_69268714)	23954
CGOV40T	chr13	g.(108112115_108112215)_(108129320_108129420)	17306
CGOV40T	chr16	g.(78169069_78169169)_(78178012_78178112)	9044
CGOV40T	chr16	g.(78581883_78581983)_(78624144_78624244)	42362
CGOV40T	chr17	g.(28939501_28940501)_(28949501_28950501)	10001
CGOV40T	chr18	g.(66745659_66745759)_(66756839_66756939)	11281
CGOV40T	chr19	g.(11130042_11131042)_(11133876_11134876)	3835
CGOV40T	chr19	g.(11153594_11154594)_(11160561_11161561)	6968
CGOV40T	chr21	g.(43343501_43344501)_(43349501_43350501)	6001
CGOV40T	chr22	g.(19892068_19892168)_(20024323_20024423)	132356
CGOV40T	chrX	g.(6855501_6856501)_(6910501_6911501)	55001
CGOV15T	chr1	g.(21966870_21966970)_(21980618_21980718)	13849
CGOV15T	chr1	g.(77031928_77032028)_(77047415_77047515)	15588
CGOV15T	chr1	g.(180742702_180742802)_(180875651_180875751)	133050
CGOV15T	chr1	g.(210582343_210582443)_(210620517_210620617)	38275
CGOV15T	chr2	g.(3732876_3732976)_(3737864_3737964)	5089
CGOV15T	chr2	g.(122767609_122767709)_(122787150_122787250)	19642
CGOV15T	chr3	g.(83342471_83342571)_(83368227_83368327)	25857
CGOV15T	chr4	g.(28131351_28131451)_(28177945_28178045)	46695
CGOV15T	chr4	g.(55072681_55072781)_(55081578_55081678)	8998
CGOV15T	chr4	g.(92100501_92101501)_(92334501_92335501)	234001
CGOV15T	chr5	g.(44548972_44549072)_(44554728_44554828)	5857
CGOV15T	chr5	g.(111939649_111939749)_(111944175_111944275)	4627
CGOV15T	chr5	g.(117400375_117401375)_(119756463_119757463)	2356089
CGOV15T	chr5	g.(179132631_179132731)_(179148657_179148757)	16127
CGOV15T	chr6	g.(62759791_62759891)_(62792146_62792246)	32456
CGOV15T	chr6	g.(65221140_65221240)_(65227676_65227776)	6637
CGOV15T	chr7	g.(49168703_49168803)_(49233800_49233900)	65198
CGOV15T	chr7	g.(107899737_107899837)_(107929802_107929902)	30166

CGOV15T	chr10	g.(1105261_1105361)_(1118994_1119094)	13834
CGOV15T	chr10	g.(23415227_23415327)_(23436931_23437031)	21805
CGOV15T	chr10	g.(51003501_51004501)_(51009501_51010501)	6001
CGOV15T	chr12	g.(8378501_8379501)_(8411501_8412501)	33001
CGOV15T	chr12	g.(104282150_104282250)_(104311358_104311458)	29309
CGOV15T	chr12	g.(106811523_106811623)_(106824336_106824436)	12914
CGOV15T	chr13	g.(110177155_110177255)_(110468862_110468962)	291808
CGOV15T	chr14	g.(25373790_25373890)_(25458530_25458630)	84841
CGOV15T	chr15	g.(29864654_29864754)_(29918051_29918151)	53498
CGOV15T	chr15	g.(54851057_54851157)_(54973874_54973974)	122918
CGOV15T	chr16	g.(19945577_19945677)_(19967459_19967559)	21983
CGOV15T	chr16	g.(55956023_55956123)_(56056729_56056829)	100807
CGOV15T	chr16	g.(62612601_62612701)_(62833269_62833369)	220769
CGOV15T	chr17	g.(151746_151846)_(227412_227512)	75767
CGOV15T	chr17	g.(9590501_9591501)_(9946501_9947501)	356001
CGOV15T	chr17	g.(10619784_10620784)_(12488757_12489757)	186897
CGOV15T	chr17	g.(13082022_13082122)_(13822892_13822992)	740971
CGOV15T	chr17	g.(19615501_19616501)_(20548501_20549501)	933001
CGOV15T	chr17	g.(20785501_20786501)_(21504501_21505501)	719001
CGOV15T	chr18	g.(75508039_75508139)_(75555191_75555291)	47253
CGOV15T	chr19	g.(3350028_3350128)_(3394707_3394807)	44780
CGOV15T	chr20	g.(15927164_15927264)_(16058289_16058389)	131226
CGOV15T	chr21	g.(15957697_15958697)_(16976324_16977324)	101862
CGOV15T	chr22	g.(46475503_46475603)_(46492250_46492350)	16848
CGOV15T	chrX	g.(26225501_26226501)_(26710501_26711501)	485001
CGOV15T	chrX	g.(39610501_39611501)_(39623501_39624501)	13001
CGOV15T	chrX	g.(57745501_57746501)_(57767501_57768501)	22001
CGOV15T	chrX	g.(71347989_71348089)_(71433156_71433256)	85268
CGOV15T	chrX	g.(86649199_86649299)_(86658925_86659025)	9827
CGOV15T	chrX	g.(140344044_140345044)_(140562189_140563189)	218146

CGOV15T	chrX	g.(143628754_143628854)_(143637595_143637695)	8942
CGOV1T	chr1	g.(19599702_19599802)_(19614010_19614110)	14409
CGOV1T	chr1	g.(26459640_26460640)_(26464310_26465310)	4671
CGOV1T	chr1	g.(98689985_98690085)_(99141697_99141797)	451813
CGOV1T	chr2	g.(7229968_7230068)_(7235598_7235698)	5731
CGOV1T	chr2	g.(9925530_9925630)_(9928887_9928987)	3458
CGOV1T	chr3	g.(60345982_60346082)_(60383574_60383674)	37693
CGOV1T	chr4	g.(19278234_19278334)_(19460166_19460266)	182033
CGOV1T	chr4	g.(156594266_156594366)_(156598138_156598238)	3973
CGOV1T	chr4	g.(181848196_181848296)_(182031250_182031350)	183155
CGOV1T	chr4	g.(182123700_182123800)_(182647725_182647825)	524126
CGOV1T	chr5	g.(155577264_155577364)_(155591242_155591342)	14079
CGOV1T	chr6	g.(21090286_21090386)_(21160245_21160345)	70060
CGOV1T	chr6	g.(121795537_121795637)_(121800209_121800309)	4773
CGOV1T	chr6	g.(140530722_140530822)_(140537014_140537114)	6393
CGOV1T	chr7	g.(6908501_6909501)_(6915501_6916501)	7001
CGOV1T	chr7	g.(40085858_40085958)_(40124311_40124411)	38554
CGOV1T	chr7	g.(69458323_69458423)_(69800753_69800853)	342531
CGOV1T	chr7	g.(110580825_110580925)_(110634198_110634298)	53474
CGOV1T	chr7	g.(133043937_133044037)_(133408317_133408417)	364481
CGOV1T	chr8	g.(16262064_16262164)_(16274526_16274626)	12563
CGOV1T	chr8	g.(82974620_82975620)_(82980136_82981136)	5517
CGOV1T	chr10	g.(67324149_67324249)_(67336328_67336428)	12280
CGOV1T	chr11	g.(15807501_15808501)_(15814501_15815501)	7001
CGOV1T	chr11	g.(25019501_25020501)_(25034501_25035501)	15001
CGOV1T	chr11	g.(25702329_25702429)_(25720746_25720846)	18518
CGOV1T	chr11	g.(84163691_84163791)_(84211492_84211592)	47902
CGOV1T	chr11	g.(84389850_84389950)_(84418921_84419021)	29172
CGOV1T	chr13	g.(92386303_92386403)_(92392209_92392309)	6007
CGOV1T	chr13	g.(93962563_93962663)_(93995411_93995511)	32949
CGOV1T	chr14	g.(68712272_68712372)_(69157739_69157839)	445568
CGOV1T	chr15	g.(24055429_24055529)_(24061470_24061570)	6142
CGOV1T	chr15	g.(25420182_25420282)_(25430634_25430734)	10553
CGOV1T	chr16	g.(78925208_78925308)_(79006380_79006480)	81273
CGOV1T	chr17	g.(13876885_13876985)_(14059858_14059958)	183074

CGOV1T	chr18	g.(36656930_36657030)_(36666550_36666650)	9721
CGOV1T	chr18	g.(36905374_36905474)_(37108979_37109079)	203706
CGOV1T	chrX	g.(32475980_32476080)_(32598402_32598502)	122523
CGOV26T	chr2	g.(184794361_184794461)_(184803883_184803983)	9623
CGOV26T	chr3	g.(59763028_59763128)_(59894791_59894891)	131864
CGOV26T	chr4	g.(37925922_37926022)_(37960519_37960619)	34698
CGOV26T	chr4	g.(39704426_39704526)_(39713802_39713902)	9477
CGOV26T	chr5	g.(97047921_97048021)_(97096045_97096145)	48225
CGOV26T	chr7	g.(3863809_3863909)_(3911770_3911870)	48062
CGOV26T	chr7	g.(48581358_48581458)_(48592493_48592593)	11236
CGOV26T	chr7	g.(145997335_145997435)_(146005687_146005787)	8453
CGOV26T	chr7	g.(145996923_145997923)_(146000290_146001290)	3368
CGOV26T	chr9	g.(21714247_21714347)_(22214586_22214686)	500440
CGOV26T	chr9	g.(30501164_30501264)_(30537747_30537847)	36684
CGOV26T	chr9	g.(133030507_133030607)_(133034660_133034760)	4254
CGOV26T	chr9	g.(139365645_139365745)_(139384969_139385069)	19425
CGOV26T	chr10	g.(58512930_58513030)_(58526800_58526900)	13971
CGOV26T	chr12	g.(51376582_51376682)_(51380169_51380269)	3688
CGOV26T	chr14	g.(55788248_55788348)_(56113943_56114043)	325796
CGOV26T	chr17	g.(49079114_49079214)_(49109589_49109689)	30576
CGOV26T	chr19	g.(348972_349072)_(364146_364246)	15275
CGOV26T	chr20	g.(7398616_7398716)_(7403427_7403527)	4912
CGOV26T	chr20	g.(52647045_52647145)_(52657841_52657941)	10897
CGOV26T	chr22	g.(46515882_46515982)_(46521451_46521551)	5670
CGOV26T	chrX	g.(127626935_127627035)_(127719603_127719703)	92769
CGOV2T	chr1	g.(31600723_31600823)_(31624480_31624580)	23858
CGOV2T	chr1	g.(71728900_71729000)_(71829880_71829980)	101081
CGOV2T	chr1	g.(158624153_158624253)_(158633733_158633833)	9681
CGOV2T	chr1	g.(161573501_161574501)_(161618501_161619501)	45001
CGOV2T	chr1	g.(162830890_162830990)_(162845977_162846077)	15188
CGOV2T	chr2	g.(18597257_18597357)_(18630511_18630611)	33355
CGOV2T	chr3	g.(33136817_33137817)_(33142637_33143637)	5821
CGOV2T	chr3	g.(187567957_187568957)_(187833820_187834820)	265864

CGOV2T	chr3	g.(187834830_187835830)_(192707252_192708252)	4872423
CGOV2T	chr4	g.(43408501_43409501)_(45009501_45010501)	160100
CGOV2T	chr4	g.(45032340_45033340)_(46949830_46950830)	191749
CGOV2T	chr4	g.(155875122_155876122)_(163851396_163852396)	7976275
CGOV2T	chr5	g.(16115873_16115973)_(16126604_16126704)	10832
CGOV2T	chr5	g.(87378949_87379049)_(87381901_87382001)	3053
CGOV2T	chr8	g.(7224501_7225501)_(8085501_8086501)	861001
CGOV2T	chr8	g.(40182925_40183025)_(40189629_40189729)	6805
CGOV2T	chr8	g.(140371181_140371281)_(140468282_140468382)	97202
CGOV2T	chr10	g.(67298233_67298333)_(67436538_67436638)	138406
CGOV2T	chr10	g.(87781729_87781829)_(87803914_87804014)	22286
CGOV2T	chr11	g.(63918342_63918442)_(63984807_63984907)	66566
CGOV2T	chr11	g.(134927501_134928501)_(134945501_134946501)	18001
CGOV2T	chr12	g.(86426154_86426254)_(86432770_86432870)	6717
CGOV2T	chr13	g.(67377894_67377994)_(67397021_67397121)	19228

CGOV2T	chr15	g.(39995634_39995734)_(41216175_41216275)	122064
CGOV2T	chr16	g.(8615789_8616789)_(8622860_8623860)	7072
CGOV2T	chr17	g.(39211079_39212079)_(39221423_39222423)	10345
CGOV2T	chr18	g.(4780017_4780117)_(4790262_4790362)	10346
CGOV2T	chr19	g.(1119281_1119381)_(1229318_1229418)	110138
CGOV2T	chr22	g.(37744478_37744578)_(37749835_37749935)	5458
CGOV2T	chr22	g.(46809126_46809226)_(46969802_46969902)	160777
CGOV2T	chrX	g.(63188501_63189501)_(63866501_63867501)	678001
CGOV2T	chrX	g.(74871448_74871548)_(75307078_75307178)	435731
CGOV33T	chr1	g.(82370899_82370999)_(82391959_82392059)	21161
CGOV33T	chr1	g.(164263758_164263858)_(164271462_164271562)	7805
CGOV33T	chr2	g.(213184027_213184127)_(213191834_213191934)	7908
CGOV33T	chr2	g.(224183534_224183634)_(225009990_225010090)	826557
CGOV33T	chr3	g.(13670383_13670483)_(13685181_13685281)	14899
CGOV33T	chr3	g.(116750517_116750617)_(116925985_116926085)	175569
CGOV33T	chr3	g.(197050011_197051011)_(197056527_197057527)	6517
CGOV33T	chr4	g.(187294251_187295251)_(188895548_188896548)	160129
CGOV33T	chr5	g.(801501_802501)_(835501_836501)	34001
CGOV33T	chr5	g.(97047920_97048020)_(97095996_97096096)	48177
CGOV33T	chr7	g.(115931689_115931789)_(115941208_115941308)	9620
CGOV33T	chr9	g.(6700548_6700648)_(6710469_6710569)	10022
CGOV33T	chr11	g.(78768586_78768686)_(78783435_78783535)	14950
CGOV33T	chr11	g.(115161091_115161191)_(115167329_115167429)	6339
CGOV33T	chr13	g.(69244758_69244858)_(69268600_69268700)	23943
CGOV33T	chr15	g.(83353829_83353929)_(83384013_83384113)	30285
CGOV33T	chr16	g.(78507078_78507178)_(78703215_78703315)	196238
CGOV33T	chr17	g.(9218275_9218375)_(9222529_9222629)	4355
CGOV33T	chr21	g.(38742100_38742200)_(38758613_38758713)	16614
CGOV33T	chr22	g.(18625566_18626566)_(18629269_18630269)	3704
CGOV33T	chrX	g.(82319877_82320877)_(82324858_82325858)	4982

CGOV3T	chr4	g.(112236959_112237959)_(112241898_112242898)	4940
CGOV3T	chr9	g.(134260046_134261046)_(134265461_134266461)	5416
CGOV3T	chr10	g.(82879485_82879585)_(82891184_82891284)	11800
CGOV3T	chr11	g.(85263096_85263196)_(85274620_85274720)	11625
CGOV3T	chr13	g.(83788283_83788383)_(83792440_83792540)	4258
CGOV3T	chr13	g.(98529959_98530059)_(98532905_98533005)	3047
CGOV3T	chr17	g.(22060527_22060627)_(22066594_22066694)	6168
CGOV42T	chr1	g.(182728047_182728147)_(182732806_182732906)	4860
CGOV42T	chr1	g.(183501670_183501770)_(183507549_183507649)	5980
CGOV42T	chr2	g.(14843450_14843550)_(14941023_14941123)	97674
CGOV42T	chr2	g.(15217654_15217754)_(15405895_15405995)	188342
CGOV42T	chr2	g.(33852018_33852118)_(33937227_33937327)	85310
CGOV42T	chr3	g.(21338538_21338638)_(21397459_21397559)	59022
CGOV42T	chr3	g.(161987195_161988195)_(167919395_167920395)	593220
CGOV42T	chr3	g.(167922501_167923501)_(169239501_169240501)	131700
CGOV42T	chr4	g.(16343864_16343964)_(16356548_16356648)	12785
CGOV42T	chr4	g.(81209059_81209159)_(81228236_81228336)	19278
CGOV42T	chr4	g.(166772764_166772864)_(166780052_166780152)	7389
CGOV42T	chr4	g.(177955251_177956251)_(179420870_179421870)	146562
CGOV42T	chr5	g.(1489490_1489590)_(1525158_1525258)	35769
CGOV42T	chr5	g.(125109232_125109332)_(125143529_125143629)	34398
CGOV42T	chr5	g.(162048798_162048898)_(162055663_162055763)	6966
CGOV42T	chr5	g.(178348356_178348456)_(178352983_178353083)	4728
CGOV42T	chr6	g.(126839504_126839604)_(126941747_126941847)	102344
CGOV42T	chr7	g.(69834817_69834917)_(69890868_69890968)	56152
CGOV42T	chr7	g.(78035451_78035551)_(78379562_78379662)	344212
CGOV42T	chr7	g.(101724570_101724670)_(101727913_101728013)	3444
CGOV42T	chr8	g.(89828384_89828484)_(89922135_89922235)	93852
CGOV42T	chr11	g.(28184661_28184761)_(28461232_28461332)	276672
CGOV42T	chr11	g.(123866862_123866962)_(123909743_123909843)	42982
CGOV42T	chr12	g.(29316667_29316767)_(29697815_29697915)	381249
CGOV42T	chr12	g.(86426152_86426252)_(86432770_86432870)	6719
CGOV42T	chr12	g.(111976338_111976438)_(111979740_111979840)	3503

CGOV42T	chr13	g.(80681134_80681234)_(80686285_80686385)	5252
CGOV42T	chr13	g.(109949122_109949222)_(109957783_109957883)	8762
CGOV42T	chr15	g.(33986177_33986277)_(34030418_34030518)	44342
CGOV42T	chr16	g.(78262211_78262311)_(78326681_78326781)	64571
CGOV42T	chr16	g.(79015446_79015546)_(79057892_79057992)	42547
CGOV42T	chr16	g.(83566487_83566587)_(83572114_83572214)	5728
CGOV42T	chr16	g.(88895413_88895513)_(88905737_88905837)	10425
CGOV42T	chr19	g.(244501_245501)_(437501_438501)	193001
CGOV42T	chr19	g.(51467945_51468945)_(51493584_51494584)	25640
CGOV42T	chr19	g.(54356009_54356109)_(54369515_54369615)	13607
CGOV42T	chr20	g.(52285529_52285629)_(52291766_52291866)	6338
CGOV42T	chr21	g.(46057573_46057673)_(46066375_46066475)	8903
CGOV42T	chrX	g.(3703400_3703500)_(3711152_3711252)	7853
CGOV42T	chrX	g.(6501501_6502501)_(6505501_6506501)	4001
CGOV42T	chrX	g.(10390812_10390912)_(10559740_10559840)	169029
CGOV42T	chrX	g.(63700501_63701501)_(63715501_63716501)	15001
CGOV42T	chrX	g.(74663501_74664501)_(74666501_74667501)	3001
CGOV42T	chrX	g.(96006783_96006883)_(96025741_96025841)	19059
CGOV53T	chr1	g.(7975030_7975130)_(7987470_7987570)	12541
CGOV53T	chr2	g.(184794483_184794583)_(184803894_184803994)	9512
CGOV53T	chr2	g.(212274020_212274120)_(212485092_212485192)	211173
CGOV53T	chr3	g.(59763116_59763216)_(59894753_59894853)	131738
CGOV53T	chr3	g.(60477380_60477480)_(60692910_60693010)	215631
CGOV53T	chr4	g.(37925940_37926040)_(37960502_37960602)	34663
CGOV53T	chr4	g.(39704403_39704503)_(39713735_39713835)	9433
CGOV53T	chr4	g.(143066945_143067045)_(143745255_143745355)	678411
CGOV53T	chr5	g.(97047935_97048035)_(97095991_97096091)	48157
CGOV53T	chr5	g.(178348453_178348553)_(178353016_178353116)	4664
CGOV53T	chr7	g.(3863816_3863916)_(3911763_3911863)	48048
CGOV53T	chr7	g.(48581358_48581458)_(48592487_48592587)	11230
CGOV53T	chr7	g.(145997407_145997507)_(146005681_146005781)	8375
CGOV53T	chr7	g.(145997501_145998501)_(145999501_146000501)	2001
CGOV53T	chr8	g.(131253805_131253905)_(131333657_131333757)	79953
CGOV53T	chr9	g.(21714106_21714206)_(22214507_22214607)	500502
CGOV53T	chr10	g.(58513114_58513214)_(58526789_58526889)	13776
CGOV53T	chr10	g.(72599046_72599146)_(72602587_72602687)	3642
CGOV53T	chr11	g.(102303643_102303743)_(102307320_102307420)	3778

CGOV53T	chr12	g.(20808640_20808740)_(20950019_20950119)	141480
CGOV53T	chr12	g.(44456088_44456188)_(44630675_44630775)	174688
CGOV53T	chr12	g.(51376835_51376935)_(51380217_51380317)	3483
CGOV53T	chr12	g.(81711183_81711283)_(81773125_81773225)	62043
CGOV53T	chr16	g.(78686925_78687025)_(78860448_78860548)	173624
CGOV53T	chr16	g.(78779546_78779646)_(78796468_78796568)	17023
CGOV53T	chr16	g.(78811577_78812577)_(78858501_78859501)	46925
CGOV53T	chr16	g.(78812077_78812177)_(78863098_78863198)	51122
CGOV53T	chr17	g.(49079112_49079212)_(49109481_49109581)	30470
CGOV53T	chr20	g.(7398778_7398878)_(7403413_7403513)	4736
CGOV53T	chr20	g.(52647122_52647222)_(52657842_52657942)	10821
CGOV53T	chr22	g.(46516094_46516194)_(46521450_46521550)	5457
CGOV53T	chrX	g.(17167316_17167416)_(17179418_17179518)	12203
CGOV53T	chrX	g.(104368659_104368759)_(104520276_104520376)	151718
CGOV53T	chrX	g.(104368501_104369501)_(104443501_104444501)	75001
CGOV53T	chrX	g.(104443941_104444941)_(104519867_104520867)	75927
CGOV53T	chrX	g.(127626941_127627041)_(127719603_127719703)	92763
CGOV37T_3	chr1	g.(41087863_41087963)_(41221210_41221310)	133448
CGOV37T_3	chr1	g.(72755758_72755858)_(72763943_72764043)	8286
CGOV37T_3	chr1	g.(152311258_152311358)_(152351084_152351184)	39927
CGOV37T_3	chr2	g.(153795954_153796054)_(153799583_153799683)	3730
CGOV37T_3	chr3	g.(37046030_37046130)_(37185482_37185582)	139553
CGOV37T_3	chr3	g.(160680330_160680430)_(160685849_160685949)	5620
CGOV37T_3	chr3	g.(165041000_165041100)_(165083201_165083301)	42302
CGOV37T_3	chr3	g.(192776933_192777033)_(192782436_192782536)	5604
CGOV37T_3	chr4	g.(64134360_64134460)_(64154376_64154476)	20117
CGOV37T_3	chr7	g.(36037453_36037553)_(36041197_36041297)	3845
CGOV37T_3	chr7	g.(159117501_159118501)_(159127501_159128501)	10001
CGOV37T_3	chr8	g.(40182920_40183020)_(40189648_40189748)	6829
CGOV37T_3	chr8	g.(90171824_90171924)_(90277807_90277907)	106084
CGOV37T_3	chr9	g.(21968502_21968602)_(22129928_22130028)	161527
CGOV37T_3	chr10	g.(58513132_58513232)_(58526794_58526894)	13763
CGOV37T_3	chr12	g.(99041398_99041498)_(99503060_99503160)	461763
CGOV37T_3	chr14	g.(46749199_46749299)_(46770458_46770558)	21360
CGOV37T_3	chr14	g.(73526897_73526997)_(73531837_73531937)	5041

CGOV37T_3	chr17	g.(3914657_3915657)_(4208274_4209274)	293618
CGOV37T_3	chr18	g.(7920468_7920568)_(7988489_7988589)	68122
CGOV37T_3	chr18	g.(41764002_41764102)_(41776785_41776885)	12884
CGOV37T_3	chr20	g.(15726759_15726859)_(15789129_15789229)	62471
CGOV37T_3	chrX	g.(143628759_143628859)_(143637626_143637726)	8968

* Deletions were identified by segmentation of the normalized read depth. Deletions were called as hemizygous+
(Start, End) were refined based on the alignments of the rearranged read pairs. For annotation of affected coding

Table S3.1i. Predicted in-frame coding fusions*

Lab id	Cell line	Gene 5'	Gene 3'	Tx 5'
CGOV16T	OAW-42	TICAM1	PKN1	NM_182919
CGOV16T	OAW-42	HORMAD2	BAIAP2L2	NM_152510
CGOV16T	OAW-42	BAIAP2L2	HORMAD2	NM_025045
CGOV16T	OAW-42	SLC9A4	PSMD14	NM_001011552
CGOV16T	OAW-42	ACOXL	RYR3	NM_001142807
CGOV16T	OAW-42	RYR3	ACOXL	NM_001036
CGOV16T	OAW-42	ZNF619	ADAMTS9	NM_001145082
CGOV16T	OAW-42	ADAMTS9	ZNF619	NM_182920
CGOV16T	OAW-42	SLC44A1	FSD1L	NM_001286730
CGOV16T	OAW-42	FSD1L	SLC44A1	NM_001145313
CGOV16T	OAW-42	IQGAP1	PIR	NM_003870
CGOV16T	OAW-42	PIR	IQGAP1	NM_001018109
CGOV17T	OV-167	FHIT	NLGN1	NM_001166243
CGOV17T	OV-167	NLGN1	FHIT	NM_014932
CGOV17T	OV-167	INTS12	GSTCD	NM_001142471
CGOV17T	OV-167	GSTCD	INTS12	NM_024751
CGOV17T	OV-167	ADCY10	MPC2	NM_001167749
CGOV17T	OV-167	MPC2	ADCY10	NM_001143674
CGOV17T	OV-167	LMO7	TFDP1	NM_005358
CGOV17T	OV-167	TFDP1	LMO7	NM_007111
CGOV17T	OV-167	FBXL3	COL4A2	NM_012158
CGOV18T	OV177	BPIFB2	CCM2L	NM_025227

CGOV18T	OV177	GK	DMD	NM_000167
CGOV18T	OV177	DMD	GK	NM_004014
CGOV18T	OV177	VAMP8	TCF7L1	NM_003761
CGOV18T	OV177	CPAMD8	EPB41L5	NM_015692
CGOV18T	OV177	RASSF1	GNAI2	NM_170713
CGOV18T	OV177	MARCH6	ANKRD33B	NM_001270660
CGOV18T	OV177	ANKRD33B	MARCH6	NM_001164440
CGOV18T	OV177	FBXO32	ANXA13	NM_001242463
CGOV18T	OV177	NEK6	UROS	NM_001145001
CGOV18T	OV177	UROS	NEK6	NM_000375
CGOV18T	OV177	NRXN2	LRRC4B	NM_015080
CGOV18T	OV177	LRRC4B	NRXN2	NM_001080457
CGOV18T	OV177	KLC2	KDM2A	NM_001134775
CGOV18T	OV177	KDM2A	KLC2	NM_012308
CGOV18T	OV177	UVRAG	CAPN5	NM_003369
CGOV18T	OV177	CAPN5	UVRAG	NM_004055
CGOV18T	OV177	KSR2	WSB2	NM_173598
CGOV18T	OV177	WSB2	KSR2	NM_001278558
CGOV18T	OV177	PTP4A2	MYH14	NM_080391
CGOV18T	OV177	TMEM63C	SPTLC2	NM_020431
CGOV18T	OV177	SPTLC2	TMEM63C	NM_004863
CGOV18T	OV177	PCSK6	LINS	NM_001291309
CGOV18T	OV177	PDPR	VAC14	NM_017990
CGOV18T	OV177	VAC14	PDPR	NM_018052
CGOV18T	OV177	SUMO2	UBE2O	NM_001005849

CGOV18T	OV177	UBE2O	SUMO2	NM_022066
CGOV21T	OV-90	RIPK2	GPR158	NM_003821
CGOV21T	OV-90	GPR158	RIPK2	NM_020752
CGOV25T	OVCAR-3	SEMA5B	DYM	NM_001031702
CGOV25T	OVCAR-3	DYM	SEMA5B	NM_017653
CGOV25T	OVCAR-3	ENDOU	PEF1	NM_001172439
CGOV25T	OVCAR-3	TET2	GSTCD	NM_001127208
CGOV25T	OVCAR-3	MZB1	GAB2	NM_016459
CGOV25T	OVCAR-3	ANKS1A	PPARD	NM_015245
CGOV25T	OVCAR-3	PPARD	ANKS1A	NM_177435
CGOV25T	OVCAR-3	PGC	TFEB	NM_002630
CGOV25T	OVCAR-3	KCNN3	ASH1L	NM_170782
CGOV25T	OVCAR-3	ASH1L	KCNN3	NM_018489
CGOV25T	OVCAR-3	MPP7	BICD1	NM_173496
CGOV25T	OVCAR-3	BICD1	MPP7	NM_001003398
CGOV25T	OVCAR-3	ANK3	CCDC6	NM_001149
CGOV25T	OVCAR-3	NUP98	BEAN1	NM_016320
CGOV25T	OVCAR-3	BEAN1	NUP98	NM_001136106
CGOV25T	OVCAR-3	SLC1A2	LDLRAD3	NM_001195728
CGOV25T	OVCAR-3	LDLRAD3	SLC1A2	NM_001304264
CGOV25T	OVCAR-3	RBM14	PELI3	NM_001198836
CGOV25T	OVCAR-3	FCHSD2	P2RY6	NM_014824
CGOV25T	OVCAR-3	P2RY6	FCHSD2	NM_001277205
CGOV25T	OVCAR-3	PRDM10	APLP2	NM_020228
CGOV25T	OVCAR-3	APLP2	PRDM10	NM_001142276

CGOV25T	OVCAR-3	TEAD4	TSPAN9	NM_003213
CGOV25T	OVCAR-3	TSPAN9	TEAD4	NM_001168320
CGOV25T	OVCAR-3	UBALD1	UBN1	NM_145253
CGOV25T	OVCAR-3	UBN1	UBALD1	NM_001079514
CGOV25T	OVCAR-3	RASD1	LRRC75A	NM_001199989
CGOV25T	OVCAR-3	PCTP	ANKFN1	NM_021213
CGOV25T	OVCAR-3	ANKFN1	PCTP	NM_153228
CGOV25T	OVCAR-3	ZNF142	POLR1A	NM_001105537
CGOV28T	OVKATE	PHOSPHO2-KLHL23	NALCN	NM_001199290
CGOV28T	OVKATE	NALCN	PHOSPHO2-KLHL23	NM_052867
CGOV28T	OVKATE	PHOSPHO2-KLHL23	NALCN	NM_001199290
CGOV28T	OVKATE	NALCN	PHOSPHO2-KLHL23	NM_052867
CGOV28T	OVKATE	HELQ	FAM175A	NM_001297755
CGOV28T	OVKATE	FAM175A	HELQ	NM_139076
CGOV30T	OVSAHO	PDE4D	UBE2D2	NM_001165899
CGOV30T	OVSAHO	UBE2D2	PDE4D	NM_003339
CGOV30T	OVSAHO	DDX46	CATSPER3	NM_001300860
CGOV30T	OVSAHO	CATSPER3	DDX46	NM_178019
CGOV30T	OVSAHO	RNF8	GRID1	NM_003958
CGOV30T	OVSAHO	GRID1	RNF8	NM_017551
CGOV30T	OVSAHO	KIFC2	UBE2V1	NM_145754
CGOV30T	OVSAHO	UBE2V1	KIFC2	NM_001032288
CGOV30T	OVSAHO	RALGPS1	ENG	NM_001190730
CGOV30T	OVSAHO	ENG	RALGPS1	NM_001278138
CGOV30T	OVSAHO	CFAP43	CFAP58	NM_025145

CGOV30T	OVSAHO	CFAP58	CFAP43	NM_001008723
CGOV30T	OVSAHO	LGALS14	KLF12	NM_020129
CGOV30T	OVSAHO	ISM2	COX16	NM_182509
CGOV30T	OVSAHO	CSNK1G2	AP3D1	NM_001319
CGOV30T	OVSAHO	AP3D1	CSNK1G2	NM_001261826
CGOV30T	OVSAHO	GNB1L	MKL1	NM_053004
CGOV30T	OVSAHO	MKL1	HDAC10	NM_001282661
CGOV30T	OVSAHO	TUBGCP6	MKL1	NM_020461
CGOV30T	OVSAHO	ZCWPW2	RBMS3	NM_001040432
CGOV30T	OVSAHO	RBMS3	ZCWPW2	NM_001177712
CGOV32T	PEO-14	NFASC	TMCC2	NM_001005389
CGOV32T	PEO-14	TMCC2	NFASC	NM_014858
CGOV32T	PEO-14	PUM1	SDC3	NM_001020658
CGOV32T	PEO-14	GMPS	RNF180	NM_003875
CGOV32T	PEO-14	MECOM	TNIK	NM_001205194
CGOV32T	PEO-14	TNIK	MECOM	NM_001161560
CGOV32T	PEO-14	ADCY1	C7orf72	NM_021116
CGOV32T	PEO-14	C7orf72	ADCY1	NM_001161834
CGOV32T	PEO-14	UPP1	ABCA13	NM_001287426
CGOV32T	PEO-14	ABCA13	UPP1	NM_152701
CGOV32T	PEO-14	AIFM2	LRRC20	NM_001198696
CGOV32T	PEO-14	LRRC20	AIFM2	NM_001278214
CGOV32T	PEO-14	MAT1A	TSPAN14	NM_000429
CGOV32T	PEO-14	KCNC1	SAA4	NM_001112741
CGOV32T	PEO-14	SAA4	KCNC1	NM_006512

CGOV32T	PEO-14	SOX5	CCDC91	NM_001261414
CGOV32T	PEO-14	CCDC91	SOX5	NM_018318
CGOV32T	PEO-14	SOX5	CCDC91	NM_001261414
CGOV32T	PEO-14	CCDC91	SOX5	NM_018318
CGOV32T	PEO-14	GEMIN2	CTAGE5	NM_001009182
CGOV32T	PEO-14	CTAGE5	GEMIN2	NM_001247988
CGOV32T	PEO-14	KLC1	PPP1R13B	NM_182923
CGOV32T	PEO-14	PPP1R13B	KLC1	NM_015316
CGOV32T	PEO-14	ZNF106	JMJD7-PLA2G4B	NM_001284306
CGOV32T	PEO-14	UPF1	NCAN	NM_002911
CGOV32T	PEO-14	NCAN	UPF1	NM_004386
CGOV32T	PEO-14	DLGAP4	NDRG3	NM_001042486
CGOV32T	PEO-14	NDRG3	DLGAP4	NM_022477
CGOV32T	PEO-14	TOMM22	TAB1	NM_020243
CGOV32T	PEO-14	TAB1	TOMM22	NM_006116
CGOV32T	PEO-14	CAMSAP2	PPP1R12B	NM_001297707
CGOV32T	PEO-14	PPP1R12B	CAMSAP2	NM_001167857
CGOV34T	PEO-6	NFASC	USP32	NM_001005388
CGOV34T	PEO-6	USP32	NFASC	NM_032582
CGOV34T	PEO-6	ATL1	SAV1	NM_001127713
CGOV34T	PEO-6	SAV1	ATL1	NM_021818
CGOV34T	PEO-6	MLPH	PRDM12	NM_001281474
CGOV34T	PEO-6	PRDM12	MLPH	NM_021619
CGOV44T	FU-OV-1	PTPRZ1	AASS	NM_001206838
CGOV44T	FU-OV-1	AASS	PTPRZ1	NM_005763

CGOV44T	FU-OV-1	GLS2	RBMS2	NM_001280796
CGOV44T	FU-OV-1	RBMS2	GLS2	NM_002898
CGOV44T	FU-OV-1	IFNL1	ACTN4	NM_172140
CGOV44T	FU-OV-1	DEFB123	REM1	NM_153324
CGOV44T	FU-OV-1	CMTM8	CLASP2	NM_178868
CGOV44T	FU-OV-1	DOK3	ZNF527	NM_001144875
CGOV44T	FU-OV-1	ZNF527	DOK3	NM_032453
CGOV45T	COV-318	C3orf22	FBXO42	NM_152533
CGOV45T	COV-318	MAST4	CHD1	NM_198828
CGOV45T	COV-318	CHD1	MAST4	NM_001270
CGOV45T	COV-318	BSCL2	ZNF536	NM_001130702
CGOV45T	COV-318	ZNF536	BSCL2	NM_014717
CGOV46T	JHOS-2	CDK11B	KIAA2013	NM_001291345
CGOV46T	JHOS-2	KIAA2013	CDK11B	NM_138346
CGOV46T	JHOS-2	STAB1	UBE3C	NM_015136
CGOV46T	JHOS-2	UBE3C	STAB1	NM_014671
CGOV46T	JHOS-2	ARMC8	SF3B3	NM_001282342
CGOV46T	JHOS-2	SF3B3	ARMC8	NM_012426
CGOV46T	JHOS-2	NUB1	ABCF2	NM_001243351
CGOV46T	JHOS-2	THEM6	FANCI	NM_016647
CGOV46T	JHOS-2	FANCI	THEM6	NM_001113378
CGOV46T	JHOS-2	PAAF1	RBFOX3	NM_001267806
CGOV46T	JHOS-2	RBFOX3	PAAF1	NM_001082575
CGOV46T	JHOS-2	ITGA7	SARNP	NM_001144996
CGOV46T	JHOS-2	SARNP	ITGA7	NM_033082

CGOV46T	JHOS-2	DOCK9	STK24	NM_001130048
CGOV46T	JHOS-2	MBTPS1	CDH13	NM_003791
CGOV46T	JHOS-2	SCAF4	KCNE1	NM_001145444
CGOV46T	JHOS-2	KCNE1	SCAF4	NM_001270403
CGOV47T	JHOS-4	NEGR1	CNTNAP5	NM_173808
CGOV47T	JHOS-4	CNTNAP5	NEGR1	NM_130773
CGOV47T	JHOS-4	PHF3	PNISR	NM_001290259
CGOV47T	JHOS-4	PNISR	PHF3	NM_015491
CGOV47T	JHOS-4	TTF2	SGK1	NM_003594
CGOV47T	JHOS-4	SGK1	TTF2	NM_001143676
CGOV47T	JHOS-4	PFN4	ATAD2B	NM_199346
CGOV47T	JHOS-4	TMEM108	KNG1	NM_001136469
CGOV47T	JHOS-4	KNG1	TMEM108	NM_001102416
CGOV4T	DOV-13	CCL27	PHF21B	NM_006664
CGOV4T	DOV-13	POU6F1	GLTSCR2	NM_002702
CGOV4T	DOV-13	GLTSCR2	POU6F1	NM_015710
CGOV5T	EFO-21	CEMIP	RYR1	NM_001293298
CGOV5T	EFO-21	RYR1	CEMIP	NM_000540
CGOV5T	EFO-21	ZFR	KIAA0226L	NM_016107
CGOV5T	EFO-21	KIAA0226L	ZFR	NM_001286762
CGOV5T	EFO-21	HCN1	PALM2-AKAP2	NM_021072
CGOV5T	EFO-21	PALM2-AKAP2	HCN1	NM_007203
CGOV5T	EFO-21	FAM193B	B4GALT7	NM_001190946
CGOV92T	JHOS-3	NDUFAF2	ZNF366	NM_174889
CGOV92T	JHOS-3	ZNF366	NDUFAF2	NM_152625

CGOV92T	JHOS-3	ANK1	DEPTOR	NM_001142446
CGOV92T	JHOS-3	DEPTOR	ANK1	NM_001283012
CGOV92T	JHOS-3	PRKDC	SPIDR	NM_001081640
CGOV92T	JHOS-3	CASQ2	NIN	NM_001232
CGOV92T	JHOS-3	DDX21	DDX50	NM_004728
CGOV92T	JHOS-3	ERLIN1	CHUK	NM_006459
CGOV92T	JHOS-3	API5	SIK3	NM_001142930
CGOV92T	JHOS-3	CHD4	NCAPD2	NM_001297553
CGOV92T	JHOS-3	WFIKKN1	FRY	NM_053284
CGOV92T	JHOS-3	RCBTB2	CYSLTR2	NM_001268
CGOV92T	JHOS-3	CYSLTR2	RCBTB2	NM_001308465
CGOV92T	JHOS-3	NETO2	ITFG1	NM_001201477
CGOV92T	JHOS-3	ITFG1	NETO2	NM_001305002
CGOV92T	JHOS-3	TANGO6	CIRH1A	NM_024562
CGOV92T	JHOS-3	CHTF8	TANGO6	NM_001040146
CGOV92T	JHOS-3	WNK4	GNA13	NM_032387
CGOV92T	JHOS-3	LAMA3	OSBPL1A	NM_001127717
CGOV92T	JHOS-3	CAMSAP2	ASZ1	NM_001297707
CGOV92T	JHOS-3	ASZ1	CAMSAP2	NM_001301821
CGOV92T	JHOS-3	ADORA1	KDM5B	NM_000674
CGOV92T	JHOS-3	TTC28	ZNRF3	NM_001145418
CGOV92T	JHOS-3	ZNRF3	TTC28	NM_001206998
CGOV92T	JHOS-3	HORMAD2	SF3A1	NM_152510
CGOV92T	JHOS-3	CCDC157	HORMAD2	NM_001017437
CGOV92T	JHOS-3	SMYD3	ZHX3	NM_022743

CGOV92T	JHOS-3	ZHX3	SMYD3	NM_015035
CGOV12T	KOC-7C	PKLR	FAM189B	NM_181871
CGOV12T	KOC-7C	NR2E3	THSD4	NM_016346
CGOV12T	KOC-7C	C22orf39	ACOT11	NM_001166242
CGOV20T	OV207	MEGF8	MUC21	NM_001271938
CGOV20T	OV207	ATG5	TRUB2	NM_001286106
CGOV20T	OV207	COQ4	ATG5	NM_001305942
CGOV20T	OV207	STOX1	IZUMO2	NM_001130159
CGOV20T	OV207	IZUMO2	STOX1	NM_152358
CGOV20T	OV207	C10orf76	CUEDC2	NM_024541
CGOV20T	OV207	CUEDC2	C10orf76	NM_024040
CGOV20T	OV207	RPAP3	VDR	NM_001146075
CGOV20T	OV207	VDR	RPAP3	NM_000376
CGOV20T	OV207	SLC4A8	GALNT6	NM_001267615
CGOV20T	OV207	MYL6	INHBC	NM_021019
CGOV20T	OV207	INHBC	MYL6	NM_005538
CGOV20T	OV207	RUSC1	ACLY	NM_001105203
CGOV20T	OV207	ACLY	FDPS	NM_001303274
CGOV20T	OV207	ITPK1	BTBD7	NM_001142594
CGOV20T	OV207	BTBD7	ITPK1	NM_001289133
CGOV20T	OV207	LAMC1	NMNAT2	NM_002293
CGOV20T	OV207	NMNAT2	LAMC1	NM_015039
CGOV20T	OV207	MIEN1	KIAA0195	NM_032339
CGOV20T	OV207	DNTTIP1	SNX21	NM_052951
CGOV20T	OV207	SNX21	DNTTIP1	NM_001042633

CGOV20T	OV207	STK40	CFTR	NM_001282546
CGOV20T	OV207	FMNL2	FOXP1	NM_052905
CGOV20T	OV207	FOXP1	FMNL2	NM_001244816
CGOV20T	OV207	CERS6	ABCB11	NM_001256126
CGOV20T	OV207	ABCB11	CERS6	NM_003742
CGOV20T	OV207	METAP1D	SLC25A12	NM_199227
CGOV20T	OV207	DGKD	YAP1	NM_152879
CGOV20T	OV207	YAP1	DGKD	NM_001130145
CGOV20T	OV207	CCDC51	CABIN1	NM_001256964
CGOV20T	OV207	CABIN1	CCDC51	NM_001201429
CGOV20T	OV207	BTLA	TMEM175	NM_001085357
CGOV20T	OV207	SEC22A	ADCY5	NM_012430
CGOV20T	OV207	ADCY5	SEC22A	NM_001199642
CGOV20T	OV207	SMARCAD1	PDLIM5	NM_001128430
CGOV20T	OV207	PDLIM5	SMARCAD1	NM_001256425
CGOV20T	OV207	KIF2A	ADGRV1	NM_001098511
CGOV20T	OV207	ADGRV1	KIF2A	NM_032119
CGOV27T	OVISE	TNXB	CREB5	NM_019105
CGOV27T	OVISE	DLL3	BCLAF1	NM_016941
CGOV27T	OVISE	DUSP27	DIAPH3	NM_001080426
CGOV27T	OVISE	DIAPH3	DUSP27	NM_001258366
CGOV27T	OVISE	RFX3	GLIS3	NM_001282116
CGOV27T	OVISE	GLIS3	RFX3	NM_152629
CGOV27T	OVISE	MDM1	BEST3	NM_001205028
CGOV27T	OVISE	NLRP8	GP6	NM_176811

CGOV27T	OVISE	MAP1LC3A	BPIFB4	NM_032514
CGOV29T	OVMANA	PTPN7	ASH1L	NM_080588
CGOV29T	OVMANA	KAT5	RASIP1	NM_001206833
CGOV29T	OVMANA	ATXN10	ABCA7	NM_001167621
CGOV29T	OVMANA	ZNF14	EPS15L1	NM_021030
CGOV29T	OVMANA	EIF2B4	BRE	NM_172195
CGOV29T	OVMANA	BRE	SNX17	NM_001261840
CGOV29T	OVMANA	SEC14L4	HORMAD2	NM_001161368
CGOV29T	OVMANA	HERC1	RELB	NM_003922
CGOV31T	OVTOKO	ST6GALNAC4	CIZ1	NM_175039
CGOV31T	OVTOKO	RBCK1	SLC52A3	NM_006462
CGOV31T	OVTOKO	CRELD2	PIM3	NM_001135101
CGOV31T	OVTOKO	PIM3	ALG12	NM_001001852
CGOV31T	OVTOKO	NKAIN1	KDM4B	NM_024522
CGOV31T	OVTOKO	KDM4B	NKAIN1	NM_015015
CGOV35T	RMG-I	CD164L2	AHDC1	NM_207397
CGOV35T	RMG-I	KLF16	FANCD2	NM_031918
CGOV35T	RMG-I	C22orf39	ACOT11	NM_001166242
CGOV35T	RMG-I	GDA	CCDC7	NM_001242507
CGOV35T	RMG-I	CCDC7	GDA	NM_024688
CGOV35T	RMG-I	TRAF2	MYADML2	NM_021138
CGOV35T	RMG-I	MYADML2	TRAF2	NM_001145113
CGOV35T	RMG-I	RAB3IP	CNOT2	NM_022456
CGOV35T	RMG-I	CNOT2	RAB3IP	NM_014515
CGOV35T	RMG-I	COL4A1	NUMB	NM_001845

CGOV35T	RMG-I	NUMB	COL4A1	NM_001005743
CGOV35T	RMG-I	GRB7	IKZF3	NM_005310
CGOV35T	RMG-I	IKZF3	GRB7	NM_001284514
CGOV7T	ES-2	CCND1	SHANK2	NM_053056
CGOV7T	ES-2	SHANK2	CCND1	NM_133266
CGOV7T	ES-2	SHANK2	CNTN5	NM_133266
CGOV7T	ES-2	CNTN5	SHANK2	NM_001243271
CGOV7T	ES-2	SHANK2	CNTN5	NM_133266
CGOV7T	ES-2	CNTN5	SHANK2	NM_001243271
CGOV7T	ES-2	SHANK2	AAMDC	NM_133266
CGOV7T	ES-2	AAMDC	SHANK2	NM_024684
CGOV7T	ES-2	MAML2	YAP1	NM_032427
CGOV7T	ES-2	YAP1	MAML2	NM_001130145
CGOV7T	ES-2	FAM53A	CNTN5	NM_001013622
CGOV7T	ES-2	CNTN5	FAM53A	NM_001243271
CGOV7T	ES-2	CRMP1	AMOTL1	NM_001288662
CGOV7T	ES-2	AMOTL1	CRMP1	NM_001301007
CGOV7T	ES-2	CRMP1	CHKA	NM_001288662
CGOV7T	ES-2	CHKA	CRMP1	NM_001277
CGOV7T	ES-2	SORCS2	TYR	NM_020777
CGOV7T	ES-2	TYR	SORCS2	NM_000372
CGOV11T_1	KK	C3orf67	FHIT	NM_198463
CGOV11T_1	KK	FHIT	C3orf67	NM_001166243
CGOV11T_1	KK	FNDC3B	PGPEP1L	NM_022763
CGOV11T_1	KK	SST	LPP	NM_001048

CGOV11T_1	KK	TMEM219	ACSM3	NM_001083613
CGOV11T_1	KK	ERBB4	IKZF2	NM_001042599
CGOV11T_1	KK	IKZF2	ERBB4	NM_016260
CGOV11T_1	KK	USP37	MTA2	NM_020935
CGOV11T_1	KK	TUT1	USP37	NM_022830
CGOV14T	MCAS	C22orf39	ACOT11	NM_001166242
CGOV14T	MCAS	ARL4A	RAB11FIP4	NM_001037164
CGOV14T	MCAS	ISPD	TRAF4	NM_001101417
CGOV14T	MCAS	TRAF4	ISPD	NM_004295
CGOV14T	MCAS	AUTS2	GTF2IRD1	NM_001127231
CGOV14T	MCAS	GTF2IRD1	AUTS2	NM_001199207
CGOV48T	JHOM-1	ATAD2	PPHLN1	NM_014109
CGOV48T	JHOM-1	PPHLN1	ATAD2	NM_001143788
CGOV48T	JHOM-1	XRRA1	ACER3	NM_001270380
CGOV48T	JHOM-1	ACER3	XRRA1	NM_001300954
CGOV48T	JHOM-1	SLCO2B1	RAB30	NM_001145212
CGOV48T	JHOM-1	RAB30	SLCO2B1	NM_001286061
CGOV48T	JHOM-1	TMEM133	RAB30	NM_032021
CGOV48T	JHOM-1	CNTN1	ADAMTS20	NM_001256063
CGOV48T	JHOM-1	ADAMTS20	CNTN1	NM_025003
CGOV48T	JHOM-1	ADAMTS20	USP15	NM_025003
CGOV48T	JHOM-1	USP15	ADAMTS20	NM_001252079
CGOV48T	JHOM-1	SDSL	ATF7	NM_001304993
CGOV10T	IGROV-1	GTF2IRD1	GTF2I	NM_001199207
CGOV10T	IGROV-1	GTF2I	GTF2IRD1	NM_001280800

CGOV10T	IGROV-1	CALD1	AGBL3	NM_004342
CGOV10T	IGROV-1	AGBL3	CALD1	NM_178563
CGOV10T	IGROV-1	ZFYVE27	MMS19	NM_001002262
CGOV10T	IGROV-1	TWSG1	RALBP1	NM_020648
CGOV10T	IGROV-1	RALBP1	TWSG1	NM_006788
CGOV13T	Kuramochi	FAM65B	LRRC16A	NM_014722
CGOV13T	Kuramochi	LRRC16A	FAM65B	NM_001173977
CGOV13T	Kuramochi	LRP5	SORL1	NM_002335
CGOV40T	TYK-nu	KITLG	MTMR4	NM_000899
CGOV40T	TYK-nu	HSF5	KITLG	NM_001080439
CGOV40T	TYK-nu	NF1	TMEM104	NM_001128147
CGOV40T	TYK-nu	TMEM104	NF1	NM_017728
CGOV40T	TYK-nu	OSBPL5	LUZP2	NM_001144063
CGOV40T	TYK-nu	LUZP2	OSBPL5	NM_001009909
CGOV15T	OAW-28	HMG20A	LINGO1	NM_001304504
CGOV15T	OAW-28	LINGO1	HMG20A	NM_032808
CGOV15T	OAW-28	EBF4	IFNAR2	NM_001110514
CGOV15T	OAW-28	IFNAR2	EBF4	NM_000874
CGOV15T	OAW-28	ATP9A	PMEPA1	NM_006045
CGOV15T	OAW-28	PMEPA1	ATP9A	NM_001255976
CGOV15T	OAW-28	ADGRF3	OTOF	NM_153835
CGOV15T	OAW-28	OTOF	ADGRF3	NM_004802
CGOV15T	OAW-28	MAP4	CBFA2T3	NM_001134364
CGOV15T	OAW-28	CBFA2T3	MAP4	NM_005187
CGOV15T	OAW-28	MVD	NME6	NM_002461

CGOV15T	OAW-28	EPHA6	FAM19A2	NM_001080448
CGOV15T	OAW-28	FAM19A2	EPHA6	NM_178539
CGOV15T	OAW-28	RASGRF2	CCDC77	NM_006909
CGOV15T	OAW-28	CCDC77	RASGRF2	NM_001130147
CGOV15T	OAW-28	FAM26D	RWDD1	NM_001256887
CGOV15T	OAW-28	RWDD1	FAM26D	NM_001007464
CGOV15T	OAW-28	NAPEPLD	MET	NM_001122838
CGOV15T	OAW-28	MET	NAPEPLD	NM_000245
CGOV15T	OAW-28	UMOD	PLXNA4	NM_001008389
CGOV1T	A2780	RAB11FIP5	ALMS1	NM_015470
CGOV1T	A2780	C22orf39	ACOT11	NM_001166242
CGOV26T	OVCAR-5	RSRC1	NDUFAF2	NM_001271834
CGOV2T	Caov-3	ZBTB20	GAP43	NM_001164343
CGOV2T	Caov-3	GAP43	ZBTB20	NM_001130064
CGOV2T	Caov-3	KALRN	PLXNA1	NM_001024660
CGOV2T	Caov-3	GABRA4	TMUB2	NM_001204266
CGOV2T	Caov-3	TMUB2	GABRA4	NM_001076674
CGOV2T	Caov-3	CTNND2	TRIO	NM_001288715
CGOV2T	Caov-3	TRIO	CTNND2	NM_007118
CGOV2T	Caov-3	CSF1R	PDGFRB	NM_005211
CGOV2T	Caov-3	PDGFRB	CSF1R	NM_002609
CGOV2T	Caov-3	OPRM1	IPCEF1	NM_001145280
CGOV2T	Caov-3	IPCEF1	OPRM1	NM_001130699
CGOV2T	Caov-3	WIPF3	NUDCD3	NM_001080529
CGOV2T	Caov-3	NUDCD3	WIPF3	NM_015332

CGOV2T	Caov-3	GRM8	ZNF800	NM_000845
CGOV2T	Caov-3	ZNF800	GRM8	NM_176814
CGOV2T	Caov-3	DDAH1	FAM189B	NM_001134445
CGOV2T	Caov-3	GBA	DDAH1	NM_001005741
CGOV2T	Caov-3	FZD3	INTS9	NM_017412
CGOV2T	Caov-3	INTS9	FZD3	NM_001172562
CGOV2T	Caov-3	KCNB2	GSDMD	NM_004770
CGOV2T	Caov-3	GSDMD	KCNB2	NM_001166237
CGOV2T	Caov-3	RUSC2	MTUS2	NM_014806
CGOV2T	Caov-3	APBA1	MAMDC2	NM_001163
CGOV2T	Caov-3	SFXN2	WBP1L	NM_178858
CGOV2T	Caov-3	WBP1L	ARL3	NM_017787
CGOV2T	Caov-3	OR2H1	RCSD1	NM_030883
CGOV2T	Caov-3	OR4K14	HNRNPC	NM_001004712
CGOV2T	Caov-3	NOL4L	HNF4A	NM_080616
CGOV2T	Caov-3	HNF4A	NOL4L	NM_001030004
CGOV2T	Caov-3	ITM2C	CAB39	NM_001287240
CGOV2T	Caov-3	HDLBP	FARP2	NM_001243900
CGOV2T	Caov-3	FARP2	HDLBP	NM_001282983
CGOV33T	PEA2	MTFR1	NCOA2	NM_014637
CGOV33T	PEA2	SPATA13	ATP8A2	NM_001286792
CGOV33T	PEA2	ATP8A2	SPATA13	NM_016529
CGOV33T	PEA2	NUMB	RPS6KA5	NM_001005743
CGOV33T	PEA2	RPS6KA5	NUMB	NM_004755
CGOV3T	COLO-704	SLC8A2	CYTH2	NM_015063

CGOV3T	COLO-704	CYTH2	SLC8A2	NM_004228
CGOV42T	OVCAR-8	FAM160A1	FBXW7	NM_001109977
CGOV42T	OVCAR-8	FBXW7	FAM160A1	NM_033632
CGOV42T	OVCAR-8	PODXL	CHST8	NM_001018111
CGOV42T	OVCAR-8	NRXN2	SLCO2B1	NM_138734
CGOV42T	OVCAR-8	FLYWCH2	FLYWCH1	NM_001142499
CGOV42T	OVCAR-8	FLYWCH1	FLYWCH2	NM_020912
CGOV42T	OVCAR-8	KCNE5	DCX	NM_012282
CGOV53T	OVCAR-5-CisR	BLVRA	STK17A	NM_000712
CGOV53T	OVCAR-5-CisR	CUBN	TRDMT1	NM_001081
CGOV53T	OVCAR-5-CisR	TRDMT1	CUBN	NM_004412
CGOV53T	OVCAR-5-CisR	DLG2	USP25	NM_001300983
CGOV53T	OVCAR-5-CisR	USP25	DLG2	NM_001283041
CGOV53T	OVCAR-5-CisR	PEX5L	ASH2L	NM_001256750
CGOV53T	OVCAR-5-CisR	ASH2L	PEX5L	NM_001282272
CGOV37T_3	SK-OV-3	KDM3B	SIL1	NM_016604
CGOV37T_3	SK-OV-3	SIL1	KDM3B	NM_001037633
CGOV37T_3	SK-OV-3	NOTCH1	NBPF10	NM_017617
CGOV37T_3	SK-OV-3	NUDT17	RNF130	NM_001012758
CGOV37T_3	SK-OV-3	TMEM180	FAM213A	NM_024789
CGOV37T_3	SK-OV-3	AP2A2	CHID1	NM_001242837
CGOV37T_3	SK-OV-3	LOR	GATAD2B	NM_000427
CGOV37T_3	SK-OV-3	SMCO2	PPFIBP1	NM_001145010
CGOV37T_3	SK-OV-3	PPFIBP1	SMCO2	NM_001198915
CGOV37T_3	SK-OV-3	ANKS1B	SCYL2	NM_152788

CGOV37T_3	SK-OV-3	SCYL2	ANKS1B	NM_017988
CGOV37T_3	SK-OV-3	SPINT1	HIF1A	NM_003710
CGOV37T_3	SK-OV-3	LAMC1	SH2D4B	NM_002293
CGOV37T_3	SK-OV-3	SH2D4B	LAMC1	NM_207372
CGOV37T_3	SK-OV-3	RASL12	MTFMT	NM_001307930
CGOV37T_3	SK-OV-3	MLST8	TSC2	NM_001199173
CGOV37T_3	SK-OV-3	CTCF	PSKH1	NM_001191022
CGOV37T_3	SK-OV-3	PSKH1	CTCF	NM_006742
CGOV37T_3	SK-OV-3	FAM222B	MYO18A	NM_001288634
CGOV37T_3	SK-OV-3	MYO18A	FAM222B	NM_078471
CGOV37T_3	SK-OV-3	FBXL20	RFX2	NM_001184906
CGOV37T_3	SK-OV-3	CNBD2	HSF2BP	NM_001207076
CGOV37T_3	SK-OV-3	HSF2BP	CNBD2	NM_007031
CGOV37T_3	SK-OV-3	PTTG1IP	ITGB2	NM_001286822
CGOV37T_3	SK-OV-3	GRAMD4	TBC1D22A	NM_015124
CGOV37T_3	SK-OV-3	MLPH	LRRFIP1	NM_001281474
CGOV37T_3	SK-OV-3	LRRFIP1	MLPH	NM_001137550

* In-frame rearrangements were identified from rearranged read pairs and split reads.

Table S3.1k. Pathway inhibitors

Drug	Pathway inhibition	Cell line	Lab id	IC20	IC50
BMN673	PARP inhibitor	JHOS-4	CGOV47T	-8.76	-7.7
BMN673	PARP inhibitor	JHOS-3	CGOV92T	-9.07	-7.62
BMN673	PARP inhibitor	OVMANA	CGOV29T	-8.59	-6.89
BMN673	PARP inhibitor	OV177	CGOV18T	-8.14	-6.5
BMN673	PARP inhibitor	PEO-14	CGOV32T	-7.31	-5.52
BMN673	PARP inhibitor	FU-OV-1	CGOV44T	-6.9	-4.79
BMN673	PARP inhibitor	A2780	CGOV1T	-6.21	-4.42
BMN673	PARP inhibitor	TYK-nu	CGOV40T	-5.7	-4.21
BMN673	PARP inhibitor	COV-318	CGOV45T	-6.7	-4.2
BMN673	PARP inhibitor	OAW-28	CGOV15T	-5.94	-4.19
BMN673	PARP inhibitor	JHOM-1	CGOV48T	-6.45	-4.13
BMN673	PARP inhibitor	OVSAHO	CGOV30T	-7.38	-3.92
BMN673	PARP inhibitor	Caov-3	CGOV2T	-5.86	-3.54
BMN673	PARP inhibitor	JHOS-2	CGOV46T	-5.93	-3.49
BMN673	PARP inhibitor	Kuramochi	CGOV13T	-5.33	-3.32
BMN673	PARP inhibitor	OV-167	CGOV17T	-4.97	-2.46
BMN673	PARP inhibitor	OAW-42	CGOV16T	-3.98	-2.27
BMN673	PARP inhibitor	KK	CGOV11T_1	-4.71	-2.11
BMN673	PARP inhibitor	OVISE	CGOV27T	-4.61	-2.04
BMN673	PARP inhibitor	ES-2	CGOV7T	-2.97	-1.58
BMN673	PARP inhibitor	OVCAR-8	CGOV42T	-3.96	-1.3
BMN673	PARP inhibitor	OVCA-429	CGOV23T	-2.85	-0.85
BMN673	PARP inhibitor	OVCAR-5	CGOV26T	-2.16	-0.79

BMN673	PARP inhibitor	OVTOKO	CGOV31T	-3.83	-0.69
BMN673	PARP inhibitor	RMUG-S	CGOV36T	-3.28	-0.48
BMN673	PARP inhibitor	OV207	CGOV20T	-2.37	-0.21
BMN673	PARP inhibitor	OV-90	CGOV21T	-2.49	-0.16
BMN673	PARP inhibitor	DOV-13	CGOV4T	-2.18	-0.14
BMN673	PARP inhibitor	OVKATE	CGOV28T	-1.06	0
BMN673	PARP inhibitor	HEY	CGOV8T	-2.82	0.09
BMN673	PARP inhibitor	RMG-I	CGOV35T	-1.5	0.14
BMN673	PARP inhibitor	OVCAR-3	CGOV25T	-2.2	0.15
BMN673	PARP inhibitor	TOV-112D	CGOV38T	-1.24	0.2
BMN673	PARP inhibitor	EFO-21	CGOV5T	-3.09	0.21
BMN673	PARP inhibitor	MCAS	CGOV14T	-1.4	0.68
BMN673	PARP inhibitor	PEA2	CGOV33T	-1.41	0.7
BMN673	PARP inhibitor	PEO-6	CGOV34T	-2.43	0.83
GNE-493	PI3K inhibitor	A2780	CGOV1T	-3.29	-1.78
GNE-493	PI3K inhibitor	Caov-3	CGOV2T	-2.74	-1.05
GNE-493	PI3K inhibitor	COV-318	CGOV45T	-2.32	-0.99
GNE-493	PI3K inhibitor	DOV-13	CGOV4T	-2.1	-0.64
GNE-493	PI3K inhibitor	EFO-21	CGOV5T	-1.42	-0.33
GNE-493	PI3K inhibitor	ES-2	CGOV7T	-0.53	0.73
GNE-493	PI3K inhibitor	HEY	CGOV8T	-1.52	-0.1
GNE-493	PI3K inhibitor	JHOM-1	CGOV48T	-0.55	0.85
GNE-493	PI3K inhibitor	JHOS-2	CGOV46T	-0.67	0.03
GNE-493	PI3K inhibitor	JHOS-4	CGOV47T	-1.62	-0.67
GNE-493	PI3K inhibitor	KK	CGOV11T_1	-2	-0.95

GNE-493	PI3K inhibitor	Kuramochi	CGOV13T	-2.8	-1.4
GNE-493	PI3K inhibitor	MCAS	CGOV14T	-1.09	-0.64
GNE-493	PI3K inhibitor	OAW-28	CGOV15T	-0.83	0.06
GNE-493	PI3K inhibitor	OAW-42	CGOV16T	-1.43	-0.56
GNE-493	PI3K inhibitor	OV-167	CGOV17T	-2.05	-0.78
GNE-493	PI3K inhibitor	OV177	CGOV18T	-3.91	-2.63
GNE-493	PI3K inhibitor	OV207	CGOV20T	-1.78	-0.54
GNE-493	PI3K inhibitor	OV-90	CGOV21T	-1.34	-0.35
GNE-493	PI3K inhibitor	OVCA-429	CGOV23T	-0.45	0.39
GNE-493	PI3K inhibitor	OVCAR-3	CGOV25T	-1.27	-0.58
GNE-493	PI3K inhibitor	OVCAR-5	CGOV26T	-2.69	-0.23
GNE-493	PI3K inhibitor	OVCAR-8	CGOV42T	-0.27	1.06
GNE-493	PI3K inhibitor	OVISE	CGOV27T	-2.87	-2.06
GNE-493	PI3K inhibitor	OVKATE	CGOV28T	-3.85	-2.59
GNE-493	PI3K inhibitor	OVMANA	CGOV29T	-2.35	-1.28
GNE-493	PI3K inhibitor	OVSAHO	CGOV30T	-2.48	-1.37
GNE-493	PI3K inhibitor	OVTOKO	CGOV31T	-2.41	-1.54
GNE-493	PI3K inhibitor	PEA2	CGOV33T	-1.08	-0.52
GNE-493	PI3K inhibitor	PEO-14	CGOV32T	-1.65	-0.81
GNE-493	PI3K inhibitor	RMG-I	CGOV35T	-3.52	-1.92
GNE-493	PI3K inhibitor	RMUG-S	CGOV36T	-2.06	-0.59
GNE-493	PI3K inhibitor	SK-OV-3	CGOV37T_3	-1.97	-1.47
GNE-493	PI3K inhibitor	TOV-112D	CGOV38T	-1.07	0.31
GNE-493	PI3K inhibitor	TYK-nu	CGOV40T	-1.16	-0.06
MEK162	MEK inhibitor	A2780	CGOV1T	-0.72	1.59

MEK162	MEK inhibitor	Caov-3	CGOV2T	-3.02	1.82
MEK162	MEK inhibitor	DOV-13	CGOV4T	-1.15	1.97
MEK162	MEK inhibitor	EFO-21	CGOV5T	0.05	1.48
MEK162	MEK inhibitor	ES-2	CGOV7T	-2.48	-1.07
MEK162	MEK inhibitor	HEY	CGOV8T	-2.5	-0.63
MEK162	MEK inhibitor	KK	CGOV11T_1	0.33	1.55
MEK162	MEK inhibitor	Kuramochi	CGOV13T	0.27	1.93
MEK162	MEK inhibitor	MCAS	CGOV14T	-4.47	-2.33
MEK162	MEK inhibitor	OAW-28	CGOV15T	-1.69	0.33
MEK162	MEK inhibitor	OAW-42	CGOV16T	0.25	1.27
MEK162	MEK inhibitor	OV-167	CGOV17T	-4.24	-1.51
MEK162	MEK inhibitor	OV177	CGOV18T	-2.5	-0.92
MEK162	MEK inhibitor	OV207	CGOV20T	-1.23	1.56
MEK162	MEK inhibitor	OV-90	CGOV21T	-4	-2.86
MEK162	MEK inhibitor	OVCA-429	CGOV23T	-1.49	2.11
MEK162	MEK inhibitor	OVCAR-5	CGOV26T	-4.31	-0.91
MEK162	MEK inhibitor	OVISE	CGOV27T	-2.5	0.25
MEK162	MEK inhibitor	OVKATE	CGOV28T	-4.98	-3.7
MEK162	MEK inhibitor	OVMANA	CGOV29T	-5.14	-4.11
MEK162	MEK inhibitor	OVSAHO	CGOV30T	-3.7	0.44
MEK162	MEK inhibitor	OVTOKO	CGOV31T	-3.8	-1.62
MEK162	MEK inhibitor	PEA2	CGOV33T	-3.34	-1.51
MEK162	MEK inhibitor	PEO-14	CGOV32T	-1.35	1.52
MEK162	MEK inhibitor	PEO-6	CGOV34T	-3.22	-0.18
MEK162	MEK inhibitor	RMG-I	CGOV35T	-4.28	-3.19

MEK162	MEK inhibitor	RMUG-S	CGOV36T	-3.64	-2
MEK162	MEK inhibitor	TOV-112D	CGOV38T	1.84	3.76
MEK162	MEK inhibitor	TYK-nu	CGOV40T	-2.19	-0.26

Table S3.1l. Rearrangement types identified from improperly paired reads

Type	R1 strand	R2 strand	R1 position < R2 position	Inter-chromosomal
Deletion	+	-	TRUE	FALSE
Deletion	-	+	FALSE	FALSE
Amplification	+	-	TRUE	FALSE
Amplification	+	-	FALSE	FALSE
Amplification	-	+	FALSE	FALSE
Amplification	-	+	TRUE	FALSE
Translocation	+	-	NA	TRUE
Translocation	-	+	NA	TRUE
Translocation	+	-	NA	TRUE
Translocation	-	+	NA	TRUE
Inversion	+	+	TRUE	FALSE
Inversion	+	+	FALSE	FALSE
Inversion	-	-	TRUE	FALSE
Inversion	-	-	FALSE	FALSE
Inverted translocation	+	+	NA	TRUE
Inverted translocation	+	+	NA	TRUE
Inverted translocation	-	-	NA	TRUE
Inverted translocation	-	-	NA	TRUE

Table S3.1n. R package versions*

R package	Version	Source
acepack	1.4.1	CRAN (R 3.5.0)
AnnotationDbi	1.42.1	cran (@1.42.1)
AnnotationFilter	1.4.0	Bioconductor
assertthat	0.2.0	CRAN (R 3.5.0)
backports	1.1.2	CRAN (R 3.5.0)
base	3.5.0	local
base64enc	0.1-3	CRAN (R 3.5.0)
bindr	0.1.1	CRAN (R 3.5.0)
bindrcpp	0.2.2	CRAN (R 3.5.0)
Biobase	2.40.0	Bioconductor
BiocGenerics	0.26.0	Bioconductor
BiocInstaller	1.30.0	Bioconductor
BiocParallel	1.14.1	Bioconductor
biomaRt	2.36.1	Bioconductor
Biostrings	2.48.0	Bioconductor
biovizBase	1.28.0	Bioconductor
bit	1.1-14	CRAN (R 3.5.0)
bit64	0.9-7	CRAN (R 3.5.0)
bitops	1.0-6	CRAN (R 3.5.0)
blob	1.1.1	CRAN (R 3.5.0)
boot	1.3-20	CRAN (R 3.5.0)
broom	0.4.4	CRAN (R 3.5.0)
BSgenome	1.48.0	Bioconductor
cellranger	1.1.0	CRAN (R 3.5.0)
checkmate	1.8.5	CRAN (R 3.5.0)
circlize	0.4.3	CRAN (R 3.5.0)
cli	1.0.0	CRAN (R 3.5.0)
cluster	2.0.7-1	CRAN (R 3.5.0)
CNPBayes	1.11.1	local
coda	0.19-1	CRAN (R 3.5.0)
colorspace	1.3-2	CRAN (R 3.5.0)
combinat	0.0-8	CRAN (R 3.5.0)
compiler	3.5.0	local
ComplexHeatmap	1.18.0	Bioconductor (R 3.5.0)
crayon	1.3.4	CRAN (R 3.5.0)
curl	3.2	CRAN (R 3.5.0)
data.table	1.11.4	CRAN (R 3.5.0)
datasets	3.5.0	local

DBI	1.0.0	CRAN (R 3.5.0)
deconstructSigs	1.8.0	CRAN (R 3.5.0)
DelayedArray	0.6.0	Bioconductor
devtools	1.13.5	CRAN (R 3.5.0)
dichromat	2.0-0	CRAN (R 3.5.0)
digest	0.6.15	CRAN (R 3.5.0)
DNAcopy	1.54.0	Bioconductor
dplyr	0.7.5	CRAN (R 3.5.0)
ensembldb	2.4.1	Bioconductor
evaluate	0.10.1	CRAN (R 3.5.0)
forcats	0.3.0	CRAN (R 3.5.0)
foreign	0.8-70	CRAN (R 3.5.0)
Formula	1.2-3	CRAN (R 3.5.0)
GenomeInfoDb	1.16.0	Bioconductor
GenomeInfoDbData	1.1.0	Bioconductor
GenomicAlignments	1.16.0	Bioconductor
GenomicFeatures	1.32.0	Bioconductor
GenomicRanges	1.32.3	Bioconductor
GetoptLong	0.1.6	CRAN (R 3.5.0)
GGally	1.4.0	CRAN (R 3.5.0)
ggbio	1.28.0	Bioconductor
ggplot2	2.2.1	CRAN (R 3.5.0)
GlobalOptions	0.0.13	CRAN (R 3.5.0)
glue	1.2.0	CRAN (R 3.5.0)
graph	1.58.0	Bioconductor
graphics	3.5.0	local
grDevices	3.5.0	local
grid	3.5.0	local
gridExtra	2.3	CRAN (R 3.5.0)
gtable	0.2.0	CRAN (R 3.5.0)
gtools	3.5.0	CRAN (R 3.5.0)
haven	1.1.1	CRAN (R 3.5.0)
Hmisc	4.1-1	CRAN (R 3.5.0)
hms	0.4.2	CRAN (R 3.5.0)
htmlTable	1.12	CRAN (R 3.5.0)
htmltools	0.3.6	CRAN (R 3.5.0)
htmlwidgets	1.2	CRAN (R 3.5.0)
httr	1.3.1	CRAN (R 3.5.0)
integration	0.0.3	local
integration.data	0.0.1	local

IRanges	2.14.10	Bioconductor
jsonlite	1.5	CRAN (R 3.5.0)
kableExtra	0.9.0	CRAN (R 3.5.0)
knitr	1.2	CRAN (R 3.5.0)
lattice	0.20-35	CRAN (R 3.5.0)
latticeExtra	0.6-28	CRAN (R 3.5.0)
lazyeval	0.2.1	CRAN (R 3.5.0)
lubridate	1.7.4	CRAN (R 3.5.0)
magrittr	1.5	CRAN (R 3.5.0)
Matrix	1.2-14	CRAN (R 3.5.0)
matrixStats	0.53.1	CRAN (R 3.5.0)
mclust	5.4	CRAN (R 3.5.0)
memoise	1.1.0	CRAN (R 3.5.0)
methods	3.5.0	local
mnormt	1.5-5	CRAN (R 3.5.0)
modelr	0.1.2	CRAN (R 3.5.0)
munsell	0.4.3	CRAN (R 3.5.0)
naniar	0.2.0	CRAN (R 3.5.0)
nlme	3.1-137	CRAN (R 3.5.0)
nnet	7.3-12	CRAN (R 3.5.0)
OrganismDbi	1.22.0	Bioconductor
ovarian.cell.line.data	0.0.1	local
ovarian.manuscript	0.0.34	local
ovexpress	0.0.3	local
parallel	3.5.0	local
pastecs	1.3.21	CRAN (R 3.5.0)
pillar	1.2.3	CRAN (R 3.5.0)
pkgconfig	2.0.1	CRAN (R 3.5.0)
plyr	1.8.4	CRAN (R 3.5.0)
prettyunits	1.0.2	CRAN (R 3.5.0)
progress	1.1.2	CRAN (R 3.5.0)
ProtGenerics	1.12.0	Bioconductor
psych	1.8.4	CRAN (R 3.5.0)
purrr	0.2.5	cran (@0.2.5)
R6	2.2.2	CRAN (R 3.5.0)
RBGL	1.56.0	Bioconductor
RColorBrewer	1.1-2	CRAN (R 3.5.0)
Rcpp	0.12.17	CRAN (R 3.5.0)
RCurl	1.95-4.10	CRAN (R 3.5.0)
readr	1.1.1	CRAN (R 3.5.0)

readxl	1.1.0	CRAN (R 3.5.0)
rentrez	1.2.1	CRAN (R 3.5.0)
reshape	0.8.7	CRAN (R 3.5.0)
reshape2	1.4.3	CRAN (R 3.5.0)
rjson	0.2.19	CRAN (R 3.5.0)
rlang	0.2.1	CRAN (R 3.5.0)
rmarkdown	1.9	CRAN (R 3.5.0)
rpart	4.1-13	CRAN (R 3.5.0)
rprojroot	1.3-2	CRAN (R 3.5.0)
Rsamtools	1.32.0	Bioconductor
RSQLite	2.1.1	cran (@2.1.1)
rstudioapi	0.7	CRAN (R 3.5.0)
rtracklayer	1.40.3	Bioconductor
rvest	0.3.2	CRAN (R 3.5.0)
S4Vectors	0.18.2	Bioconductor
scales	0.5.0	CRAN (R 3.5.0)
shape	1.4.4	CRAN (R 3.5.0)
splines	3.5.0	local
stats	3.5.0	local
stats4	3.5.0	local
stringi	1.2.2	CRAN (R 3.5.0)
stringr	1.3.1	cran (@1.3.1)
SummarizedExperiment	1.10.1	cran (@1.10.1)
survival	2.42-3	CRAN (R 3.5.0)
svovarian	0.0.7	local
tibble	1.4.2	CRAN (R 3.5.0)
tidyr	0.8.1	CRAN (R 3.5.0)
tidyselect	0.2.4	CRAN (R 3.5.0)
tidyverse	1.2.1	CRAN (R 3.5.0)
tools	3.5.0	local
trellis	0.0.36	local
utils	3.5.0	local
VariantAnnotation	1.26.0	Bioconductor
viridisLite	0.3.0	CRAN (R 3.5.0)
visdat	0.2.3.9500	Github (njtierney/visdat@364eded)
withr	2.1.2	Github (jimhester/withr@79d7b0d)
XML	3.98-1.11	CRAN (R 3.5.0)
xml2	1.2.0	CRAN (R 3.5.0)
XVector	0.20.0	Bioconductor

zlibbioc	1.26.0	Bioconductor

* Packages were built using R 3.5.0.

CHAPTER 4:

GENOMIC LANDSCAPES OF ENDOMETRIOID AND MUCINOUS OVARIAN CANCERS

METHODS

Specimens obtained for sequencing analysis

Matched tumor and normal tissue was collected from patients at time of resection. All tumor samples analyzed had ≥20% viable tumor cell content by histopathologic assessment. Clinical data for all patients included and sample data for the tissue types assayed in this study are listed in Table S1. All samples were obtained under Institutional Review Board (IRB) approved protocols with informed consent for research use at participating institutions.

Sample preparation and next-generation sequencing

DNA was extracted from patient whole blood using a QIAamp DNA Blood Mini QIAcube Kit (Qiagen Valencia, CA). Genomic DNA from FFPE blocks was extracted from the microdissected tissues using the QIAamp DNA FFPE Tissue kit (Qiagen, Valencia, CA). In brief, the samples were incubated in proteinase K for 16 hours before DNA extraction. The digested mixture was transferred to a microtube for DNA fragmentation using the truXTRAC™ FFPE DNA Kit with 10 min shearing time as per the manufacturer's instructions (Covaris, Woburn, MA). Following fragmentation, the sample was further digested for 24 hours followed by one hour incubation at 80ºC. DNA purification was performed using the QIAamp DNA FFPE Tissue kit following the manufacturer's instructions (Qiagen, Valencia, CA). Fragmented genomic DNA from tumor and normal samples were used for Illumina TruSeq library construction (Illumina, San Diego, CA) according to the manufacturer's instructions or as previously described[111]. Exonic or targeted regions were captured in solution using the Agilent SureSelect v.4 kit or a custom targeted panel according to the manufacturer's instructions (Agilent, Santa Clara, CA). Paired-end sequencing, resulting in 100 bases from each end of the fragments for exome libraries and 150 bases from each

end of the fragment for targeted libraries, was performed using Illumina HiSeq 2000/2500 and Illumina MiSeq instrumentation (Illumina, San Diego, CA).

Next generation sequencing data and identification of somatic mutations

Somatic mutations were identified using VariantDx45 custom software for identifying mutations in matched tumor and normal samples. Prior to mutation calling, primary processing of sequence data for both tumor and normal samples were performed using Illumina CASAVA software (v1.8), including masking of adapter sequences. Sequence reads were aligned against the human reference genome (version hg18 or hg19) using ELAND. Candidate somatic mutations, consisting of point mutations, insertions, and deletions were then identified using VariantDx across the either the whole exome or regions of interest44. For samples analyzed using targeted sequencing, we identified candidate mutations that were altered in >10% of distinct reads. For samples analyzed using whole exome sequencing, we identified candidate mutations that were altered in >10% of distinct reads with ≥5 altered reads in at least one sample, where coverage at the altered base was at least as high as the TP53 alteration in that sample, and where the ratio of the coverage of the mutated base to the overall sequence coverage of that sample was >20%. Identified mutations were reported as present in other samples of the same patient if the mutation was present in at least 2 distinct altered reads. Mutations present in polyN tract ≥ 5 bases, or those with an average distinct coverage below 50x were removed from the analysis.

An analysis of each candidate mutated region was performed using BLAT. For each mutation, 101 bases including 50 bases 5' and 3' flanking the mutated base was used as query sequence (http://genome.ucsc.edu/cgi-bin/hgBlat). Candidate mutations were removed from further analysis, if the analyzed region resulted in >1 BLAT hits with 90% identity over 70 SCORE

sequence length. All candidate alterations were examined by visual inspection, and any alteration present.

Structural variant analysis from whole genome sequencing data

Structural variants were identified by modifying the trellis approach [53] for use with tumor samples with a matched normal sample available and integrating tumor purity and ploidy from FACETS.

Tumor purity and ploidy estimation

Tumor purity and ploidy were jointly estimated from each of 41 tumor-normal pairs using FACETS. These metrics were unable to be determined for four samples (PGDX3309T_WGS_Ex, PGDX4495T_WGS, PGDX4500T2_WGS, PGDX4500T3_WGS) which were further excluded from CNV analyses.

Generation of Segmented Log2 Ratios

GC-adjusted log2 ratios were obtained as previously described in both tumor samples and normal samples. To remove technical biases and germline alterations, log2 ratios from matched normal samples were subtracted from log2 ratios in tumor samples. To identify genomic segments harboring abnormal copy number, the normalized log2 ratios were segmented using the circular binary segmentation method implemented in the R package and excluded from any structural variant analyses (PGDX3302T_WGS_Ex, PGDX3303T_WGS_Ex, PGDX3308T_WGS_Ex, CGOV365T).

Generation of Integer Copy Number Estimates

The log2 ratio (R) for a segment i from a sample that is a mixture of normal and cancer cells are given by the following equation:

$$R_i = log_2\left(\frac{Ct_i \times p + Cn_i \times (1-p)}{Pt \times p + Pn \times (1-p)}\right)$$

Where p is the tumor purity, Ct_i is the number of copies of segment *i* in the tumor cells, Cn_i is the number of copies of segment *i* in the normal cells, Pt is the average ploidy of the tumor cells, and Pn is the average ploidy of the normal cells. Log2 ratios were converted to integer copy numbers for each genomic segment by solving the following equation for *Ct* and rounding to the nearest integer.

Somatic Deletions

The deletion analysis was restricted to segments less than 3 Mb where the integer copy number was either 0 or 1. At least 2 improper read pairs supporting the deletion were required to call a deletion hemizygous+ or homozygous+.

Somatic Amplifications

Using the trellis approach, amplicons were seeded with high-copy focal amplifications of greater than three times the average ploidy of the sample. Low copy gains with a copy number of greater than 1.5 times the average ploidy of the sample were linked to the seed if at least 2 read pairs supporting linking.

Somatic Copy-Neutral Intra—and Inter-chromosomal Translocations and Inversions

Somatic rearrangements were identified as previously described for each tumor sample and its matched normal sample. At least 2 improper read pairs and at least 1 split read was required to call a rearrangement. Rearrangements in tumor samples that overlapped any rearrangement identified in their matched normal samples were excluded.

In-Frame Gene Fusions

In-frame gene fusions were identified as previously described. Fusions where the left and right fusion partner were in the same gene, and also fusions where none of the exons in the three prime gene were predicted to be in the fusion protein were excluded.

Methylation Analysis

We pre-processed and normalized raw IDAT files from the Infinium MethylationEPIC array using the funnorm function in the R package minfi[69]. Probes on chomosomes X or Y, probes with detection p value greater than 0.5, or probes overlapping a SNP with dbSNP minor allele frequency greater than 10% were excluded.

Unsupervised hierarchical clustering of the 1000 probes with the highest variance in the normal samples was performed. Next we performed penalized least squares logistic regression (PLR) with leave-one-out-cross-validation that identified five methylation sites predictive of normal ovarian or GI tissue type (area under receiver operator characteristic curve). We implemented the same leave-one-out resampling scheme to cross-validate the PLR model in the cancer samples, but restricted the training set to the five methylation sites that separated the tumor ovarian and GI tissues. We next performed this same analysis on the normal samples.

Signature Analysis

Signature analysis was performed using the deconstructSigs package in R.

RESULTS

Overall approach

A total of 130 ovarian endometrioid, uterine endometrioid, ovarian mucinous, and GI mucinous tumors and matching normal tissues were collected from patients of four institutions in the US and Japan. A total of 13 ovarian or GI mucinous tumor samples had tumor cellularity below 20% and were excluded from further analyses. We performed genomic analyses of these matched tumor and normal samples to identify sequence, structural and epigenetic changes (Figure 4.1). All samples were analyzed by whole exome analyses (WES), and for the subset of cases where frozen tumors were available, we performed whole genome sequencing (WGS). Overall, we analyzed 84 tumors using WES and 33 tumors using WGS. The average coverage for WES and WGS was 221X per and 56X per sample, respectively (Table S4.2). We assessed substitutions, small insertions and deletions as well as copy number changes in samples with WES while samples with WGS were evaluated for these changes as well as for rearrangements, linked amplicons and gene fusions. Copy number analyses identifying both focal amplifications, deletions, as well as chromosomal gains and losses were performed for WES using Facets and for WGS using our recently developed Trellis approach [53,112]. We also used Trellis to evaluate linked amplicons that may be derived from an amplification of a single target gene that is connected to multiple different regions of the genome [53,74,76,77].

Ovarian endometrioid and uterine endometrioid cancers

We employed a highly sensitive mutation analysis to identify somatic alterations in ovarian endometrioid (n=36) and uterine endometrial (n=15) cancers. Consistent with previous analyses, we observed a bimodal distribution of the number of mutations for uterine endometrioid cancers, with nearly half of the 15 tumors analyzed having more than 500 mutations per exome [47]

(Supplementary Figure 4.1). In contrast, the probability of a hypermutator defect for ovarian endometrioid cancers was much lower, with only one patient out of 36 above this threshold. Evaluation of the altered genes in ovarian endometrioid and uterine endometrioid cancers revealed similar affected pathways (Figure 4.2). Mutations involving chromatin regulating genes, and PI3K and RAS pathways were common in both tumor types. The proportion of patients with alterations in the *PTEN, PIK3CA, KRAS, PIK3R1, NF1,* and *ARID1A* genes were similar among these two cancer types and consistent with previous studies [113,114]. We also observed mutations in *TP53* and *CTNNB1* in ovarian endometrioid tumors as well as in uterine endometrioid cancers as has been previously described [115].

We identified several mutations in driver genes among patients with ovarian endometrioid cancer that have not been previously reported, including the homologous recombination *RAD51C* gene, the Notch signaling genes, *NOTCH4* and *NOTCH1*, the chromatin remodeling genes *SMARCA4* and *SMARCA1,* the *E2F1* transcription factor, the *RET* receptor tyrosine kinase, and the *ABL1* kinase.

Surprisingly, we found that two of the eight non-hypermutator uterine endometrioid cancers had an identical *ESR1* hotspot mutation at Tyr537 (Y537C and Y537N) (Supplementary Figure 4.2). This hotspot has been reported in patients with breast cancer that have become resistant to tamoxifen or aromatase inhibitor therapy [116,117]. Although none of the patients in this study had been treated with these inhibitors, it is intriguing that these two women were over the age of 60 and had experienced menopause, resulting in an estrogen-free environment that may be similar to anti-estrogen therapy.

To understand the role of mutations in these ovarian cancer subtypes in the context of mutational signatures [118], we evaluated the types of mutations and linked these to mutational processes that

include exogenous or endogenous mutagen exposure, enzymatic modification of DNA, and defective DNA repair (Supplemental Figure 4.3A). As expected, we found that the age-related mutation signature, Signature 1, was present in all samples, and also identified Signatures 6 or Signature 15 in patients with hypermutator defects.

We assessed both WES and WGS information for focal amplifications. For WGS data, we examined the read-pair information to pinpoint the presence of amplicons that may be linked gnomically using the Trellis approach [53] (Figure 4.3A). In addition to sequence alterations in *KRAS*, we found amplification of this gene in ovarian endometrioid cancer CGOV61T (Figure 4.2 and 4.3A). *KRAS* has been known to be amplified in ovarian endometrioid and HGSOC [119] and has been associated with an aggressive phenotype of metastatic uterine endometrial cancer [120]. We also identified linked amplification events involving *MYC* and *JAK1* (Figure 4.3). *MYC* amplification has previously been observed in a variety of ovarian cancers including endometrioid [121]. While *JAK1* amplification has been observed in triple negative breast cancer [122], this gene has not been previously been reported to be amplified in ovarian endometrioid cancers.

We evaluated whole exome and genome sequence data for homozygous deletions and identified losses of the following genes that have been known to be altered in ovarian endometrioid cancers: *PTEN, NF1, GNAS, ARID1A, CCND1, BRCA1, RAD51C, PMS2, RET, ALK, SMAD3, TP53* and *ESR1*. Additionally, we identified deletions in *TSC2* and *STK11* that have not been previously reported in endometrioid ovarian cancer. *TSC2* deletions have been seen in high grade serous ovarian cancer [123] and mutations in *TSC2* have been associated with increased sensitivity to rapamycin-induced apoptosis, making *TSC2* a potentially targetable biomarker [94]. Germline *STK11* inactivating mutations have been associated with Peutz-Jeghers syndrome, and somatic changes in this gene have been reported in a variety of carcinomas including non-small cell lung carcinoma,

cervical cancer, colorectal cancer, melanoma, and pancreatic cancer with predominantly truncating mutations, but have not yet been reported in endometrioid ovarian cancer [124].

For samples with available WGS, we also used Trellis to identify rearrangements and fusions (Supplementary Figure 4.4). These analyses revealed several novel rearrangements that were predicted to result in in-frame protein fusions in ovarian endometrioid cancers (examples in Figure 4.3B). *ATAD2-PTEN* was found in a patient with ovarian endometrioid cancer, CGOV172T. Interestingly, this rearrangement was associated with homozygous deletion of a portion of *PTEN* in this tumor. Rearrangements of *PTEN* associated with deletions have not been previously reported in ovarian endometrioid tumors and *PTEN* loss in the ovarian surface epithelium has been shown to induce papillary serous ovarian cancer[123]. Fusions involving the neurofibromin genes NF1 and NF2 (*NF1-RAB11FIP4* and *UBXN6-NF2*) were identified in ovarian endometrioid cancer CGOV161T. Although rearrangements involving NF1 and NF2 have been reported in other cancers [53] and have been associated with therapeutic resistance in HGSOC [125], rearrangements of these genes have not been previously identified in this ovarian cancer subtype. We identified a novel fusion of *PPM1E-RAD51C* in patient CGOV172T with ovarian endometrioid cancer. Although the function of this rearrangement is unknown, germline alterations of *RAD41C* have been shown to increase the risk of breast and ovarian cancer[126,127]. Fusions of *IPO11-CDK7* and *PLK5-TCF3* were detected in two different tumors. *CDK7* is a member of the cyclin-dependent kinas family and involved in cell cycle progression and CDK7 inhibitors have been shown to exert broad cytotoxicity against ovarian tumors [128]. As the *IPO11* gene, involved in nuclear protein import, is expressed in both ovarian and endometrial cells, the fusion of *IPO11-CDK7* may lead *CDK7* to constitutively activated, promoting cell cycle progression and tumor growth. The polo like kinase 5 gene (*PLK5*) has been reported to be altered in glioblastoma [129] and along with other members of the PLK family may normally play a role in cell division and centriole duplication [130]. Increasing evidence suggests that aberrant expression of PLKs may affect cell division and play a

role in genomic instability [131,132] and may therefore be a useful target of therapeutic intervention [133].

Ovarian mucinous and GI mucinous tumors

We analyzed a total of 36 patients with ovarian mucinous carcinoma and with 14 colorectal mucinous cancers. Using a threshold of 500 mutations per exome, we identified two hypermutated tumors, including a mucinous colorectal tumor with a mutation in *POLE* (1/14) that had over 12,000 mutations per exome, and one ovarian mucinous tumor (1/36) with nearly 900 mutations (Figure 4). The hotspot somatic mutation observed in *POLE* occurred in the exonuclease domain of encoded protein and has been reported in a small subset of microsatellite-stable and hypermutated colorectal carcinomas, affecting the proofreading activity of the enzyme during DNA replication [134].

Of the genes known to be altered though sequence changes in ovarian and colorectal mucinous tumors, we found alterations at similar frequencies in *KRAS*, *PIK3CA*, *RNF43, SMAD4, GNAS* and *TP53*. We identified several genes to be known mutated in ovarian mucinous cancers including *ERBB2, ARID1A, CCND1, CTNNB1, EGFR, CREBBP,* and *ATM* [36,52,135,136]. We also identified mutations in the chromatin modifier gene *SMARCA4* that had not been previously reported in ovarian mucinous cancers. None of these genes were found to be altered in colorectal mucinous cancers other than in the *POLE* mutant tumor. In addition to the age-related mutation Signature 1 which we found in nearly half in ovarian and GI mucinous cancers, we identified a signature associated with failure of DNA double-strand break-repair by homologous recombination Signature 3, which has been previously reported in breast, ovarian, and pancreatic cancers[118] (Supplemental Figure 4.3B).

Analyses of focal copy number changes revealed amplifications of *CCND1* and *ERBB2*, and homozygous deletions of *CDK2A/B* in mucinous ovarian cancers, a finding consistent with a previous studies [53,137-139]. Amplification of *ERBB2* was observed in six of the 36 ovarian mucinous cancers, and provides a potentially useful target for trastuzumab therapy [140]. *CDKN2A* deletions were observed in six cases, and an additional eight tumors had sequence alterations in this gene [138]. None of the colorectal mucinous tumors had copy number changes alterations in *ERBB2*, *CCND1* or *CDKN2A/B*.

Interestingly, homozygous deletions of *NF1* were present in both ovarian and colorectal mucinous tumors. In addition, we identified a novel rearrangement resulting in the likely inactivation of *NF1* (*NF1-RAD51D)* in one ovarian mucinous cancer. Inactivating alterations of *NF1* has been shown to lead to RAS overactivity in HGSOC [12]. Although the role of *RAD51D* is unclear in this context, it has been reported that germline *RAD51D* carriers are likely to develop ovarian tumors at an early age [141]. We also identified a novel *MED1-STAT5B* rearrangement in the same ovarian mucinous tumor. *MED1* alterations have been implicated in bladder and breast cancers and may be a potential target for treatment in endocrine resistant breast cancer [142,143].

Integrative analyses

To facilitate comparisons of the molecular alterations between the different tumor types, we integrated the sequence and structural changes at the gene level and organized these genes by biologically relevant pathways including Ras, PI3K, BRCA, WNT, chromatin regulating, cell cycle, TK receptors, DNA repair, and TGFBR (Figures 4.2 and 4.4). Genes observed to be commonly altered through this integrative analysis of sequence mutations, amplifications and deletions included *CDKN2A, ERBB2, CCND1, EGFR, PTEN, KRAS, NF1, ARID1A, BRCA1*, and *TP53*. For example, we found changes in cell cycle genes in in 14/36 (38%) samples of ovarian

mucinous when combining mutations and deletions in *CDKN2A* and amplifications of *CCND1*. Likewise, combined analyses of the RAS pathway, including TK receptors, identified alterations in 30 of 36 (83%) of these tumors.

To assess whether cancer subtypes had differences in the molecular alterations that commonly arise in the development of these cancers, we implemented a Bayesian model averaging approach for feature selection using a logit link function[102]. This approach searches the space of 2^{11} and 2^{17}, respectively for the endometrioid and mucinous models, possible single- and multi-variate models using Markov Chain Monte Carlo, allowing for the simultaneous selection of features (genes) and estimation of effect size. Posterior summaries available from these models include the probability that the regression coefficient is non-zero (the proportion of models evaluated by MCMC that included the gene) and the posterior median and 90% credible interval of the odds ratio. For the ovarian endometrioid and uterine endometrioid subtypes, we did not find statistically significant differences in the genes/pathways that were altered in these cancers (Figure 4.5A). However, for the ovarian and GI mucinous cancers, we found that *CDKN2A* were more commonly altered in the ovarian mucinous tumors (Figure 5B). These analyses revealed statistically significant differences between the number of alterations among the cell cycle and TK receptor pathways, and suggested that ovarian mucinous and GI mucinous tumors may evolve differently.

Methylation Analyses

Given the mutational differences observed, we hypothesized that ovarian and GI mucinous cancers may also be epigenetically distinct. To evaluate this possibility, we performed genome-wide methylation analyses of the GI and mucinous cancers as well as their matched normal tissues using Infinium MethylationEPIC arrays that interrogated more than 850,000 CpG cites. Methylation levels were evaluated for a subset of 25 mucinous tumor samples and matched normal samples with

sufficient material at individual CpG sites within gene promoter regions (±1500 bp upstream of the transcription start site) or within individual genes. After normalization, we estimated the proportion of methylated CpG sites as the fraction of CpG probes with Beta > 0.3. Overall methylation was higher among normal samples and more variable in cancer (Supplemental Figure 3).

Unsupervised hierarchical clustering of the 1000 probes with the highest variance in the normal samples revealed a clear separation of the normal ovarian and GI tissues (Figure 4.6A) that was present but less pronounced in the cancer tissues (Figure 4.6B). Penalized least squares logistic regression (PLR) with leave-one-out-cross-validation identified five methylation sites predictive of normal ovarian or GI tissue type (area under receiver operator characteristic curve). Given the large range of tumor purity of the biopsied cancers (20-80%), we hypothesized that these methylation sites would not be predictive of the histopathological diagnosis if the tumors shared the same tissue of origin. To evaluate this hypothesis, we implemented the same leave-one-out resampling scheme to cross-validate the PLR model in the cancer samples, but restricted the training set to the five methylation sites that separated the tumor ovarian and GI tissues(Figure 4.6C). Applied to the mucinous cancers, the tumor-specific tissue methylation sites predicted the histopathological cancer diagnosis with a sensitivity of 100% at a specificity of 100% (AUC 1.0, 95% CI: 0.86-1.0). Additionally, we used the same leave-one-out resampling scheme to cross validate the PLR model among the cancer samples, but restricted the training set to five methylation sites that separated the normal ovarian and GI tissues. Applied to the mucinous cancers, the tissue-specific methylation sites predicted the histopathological cancer diagnosis with a sensitivity of 83% at a specificity of 77% (AUC 0.8, 95% CI : 0.59-0.93), indicating that these cancers likely have a distinct tissue of origin (Figure 4.6D). We found no relationship between tumor purity and the classifier performance, suggesting that our approach was robust to normal contamination.

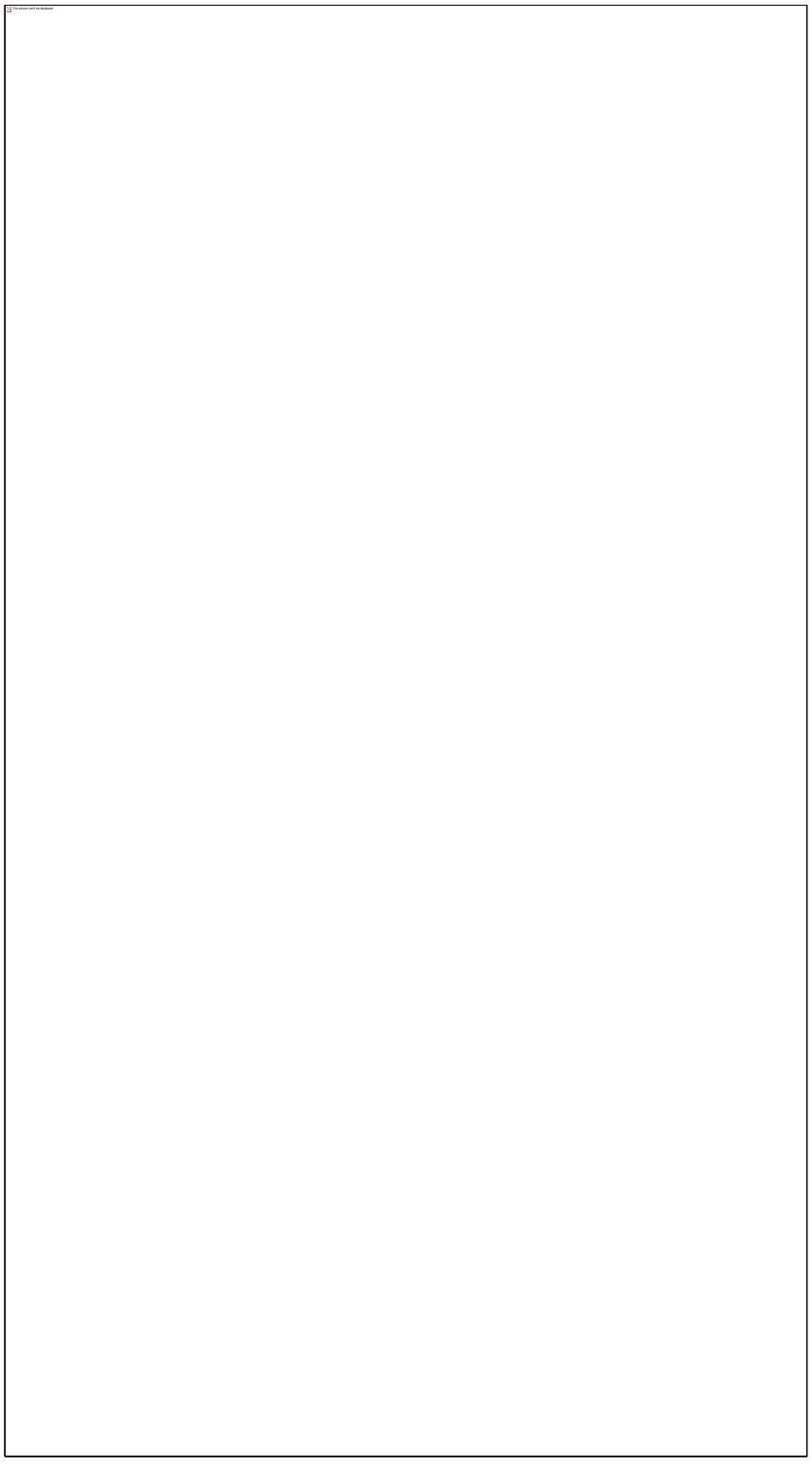

Figure 4.1. Overview of genomic analyses
We performed genomic analyses of these matched tumor and normal samples to identify sequence, structural and epigenetic changes

Figure 4.2. Integrated genomic and epigenomic analyses of ovarian endometrioid and uterine endometrial cancers

Integrated somatic point mutations, structural variants including linked amplicons, deletions and rearrangements ordered by pathway. Panels within each tile plot starting from the top represent tumor purity, number of each type of alteration, the panel of alterations present in each sample color coded based on type and finally the mutation spectra.

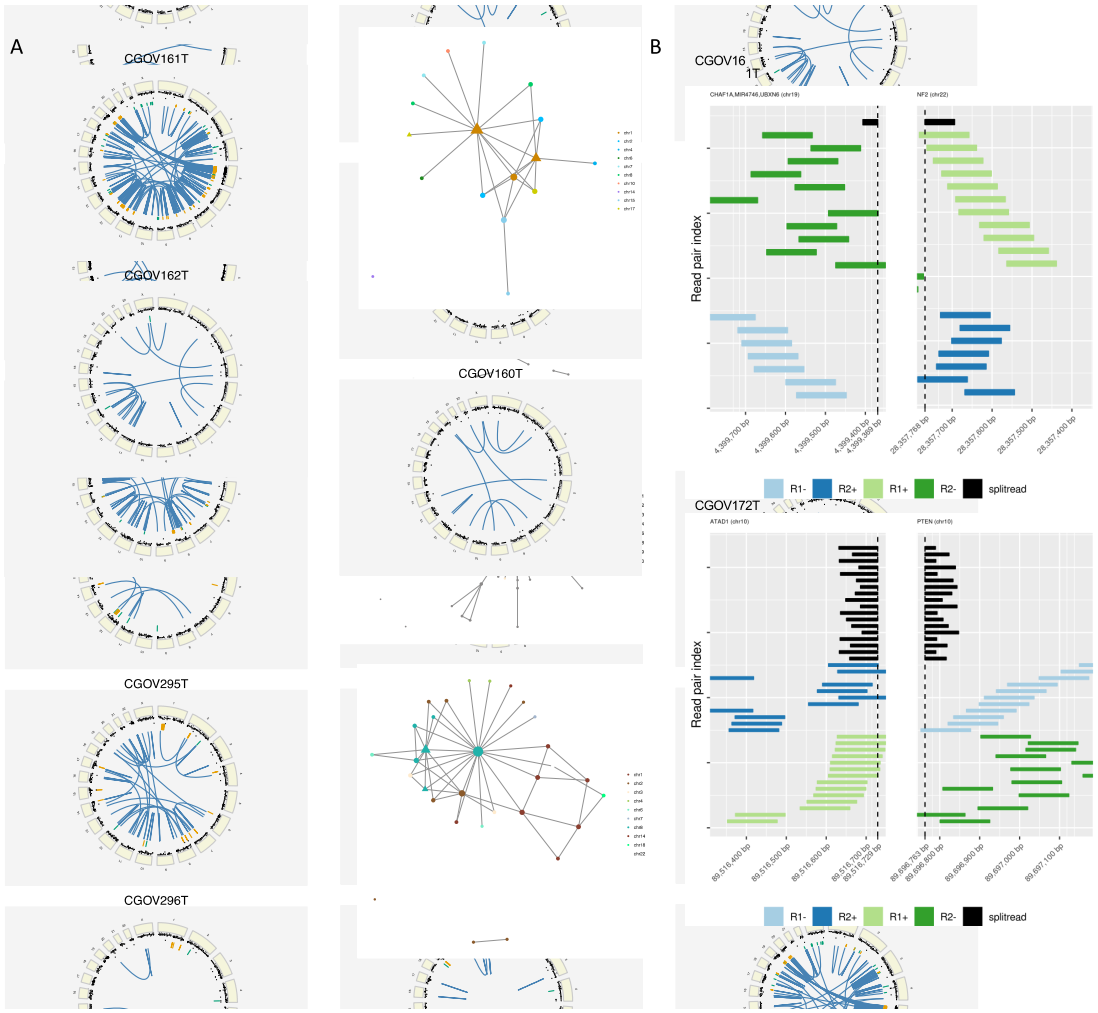

Figure 4.3. Whole genome analyses of linked amplicons and rearrangements

A) Circos plots for three tumor samples with >100 structural variants(left) each contained linked amplicons(right) with focal amplifications of known driver genes indicated by triangles. Circos plots of 19 tumor samples with few structual variants. Circos plots depict copy number alterations as well as intra- and inter-chromosomal rearrangements. Segmented normalized estimates of read depth were used to identify candidate focal amplifications in yellow and focal deletions in green. Rearranged read pairs and split reads were used to identify inter- and intra-chromosomal rearrangements in blue. For these amplicon graphs nodes represent genes, node size represents number of times the segment is represented in the genome, color indicates the chromosome the segment is located on and edges represent how the segments are connected in the genome. B) Reads aligned to the fusion junction of two representative rearrangements. Split reads, that span the fusion junction in black, and read pairs, that reside on either side of the junction in green and blue, give evidence for identifiying such rearrangements.

Figure 4.4. Integrated genomic analyses of ovarian and colorectal mucinous cancers

Integrated somatic point mutations, structural variants including linked amplicons, deletions and rearrangements ordered by pathway. Panels within each tile plot starting from the top represent tumor purity, number of each type of alteration, the panel of alterations present in each sample color coded based on type and finally the mutation spectra.

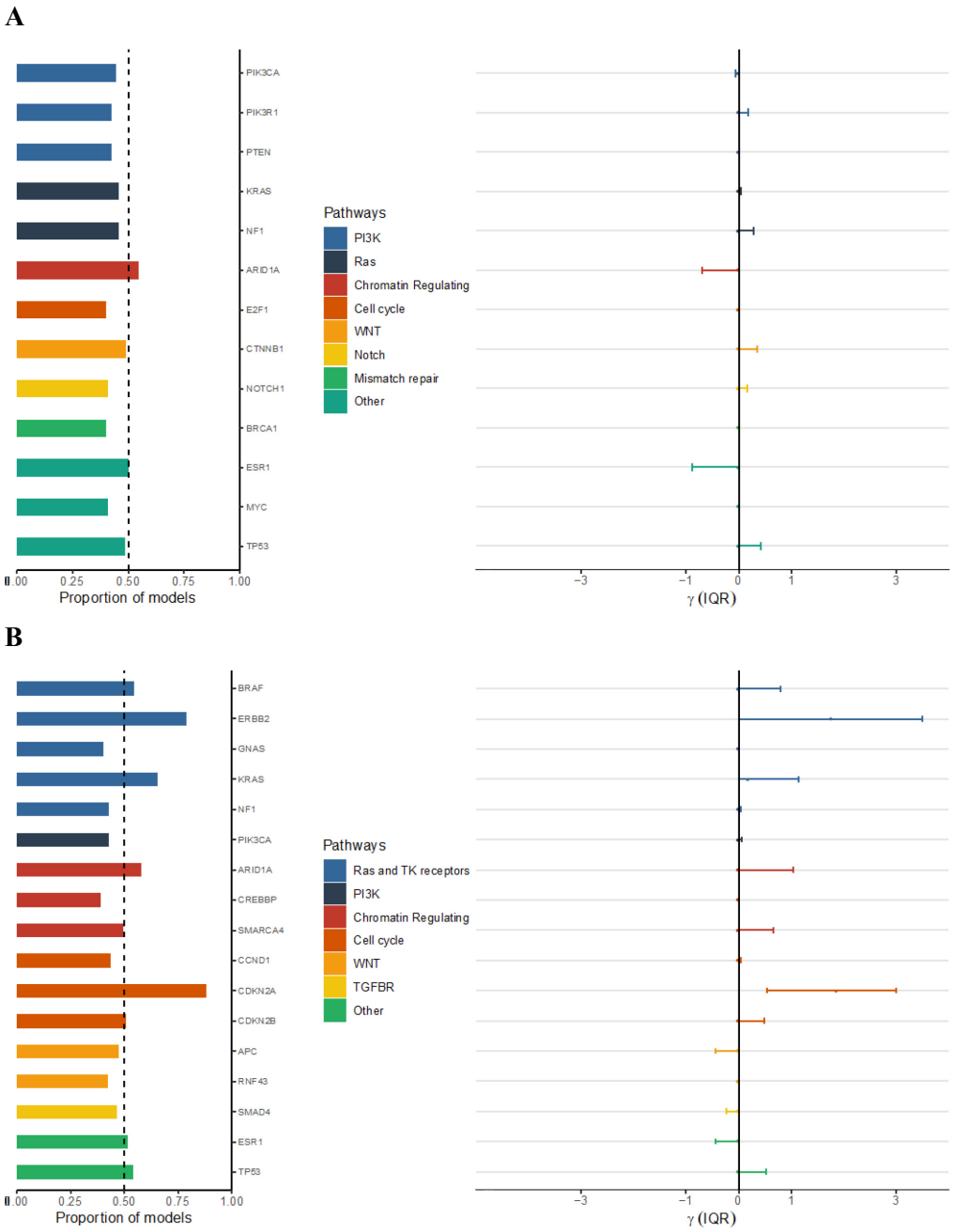

Figure 4.5. Prevalence of alterations in related tumor types.

Bayesian model averaging was used to identify alterations involving known drivers associated with ovarian and uterine endometrioid tumors(A) or ovarian and GI mucinous tumors (B). The probability that the gene coefficient (γ) in these models is non-zero is indicated by a bar graph (left). The inter-quartile range (IQR) for the difference in log odds of the regression coefficient is indicated by error bars (right). The odds of a mutation in ERBB2 and CDKN2A were higher among patients with GI mucinous cancers compared to patients with ovarian mucinous cancers.

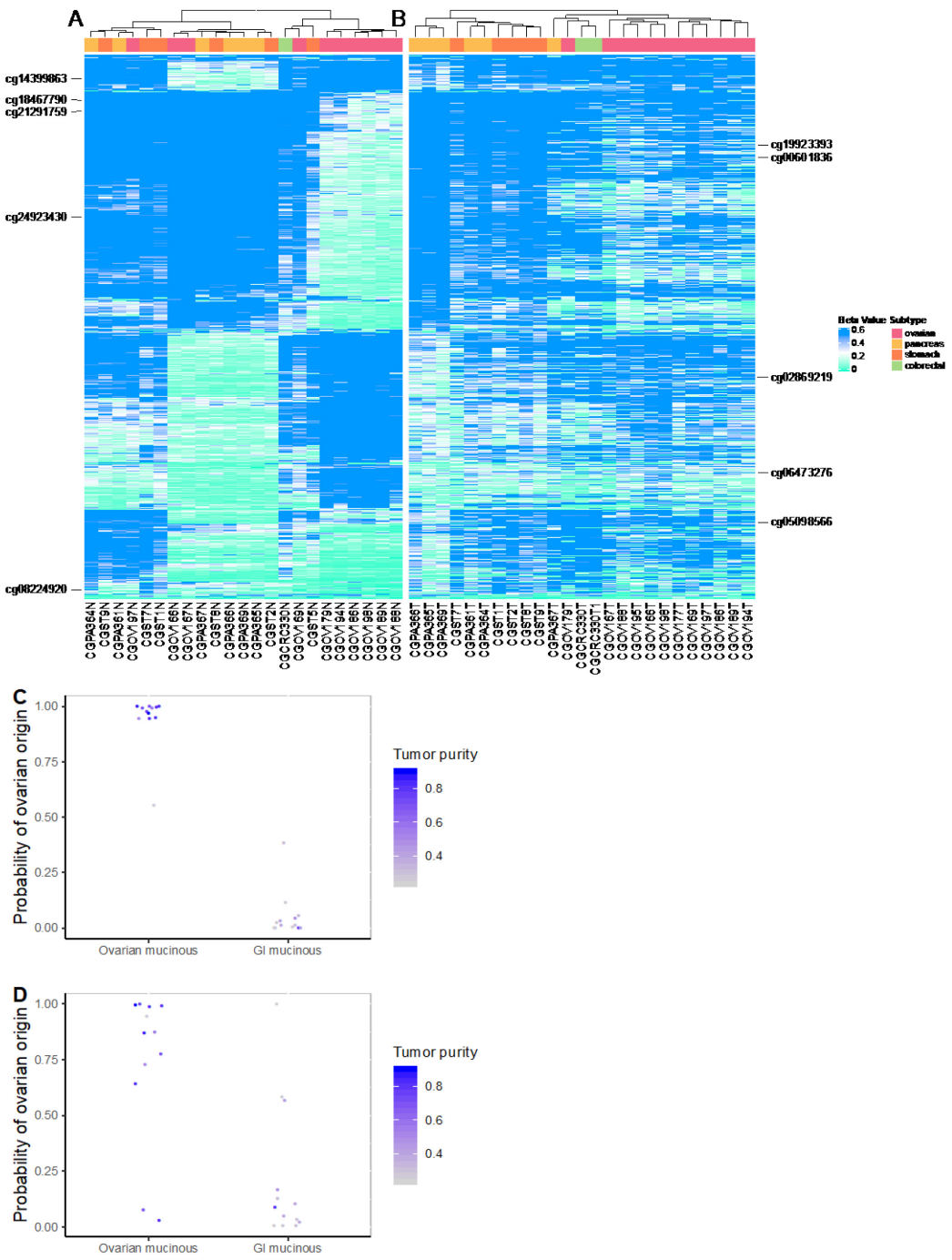

Figure 4.6. Methylation analyses of ovarian and GI mucinous tumors

1000 most variable probes among normal samples. A) Normal ovarian and GI tissues separate roughly based on the most variable porbes. B) Ovarian and GI mucinous tumor separate and resemble their normal counterparts more than each other and also segregate with the top 1000 most variable probes. C) Visualization of logistic regression modeling for each tumor sample correctly separating the mucinous tumors by tissue of origin as trained on the tumor samples. D) Visualization of logistic regression modeling for each tumor sample correctly separating the mucinous tumors by tissue of origin as trained on the normal tissue samples.

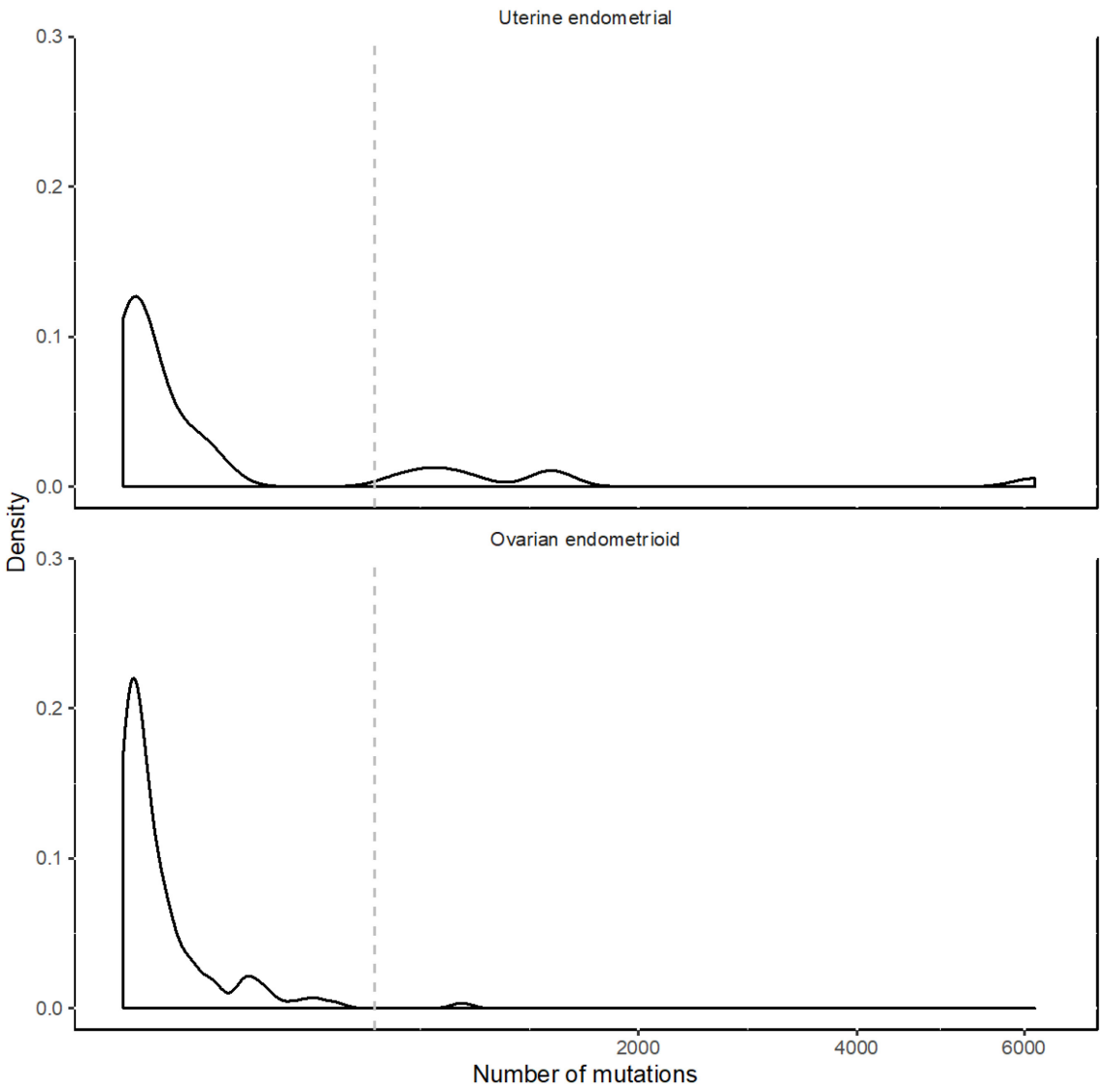

Supplemental Figure 4.1. Distribution number of mutations within the endometrioid samples Count of samples represented in the bar graph either uterine endometrial (blue) or ovarian endometrioid (red) with density curve as a black line and the cut off of hypermutators at 500 mutations on a square-root scale.

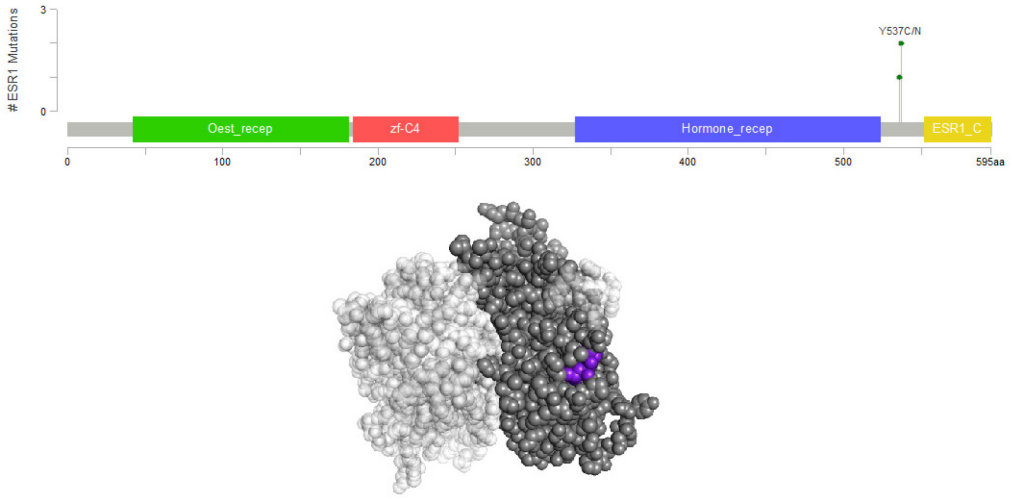

Supplemental Figure 4.2. ESR1 Y537R mutations

ESR1 mutations found in three uterine endometrioid cancer patients at Tyr357 hotspot most commonly associated with aromatase inhibitor resistance in breast cancer patients. This hotspot is located in close proximinty to the region of the estrogen receptor that is important for ligand-dependent transcriptional function. The Tyr537 mutations cause a conformational change that constitutively activates the receptor independent of ER binding. Below is the conformational structure of ESR1 with Tyr537 highlighted in purple.

A

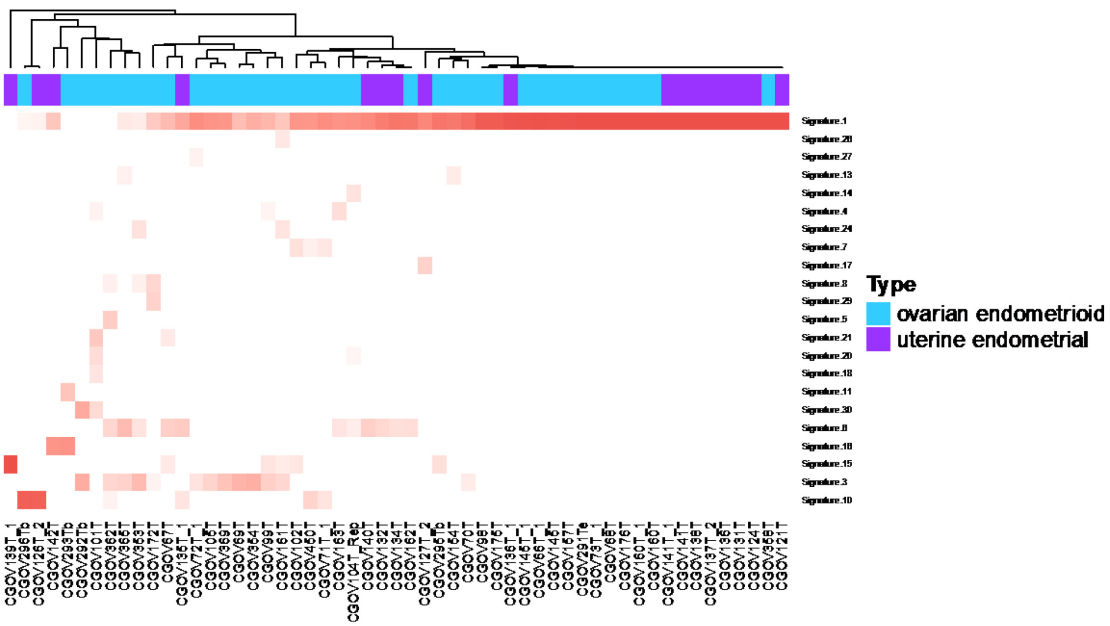

B

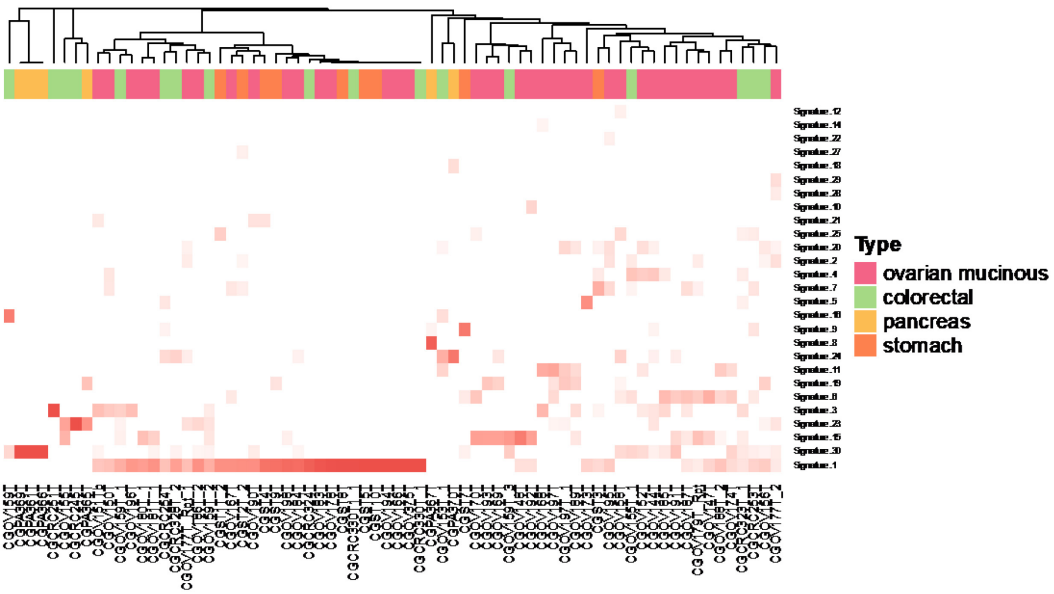

Supplemental Figure 4.3. Mutation signature analyses

Mutation signature analyses for various tumor types. Color indicates the percentage for which the signature explains the overall mutational profile of that sample.

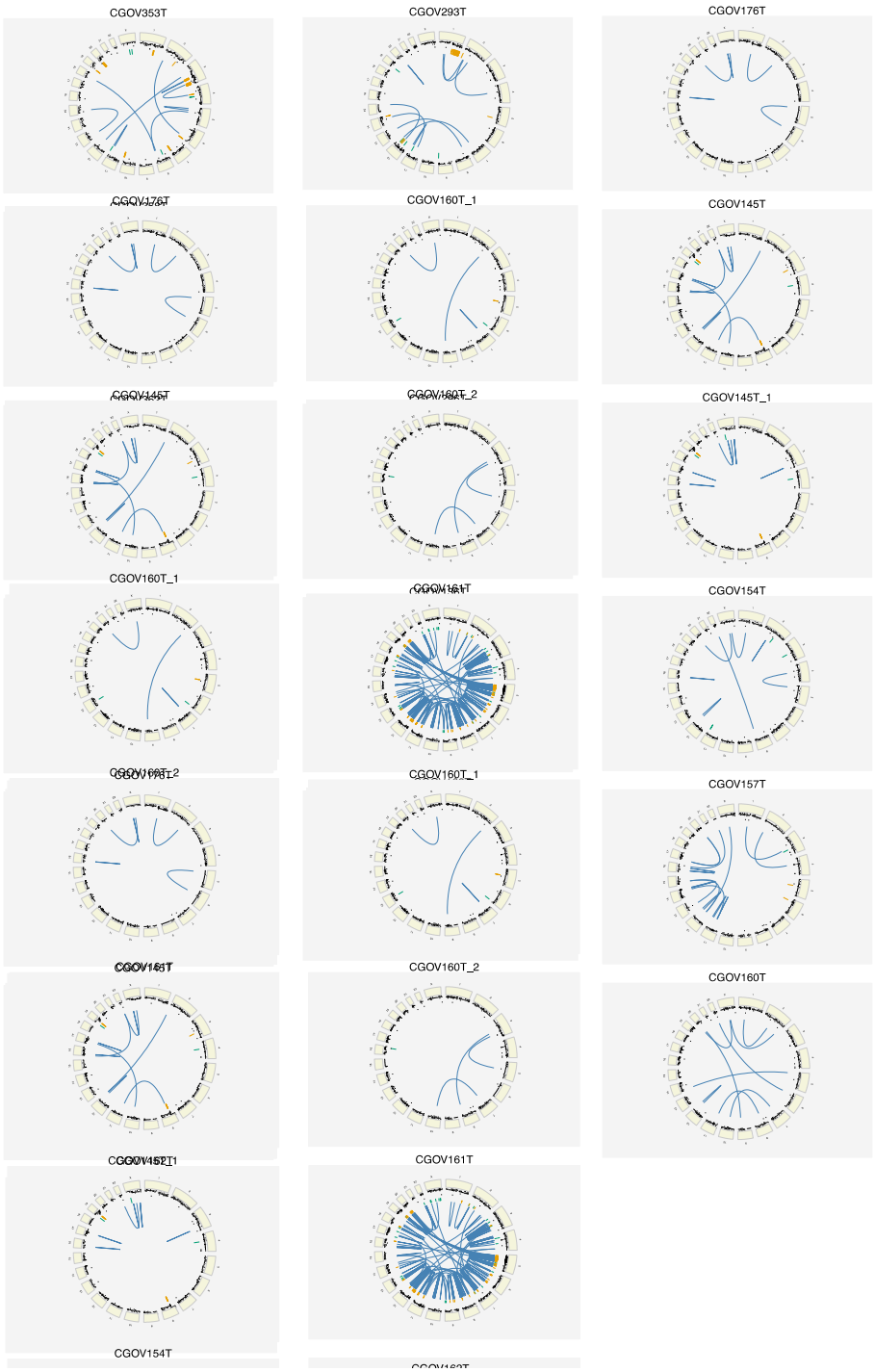

Supplemental Figure 4.4. Circos plots of 19 ovarian endometrioid tumor samples

Circos plots depict copy number alterations as well as intra- and inter-chromosomal rearrangements. Segmented normalized estimates of read depth were used to identify candidate focal amplifications in yellow and focal deletions in green. Rearranged read pairs and split reads were used to identify inter- and intra-chromosomal rearrangements in blue.

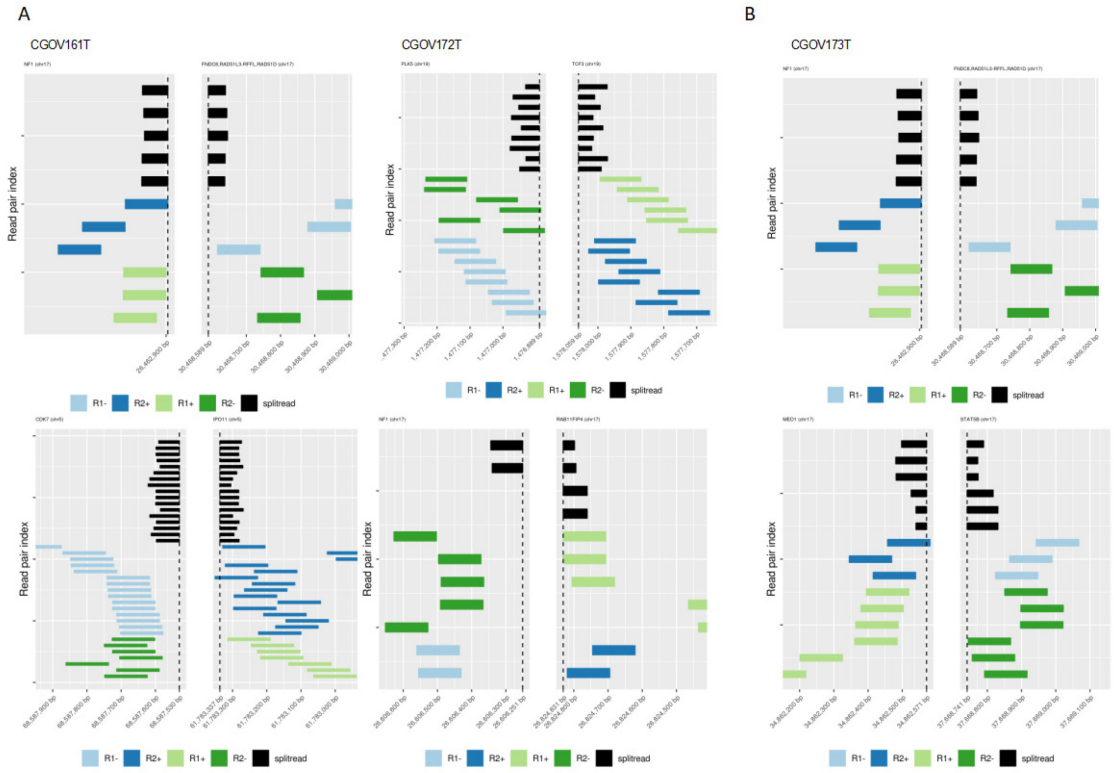

Supplemental Figure 4.5. Rearrangement analyses of ovarian endometrioid and ovarian mucinous tumors

Rearrangements present in 2 samples of ovarian endometrioid tumors (A), and one ovarian mucinous tumor sample (B). Reads aligned to the fusion junction of two representative rearrangements. Split reads, that span the fusion junction in black, and read pairs, that reside on either side of the junction in green and blue, give evidence for identifiying such rearrangements.

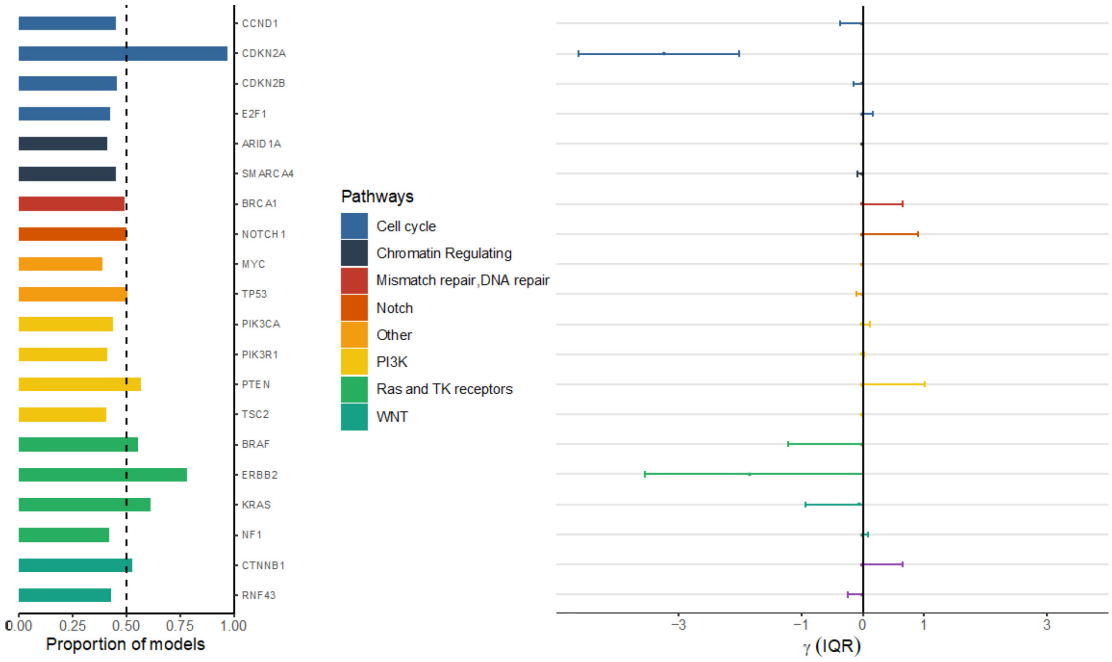

Supplemental Figure 4,6. Comparison of mutation frequencies in ovarian mucinous and endometrioid tumors

Bayesian model averaging was used to identify alterations involving known drivers associated with endometrioid and ovarian mucinous tumors. The probability that the gene coefficient (γ) in these models is non-zero is indicated by a bar graph (left). The inter-quartile range (IQR) for the difference in log odds of the regression coefficient is indicated by error bars (right). The odds of a mutation in ERBB2 and CDKN2A were higher among patients with GI mucinous cancers compared to patients with ovarian mucinous cancers.

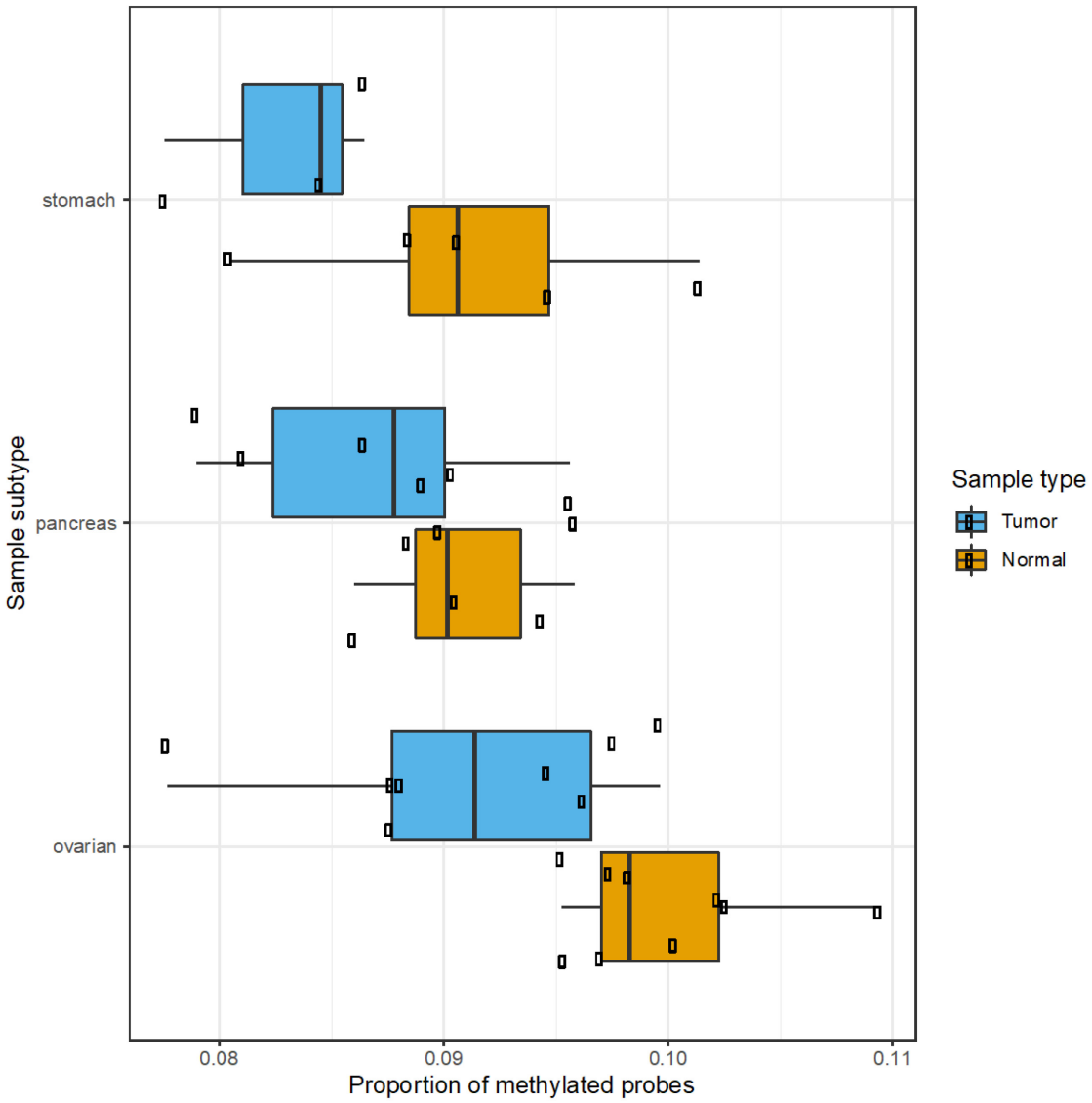

Supplemental Figure 4.7. Proportion of methylated probes in mucinous tumor samples
The proportion of methylated CpG sites (mean B >0.3) in the mucinous stomach samples, mucinous pancreas samples and mucinous ovarian samples for tumors and their matched normals.

Supplementary Table 4.1. Summary of Ovarian and CRC Mucinous Analyzed Through Whole-Exome and Whole-Genome Analyses

Case ID	Analysis Type	Tumor Type	Age at Diagnosis or Surgery	Gender
CGCRC245T	WES	colorectal	0	Female
CGCRC251T	WES	colorectal	0	Female
CGCRC253T	WES	colorectal	0	Female
CGCRC254T	WES	colorectal	0	Female
CGCRC323T_1	WES	colorectal	#N/A	Female
CGCRC324T	WES	colorectal	#N/A	Female
CGCRC325T	WES	colorectal	#N/A	Female
CGCRC328T_2	WES	colorectal	#N/A	Female
CGCRC330T_1	WES	colorectal	#N/A	Female
CGCRC331T_1	WES	colorectal	#N/A	Female
CGOV101T	WES	ovarian endometrioid	44	Female
CGOV102T	WES	ovarian endometrioid	51	Female
CGOV104T_Rep	WES	ovarian endometrioid	31	Female
CGOV105T	WES	ovarian endometrioid	64	Female
CGOV121T	WES	uterine endometrial	64	Female
CGOV124T	WES	uterine endometrial	80	Female
CGOV126T_2	WES	uterine endometrial	#N/A	Female
CGOV127T_2	WGS	uterine endometrial	76	Female
CGOV131T	WGS	uterine endometrial	71	Female
CGOV132T	WES	uterine endometrial	64	Female
CGOV134T	WES	uterine endometrial	56	Female
CGOV135T_1	WES	uterine endometrial	67	Female
CGOV136T_1	WGS	uterine endometrial	#N/A	Female
CGOV137T_2	WES	uterine endometrial	59	Female
CGOV138T	WGS	uterine endometrial	54	Female
CGOV139T_1	WGS	uterine endometrial	63	Female

CGOV140T	WGS	uterine endometrial	65	Female
CGOV141T	WES	uterine endometrial	59	Female
CGOV142T	WGS	uterine endometrial	56	Female
CGOV144T	WGS	ovarian mucinous	52	Female
CGOV145T	WGS	ovarian endometrioid	53	Female
CGOV147T	WGS	ovarian mucinous	37	Female
CGOV148T	WGS	ovarian mucinous	#N/A	Female
CGOV150T	WES	ovarian mucinous	48	Female
CGOV151Tb	WES	ovarian mucinous	51	Female
CGOV152T	WES	ovarian mucinous	58	Female
CGOV153T_1	WES	colorectal	49	Female
CGOV154T	WGS	ovarian endometrioid	62	Female
CGOV155T_1	WGS	colorectal	#N/A	Female
CGOV156T	WES	colorectal	45	Female
CGOV157T	WGS	ovarian endometrioid	54	Female
CGOV158T	WES	ovarian mucinous	78	Female
CGOV159T_1	WES	colorectal	#N/A	Female
CGOV160T	WGS	ovarian endometrioid	61	Female
CGOV161T	WGS	ovarian endometrioid	36	Female
CGOV162T	WGS	ovarian endometrioid	#N/A	Female
CGOV163T	WES	ovarian endometrioid	60	Female
CGOV166T	WES	ovarian mucinous	79/3 (y/m)	Female
CGOV167T	WES	ovarian mucinous	47/3 (y/m)	Female
CGOV168T	WES	ovarian mucinous	24/5 (y/m)	Female
CGOV169T	WES	ovarian mucinous	27/3 (y/m)	Female
CGOV170T	WGS	ovarian mucinous	63	Female
CGOV172T	WGS	ovarian endometrioid	47	Female
CGOV173T	WGS	ovarian mucinous	73	Female
CGOV174T	WGS	ovarian mucinous	57	Female
CGOV175T	WES	ovarian endometrioid	56	Female
CGOV176T	WGS	ovarian endometrioid	76	Female

CGOV177T_2	WES	ovarian mucinous	#N/A	Female
CGOV178T	WES	ovarian mucinous	65	Female
CGOV179T_Rpt	WES	ovarian mucinous	#N/A	Female
CGOV180T_1	WES	ovarian mucinous	62	Female
CGOV181T_1	WES	ovarian mucinous	#N/A	Female
CGOV183T	WES	ovarian mucinous	36	Female
CGOV184T	WES	ovarian mucinous	61	Female
CGOV185T	WES	ovarian mucinous	65	Female
CGOV186T_2	WES	ovarian mucinous	#N/A	Female
CGOV187T	WES	ovarian mucinous	88	Female
CGOV188T_2	WES	ovarian mucinous	37	Female
CGOV189T	WES	ovarian mucinous	61	Female
CGOV190T	WES	ovarian mucinous	29	Female
CGOV191T	WES	ovarian mucinous	35	Female
CGOV192T	WES	ovarian mucinous	30	Female
CGOV193T	WES	ovarian mucinous	43	Female
CGOV194T	WES	ovarian mucinous	44	Female
CGOV195T	WES	ovarian mucinous	76	Female
CGOV196T	WES	ovarian mucinous	40	Female
CGOV197T	WES	ovarian mucinous	33	Female
CGOV198T	WES	ovarian mucinous	70	Female
CGOV291Te	WGS	ovarian endometrioid	#N/A	Female
CGOV292Tb	WGS	ovarian endometrioid	#N/A	Female
CGOV293Tb	WGS	ovarian endometrioid	#N/A	Female
CGOV295Tb	WGS	ovarian endometrioid	#N/A	Female
CGOV296Tb	WGS	ovarian endometrioid	#N/A	Female
CGOV353T	WGS	ovarian endometrioid	#N/A	Female
CGOV354T	WGS	ovarian endometrioid	#N/A	Female
CGOV358T	WGS	ovarian endometrioid	#N/A	Female
CGOV362T	WGS	ovarian endometrioid	#N/A	Female
CGOV365T	WGS	ovarian endometrioid	#N/A	Female
CGOV369T	WGS	ovarian endometrioid	#N/A	Female

CGOV375T	WES	ovarian mucinous	#N/A	Female
CGOV450T	WES	ovarian endometrioid	#N/A	Female
CGOV66T_1	WES	ovarian endometrioid	63	Female
CGOV67T	WES	ovarian endometrioid	60	Female
CGOV68T	WES	ovarian endometrioid	37	Female
CGOV69T	WES	ovarian endometrioid	61	Female
CGOV70T	WES	ovarian endometrioid	55	Female
CGOV71T_1	WES	ovarian endometrioid	41	Female
CGOV72T_1	WES	ovarian endometrioid	55	Female
CGOV73T_1	WES	ovarian endometrioid	44	Female
CGOV98T	WES	ovarian endometrioid	41	Female
CGOV99T	WES	ovarian endometrioid	47	Female
CGPA361T	WES	pancreas	#N/A	Male
CGPA364T	WES	pancreas	#N/A	Female
CGPA365T	WES	pancreas	#N/A	Male
CGPA366T	WES	pancreas	#N/A	Female
CGPA367T	WES	pancreas	#N/A	Male
CGPA369T	WES	pancreas	#N/A	Male
CGPA370T	WES	pancreas	#N/A	Female
CGST10T	WES	stomach	#N/A	Male
CGST1T_2	WES	stomach	#N/A	Male
CGST2T_2	WES	stomach	#N/A	Male
CGST3T	WES	stomach	#N/A	Male
CGST4T	WES	stomach	#N/A	Male
CGST5T	WES	stomach	#N/A	Male
CGST7T	WES	stomach	#N/A	
CGST8T	WES	stomach	#N/A	Male
CGST9T	WES	stomach	#N/A	Male

Supplementary Table 4.2. Summary of Next-Generation Sequencing Analyses

Case ID	Sample Type	Analysis Type
CGOV145N_1	Normal	WGS
CGCRC245N	Normal	WES
CGCRC245T	Tumor	WES
CGCRC251N	Normal	WES
CGCRC251T	Tumor	WES
CGCRC252N	Normal	WES
CGCRC252T	Tumor	WES
CGCRC253N_1	Normal	WES
CGCRC253T	Tumor	WES
CGCRC254N_1	Normal	WES
CGCRC254T	Tumor	WES
CGCRC323N_1	Normal	WES
CGCRC323T_1	Tumor	WES
CGCRC324Na	Normal	WES
CGCRC324T	Tumor	WES
CGCRC325N	Normal	WES
CGCRC325T	Tumor	WES
CGCRC328N	Normal	WES
CGCRC328T_2	Tumor	WES
CGCRC330N_1	Normal	WES
CGCRC330T_1	Tumor	WES
CGCRC330T1_1	Tumor	WES
CGCRC331N_1	Normal	WES
CGCRC331T_1	Tumor	WES
CGOV101N	Normal	WES
CGOV101T	Tumor	WES
CGOV102N	Normal	WES
CGOV102T	Tumor	WES
CGOV103N	Normal	WES
CGOV103T	Tumor	WES
CGOV104N	Normal	WES
CGOV104T_Rep	Tumor	WES
CGOV105N	Normal	WES
CGOV105T	Tumor	WES
CGOV121N	Normal	WES
CGOV121T	Tumor	WES
CGOV124N	Normal	WES

CGOV124T	Tumor	WES
CGOV126N	Normal	WES
CGOV126T_2	Tumor	WES
CGOV127N_2	Normal	WGS
CGOV127T_2	Tumor	WGS
CGOV131N_1	Normal	WGS
CGOV131T	Tumor	WGS
CGOV132N	Normal	WES
CGOV132T	Tumor	WES
CGOV133N	Normal	WES
CGOV133T	Tumor	WES
CGOV134N	Normal	WES
CGOV134T	Tumor	WES
CGOV135N	Normal	WES
CGOV135T_1	Tumor	WES
CGOV136N	Normal	WES
CGOV136N	Normal	WGS
CGOV136T	Tumor	WES
CGOV136T_1	Tumor	WGS
CGOV137N	Normal	WES
CGOV137T_2	Tumor	WES
CGOV138N	Normal	WGS
CGOV138T	Tumor	WGS
CGOV139N	Normal	WGS
CGOV139T_1	Tumor	WGS
CGOV140N_1	Normal	WGS
CGOV140T	Tumor	WGS
CGOV141N	Normal	WES
CGOV141N	Normal	WGS
CGOV141T	Tumor	WES
CGOV141T_1	Tumor	WGS
CGOV142N_1	Normal	WGS
CGOV142T	Tumor	WGS
CGOV144N	Normal	WGS
CGOV144T	Tumor	WGS
CGOV145N	Normal	WGS
CGOV145T	Tumor	WGS
CGOV145T_1	Tumor	WGS
CGOV147N	Normal	WGS
CGOV147T	Tumor	WGS
CGOV148N	Normal	WGS
CGOV148T	Tumor	WGS
CGOV150N	Normal	WES

CGOV150T	Tumor	WES
CGOV151N	Normal	WES
CGOV151Tb	Tumor	WES
CGOV152N	Normal	WES
CGOV152T	Tumor	WES
CGOV153N	Normal	WES
CGOV153T_1	Tumor	WES
CGOV154N	Normal	WGS
CGOV154T	Tumor	WGS
CGOV155N	Normal	WGS
CGOV155T	Tumor	WES
CGOV155T_1	Tumor	WGS
CGOV156N	Normal	WES
CGOV156T	Tumor	WES
CGOV157N	Normal	WGS
CGOV157T	Tumor	WGS
CGOV158N	Normal	WES
CGOV158T	Tumor	WES
CGOV159N	Normal	WES
CGOV159N_2	Normal	WES
CGOV159T	Tumor	WGS
CGOV159T_1	Tumor	WES
CGOV159T_2	Tumor	WES
CGOV159T_3	Tumor	WGS
CGOV160N	Normal	WGS
CGOV160N_1	Normal	WGS
CGOV160N_2	Normal	WGS
CGOV160T	Tumor	WGS
CGOV160T_1	Tumor	WGS
CGOV160T_2	Tumor	WGS
CGOV161N	Normal	WGS
CGOV161T	Tumor	WGS
CGOV162N	Normal	WGS
CGOV162T	Tumor	WGS
CGOV163N	Normal	WES
CGOV163T	Tumor	WES
CGOV166N	Normal	WES
CGOV166T	Tumor	WES
CGOV167N	Normal	WES
CGOV167T	Tumor	WES
CGOV168N	Normal	WES
CGOV168T	Tumor	WES
CGOV169N	Normal	WES

CGOV169T	Tumor	WES
CGOV170N	Normal	WGS
CGOV170T	Tumor	WGS
CGOV172N	Normal	WGS
CGOV172T	Tumor	WGS
CGOV173N	Normal	WGS
CGOV173T	Tumor	WGS
CGOV174N	Normal	WGS
CGOV174T	Tumor	WGS
CGOV175N	Normal	WES
CGOV175T	Tumor	WES
CGOV176N	Normal	WGS
CGOV176T	Tumor	WGS
CGOV177N_2	Normal	WES
CGOV177N_Rpt	Normal	WES
CGOV177T_2	Tumor	WES
CGOV177T_Rpt_1	Tumor	WES
CGOV178N	Normal	WES
CGOV178T	Tumor	WES
CGOV179N	Normal	WES
CGOV179T_Rpt	Tumor	WES
CGOV180N_1	Normal	WES
CGOV180T_1	Tumor	WES
CGOV181N	Normal	WES
CGOV181T_1	Tumor	WES
CGOV183N_Rpt_1	Normal	WES
CGOV183T	Tumor	WES
CGOV184N_Rpt_1	Normal	WES
CGOV184T	Tumor	WES
CGOV185N_2	Normal	WES
CGOV185T	Tumor	WES
CGOV186N	Normal	WES
CGOV186T_2	Tumor	WES
CGOV187N	Normal	WES
CGOV187T	Tumor	WES
CGOV188N_2	Normal	WES
CGOV188T_2	Tumor	WES
CGOV189N	Normal	WES
CGOV189T	Tumor	WES
CGOV190N	Normal	WES
CGOV190T	Tumor	WES
CGOV191N	Normal	WES
CGOV191T	Tumor	WES

CGOV192N	Normal	WES
CGOV192T	Tumor	WES
CGOV193N	Normal	WES
CGOV193T	Tumor	WES
CGOV194N	Normal	WES
CGOV194T	Tumor	WES
CGOV195N	Normal	WES
CGOV195T	Tumor	WES
CGOV196N	Normal	WES
CGOV196T	Tumor	WES
CGOV197N	Normal	WES
CGOV197T	Tumor	WES
CGOV197T_1	Tumor	WES
CGOV198N	Normal	WES
CGOV198T	Tumor	WES
CGOV291N	Normal	WGS
CGOV291Te	Tumor	WGS
CGOV292Na	Normal	WGS
CGOV292Tb	Tumor	WGS
CGOV293N	Normal	WGS
CGOV293Tb	Tumor	WGS
CGOV295N	Normal	WGS
CGOV295Tb	Tumor	WGS
CGOV296N	Normal	WGS
CGOV296Tb	Tumor	WGS
CGOV353N	Normal	WGS
CGOV353T	Tumor	WGS
CGOV354N	Normal	WGS
CGOV354T	Tumor	WGS
CGOV358N	Normal	WGS
CGOV358T	Tumor	WGS
CGOV362N	Normal	WGS
CGOV362T	Tumor	WGS
CGOV365N	Normal	WGS
CGOV365T	Tumor	WGS
CGOV369N	Normal	WGS
CGOV369T	Tumor	WGS
CGOV375N	Normal	WES
CGOV375T	Tumor	WES
CGOV450N	Normal	WES
CGOV450T	Tumor	WES
CGOV66N	Normal	WES
CGOV66T_1	Tumor	WES

CGOV67N	Normal	WES
CGOV67T	Tumor	WES
CGOV68N	Normal	WES
CGOV68T	Tumor	WES
CGOV69N_2	Normal	WES
CGOV69T	Tumor	WES
CGOV70N	Normal	WES
CGOV70T	Tumor	WES
CGOV71N	Normal	WES
CGOV71T_1	Tumor	WES
CGOV72N	Normal	WES
CGOV72T_1	Tumor	WES
CGOV73N	Normal	WES
CGOV73T_1	Tumor	WES
CGOV98N	Normal	WES
CGOV98T	Tumor	WES
CGOV99N	Normal	WES
CGOV99T	Tumor	WES
CGPA361N	Normal	WES
CGPA361T	Tumor	WES
CGPA364N	Normal	WES
CGPA364T	Tumor	WES
CGPA365N	Normal	WES
CGPA365T	Tumor	WES
CGPA366N	Normal	WES
CGPA366T	Tumor	WES
CGPA367N	Normal	WES
CGPA367T	Tumor	WES
CGPA369N	Normal	WES
CGPA369T	Tumor	WES
CGPA370N	Normal	WES
CGPA370T	Tumor	WES
CGST10N_1	Normal	WES
CGST10T	Tumor	WES
CGST1N_1	Normal	WES
CGST1T_2	Tumor	WES
CGST2N	Normal	WES
CGST2T_2	Tumor	WES
CGST3N	Normal	WES
CGST3T	Tumor	WES
CGST4N	Normal	WES
CGST4T	Tumor	WES
CGST5N	Normal	WES

CGST5T	Tumor	WES
CGST7N	Normal	WES
CGST7T	Tumor	WES
CGST8N	Normal	WES
CGST8T	Tumor	WES
CGST9N	Normal	WES
CGST9T	Tumor	WES

CHAPTER 5:

DISCUSSION

5.1 High grade serous ovarian carcinomas originate in the fallopian tube discussion

These results provide a comprehensive evolutionary analysis of sporadic high-grade serous ovarian carcinoma in five patients. Given the unique nature of the multiple samples we examined from each patient, our study may have certain limitations not typical of genome-wide efforts. First, the small size of the tumor samples compared to surrounding non-neoplastic tissue could potentially lead to low tumor purity. The high mutant allele fraction of *TP53* among cancer samples (average of 56-85%) indicates that this issue was largely overcome through laser capture microdissection. Second, the small number of cells in p53 signature samples may have limited our genomic analyses for these lesions. The observation that all sequence changes in p53 signatures were also present in STIC and other carcinomas of multiple sites is consistent with our evolutionary model and suggests that these cells are likely to represent a parental clone of other neoplastic lesions. Third, our analysis was limited to ovarian cancers where STICs and other concomitant lesions were identified, and may therefore not be representative of all HGOCs. The absence of STIC lesions in ~40% of sporadic HGSOCs is likely due to an incomplete sampling of the fallopian tube or the overgrowth of the STIC by the carcinoma in the context of bulky disease, but may also reflect another site of origin that has yet to be determined for these cancers[144]. Fourth, this study did not intend to address the intra-tumoral heterogeneity within the carcinomas but rather focused on clonal changes within each tumor. Fifth, as in any evolutionary analyses, the genomic alterations we observed provide the most likely model of tumor development but do not exclude the possibility of other relationships. Nevertheless, our analyses of somatic alterations suggest that models where the ovarian cancer or metastatic lesions seed the fallopian tube tumors[25,26] (including STICs or p53 signatures) are infrequent and unlikely to be the source of most fallopian tube lesions.

Despite these potential limitations, the data we have obtained provide new insights into the etiology of ovarian Type II carcinoma and have significant implications for the prevention, early detection and therapeutic intervention of this disease. The results suggest that ovarian cancer is a disease of

the fallopian tubes, with the development of p53 signatures and STICs as early events. The subsequent formation of a cancer in the ovaries represents a seeding event from a primary tumor in the fallopian tube that already contains sequence and structural alterations in key driver genes, including those in *TP53*, PI3K pathway, and *BRCA1/BRCA2* genes. The recurrent allelic imbalances observed in chromosomes 1, 6, 16, 18, 20 and 22 may suggest additional genes that involved in this process. The timing of the progression from STICs to ovarian cancer in the cases we analyzed was on average 6.5 years, but seeding of metastatic lesions in these patients occurred rapidly thereafter. This timing is consistent with recent reports showing a difference of 7.7 years in the age of *BRCA* carriers with localized vs advanced adnexal lesions[145]. This evolutionary timeline can help explain why most HGSOC patients are diagnosed at advanced stage (III/IV) with pelvic and peritoneal spread of disease, and why among asymptomatic *BRCA* germline mutation carriers half of the cases diagnosed with asymptomatic adnexal neoplasia have already seeded to pelvis or peritoneum (>IA)[145]. These observations are largely similar to other genomic analyses of the evolution of ovarian cancer[24,25,28,146] as well as the recent analyses of STIC lesions that were reported while this study was under review[14]. Our study highlights the role of p53 signatures as early lesions in this evolutionary paradigm.

Our genomic analyses are consistent with population-based studies of the effects of salpingectomy on the risk of ovarian cancer. Prophylactic bilateral salpingo-oophorectomy has been shown to reduce the risk of developing ovarian cancer in *BRCA* mutation carriers to below 5%[147,148]. Likewise, bilateral salpingectomy, performed as a contraceptive method instead of tubal sterilization, reduced the risk of ovarian cancer by 61% at 10 years[149]. Our study provides a mechanistic basis for these observations and has implications for clinical management in prevention of ovarian cancer. In high risk *BRCA* carriers, bilateral salpingectomy with delayed oophorectomy should be considered[150] through participation in ongoing clinical trials (NCT02321228; NCT01907789). In non-carriers, our work implies that for women who undergo

surgery for benign uterine causes, total abdominal hysterectomy and bilateral salpingectomy with sparing of the ovaries should be considered[151], and that bilateral salpingectomy may be a preferred contraceptive alternative to tubal ligation. The dual concepts in these recommendations for *BRCA* carriers and non-carriers are that removal of the fallopian tubes (rather than the ovaries) may be curative as it eliminates the underlying cellular precursors of ovarian cancer, and that preservation of the ovaries provides long term benefits due to decreased risk and fatalities from coronary heart disease and other illnesses[152]. A limitation of this approach is that as the precise timing of when potentially malignant cells shed from the fallopian tube and microscopically seed the ovary is unknown, removal of the tubes may not provide optimal risk-reduction.

5.2 Integrated genomic, epigenomic and expression analyses of ovarian cancer cell lines discussion

These analyses provide the most comprehensive molecular analyses of ovarian cancer cell lines to date. Through integration of sequence, copy number, rearrangement, methylation, and expression analyses, we were able to detect frequently altered driver genes and pathways. These efforts revealed that ovarian cancer cell lines were largely representative of primary ovarian cancers and identified a variety of alterations not previously appreciated in these tumors.

One of the challenges of genomic analyses of tumor cell lines has been the lack of matched normal samples for determination of whether alterations are truly tumor-specific. Through the development of Trellis, we were able to identify high-confidence copy number and rearrangement alterations in the absence of matched normal DNA. Additionally, the grouping of structural changes allowed linking of apparently disparate events that would normally have been considered separate copy number alterations. These efforts provide a method for detecting somatic structural changes in cancer cell lines and other specimens in the absence of a matched normal, without the hundreds to

thousands of false-positive changes typically detected through other approaches. The method also permits identification of likely driver copy number changes by detecting the most connected regions of amplicons among the many such passenger alterations typically observed in human cancers. The identification of likely somatic structural and sequence alterations in a tumor-only setting is conservative. Cancer signature analyses, for example, currently require a matched normal sample to comprehensively identify somatic signatures across the genome, and our analyses based on a subset of somatic alterations may not reflect overall somatic mutation signatures.

These efforts revealed alterations in ovarian cancer that may provide insights into the biology of this disease. The integration of methylation and expression changes together with sequence and structural changes identified a larger fraction of tumors that were altered in specific genes and pathways than whole-genome sequencing alone. For example, CDKN2A was altered in over half of the serous, clear-cell, and mucinous cancer cell lines analyzed, revealing a higher fraction than previously thought to have alterations in this gene. Additionally, changes of a variety of genes, including ASXL1, H3F3B, and CDC73, as well as fusions of YAP1-MAML2, IKFZ2-ERBB4, and those disrupting FBXW7, NF1, and CCND1 were detected in these tumors, providing pathways of dysregulation within ovarian cancer.

The integrative molecular analyses of ovarian cancer cell lines provide opportunities for characterizing differences in susceptibility to targeted therapies. As an example, ovarian tumors with sequence alterations in PIK3CA and PPP2R1A had enhanced sensitivity to the GNE-493 inhibitor to achieve the same therapeutic response as tumors without these alterations. Mutations in PIK3CA and PPP2R1A are common in ovarian clear-cell cancers, suggesting that PI3K inhibitors may be an effective therapeutic strategy for this subtype.

Cancers with HRD are more prone to genomic errors resulting in loss or duplication of chromosomal regions and chromosomal instability[73]. Drugs that inhibit PARP1 cause multiple double strand breaks, and in tumors with HRD such DNA damage cannot be efficiently repaired, leading to cell death. We found that serous and endometrioid tumors with MYC amplification were highly sensitive to PARP inhibitors. PARP inhibitors have been previously shown to lead to mitotic catastrophe in neuroblastoma with amplification of the related gene MYCN on chromosome 2p[153], and MYC amplification on chromosome 8q has been shown to suppress BIN1, thereby increasing the activity of PARP1[154]. Additionally, MYCN amplified neuroblastoma cell lines were more sensitive to the PARP inhibitor BYK204165 compared to cell lines without such alterations[155]. In our study, MYC was the central driver in multiple ovarian cancers cell lines with highly linked amplicon groups (Table S1g; Figures S3, S4, and S5), suggesting that this gene plays a major role in a subset of ovarian cancers that may now be targeted therapeutically. Interestingly, we found that genome-wide rearrangements were a more useful biomarker of sensitivity to this therapy compared to the commonly used HRD scores[156-158], perhaps because these latter measurements only identify a subset of patients that respond to PARP inhibitors, especially as shown in clinical trials that enriched for tumors with previous sensitivity to DNA-damaging agents[159,160]. Although there is a correlation between the HRD score and the number of inversions and intra-chromosomal rearrangements (Spearman correlation coefficient = 0.5), the genome-wide rearrangements we identified may provide a more informative signature of the underlying recombination deficiency in these tumors and together with MYC amplification offer potentially improved opportunities for identifying responsive patients.

5.3 Genomic landscapes of endometrioid and mucinous ovarian cancers discussion

These analyses provide an extensive genomic and epigenomic analysis of ovarian mucinous and endometrioid cancers. Through the integration of somatic mutations, structural variants, including

deletions, linked amplicons, intra and inter-chromosomal rearrangements, as well as methylation analyses, we were able to detect frequently altered genes and pathways that describe the genomic landscape of these tumor types. These efforts revealed that ovarian endometrioid and uterine endometrial cancers were genetically similar, suggesting they may share a common cellular precursor. In contrast, at both genetic and epigenetic levels, ovarian and GI mucinous tumors had different characteristics, highlighting the unique origins of these tumors.

We identified novel alterations that have not been previously observed in these tumors. These included alterations in *RAD51C, NOTCH4, SMARCA4, SMARCA1* and *JAK1* in ovarian endometrioid, and *SMARCA4* genes in ovarian mucinous cancers. Whole genome sequence analyses using our Trellis pipeline revealed novel rearrangements involving *PTEN*, *NF1,* and *NF2* in ovarian endometrioid tumors, and *NF1* and *MED1* in ovarian mucinous cancers. Many of these novel alterations provide new avenues for potential therapeutic intervention or new insights into the biology of these cancers. For example, patients with germline *NF1* mutations have shown to respond well to MEK1/2 inhibitors, providing a new treatment avenue for tumors with alterations in this gene [161]. *SMARCA4* loss, while not directly targetable, may result in cyclin D1 deficiency leading to susceptibility to CDK4/6 inhibition and thus provide another targetable treatment avenue to patients with *SMARCA4* mutant ovarian endometrioid tumors [162]. *JAK1* is essential for IL-6-class inflammatory cytokine signaling and plays a critical role in metastatic cancer progression in breast cancer, and may provide a similar role in ovarian endometrioid cancer [163]. *MED1* is a tissue-specific coactivator of the estrogen receptor that mediates breast cancer metastasis and treatment resistance [164] and when targeted in model systems results in reduced growth and metastasis of breast cancer xenografts [165]. *MED1* rearrangements involving exons may lead to overexpression of this protein that could be exploited in ovarian mucinous cancer patients.

In uterine endometrioid cancers, we identified *ESR1* activating mutations in three of 15 patients at amino acid residue 537 resulting in a mutation hotspot commonly seen in breast cancer patients who have become resistant to estrogen targeted therapies. Although aromatase inhibitors have been shown to select for Tyr537 *ESR1* mutations [116,117], none of the patients in this study had been treated with these therapies. We hypothesize that these three women, each over the age of 60, may have been in a post-menopausal estrogen-free environment similar to estrogen therapy that increased selection for *ESR1* mutations. The significant interest in overcoming ESR1 mutations for patients with resistance to aromatase inhibitors may ultimately provide new avenues for patients with these *de novo* alterations in uterine endometrioid cancers.

5.4 Overall Discussion

Our observations also have implications for improved detection of ovarian cancer. Unfortunately, less than 1.25% of HGSOC are confined to the ovary at diagnosis[27]. Earlier detection of this disease is likely to benefit from the identification of a precursor lesion, as has been the case for many other tumor types. Our data suggest that fallopian tube neoplasia is the origin of ovarian serous carcinogenesis, and can directly lead to cancer of the ovaries and of other sites. Currently, the typical histopathologic evaluation of fallopian tubes typically involves a cursory evaluation of one or two representative sections. Our study suggests that systematic sectioning and extensive examination of total fallopian tubes[21] should become common practice in pathology, and not confined to academic tertiary care centers. Depending on whether the fallopian tubes are removed for benign conditions, risk-reducing bilateral salpingectomy, or gynecological cancers, specific examination protocols should be applied[21,166]. Given the window of time that appears to exist between the formation of fallopian tube lesions and development of ovarian cancer, these insights open the prospect of novel approaches for screening. Such approaches may be especially important given the limited therapeutic options currently available for ovarian cancer[4,5]. Recent advances for

ultrasensitive detection of genetic alterations in blood-based liquid biopsies, pap smears, and other bodily fluids[167] [168] or imaging approaches may provide opportunities in early diagnosis and intervention.

Although our analyses provide a comprehensive integration of molecular alterations for ovarian cancer, certain types of changes have not been evaluated. In the future, proteomic, metabolomic, and carbohydrate changes can be added to the compendium of genomic, epigenomic, and transcriptomic information for these cell lines. Additionally, further efforts will be needed to demonstrate that these observations can be translated broadly to ovarian cancer patients. Nevertheless, these data provide a foundation for using ovarian cell line models in screening novel therapeutic strategies. Evaluation of additional compounds using these well-characterized tumor cell lines will provide rational translational opportunities for development of new therapies in ovarian cancer.

Integrated analyses of the sequence and structural changes through Bayesian modeling revealed that the genomic landscapes of ovarian GI mucinous tumors were different, but that ovarian endometrioid and uterine endometrial tumors were related and may share similar origins. Our observation that ovarian and uterine endometrioid tumors may share a similar cellular precursor is consistent with previous observations of co-occurrence of these diseases at a higher than expected frequency based on the individual prevalence of these cancers . The common origin of these tumors remains to be determined, but accumulating evidence that that other ovarian cancers such as HGSOC arise in the fallopian tube [13], together with pathologic evidence suggests that the endometrium is the likely source of this cancer. These observations have important implications for the management of these patients and may suggest new methods for disease prevention.

REFERENCES

1. Ferlay J, Steliarova-Foucher E, Lortet-Tieulent J, et al. Cancer incidence and mortality patterns in Europe: estimates for 40 countries in 2012. Eur J Cancer 2013;49:1374-403.
2. Siegel RL, Miller KD, Jemal A. Cancer statistics, 2015. CA Cancer J Clin 2015;65:5-29.
3. Cress RD, Chen YS, Morris CR, Petersen M, Leiserowitz GS. Characteristics of Long-Term Survivors of Epithelial Ovarian Cancer. Obstetrics and gynecology 2015;126:491-7.
4. Menon U, Griffin M, Gentry-Maharaj A. Ovarian cancer screening--current status, future directions. Gynecologic oncology 2014;132:490-5.
5. Jacobs IJ, Menon U, Ryan A, et al. Ovarian cancer screening and mortality in the UK Collaborative Trial of Ovarian Cancer Screening (UKCTOCS): a randomised controlled trial. Lancet 2015.
6. Kurman RJ, Shih Ie M. The Dualistic Model of Ovarian Carcinogenesis: Revisited, Revised, and Expanded. Am J Pathol 2016;186:733-47.
7. Kurman RJ, Shih Ie M. The origin and pathogenesis of epithelial ovarian cancer: a proposed unifying theory. Am J Surg Pathol 2010;34:433-43.
8. Karst AM, Drapkin R. Ovarian cancer pathogenesis: a model in evolution. J Oncol 2010;2010:932371.
9. Levanon K, Crum C, Drapkin R. New insights into the pathogenesis of serous ovarian cancer and its clinical impact. J Clin Oncol 2008;26:5284-93.
10. Bowtell DD, Bohm S, Ahmed AA, et al. Rethinking ovarian cancer II: reducing mortality from high-grade serous ovarian cancer. Nat Rev Cancer 2015;15:668-79.
11. Torre LA, Trabert B, DeSantis CE, et al. Ovarian cancer statistics, 2018. CA: a cancer journal for clinicians 2018;68:284-96.
12. Integrated genomic analyses of ovarian carcinoma. Nature 2011;474:609-15.
13. Labidi-Galy SI, Papp E, Hallberg D, et al. High grade serous ovarian carcinomas originate in the fallopian tube. Nature communications 2017;8:1093.
14. Eckert MA, Pan S, Hernandez KM, et al. Genomics of Ovarian Cancer Progression Reveals Diverse Metastatic Trajectories Including Intraepithelial Metastasis to the Fallopian Tube. Cancer discovery 2016;6:1342-51.
15. Ducie J, Dao F, Considine M, et al. Molecular analysis of high-grade serous ovarian carcinoma with and without associated serous tubal intra-epithelial carcinoma. Nature communications 2017;8:990-.
16. Cancer Genome Atlas Research N. Integrated genomic analyses of ovarian carcinoma. Nature 2011;474:609-15.
17. Patch AM, Christie EL, Etemadmoghadam D, et al. Whole-genome characterization of chemoresistant ovarian cancer. Nature 2015;521:489-94.
18. Cass I, Holschneider C, Datta N, Barbuto D, Walts AE, Karlan BY. BRCA-mutation-associated fallopian tube carcinoma: a distinct clinical phenotype? Obstetrics and gynecology 2005;106:1327-34.
19. Piek JM, Verheijen RH, Kenemans P, Massuger LF, Bulten H, van Diest PJ. BRCA1/2-related ovarian cancers are of tubal origin: a hypothesis. Gynecologic oncology 2003;90:491.
20. Piek JM, van Diest PJ, Zweemer RP, et al. Dysplastic changes in prophylactically removed Fallopian tubes of women predisposed to developing ovarian cancer. J Pathol 2001;195:451-6.
21. Medeiros F, Muto MG, Lee Y, et al. The tubal fimbria is a preferred site for early adenocarcinoma in women with familial ovarian cancer syndrome. Am J Surg Pathol 2006;30:230-6.
22. Lee Y, Miron A, Drapkin R, et al. A candidate precursor to serous carcinoma that originates in the distal fallopian tube. J Pathol 2007;211:26-35.

23. Kindelberger DW, Lee Y, Miron A, et al. Intraepithelial carcinoma of the fimbria and pelvic serous carcinoma: Evidence for a causal relationship. Am J Surg Pathol 2007;31:161-9.
24. Kuhn E, Kurman RJ, Vang R, et al. TP53 mutations in serous tubal intraepithelial carcinoma and concurrent pelvic high-grade serous carcinoma--evidence supporting the clonal relationship of the two lesions. J Pathol 2012;226:421-6.
25. McDaniel AS, Stall JN, Hovelson DH, et al. Next-Generation Sequencing of Tubal Intraepithelial Carcinomas. JAMA Oncol 2015;1:1128-32.
26. Bashashati A, Ha G, Tone A, et al. Distinct evolutionary trajectories of primary high-grade serous ovarian cancers revealed through spatial mutational profiling. J Pathol 2013;231:21-34.
27. Nik NN, Vang R, Shih Ie M, Kurman RJ. Origin and pathogenesis of pelvic (ovarian, tubal, and primary peritoneal) serous carcinoma. Annu Rev Pathol 2014;9:27-45.
28. McPherson A, Roth A, Laks E, et al. Divergent modes of clonal spread and intraperitoneal mixing in high-grade serous ovarian cancer. Nat Genet 2016;48:758-67.
29. Yachida S, Jones S, Bozic I, et al. Distant metastasis occurs late during the genetic evolution of pancreatic cancer. Nature 2010;467:1114-7.
30. Jones S, Anagnostou V, Lytle K, et al. Personalized genomic analyses for cancer mutation discovery and interpretation. Science translational medicine 2015;7:283ra53.
31. Jones S, Wang TL, Kurman RJ, et al. Low-grade serous carcinomas of the ovary contain very few point mutations. The Journal of pathology 2012;226:413-20.
32. Zhang H, Liu T, Zhang Z, et al. Integrated Proteogenomic Characterization of Human High-Grade Serous Ovarian Cancer. Cell 2016;166:755-65.
33. Garnett MJ, Edelman EJ, Heidorn SJ, et al. Systematic identification of genomic markers of drug sensitivity in cancer cells. Nature 2012;483:570-5.
34. Barretina J, Caponigro G, Stransky N, et al. The Cancer Cell Line Encyclopedia enables predictive modelling of anticancer drug sensitivity. Nature 2012;483:603-7.
35. Domcke S, Sinha R, Levine DA, Sander C, Schultz N. Evaluating cell lines as tumour models by comparison of genomic profiles. Nature communications 2013;4:2126.
36. Anglesio MS, Kommoss S, Tolcher MC, et al. Molecular characterization of mucinous ovarian tumours supports a stratified treatment approach with HER2 targeting in 19% of carcinomas. The Journal of pathology 2013;229:111-20.
37. Ince TA, Sousa AD, Jones MA, et al. Characterization of twenty-five ovarian tumour cell lines that phenocopy primary tumours. Nature communications 2015;6:7419.
38. Iorio F, Knijnenburg TA, Vis DJ, et al. A Landscape of Pharmacogenomic Interactions in Cancer. Cell 2016;166:740-54.
39. Buhtoiarova TN, Brenner CA, Singh M. Endometrial Carcinoma: Role of Current and Emerging Biomarkers in Resolving Persistent Clinical Dilemmas. American journal of clinical pathology 2016;145:8-21.
40. Makris GM, Manousopoulou G, Battista MJ, Salloum I, Chrelias G, Chrelias C. Synchronous Endometrial and Ovarian Carcinoma: A Case Series. Case reports in oncology 2017;10:732-6.
41. Hajkova N, Ticha I, Hojny J, et al. Synchronous endometrioid endometrial and ovarian carcinomas are biologically related: A clinico-pathological and molecular (next generation sequencing) study of 22 cases. Oncology letters 2019;17:2207-14.
42. Wu R, Zhai Y, Fearon ER, Cho KR. Diverse mechanisms of beta-catenin deregulation in ovarian endometrioid adenocarcinomas. Cancer research 2001;61:8247-55.
43. Wu R-C, Veras E, Lin J, et al. Elucidating the pathogenesis of synchronous and metachronous tumors in a woman with endometrioid carcinomas using a whole-exome sequencing approach. Cold Spring Harb Mol Case Stud 2017;3:a001693.
44. Matsuo K, Machida H, Blake EA, et al. Trends and outcomes of women with synchronous endometrial and ovarian cancer. Oncotarget 2018;9:28757-71.

45. Wang YK, Bashashati A, Anglesio MS, et al. Genomic consequences of aberrant DNA repair mechanisms stratify ovarian cancer histotypes. Nature genetics 2017;49:856-65.
46. Hoang LN, McConechy MK, Meng B, et al. Targeted mutation analysis of endometrial clear cell carcinoma. Histopathology 2015;66:664-74.
47. Kandoth C, Schultz N, Cherniack AD, et al. Integrated genomic characterization of endometrial carcinoma. Nature 2013;497:67-73.
48. Brown J, Frumovitz M. Mucinous tumors of the ovary: current thoughts on diagnosis and management. Current oncology reports 2014;16:389.
49. Lee CT, Huang YC, Hung LY, et al. Serrated adenocarcinoma morphology in colorectal mucinous adenocarcinoma is associated with improved patient survival. Oncotarget 2017;8:35165-75.
50. Khan M, Loree JM, Advani SM, et al. Prognostic Implications of Mucinous Differentiation in Metastatic Colorectal Carcinoma Can Be Explained by Distinct Molecular and Clinicopathologic Characteristics. Clinical colorectal cancer 2018;17:e699-e709.
51. Nakata B, Yashiro M, Nishioka N, et al. Genetic alterations in adenoma-carcinoma sequencing of intraductal papillary-mucinous neoplasm of the pancreas. International journal of oncology 2002;21:1067-72.
52. Cheasley D, Wakefield MJ, Ryland GL, et al. The molecular origin and taxonomy of mucinous ovarian carcinoma. Nature communications 2019;10:3935.
53. Papp E, Hallberg D, Konecny GE, et al. Integrated Genomic, Epigenomic, and Expression Analyses of Ovarian Cancer Cell Lines. Cell reports 2018;25:2617-33.
54. Niknafs N, Beleva-Guthrie V, Naiman DQ, Karchin R. SubClonal Hierarchy Inference from Somatic Mutations: Automatic Reconstruction of Cancer Evolutionary Trees from Multi-region Next Generation Sequencing. PLoS Comput Biol 2015;11:e1004416.
55. Leeper K, Garcia R, Swisher E, Goff B, Greer B, Paley P. Pathologic findings in prophylactic oophorectomy specimens in high-risk women. Gynecol Oncol 2002;87:52-6.
56. Roh MH, Yassin Y, Miron A, et al. High-grade fimbrial-ovarian carcinomas are unified by altered p53, PTEN and PAX2 expression. Mod Pathol 2010;23:1316-24.
57. Perets R, Wyant GA, Muto KW, et al. Transformation of the fallopian tube secretory epithelium leads to high-grade serous ovarian cancer in Brca;Tp53;Pten models. Cancer Cell 2013;24:751-65.
58. Jones S, Chen WD, Parmigiani G, et al. Comparative lesion sequencing provides insights into tumor evolution. Proc Natl Acad Sci U S A 2008;105:4283-8.
59. Korch C, Spillman MA, Jackson TA, et al. DNA profiling analysis of endometrial and ovarian cell lines reveals misidentification, redundancy and contamination. Gynecologic oncology 2012;127:241-8.
60. Yu M, Selvaraj SK, Liang-Chu MM, et al. A resource for cell line authentication, annotation and quality control. Nature 2015;520:307-11.
61. Alexandrov LB, Nik-Zainal S, Wedge DC, et al. Signatures of mutational processes in human cancer. Nature 2013;500:415-21.
62. Rausch T, Zichner T, Schlattl A, Stutz AM, Benes V, Korbel JO. DELLY: structural variant discovery by integrated paired-end and split-read analysis. Bioinformatics 2012;28:i333-i9.
63. Layer RM, Chiang C, Quinlan AR, Hall IM. LUMPY: a probabilistic framework for structural variant discovery. Genome Biol 2014;15:R84.
64. Li H, Durbin R. Fast and accurate short read alignment with Burrows-Wheeler transform. Bioinformatics 2009;25:1754-60.
65. Fujita PA, Rhead B, Zweig AS, et al. The UCSC Genome Browser database: update 2011. Nucleic Acids Res 2011;39:D876-82.
66. Olshen AB, Venkatraman ES, Lucito R, Wigler M. Circular binary segmentation for the analysis of array-based DNA copy number data. Biostatistics 2004;5:557-72.

67. Venkatraman ES, Olshen AB. A faster circular binary segmentation algorithm for the analysis of array CGH data. Bioinformatics 2007;23:657-63.
68. Kent WJ. BLAT--the BLAST-like alignment tool. Genome Res 2002;12:656-64.
69. Aryee MJ, Jaffe AE, Corrada-Bravo H, et al. Minfi: a flexible and comprehensive Bioconductor package for the analysis of Infinium DNA methylation microarrays. Bioinformatics 2014;30:1363-9.
70. Konecny GE, Winterhoff B, Kolarova T, et al. Expression of p16 and retinoblastoma determines response to CDK4/6 inhibition in ovarian cancer. Clinical cancer research : an official journal of the American Association for Cancer Research 2011;17:1591-602.
71. Hoff P. A First Course in Bayesian Statistical Methods Springer 2009.
72. Forbes SA, Tang G, Bindal N, et al. COSMIC (the Catalogue of Somatic Mutations in Cancer): a resource to investigate acquired mutations in human cancer. Nucleic Acids Res 2010;38:D652-7.
73. Wang TL, Maierhofer C, Speicher MR, et al. Digital karyotyping. Proceedings of the National Academy of Sciences of the United States of America 2002;99:16156-61.
74. Leary RJ, Lin JC, Cummins J, et al. Integrated analysis of homozygous deletions, focal amplifications, and sequence alterations in breast and colorectal cancers. Proceedings of the National Academy of Sciences of the United States of America 2008;105:16224-9.
75. Shirley MD, Baugher JD, Stevens EL, et al. Chromosomal variation in lymphoblastoid cell lines. Hum Mutat 2012;33:1075-86.
76. Campbell PJ, Stephens PJ, Pleasance ED, et al. Identification of somatically acquired rearrangements in cancer using genome-wide massively parallel paired-end sequencing. Nature genetics 2008;40:722-9.
77. Greenman CD, Cooke SL, Marshall J, Stratton MR, Campbell PJ. Modeling the evolution space of breakage fusion bridge cycles with a stochastic folding process. Journal of mathematical biology 2016;72:47-86.
78. Katoh M. Functional proteomics of the epigenetic regulators ASXL1, ASXL2 and ASXL3: a convergence of proteomics and epigenetics for translational medicine. Expert Rev Proteomics 2015;12:317-28.
79. Ayoubi HA, Mahjoubi F, Mirzaei R. Investigation of the human H3.3B (H3F3B) gene expression as a novel marker in patients with colorectal cancer. J Gastrointest Oncol 2017;8:64-9.
80. Huang RY, Chen GB, Matsumura N, et al. Histotype-specific copy-number alterations in ovarian cancer. BMC Med Genomics 2012;5:47.
81. Ohta M, Inoue H, Cotticelli MG, et al. The FHIT gene, spanning the chromosome 3p14.2 fragile site and renal carcinoma-associated t(3;8) breakpoint, is abnormal in digestive tract cancers. Cell 1996;84:587-97.
82. Zochbauer-Muller S, Wistuba, II, Minna JD, Gazdar AF. Fragile histidine triad (FHIT) gene abnormalities in lung cancer. Clin Lung Cancer 2000;2:141-5.
83. Roy D, Sin SH, Damania B, Dittmer DP. Tumor suppressor genes FHIT and WWOX are deleted in primary effusion lymphoma (PEL) cell lines. Blood 2011;118:e32-9.
84. Aldaz CM, Ferguson BW, Abba MC. WWOX at the crossroads of cancer, metabolic syndrome related traits and CNS pathologies. Biochim Biophys Acta 2014;1846:188-200.
85. Cowin PA, George J, Fereday S, et al. LRP1B deletion in high-grade serous ovarian cancers is associated with acquired chemotherapy resistance to liposomal doxorubicin. Cancer research 2012;72:4060-73.
86. Zhang H, Chen ZH, Savarese TM. Codeletion of the genes for p16INK4, methylthioadenosine phosphorylase, interferon-alpha1, interferon-beta1, and other 9p21 markers in human malignant cell lines. Cancer Genet Cytogenet 1996;86:22-8.
87. Marjon K, Cameron MJ, Quang P, et al. MTAP Deletions in Cancer Create Vulnerability to Targeting of the MAT2A/PRMT5/RIOK1 Axis. Cell reports 2016;15:574-87.

88. Tonon G, Modi S, Wu L, et al. t(11;19)(q21;p13) translocation in mucoepidermoid carcinoma creates a novel fusion product that disrupts a Notch signaling pathway. Nature genetics 2003;33:208-13.
89. Coxon A, Rozenblum E, Park YS, et al. Mect1-Maml2 fusion oncogene linked to the aberrant activation of cyclic AMP/CREB regulated genes. Cancer research 2005;65:7137-44.
90. Valouev A, Weng Z, Sweeney RT, et al. Discovery of recurrent structural variants in nasopharyngeal carcinoma. Genome Res 2014;24:300-9.
91. Boddicker RL, Razidlo GL, Dasari S, et al. Integrated mate-pair and RNA sequencing identifies novel, targetable gene fusions in peripheral T-cell lymphoma. Blood 2016;128:1234-45.
92. Gruszka-Westwood AM, Atkinson S, Summersgill BM, et al. Unusual case of leukemic mantle cell lymphoma with amplified CCND1/IGH fusion gene. Genes, chromosomes & cancer 2002;33:206-12.
93. Saglam O, Xiong Y, Marchion DC, et al. ERBB4 Expression in Ovarian Serous Carcinoma Resistant to Platinum-Based Therapy. Cancer Control 2017;24:89-95.
94. Guertin DA, Sabatini DM. An expanding role for mTOR in cancer. Trends in molecular medicine 2005;11:353-61.
95. Cumbo C, Impera L, Minervini CF, et al. Genomic BCR-ABL1 breakpoint characterization by a multi-strategy approach for "personalized monitoring" of residual disease in chronic myeloid leukemia patients. Oncotarget 2018;9:10978-86.
96. Smiraglia DJ, Rush LJ, Fruhwald MC, et al. Excessive CpG island hypermethylation in cancer cell lines versus primary human malignancies. Hum Mol Genet 2001;10:1413-9.
97. Paz MF, Fraga MF, Avila S, et al. A systematic profile of DNA methylation in human cancer cell lines. Cancer research 2003;63:1114-21.
98. Varley KE, Gertz J, Bowling KM, et al. Dynamic DNA methylation across diverse human cell lines and tissues. Genome Res 2013;23:555-67.
99. Imura M, Yamashita S, Cai LY, et al. Methylation and expression analysis of 15 genes and three normally-methylated genes in 13 Ovarian cancer cell lines. Cancer Lett 2006;241:213-20.
100. Wiley A, Katsaros D, Chen H, et al. Aberrant promoter methylation of multiple genes in malignant ovarian tumors and in ovarian tumors with low malignant potential. Cancer 2006;107:299-308.
101. Akhoondi S, Sun D, von der Lehr N, et al. FBXW7/hCDC4 is a general tumor suppressor in human cancer. Cancer research 2007;67:9006-12.
102. Viallefont V, Raftery AE, Richardson S. Variable selection and Bayesian model averaging in case-control studies. Statistics in medicine 2001;20:3215-30.
103. Neto EC, Jang IS, Friend SH, Margolin AA. The Stream algorithm: computationally efficient ridge-regression via Bayesian model averaging, and applications to pharmacogenomic prediction of cancer cell line sensitivity. Pac Symp Biocomput 2014:27-38.
104. Meisner A, Kerr KF, Thiessen-Philbrook H, et al. Development of biomarker combinations for postoperative acute kidney injury via Bayesian model selection in a multicenter cohort study. Biomark Res 2018;6:3.
105. Nik-Zainal S, Davies H, Staaf J, et al. Landscape of somatic mutations in 560 breast cancer whole-genome sequences. Nature 2016;534:47-54.
106. Basu S. PP2A in the regulation of cell motility and invasion. Curr Protein Pept Sci 2011;12:3-11.
107. Shih Ie M, Panuganti PK, Kuo KT, et al. Somatic mutations of PPP2R1A in ovarian and uterine carcinomas. Am J Pathol 2011;178:1442-7.
108. McConechy MK, Anglesio MS, Kalloger SE, et al. Subtype-specific mutation of PPP2R1A in endometrial and ovarian carcinomas. The Journal of pathology 2011;223:567-73.

109. Zhang L, Duan CJ, Binkley C, et al. A transforming growth factor beta-induced Smad3/Smad4 complex directly activates protein kinase A. Molecular and cellular biology 2004;24:2169-80.
110. Ai X, Wu Y, Zhang W, et al. Targeting the ERK pathway reduces liver metastasis of Smad4-inactivated colorectal cancer. Cancer Biol Ther 2013;14:1059-67.
111. Bertotti A, Papp E, Jones S, et al. The genomic landscape of response to EGFR blockade in colorectal cancer. Nature 2015;526:263-7.
112. Linacre JM. Facets computer program for many-facet Rasch measurement. 2019;version 3.82.0.
113. Le Gallo M, Bell DW. The emerging genomic landscape of endometrial cancer. Clinical chemistry 2014;60:98-110.
114. Talhouk A, McConechy MK, Leung S, et al. A clinically applicable molecular-based classification for endometrial cancers. British journal of cancer 2015;113:299-310.
115. McConechy MK, Ding J, Senz J, et al. Ovarian and endometrial endometrioid carcinomas have distinct CTNNB1 and PTEN mutation profiles. Modern pathology : an official journal of the United States and Canadian Academy of Pathology, Inc 2014;27:128-34.
116. Toy W, Shen Y, Won H, et al. ESR1 ligand-binding domain mutations in hormone-resistant breast cancer. Nature genetics 2013;45:1439-45.
117. Robinson DR, Wu YM, Vats P, et al. Activating ESR1 mutations in hormone-resistant metastatic breast cancer. Nature genetics 2013;45:1446-51.
118. Alexandrov LB, Kim J, Haradhvala NJ, et al. The Repertoire of Mutational Signatures in Human Cancer. bioRxiv 2018:322859.
119. Rahman MT, Nakayama K, Rahman M, et al. KRAS and MAPK1 gene amplification in type II ovarian carcinomas. International journal of molecular sciences 2013;14:13748-62.
120. Birkeland E, Wik E, Mjøs S, et al. KRAS gene amplification and overexpression but not mutation associates with aggressive and metastatic endometrial cancer. British journal of cancer 2012;107:1997-2004.
121. Jung M, Russell AJ, Kennedy C, et al. Clinical Importance of Myc Family Oncogene Aberrations in Epithelial Ovarian Cancer. JNCI Cancer Spectrum 2018;2.
122. Chen M, Pockaj B, Andreozzi M, et al. JAK2 and PD-L1 Amplification Enhance the Dynamic Expression of PD-L1 in Triple-negative Breast Cancer. Clinical breast cancer 2018;18:e1205-e15.
123. Tanwar PS, Mohapatra G, Chiang S, et al. Loss of LKB1 and PTEN tumor suppressor genes in the ovarian surface epithelium induces papillary serous ovarian cancer. Carcinogenesis 2014;35:546-53.
124. Schumacher V, Vogel T, Leube B, et al. STK11 genotyping and cancer risk in Peutz-Jeghers syndrome. Journal of medical genetics 2005;42:428-35.
125. Philpott C, Tovell H, Frayling IM, Cooper DN, Upadhyaya M. The NF1 somatic mutational landscape in sporadic human cancers. Human genomics 2017;11:13.
126. Clague J, Wilhoite G, Adamson A, Bailis A, Weitzel JN, Neuhausen SL. RAD51C germline mutations in breast and ovarian cancer cases from high-risk families. PloS one 2011;6:e25632.
127. Krivokuca A, Yanowski K, Rakobradovic J, Benitez J, Brankovic-Magic M. RAD51C mutation screening in high-risk patients from Serbian hereditary breast/ovarian cancer families. Cancer biomarkers : section A of Disease markers 2015;15:775-81.
128. Zhang Z, Peng H, Wang X, et al. Preclinical Efficacy and Molecular Mechanism of Targeting CDK7-Dependent Transcriptional Addiction in Ovarian Cancer. Molecular cancer therapeutics 2017;16:1739-50.
129. de Carcer G, Escobar B, Higuero AM, et al. Plk5, a polo box domain-only protein with specific roles in neuron differentiation and glioblastoma suppression. Molecular and cellular biology 2011;31:1225-39.

130. Moyer T, Holland A. PLK4 promotes centriole duplication by phosphorylating STIL to link the procentriole cartwheel to the microtubule wall. eLife 2019.
131. Habedanck R, Stierhof YD, Wilkinson CJ, Nigg EA. The Polo kinase Plk4 functions in centriole duplication. Nature cell biology 2005;7:1140-6.
132. Kuriyama R, Bettencourt-Dias M, Hoffmann I, Arnold M, Sandvig L. Gamma-tubulin-containing abnormal centrioles are induced by insufficient Plk4 in human HCT116 colorectal cancer cells. Journal of cell science 2009;122:2014-23.
133. Press MF, Xie B, Davenport S, et al. Role for polo-like kinase 4 in mediation of cytokinesis. Proceedings of the National Academy of Sciences of the United States of America 2019;116:11309-18.
134. Guerra J, Pinto C, Pinto D, et al. POLE somatic mutations in advanced colorectal cancer. Cancer medicine 2017;6:2966-71.
135. Ricci F, Affatato R, Carrassa L, Damia G. Recent Insights into Mucinous Ovarian Carcinoma. International journal of molecular sciences 2018;19.
136. Lin WL, Kuo WH, Chen FL, et al. Identification of the coexisting HER2 gene amplification and novel mutations in the HER2 protein-overexpressed mucinous epithelial ovarian cancer. Annals of surgical oncology 2011;18:2388-94.
137. Dimova I, Zaharieva B, Raicheva S, et al. Association of CyclinD1 copy number changes with histological type in ovarian tumors. Acta oncologica (Stockholm, Sweden) 2004;43:675-9.
138. Niederacher D, Yan HY, An HX, Bender HG, Beckmann MW. CDKN2A gene inactivation in epithelial sporadic ovarian cancer. British journal of cancer 1999;80:1920-6.
139. Ryland GL, Hunter SM, Doyle MA, et al. RNF43 is a tumour suppressor gene mutated in mucinous tumours of the ovary. The Journal of pathology 2013;229:469-76.
140. McAlpine JN, Wiegand KC, Vang R, et al. HER2 overexpression and amplification is present in a subset of ovarian mucinous carcinomas and can be targeted with trastuzumab therapy. BMC Cancer 2009;9:433.
141. Sanchez-Bermudez AI, Sarabia-Meseguer MD, Garcia-Aliaga A, et al. Mutational analysis of RAD51C and RAD51D genes in hereditary breast and ovarian cancer families from Murcia (southeastern Spain). European journal of medical genetics 2018;61:355-61.
142. Klumper N, Syring I, Vogel W, et al. Mediator Complex Subunit MED1 Protein Expression Is Decreased during Bladder Cancer Progression. Frontiers in medicine 2017;4:30.
143. Cui J, Germer K, Wu T, et al. Cross-talk between HER2 and MED1 regulates tamoxifen resistance of human breast cancer cells. Cancer research 2012;72:5625-34.
144. Perets R, Drapkin R. It's Totally Tubular...Riding The New Wave of Ovarian Cancer Research. Cancer Res 2016;76:10-7.
145. Conner JR, Meserve E, Pizer E, et al. Outcome of unexpected adnexal neoplasia discovered during risk reduction salpingo-oophorectomy in women with germ-line BRCA1 or BRCA2 mutations. Gynecologic oncology 2014;132:280-6.
146. Karnezis AN, Cho KR. Of mice and women - Non-ovarian origins of "ovarian" cancer. Gynecologic oncology 2016.
147. Rebbeck TR, Lynch HT, Neuhausen SL, et al. Prophylactic oophorectomy in carriers of BRCA1 or BRCA2 mutations. N Engl J Med 2002;346:1616-22.
148. Kauff ND, Satagopan JM, Robson ME, et al. Risk-reducing salpingo-oophorectomy in women with a BRCA1 or BRCA2 mutation. N Engl J Med 2002;346:1609-15.
149. Falconer H, Yin L, Gronberg H, Altman D. Ovarian cancer risk after salpingectomy: a nationwide population-based study. J Natl Cancer Inst 2015;107.
150. Kwon JS, Tinker A, Pansegrau G, et al. Prophylactic salpingectomy and delayed oophorectomy as an alternative for BRCA mutation carriers. Obstetrics and gynecology 2013;121:14-24.

151. McAlpine JN, Hanley GE, Woo MM, et al. Opportunistic salpingectomy: uptake, risks, and complications of a regional initiative for ovarian cancer prevention. Am J Obstet Gynecol 2014;210:471 e1-11.
152. Parker WH, Broder MS, Chang E, et al. Ovarian conservation at the time of hysterectomy and long-term health outcomes in the nurses' health study. Obstetrics and gynecology 2009;113:1027-37.
153. Colicchia V, Petroni M, Guarguaglini G, et al. PARP inhibitors enhance replication stress and cause mitotic catastrophe in MYCN-dependent neuroblastoma. Oncogene 2017;36:4682-91.
154. Pyndiah S, Tanida S, Ahmed KM, Cassimere EK, Choe C, Sakamuro D. c-MYC suppresses BIN1 to release poly(ADP-ribose) polymerase 1: a mechanism by which cancer cells acquire cisplatin resistance. Sci Signal 2011;4:ra19.
155. Hallett RM, Seong AB, Kaplan DR, Irwin MS. Transcript signatures that predict outcome and identify targetable pathways in MYCN-amplified neuroblastoma. Mol Oncol 2016;10:1461-72.
156. Abkevich V, Timms KM, Hennessy BT, et al. Patterns of genomic loss of heterozygosity predict homologous recombination repair defects in epithelial ovarian cancer. British journal of cancer 2012;107:1776-82.
157. Frey MK, Pothuri B. Homologous recombination deficiency (HRD) testing in ovarian cancer clinical practice: a review of the literature. Gynecol Oncol Res Pract 2017;4:4.
158. Swisher EM, Lin KK, Oza AM, et al. Rucaparib in relapsed, platinum-sensitive high-grade ovarian carcinoma (ARIEL2 Part 1): an international, multicentre, open-label, phase 2 trial. Lancet Oncol 2017;18:75-87.
159. Mirza MR, Monk BJ, Herrstedt J, et al. Niraparib Maintenance Therapy in Platinum-Sensitive, Recurrent Ovarian Cancer. The New England journal of medicine 2016;375:2154-64.
160. Coleman RL, Oza AM, Lorusso D, et al. Rucaparib maintenance treatment for recurrent ovarian carcinoma after response to platinum therapy (ARIEL3): a randomised, double-blind, placebo-controlled, phase 3 trial. Lancet 2017;390:1949-61.
161. Papalia H, Audic F, Riviere GR, Verschuur A, Andre N. Quick and sustained clinical response to MEK inhibitor I in a NF1 patient with neurofibromas. Ecancermedicalscience 2018;12:862.
162. Xue Y, Meehan B, Fu Z, et al. SMARCA4 loss is synthetic lethal with CDK4/6 inhibition in non-small cell lung cancer. Nature communications 2019;10:557.
163. Wehde BL, Radler PD, Shrestha H, Johnson SJ, Triplett AA, Wagner KU. Janus Kinase 1 Plays a Critical Role in Mammary Cancer Progression. Cell reports 2018;25:2192-207.e5.
164. Leonard M, Zhang X. Estrogen receptor coactivator Mediator Subunit 1 (MED1) as a tissue-specific therapeutic target in breast cancer. Journal of Zhejiang University Science B 2019;20:381-90.
165. Zhang Y, Leonard M, Shu Y, et al. Overcoming Tamoxifen Resistance of Human Breast Cancer by Targeted Gene Silencing Using Multifunctional pRNA Nanoparticles. ACS nano 2017;11:335-46.
166. Longacre TA, Oliva E, Soslow RA, Association of Directors of A, Surgical P. Recommendations for the reporting of fallopian tube neoplasms. Hum Pathol 2007;38:1160-3.
167. Haber DA, Velculescu VE. Blood-based analyses of cancer: circulating tumor cells and circulating tumor DNA. Cancer Discov 2014;4:650-61.
168. Kinde I, Bettegowda C, Wang Y, et al. Evaluation of DNA from the Papanicolaou test to detect ovarian and endometrial cancers. Sci Transl Med 2013;5:167ra4.

CURRICULUM VITAE

DOROTHY LEIGH HALLBERG

Johns Hopkins University School of Medicine
The Sydney Kimmel Comprehensive Cancer Center
The Koch Cancer Research Building
1550 Orleans Street
CRB2 Room 532
Baltimore, Maryland 21287
P: 410-614-4631
dhallbe2@jhmi.edu
DOB: 09/17/91 Mt.Kisco, NY

EDUCATION

2014 – Present **Human Genetics PhD Candidate**
Johns Hopkins School of Medicine, Baltimore, Maryland
Advisor: Victor E. Velculescu M.D, Ph.D.

2013 –2014 **Oncology Master of Science by Research**
Oxford University, Oxford, England
Advisor: Sir Walter Bodmer Ph.D.

2009 –3013 **Anthropology and Biology BS**
Bucknell University, Lewisburg, Pennyslvania

RESEARCH EXPERIENCE

2014 – Present **Graduate Research Assistant, Johns Hopkins School of Medicine, Baltimore,Maryland**

Project: Spearheaded efforts to understand the evolution of high grade serous ovarian cancer and the genomic landscapes of many subtypes of rare ovarian cancer.

- Co-developed bioinformatics software, Trellis, to identify structural alterations in tumor only ovarian cancer samples.
- Research validated the origin of high grade serous ovarian carcinoma in the fallopian tube (2016, *Cancer Genomics)*
- Write research summary and contribute research strategy content for annual American Medical Resources Foundation Adelson grant renewal
- Trained both a new postdoc and a younger graduate student in the lab in next generation sequencing techniques and analysis

2013 – 2014 Graduate Research Assistant, Oxford University, Oxford, England.
Project: Utilized flow cytometry and cell culture to understand the differentiation of goblet cells in colorectal cancer

- Designed independent experiments to understand the pathway of differentiation of goblet cells in colorectal cancer cell lines.

2012-2013 Undergraduate Research Assistant, Bucknell University
Advisor: Dr Ken Field, FTIs and Burkitt's Lymphoma

2012 **Summer Research Intern, Mt. Sinai Hospital.**
Advisor: Dr. Shu-hsai Chen

TEACHING EXPERIENCE

2015 TA for Pathology Biology

2015-2016 TA for Introduction into Bioinformatics

2018 TA for 4 day intensive Practical Genomics Workshop

LEADERSHIP EXPERIENCE

2014-2016 Captain of Soccer Team

2012-2013 Global Ambassador for IFSA-Butler

2011-2012 Senior Coxswain for St. Catherine's Boat Club at Oxford University

2010-2011 Rowing Coach at Norwalk River Rowing Association

PUBLICATIONS:

Dutke, T., **Hallberg, D**. and Reeves, R.H. (2014) Chronic up-regulation of the SHH pathway normalizes some developmental effects of trisomy in Ts65Dn mice. *Mechanisms of Development* 135

*Labidi-Galy, S.I., *Papp, E., **Hallberg, D.**, Niknafs, N., Adleff, V., Noes, M., Bhattacharya, R., Novak, M., Jones, S., Phallen, J., Hruban, C.A., Hirsch, M.S., Lin, D.I., Schwatz, L., Maire, C/L/. Tille, J.-C., Bowden, M., Ayhan, A., Wood, L.D., Scharpf, R.B., Kurman, R., Wang, T.-L., Shih, I.-M., Karchin, R., Drapkin, R., and Velculescu, V.E. (2017) High grade serous ovarian carcinomas originate in the fallopian tube. *Nature communications*, 8:1093

Camps, M.P., Cohen, M., Von Euw, E., **Hallberg, D**., Velculescu, V.E., Kujak, J.L., Conklin, D., Slamon, D.J., Elvin, J., Konecny, G.E. (*In Press*) BRAF Mutations Occur Infrequently in Ovarian Cancer but Suggest Responsiveness to BRAF and MEK Inhibition. *JCO Precision Oncology*

*Papp, E., ***Hallberg, D.**, Konecny, G.E., Bruhm, D.C., Adleff, V., Noe, M., Kagiampakis, I., Conklin, D., Kinose, Y., White, J.R., Press, M.P., Drapkin, R., Easwaran, H., Baylin, E., Slamon, D., Velculescu, V.E., Scharpf, R.B. (*In Press*) Integrated Genomic, Epigenetic, and Expression Analyses of Ovarian Cancer Cell Line. *Cell Reports*

Claudia Iavarone, Ioannis K. Zervantonakis, Laura M Selfors, Sangeetha Palakurthi, Joyce Liu, Ronny Drapkin, Ursula A Matulonis, **Dorothy Hallberg**, Victor E. Velculescu, Joel D. Leverson, Deepak Sampath, Gordon B. Mills, and Joan S. Brugge. (*In Press*) Combined MEK and BCL-2/XL inhibition is effective in high-grade serous ovarian cancer patient-derived xenograft models and BIM levels are predictive of responsiveness. *Molecular Cancer Therapeutics*

*= co-first

POSTERS:

Dorothy Hallberg, Eniko Papp, Gottfried E. Konecny, Daniel C. Bruhm, Vilmos Adleff, Michaël Noë, Ioannis Kagiampakis, Doreen Palsgrove, Dylan Conklin, Yasuto Kinose, James R. White, Michael F. Press, Ronny Drapkin, Hariharan Easwaran, Steve Baylin, Dennis Slamon, Victor E. Velculescu, Robert B.Scharpf. (2018) Integrated Genomic, Epigenetic, and Expression Analyses of Ovarian Cancer Cell Lines. *American Society of Human Genetics*